Flying Hospitals

June, 2013

Design of a Next Generation Disaster Relief System

Design Synthesis Exercise

TU Delft Delft University of Technology

Aerospace Engineering

Delft University of Technology
Faculty of Aerospace Engineering

AE3200: Design Synthesis Exercise

Final Report

FLYING HOSPITALS

GROUP MEMBERS

Britta Wilken - 4056426
Alexander Vanwelsenaere - 4108248
Yvonne Haartsen - 4079973
Anton de Bode - 4124944
Timo Sanders - 4036352
Brynn Appeldoorn - 1506625
Bart Meijer - 4016750
Balraj Singh - 4116879
Said Idoum - 4076648
Jochem Delsen - 1369121

TUTORS AND COACHES

Prof. Dr. ir. John Stoop
Dr. Dipanjay Dewanji
Pedro Pinto Rebelo

Delft, The Netherlands
July 2, 2013

Document Management

Version	Date	Pages Affected	Description of Change
2.0	July 2, 2013	All	Changes after feedback from tutor and coaches
1.0	June 24, 2013	All	New Document

Written by	Group 15
Written for Client	Red Cross
Date	July 2, 2013

Progress	**External Release**
Review	**External Release**

Checked by

Britta Wilken
Alexander Vanwelsenaere
Yvonne Haartsen
Anton de Bode
Timo Sanders
Brynn Appeldoorn
Bart Meijer
Balraj Singh
Said Idoum
Jochem Delsen

Table of Contents

Preface

In case of a military conflict or environmental disaster it is very hard to get resources and health support quickly to (remote) disaster areas. Red Cross, an organization providing international support, wants to provide self-reliant, adaptive and rapidly deployable support. Throughout the years, large commercial aircraft have been used for this purpose, with promising results. However, the application of large aircraft is limited in penetrating some event sites with limited space. Therefore, a more dedicated solution should be found that can cope with specifics of emergency support, eliminating the constraints of large aircraft. During the ten week Design Synthesis project, a group of ten aerospace engineering students of the TU Delft was occupied by the redesign of an aircraft being able to cope with this situation.

We want to thank our tutor Prof. Dr. John Stoop and our coaches Dr. Dipanjay Dewanji and Pedro Pinto Rebelo for their intensive support and assistance during the project. Additionally we would like to thank Herman Becking and Eelco Brouwer for their input from the Red Cross, Dries Blommers for his market suggestions and Dr. Adel Ghobbar for the cooperation with the Global Peace Partners. Moreover, our thanks goes to Stichting Behoud Erfgoed De Vries Robbé and to Damen Shipyards Group for their inspiring input. Also, Ir. Nando Timmer is thanked for his advice concerning the application of vortex generators. Furthermore, we would like to thank Eddy van den Bos and Martijn Stellingwerff for their help with the 3D printed scale model. Finally, we appreciate the cooperation with Rolof Mulder and Peter Hazendonk from the Hospitainer company.

This final report is the last progress report of the DSE. It summarizes the detailed design phase of the Flying Hospital project so it will be of primary interest for any parties that are providing emergency aid in inaccessible areas.

Summary

The objective of this project was to create a preliminary design of a Flying Hospital, a modular aircraft capable of providing medical and humanitarian aid to disaster areas inaccessible by conventional transport, to fulfill the disaster response needs of the Red Cross. Motivating the development of the Flying Hospital were the experiences of aid groups in recent disasters such as Haiti, which demonstrated the potential inadequacy of existing relief systems when local infrastructure was compromised. The envisioned Flying Hospital addresses these shortcomings by being self-sustaining and circumventing dependency on local infrastructure. Documented in the following report is the detailed design phase of the project where the conceptual design was evaluated and refined towards the final design of the Flying Hospital system.

Conceptual Design

The Flying Hospital mission was determined by investigating different disaster types, level of occurrence and typical injuries and past relief operations in the mid-term report. Thereafter, the different aircraft types were analyzed and one aircraft type was chosen to be implemented in the Flying Hospital concept. Red Cross, the main stakeholder, requested that the focus would shift more towards the financial side so adjustments in the mission were needed. Additionally, the retrofitted aircraft shall have improved STOL (Short Takeoff and Landing) capabilities.

Therefore, the Antonov was chosen for its performance characteristics and robust design. This aircraft will fly in supplies, customized containers, a field hospital, medical staff and may evacuate people if necessary. The field hospital will be set up outside the aircraft in the disaster area. This way, the aircraft can shuttle back and forth from the disaster area to the mission base that is located at the airport closest to the disaster area. Surgery will be performed in the specially designed surgery rooms made by Hospitainer. Other activities can be performed in the tents supplementing the field hospital. The mission concept can be scaled up and down in every aspect, in order to provide medical aid in all kind of disaster areas.
The recommended mission consists of operational bases all over the world in locations close to disaster sensitive areas. The bases were chosen with respect to already existing logistic center of the Red Cross so that the supplies can be relatively easily distributed. From the position where the aircraft is stalled, the Antonov An-74 will be flying to the spot where Hospitainer is positioned. It picks up the Hospitainer and transports it to an airport in the vicinity of the disaster area and from there into the disaster area itself.

Technical resources like weight, cost and performance had to be carefully tracked throughout the design process. Since the design started with an already existing Antonov An-74, some resources like MTOW (Maximum Takeoff Weight) did not allow for a deviation from the starting values. Using the technical performance management (TPM) method, the contingency and variation of this factor was tracked throughout the whole process.

With the mission and aircraft determined, two risk analyses were performed to investigate the critical aspects of the entire mission and aircraft. The risk analysis consisted of the description of potential risks, an assessment of their probability of occurrence and consequences of impact that led to a risk mitigation plan. A distinction was made between technical risks, schedule risks, cost risks and environmental risks for both the mission and the aircraft. Potential risks for the mission concern hazardous landing zone, operational delays and budget related problems. For the aircraft aspect, potential risks include aircraft takeoff and landing performance issues, technical malfunction or failure and the production time.

Detailed Design

The current D-36 2A engine is proposed to be changed to an engine that is able to deliver more thrust. A literature study was performed based on experiences Antonov has with certain engine types. The Ivchenko Progress D-436-T3 engine was chosen during the engine selection procedure because it has a significantly higher trust to weight ratio which is beneficial to reduce the takeoff distance. In the design process the D-36 2A engine, as well as the

D-436-T3 engine, were modeled. The D-36 2A engine was modeled during takeoff, whereas the D-436-T3 engine was modeled during takeoff and cruise. Additionally, an optimization procedure for cruise condition was performed for the D-436-T3 engine.

The retrofitting of the larger engines on the An-74 also has considerable implications on its performance due to the unique engine configuration. An-74 is the sole aircraft in production that uses upper surfacing blowing (USB): the blowing of engine exhaust over the wing surface generates additional aerodynamic forces. By installing the new engines, the performance of the aircraft is not only affected directly by the increased thrust, but also by the larger USB effect.

It was calculated that the placement of D-436 engines would have appreciable contribution to the STOL characteristics of the aircraft due to the USB effects. The larger mass flow and exhaust velocity of these engines, compared to the stock D-36, generate increased lift in two manners. Firstly, the greater mass flow results in additional jet momentum being vectored downwards by the wing surface in what is known as the Coanda effect. Secondly, the higher exhaust velocity induces lower pressures along the blown surface of the wing that result in increased aerodynamic forces. Inherit to the increase of these forces are larger drag and pitching moment. However, emphasizing the STOL aspect of the Flying Hospital, it was determined that the potential gain in lift outweighed the accompanying drag and pitching penalties. Modeling of the An-74 USB configuration demonstrated 8% and 2% increases in lift and drag respectively for the entire aircraft in flapped configuration. For cruise configuration, the increases were and 4% and 5% in lift and drag respectively. Thus the D-436 engines were deemed to have a beneficial contribution to STOL at a minor expense of cruise efficiency.

As a second alternative to increase the STOL capabilities of the aircraft, the option of adding vortex generators on the wing and flaps was considered. There was opted to perform a literature study, since this provided the most efficient way to design and estimate the performance effect due to the devices. Two configurations of vortex generators were considered: (1) placing devices at 25% of the flap chord length. By delaying the separation point, the stall speed can be reduced; lift-off speed, approach speed and landing speed are reduced meanwhile as well. (2) By placing vortex generators at 0.2·c, the transition point can be delayed. Laminar boundary layers produce less drag than turbulent boundary layers. By delaying the transition point, less drag is thus produced.
In order to reduce maintenance costs, the devices were not set to the minimal possible size (approximately 0.1 mm). The height of each device (h) is defined as function of the boundary layer thickness (δ): $h/\delta = 0.5$. The remainder device dimensions, as well as the spacing between the pairs and elements of a pair, are defined as a function of the device height. Thereafter, properties such as vortex strength, decay and core radius were determined. Also the direct drag contribution of the devices was defined.
The performance analysis of the vortex generators placed on the flaps (1) concluded that the devices effectively increase lift and reduce drag in typical landing descend and takeoff climb conditions. By placing the devices on the flaps, they no dot produce drag during cruise conditions and only affect the performance in case flaps are extracted. Since these are the flight phases in which separation alleviation is most important, this option is proposed as a feasible modification in order to improve the STOL performance. The analysis of the devices placed at 0.2·c of the wing (2) showed that the drag reduction due to the delay of the transition point was smaller than the device drag induced by the devices themselves. Therefore, this option is not proposed as modification.
The overall performance analysis due to the addition of vortex generators was analyzed further. It was determined that during landing descend and takeoff climb, lift is increased by 9% whereas drag is reduced by 37.5%. In the end the manufacturing cost and certification cost were estimated.

The aim of the structural analysis was to investigate the differences in normal and shear stress in the wing and fuselage between the stock and new engine. A simulation model of the wing and fuselage was made to investigate the structural capabilities. The differences in the loads on the structure due the heavier and more powerful new engine were investigated. Since no reliable data about the structure of the airplane is available, a general representation of the wing and fuselage structure is taken into consideration based on the available technical drawings of the aircraft. The maximum normal and shear stresses on the structure increase due to the new engine.

The stability and control analysis started with a detailed reconstruction of the geometry of the aircraft through careful measurements. With this information, the Class II weight estimation method was used to find the weight of individual components of the aircraft. Using these weights and dimensions, an estimation of the c.g. was constructed. This was necessary to obtain a loading diagram. Using stability calculations and simulation, the c.g. of

the aircraft at certain fuel, cargo and crew load and distribution was computed. This results in an output stating whether the aircraft is within its stable limits. Finally, some monitoring and redesign options were mentioned for future implementation.

The modifications introduce new operating conditions for the material therefore the material properties of the Antonov have to be analyzed. First the mechanical strain was considered. The normal stresses in the wing and fuselage increased thus the material strain decreased. Also, the shear stresses in the wing and fuselage increased and therefore the material strain was further reduced. The normal strains and shear strains can be expressed in a matrix which can be used to verify the materials' capabilities to operate in new conditions. Not only external loads but also thermal loads have an effect on the material. Due to the new engine with high exhaust velocity, high temperatures occur at the aft of the engine. The components behind the new engine are made from titanium. In these conditions the material will try to expand but it is constrained by fastening systems. High thermal stresses will be induced which will contribute to the total stress in the material.

The main purpose of the detailed design phase was to increase the STOL capabilities of the An-74. By adding the performance increase due to both the engine change and addition of the vortex generators, the total change in performance due to the technical modifications could be determined. Due to the increase in lift, the stall speed is reduced. Lift-off speed, approach speed and touch-down speed are reduced because they are proportional to the stall speed. Dynamic relations were used in order to determine the effect of the reduced speeds on takeoff and landing distance required. Furthermore, the effect of the new engine and increased USB has an effect on range which has been determined as well.
It was determined that takeoff distance is reduced by 40%-60%; landing distance is decreased by ∼12%; range is reduced by 10%-15%. For a typical operating weight of 28 ton, the aircraft with proposed modifications has a takeoff distance of 278 m, and landing distance of 329 m. In case the aircraft takes off with 1.5 ton payload and max fuel, the range is 2908 km.

Implementation

In the project design and development logic, the continuation from the end of the project towards the product delivery is given in a flow block diagram. This lists the steps taken during the lead time phase of three years. The first step after the project is to order the aircraft itself (Antonov An-74-200). This is followed by zeroing and stripping it for retrofitting. After retrofitting, the prototype is tested and certified. Once certified, the final product is produced and delivered to the stakeholder.

All post-DSE activity costs are estimated in the cost breakdown structure. From this breakdown, it became clear that the retrofitting phase of the aircraft is the most costly (€25M). Some costs will only come across once, such as prototype testing and certification of the retrofits.

The manufacturing plan explains the manufacturing phase of the retrofit modifications. The wing has to be structurally reinforced and provided with a new material panel behind the engine to cope with the change in weight of the engine, as well as with the higher temperature of the exhaust flow. Also, the vortex generators shall be mounted on the wing to provide more lift. Furthermore, the interior has to be stripped and the loading of the customized containers has to be made possible by means of the rear ramp entry. When all technical features are manufactured, the aircraft is assembled then delivered to the stakeholder.

The success of the humanitarian project depends on its cost feasibility. Therefore, a business model was developed to suit the needs of relief organization. Further, it was also extended to include prospective for-profit companies and educational institutions. Time wise, the Flying Hospital project was broken into two phases: disaster and disaster-free phase. During disasters, humanitarian non-profit aspects are important and the Flying Hospital operates as such. Outside disaster times, the hospital can either continue its charitable activities or can be made profitable. The Flying Hospital system was divided into two parts: the hospital and the aircraft. These can be managed jointly or independently. Furthermore, they can be fully owned, co-owned, dry or wet leased by the operating organization or in partnership with others. In total, this will reduce the costs of the humanitarian aid and make it more attractive and feasible for both profit and non-profit markets.
The key to sustainable development is to consider the life cycle of a product and to design for future problems that may arise during the product's life time.

The sustainability strategy can be conducted via several methods, such as utilizing sustainable materials, applying used material, applying sustainable manufacturing methods and predicting the end-of-life value of the end product. However, reuse of products has limitations such as safety regulations. Therefore, the materials should be checked for fatigue and corrosion thoroughly, which is a costly operation.
Different kinds of materials could be used in future designs such as AEROCORK and composites like GLARE. Another possibility is to retrofit with more efficient engines with engine optimization. To reduce emission these engines will operate on biofuel.
After 20 or 30 years of service the aircraft is at the end of its life. There are several options to dispose of the aircraft in a sustainable way.

System Overview

Four types of bases exist: the organizational, operational and mission base, as well as the disaster area. Between each of this bases long distance communication is needed. The pre-mission organization takes place from the organizational base. From there, the relief organization communicates the mission needs and the cargo (medicines, food etc.) that have to be taken on-board by the Flying Hospital. These are brought to the mission base that is positioned at the closest airport to the disaster area. At the mission base the Global Peace Partners perform medical help on larger scale. The An-74 is shuttling between the mission base and the disaster area to bring in supplies and evacuate patients that will be helped by the Global Peace Partners. In the disaster area the PAV EMS vehicle can be integrated in the system. This vehicle can penetrate deeper into the disaster area to bring injured people to the field hospital that cannot reach the Flying Hospital independently. The communications with the aircraft are of high importance at this stage since the primary mission of helping people in the disaster area then begins. After the provision of aid, the Flying Hospital leaves the disaster area and goes back to the position where it is stalled. There, the aircraft is checked and supplies are refilled for the following mission. The collaboration with the Global Peace Partners and PAV EMS Vehicle accomplishes a seamless connectivity between all parts the Flying Hospital system. This Flying Hospital system results in a resilient medical relief environment.

The compliance matrix and feasibility analysis present the requirements of the design and analyze if the requirements are met. The majority of the requirements of the system are met by the Flying Hospital design. After consultation with the main stakeholder, the Red Cross, the focus of the requirements shift towards a cost efficient design. The medical requirements are put to the side since the surgery room is placed in the Hospitainer. Also, the crew, patients, supplies and medical equipment requirements are taken over by the Red Cross.

List of Symbols

Roman Symbols

Variable	Description	Unit
A	Cross-sectional area	[mm^2]
A_0	Fourier coefficient	[-]
A_g	Constant	[-]
A_s	Cross-sectional area boom	[mm^2]
A_v	Aspect ratio vane vortex generator	[-]
AR	Aspect ratio	[-]
b	Width (Section 2.4)	[mm]
b	Span (Section 2.5)	[m]
B	Boom area	[mm^2]
B_0	Fourier coefficient	[-]
B_g	Constant	[-]
c	Chord length	[mm]
c_r	Root chord	[mm]
c_t	Tip chord	[mm]
c_f	Skin friction coefficient	[-]
C_D	Drag coefficient	[-]
C_d	Friction drag coefficient	[-]
C_{d0}	Zero lift drag coefficient	[-]
C_f	Friction drag coefficient	[-]
C_g	Constant	[-]
C_j	Jet coefficient	[-]
C_l	2D lift coefficient	[-]
C_L	3D Lift coefficient	[-]
C_{Lmax}	Maximum lift coefficient	[-]
C_m	Pitching moment coefficient	[-]
C_p	Pressure Coefficient	[-]
$C_{L\alpha}$	Slope C_L - α graph	[-]
d	Distance between toed-in and toed-out vane	[mm]
D	Distance between pairs	[mm]
D_0	Fourier coefficient	[-]
D_g	Constant	[-]
E	Young's modulus (Section 2.6)	[N·m^{-2}]
E	Ratio of flap chord to airfoil chord (Section 2.2)	[-]
E_0	Fourier coefficient	[-]
EI_{NO_x}	Emission index of NO_x	[-]
f	Induced pressure	[N·m^{-2}]
F	Force Vector	[N]
F_0	Fourier coefficient	[-]
FF	Form Factor	[-]
G	Shear Modulus	[N·m^{-2}]
G_0	Fourier coefficient	[-]
h	Height	[mm]
h^+	Non-dimensional effective vortex generator height	[-]
I_{xy}	Product second moment of area	[mm^4]
I_{xx}	Second moment of area about the x-axis	[mm^4]
I_{yy}	Second moment of area about the y-axis	[mm^4]
k_n	Constant	[-]
K	Constant (Section 2.5)	[-]
K	Local vortex strength (Section 2.3)	[m^2·s^{-1}]
l_h	Quarter chord of wing to quarter chord tail	[m]
L	Lift force	[N]
M	Moment (Section 2.4)	[Nm]
M	Mach number (Section 2.5)	[-]
MAC	Mean aerodynamic chord	[m]
n	Load factor (Section 2.5)	[-]
n	Number corresponding to boom numbering(Section 2.4)	[-]
n_{ult}	Ultimate load factor	[-]
N	Number of fuel tanks	[-]
N_e	Number of engines	[-]
N_i	Normal Vector	[N]
P	Pressure differential fuselage	[N·mm^{-2}]
P	Pressure	[N·m^{-2}]
q	Shear flow (Section 2.4)	[N·mm^{-1}]
q	Dynamic Pressure (Section 2.5)	[N·m^{-2}]
r	Radius of the fuselage	[m]
r_c	Vortex core radius	[mm]
R	Radius	[m]
Re	Reynolds number	[-]
s	Distance between booms	[mm]
S	Shear force (Section 2.4)	[N]
S	Wing area (Section 2.5)	[m^2]
S_{fgs}	Fuselage gross shell area	[m^2]
S_{net}	Net wing surface area	[m^2]
S_r	Rudder area	[m^2]
S_v	Planform area of vane vortex generator together with reflection	[m^2]
t	Thickness	[mm]
t/c	Thickness to chord ratio	[-]
t_r	Thickness at the root	[mm]
T	Torsion (Section 2.4)	[Nm]
T	Thrust vector (Section 2.2)	[N]
T	Temperature (Section 2.6)	[K]
T_{TO}	Total required takeoff thrust	[N]
U	Velocity	[m·s^{-1}]
U_e	Boundary layer edge velocity	[m·s^{-1}]
V	Velocity	[m·s^{-1}]
V_D	Dive Velocty	[m·s^{-1}]
W_{ac}	Aircraft Weight	[N]
W_{emp}	Empennage weight	[N]
W_{engine}	Engine weight	[N]
W_f	Fuselage weight	[N]
W_g	Landing gear weight	[N]
W_{MZF}	Maximum zero fuel weight	[N]
W_n	Nacelle weight	[N]
W_p	Payload weight	[N]
W_{struct}	Structural weight	[N]
W_{TO}	Takeoff Weight	[N]
$\bar{x}_{ac}$	Location aerodynamic center	[m]
$\bar{x}_{cg}$	Location center of gravity	[m]
$\bar{x}_{np}$	Location neutral point	[m]

Greek Symbols

Variable	Description	Unit
α	Angle of attack	[°]
Γ	Vortex strength	[$m^2 \cdot s^{-1}$]
γ	Shear strain	[-]
Δ	Difference	[-]
$\Delta\epsilon$	Downwash angle	[°]
δ	Boundary layer thickness	[mm]
δ_f	Flap deflection	[°]
ϵ	Normal strain	[-]
η	Airfoil efficiency coefficient	[-]
θ_i	Angle of panel i wrt angle of attack	[°]
Λ_{LE}	Sweep angle at the leading edge	[°]
$\Lambda_{0.25c}$	Sweep angle at the quarter chord length	[°]
$\Lambda_{0.5c}$	Sweep angle at the semi chord length	[°]
$\Lambda_{0.75c}$	Sweep angle at the third quarter chord length	[°]
λ	Taper ratio	[-]
μ	Viscosity air	[$kg \cdot (s \cdot m)^{-1}$]
μ_τ	Wall friction velocity	[$m \cdot s^{-1}$]
ν	Poisson ratio	[-]
ν_E	Effective kinematic velocity	[$m \cdot s^{-1}$]
ρ	Density	[$kg \cdot m^{-3}$]
σ	Normal stress	[$N \cdot mm^{-2}$]
σ_v	Von Mises stress	[$N \cdot mm^{-2}$]
τ	Shear stress (Section 2.4)	[$N \cdot mm^{-2}$]
τ	Jet deflection angle (Section 2.2)	[°]

Subscripts

Variable	Description
ac	Aerodynamic center
f	Fuselage
h	Horizontal tail
v	Vertical tail
v	Vortex generator
∞	Freestream condition

Glossary of Terms

CFD	Computational Fluid Dynamics
CST	Circular Streamline Theory
CVG	Conventional Vortex Generator
DSE	Design Synthesis Exercise
EADS	European Aeronautical Defense and Space Company
EMS	Emergency Medical Service
FEM	Finite Element Method
FOD	Foreign Object Damage
HPC	High Pressure Compressor
HPT	High Pressure Turbine
ICAO	International Civil Aviation Organization
ILA	Internationale Luft- und Raumfahrtausstellung
IPT	Intermediate Pressure Turbine
ISA	International Standard Atmosphere
JIT	Just-in-Time
LE	Leading Edge
LPC	Low Pressure Compressor
LPT	Low Pressure Turbine
LPVG	low Profile Vortex Generators
LW	Landing Weight
MTOW	Maximum Takeoff Weight
MVG	Micro Vortex Generators
OEW	Operational Empty Weight
PAMELA	Process for Advanced Management of End-of-Life of Aircraft
PAV	Personal Aerial Vehicle
SFC	Specific Fuel Consumption
STOL	Short Takeoff and Landing
TE	Trailing Edge
TET	Turbine Entry Temperature
TO	Takeoff
TOW	Takeoff Weight
TPM	Technical Performance Management
USB	Upper Surface Blowing
VG	Vortex Generators
VTOL	Vertical Takeoff and Landing

Introduction

Over the past few decades, natural disasters and conflicts have continued to strike various regions, endangering afflicted populations both directly and by the long-term destruction of local infrastructure. The loss of local infrastructure, including hospitals and transportation, inhibits immediate relief but also delays, if not prevents, the deployment of external aid. This has demonstrated the need for external medical and humanitarian services to rapidly deploy relief facilities in disaster areas inaccessible by conventional means.

Traditional aircraft have proven to be essential to humanitarian efforts; their long ranges and large carrying capacities are ideal for transporting emergency response resources. However, these aircraft are generally limited by the available facilities in the stricken regions. For example, the 2010 earthquake in Haiti triggered a massive international relief effort, an effort that was unfortunately hampered and bottle-necked by the congestion of its sole functional airport [1]. A possible solution to address such setbacks in future humanitarian operations is the employment of specialized aircraft, Flying Hospitals, capable of operating independently of supporting infrastructure. This would imply not only the capability to land and takeoff in normally inaccessibly terrain but also the prolonged self-sufficiency of the Flying Hospital once deployed. The aim of this project is to create a preliminary design of such a specialized aircraft, incorporating medical equipment and facilities designed by Hospitainer, to meet the needs of the Red Cross, that is the main stakeholder of this project, in extended penetration of disaster areas.

The following report documents the detailed design phase of the project, tracking development from the initial design options to the final design of an aircraft's retrofitting and systems for operating the Flying Hospital mission. The method governing the previous phase consisted of evaluating the scale of the required humanitarian aid, identifying operational constraints imposed by the mission environments and ultimately selecting the most suitable aircraft to achieve the mission. The Antonov An-74 was selected as the base aircraft for the design and modifications to achieve the envisioned mission under the given requirements will be further considered and investigated in detail in this report.

The envisioned mission consists of four different bases: the organizational base, the operational base, the mission base and the disaster area. From the organizational base the pre-mission activities are organized. There are also four operational bases spread over the world. The operational base functions as base for the supplies and is at the same places where the Red Cross places it's logistic center. The mission base is positioned on a major airport close to the disaster area. There, the Global Peace Partners, whom work in cooperation with the Flying Hospital mission, provide medical help at larger scale. Finally, in the disaster area a field hospital and a surgery room is placed. This surgery room is located within a container and is provided by the company Hospitainer. To transport the container, the field hospital and the supplies to the disaster area the Antonov An-74 retrofit is used. Furthermore, the aircraft can evacuate patients to the mission base where further medical help can be provided. The PAV EMS vehicle, designed by another DSE group, can be integrated in the mission in such a way that it can penetrate deeper into the disaster area to save injured people that could not reach the field hospital themselves.

In the Conceptual Design chapter (Chapter 1) an overview of all the design selections made in the mid-term report [2] is given. Furthermore, a functional analysis, a budget breakdown and a risk analysis are provided. The technical modifications were selected and then analyzed in the Detailed Design chapter (Chapter 2). Six different design characteristics were investigated in more detail: engine, upper surface blowing modification, vortex generators, structural components, stability and control and material characteristics. The Implementation chapter (Chapter 3) covers the project design development, including a Gantt Chart, the cost breakdown structure and the manufacturing plan for further developments of the Flying Hospital. Additionally, the market was analyzed and sustainable development strategies were provided. In the final chapter, System Overview, (Chapter 4) the operations and logistics strategy, as well as the communication system can be found. In the end the requirements compliance matrix will check whether requirements are met and if the Flying Hospital design is a feasible product.

1 Conceptual Design

In the conceptual design chapter, the conceptual mission and aircraft choice will be discussed and evaluated in Section 1.1. Changes in requirements have stemmed from the mid-term report discussions with some stakeholders, and therefore have dictated changes in design and implementation. Functional flow and block diagrams are shown in Section 1.2 in order to give an overview of the design effort and structure. The possible modifications matching the new criteria will then be evaluated; the most appropriate selections will be specified in Section 1.3. A budget breakdown can be found in Section 1.4; pre-allocation of resources and budgets, as well as assigning minimum and maximum values where appropriate, were performed. A risk assessment will be carried out to give an evaluation of the the Flying Hospital system and lay out important risks as well as their mitigation in Section 1.5. Finally, an operational record of the Antonov An-74 is given in Section 1.6.

1.1 Conceptual Mission and Aircraft Choice

In the mid-term report of the Flying Hospitals group [2] the conceptual design of the aircraft and the mission was performed. First the mission was analyzed by looking into different disaster types and occurrences. Second, the mission was specified by the use of a weighted trade-off method. Third, the different aircraft choices were analyzed and finally one aircraft type was chosen to be implemented in the Flying Hospital concept.
At the day of the internal deadline of the mid-term report the group had its first meeting with the Red Cross that functions as the main stakeholder in this project. This was due to the unavailability of the stakeholder in the first phase of the project. The stakeholder requested major changes in the configuration of the conceptual design. The requirements shifted towards the focus on low operational cost, minimal maintenance and docking cost. Additionally the lead time should not exceed 3 years and the retrofitted aircraft should be able to perform STOL maneuvers. Also, the stakeholder requested that the Flying Hospital should arrive in the disaster area 24 hours, at the latest, after the disaster stroke it also should provide help immediately and on the spot. An overview of all the requirements and a check whether the system meets the requirements can be found in Section 4.3.

1.1.1 Mission

This concept mission is a recommendation that can be scaled up and down so that either more patients can be treated, or less money is spent. The more aircraft there are, the broader the spread could be, the smaller the reaction time would be, so the Flying Hospital can provide help more quickly. Additionally the capacity of the Flying Hospital system would increase when using more aircraft. When scaling down the mission, it would rather fit for smaller disasters and save money. In the following the new mission will be described.

The global deployment strategy stayed to be multi based, but the location of the operational bases was updated. The operational bases of the Flying Hospital will be positioned in Panama, Las Palmas, Dubai and Kuala Lumpur [3]. These cities were chosen because the Red Cross already has logistic centers placed there. Therefore the Flying Hospital does not need to build up its own logistic network but can profit from the existing one. Furthermore these spots were chosen to make sure that every disaster area can be reached within 24 hours. At each operational base a regional unit is placed; this is the base from where the supplies will be carried to the major airport. At the mission base, the Global Peace Partners are carrying out their work. The Global Peace Partners have a Boeing 747 which is equipped with an operating room, pre- and post-operational support and the ability to airlift out severely injured patients. If there are patients in the disaster area that cannot be helped by the Flying Hospital but can be helped by the Global Peace Partners the patients will be evacuated to them. An overview of the mission can be found in Figure 1.1.

The Red Cross did not want to finance the three aircraft proposed in the mid-term report [2], so now one aircraft configuration was chosen. This aircraft will have the purpose of carrying the Hospitainer to the disaster area and shuttle between the mission base and the disaster area to provide the field hospital with supplies. Additionally patients with serious injuries can be evacuated to the mission base where the Global Peace Partners are performing their work. Therefore the patients need to be stabilized during flight; removable foldable stretchers with medical equipment needed for stabilization and chairs will be placed in the aircraft. On the way from the mission base to

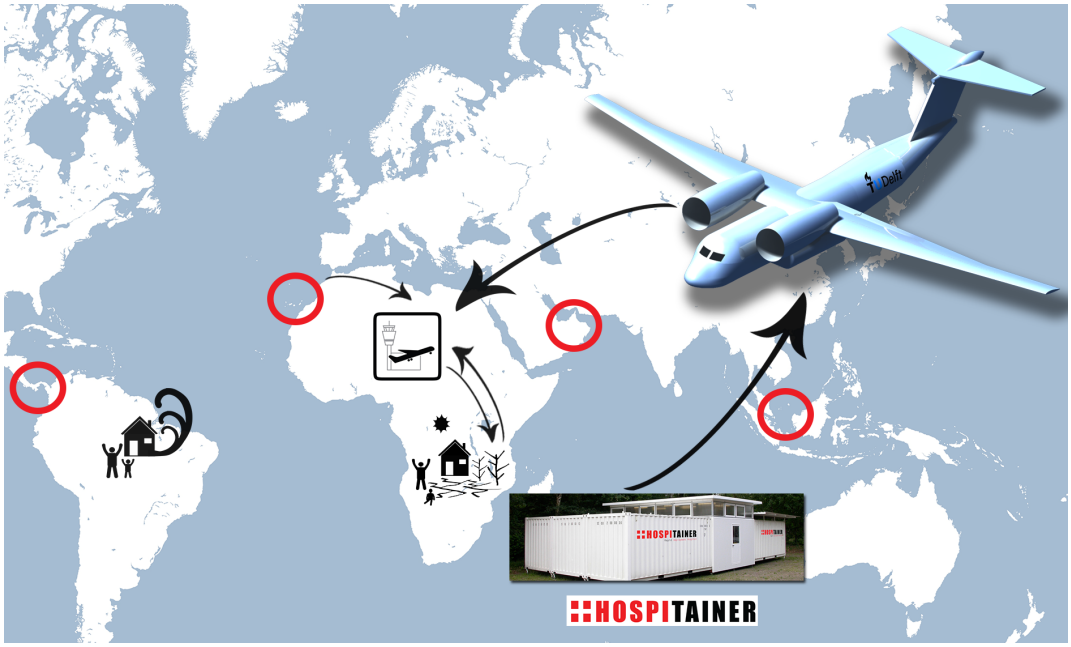

Figure 1.1: Mission overview

the disaster area, the aircraft will bring supplies so that the field hospital can operate for the required one week or longer. So the Antonov An-74 aircraft will be a cargo aircraft that can transport the Hospitainer container to the disaster area and can be equipped with removable foldable stretchers and chairs. The aircraft can be stored in a place where it is close to the area where most disasters occur but can be stored cheap. Since 39% of the disasters occur in Asia and the Pacific [2] it would be beneficial to store it within this area, but in a certain part which is not directly prone to disasters. The aircraft is not positioned within that area because it would be too risky to lose the aircraft due to a disaster. However the aircraft also needs maintenance during its storage so the aircraft has to be stored in a spot where maintenance is possible. Another option would be to lease the aircraft to a company which needs a cargo aircraft with STOL capabilities for the time the Flying Hospital is not needed. In this situation money can be earned that can be used to finance the following mission.

Since the fleet configuration changed the hospital deployment had to change as well. The new hospital deployment will be a field hospital outside the aircraft. The Hospitainer container contains a surgery room so they can be implemented in the field hospital to perform surgeries. This is beneficial because it combines the possibilities of high capacity of the field hospital and the possibility of regulating the environment of the container for surgery. The Hospitainer needs to be sterile and the temperature needs to be controllable, so that a surgery can be performed successfully. If the Hospitainer is not used the container can operate in an area where no hospital is within reach. In the surgery room patients can be treated that would not get medical treatment because their family cannot pay for it or they are not able to reach the hospital which is nearest by. If more funding is needed the hospital can also operate as a regular hospital, so that profit can be made. Furthermore it is possible that the PAV EMS Vehicle collaborates with the Flying Hospital. It will be implemented in the mission in such a way that it is responsible for evacuating injured patients from inaccessible areas. So the field hospital will be the base of the PAV EMS Vehicle and it would penetrate deeper into the disaster area to bring patients to the hospital that could not reach it otherwise.

To conclude, the new mission consists of an Antonov An-74 that is able to carry the Hospitainer. When the Flying Hospital is not needed the aircraft is stored at a place where the fees are low and it is close to possible disaster areas. The Hospitainer is placed where no regular hospital is available so that it can provide surgery where it is required. There will be one mission base at a major airport close to the disaster area where the Global Peace Partners will provide medical help. The supplies that are stored at the four operational bases get flown to the mission base, from where the Antonov An-74 can bring the supplies to the disaster area. At the disaster area the Hospitainer will be the surgery room and a field hospital is placed for medical help. Additionally, the Flying Hospital could be supported by the PAV EMS Vehicle that penetrates deeper into the disaster area so that patients can be helped that cannot reach the hospital. The collaboration with the Global Peace Partners and PAV EMS Vehicle accom-

plishes a seamless connectivity between all parts the Flying Hospital system. This Flying Hospital system results in a resilient medical relief environment. A detailed overview of the operations and logistics can be found in Section 4.1.

1.1.2 Aircraft

To select the best suitable aircraft for the mission, first several Strawman concepts were developed from which the non-feasible options were eliminated. Following from that, the three most feasible options were analyzed in more detail. These are namely the conventional STOL airplane, the conventional helicopter and the gyrocopter. Within the conventional STOL airplane analysis several different aircraft types were taken into account from which the Antonov An-74 was picked. This aircraft was chosen because it had the highest payload capacity with respect to its range. Furthermore it was able to takeoff and land within 350 m with 3500 kg of payload even before modification procedures. For the conventional helicopter the same procedure was applied and the MIL Mi-26 was chosen to be the best suitable helicopter for the mission. This is due to the fact that the payload capacity and the range of the MIL MI-26 are high compared to the other possibilities. Moreover there was no existing large gyrocopter that was suitable for the mission so a non-engine driven rotor was placed on a conventional aircraft. The aircraft which is most suitable for the gyrocopter retrofitting was the C130-H. It was chosen because it is able to carry high payloads and it is highly available. Additionally the aircraft is modular which is beneficial for implementing changes.

Next, the three different aircraft types were investigated individually into more refined detail to be applied for the eventual trade-off process. Therefore the weighting of the trade-off criteria were determined. Then one concept was selected using the trade-off criteria. The gyrocopter possibility scores highest during the trade-off, but the development risks are so high that the gyrocopter had to be disqualified. Similarly the helicopter requires significant higher maintenance hours per flight hour than the conventional STOL aircraft, so the helicopter scores a no-go value for maintenance. Therefore the conventional STOL airplane is the most suitable aircraft for the mission. With the Antonov An-74 the Flying Hospital is able to reach the disaster area within 24 hours and with internal dimension of 10.50 m (l) x 2.15 m (w) x 2.20 m (h) it is big enough to carry the required payload. Additionally its range is 3200 km with 1500 kg payload and maximum fuel [4] which is more than sufficient for the mission. If the aircraft is loaded with more payload, the range will decrease. The cost of this aircraft is relatively low with $4,000,000 [5] per aircraft because the aircraft is highly available. Also, the maintenance of the aircraft is in the allowable range. The aircraft is built for arctic missions, which is the reason why its maintenance is held low.

To achieve this mission and aircraft choice within the resources required project planning was performed in the conceptual design. Also, the system was analyzed with respect to communication, return on investment and sustainable development. Based on these choices the detailed design is performed in this present report.
Table 1.1 shows the specifications of the original Antonov An-74-200 aircraft. These are the values for the aircraft before the retrofits applied in this project.

Table 1.1: Antonov An-74-200 Specifications

Property	**Value**	**Unit**
Max. Payload	10,000	[kg]
Max. Fuel Weight	13,200	[kg]
Empty Weight	19,050	[kg]
MTOW	36,500	[kg]
Range (Max. Fuel, 1.5 ton payload)	3200	[km]
Approach Speed	180	[km·h^{-1}]
Maximum Speed	700	[km·h^{-1}]
Cruise Speed	600	[km·h^{-1}]
Ceiling	11,800	[m]
Takeoff distance (TOW = 28 ton)	515	[m]
Landing distance (LW = 28 ton)	514	[m]

1.2 Functional Analysis

In the Baseline Report [6], a functional analysis was performed. In this analysis, the ground operations (i.e. providing climate control in the hospital, check medicine inventory, perform medical activities, ...) were also seen as part of the system.

Of course, the aforementioned operations remain part of the mission. However, from this point in the design stage onward, these are not further examined. Due to the modularity of the containers, which can be (un)loaded with the appropriate equipment; the clients have to decide the equipment needed and what equipment is taken into the disaster area. Since it varies significantly from disaster to disaster, it is better to leave this part of the mission to the experts on this aspect and focus on the flying performance aspect.

The system that is being examined now focuses on the flying aspect of the mission. The functional breakdown structure, as well as the functional flow diagram, are shown in Figure 1.2 and Figure 1.3 respectively.

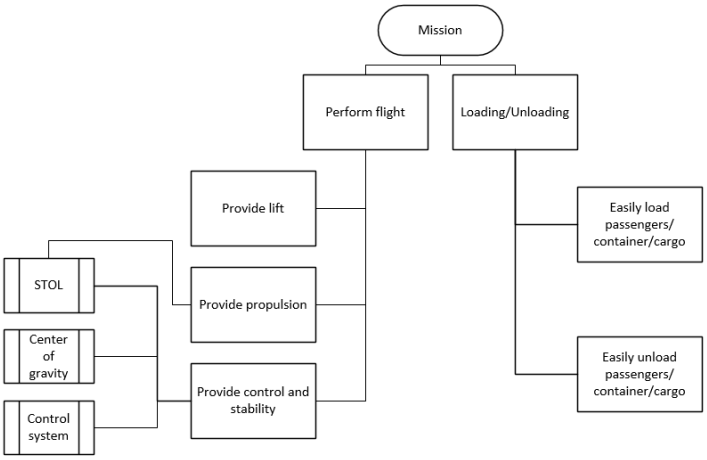

Figure 1.2: Functional Breakdown Structure

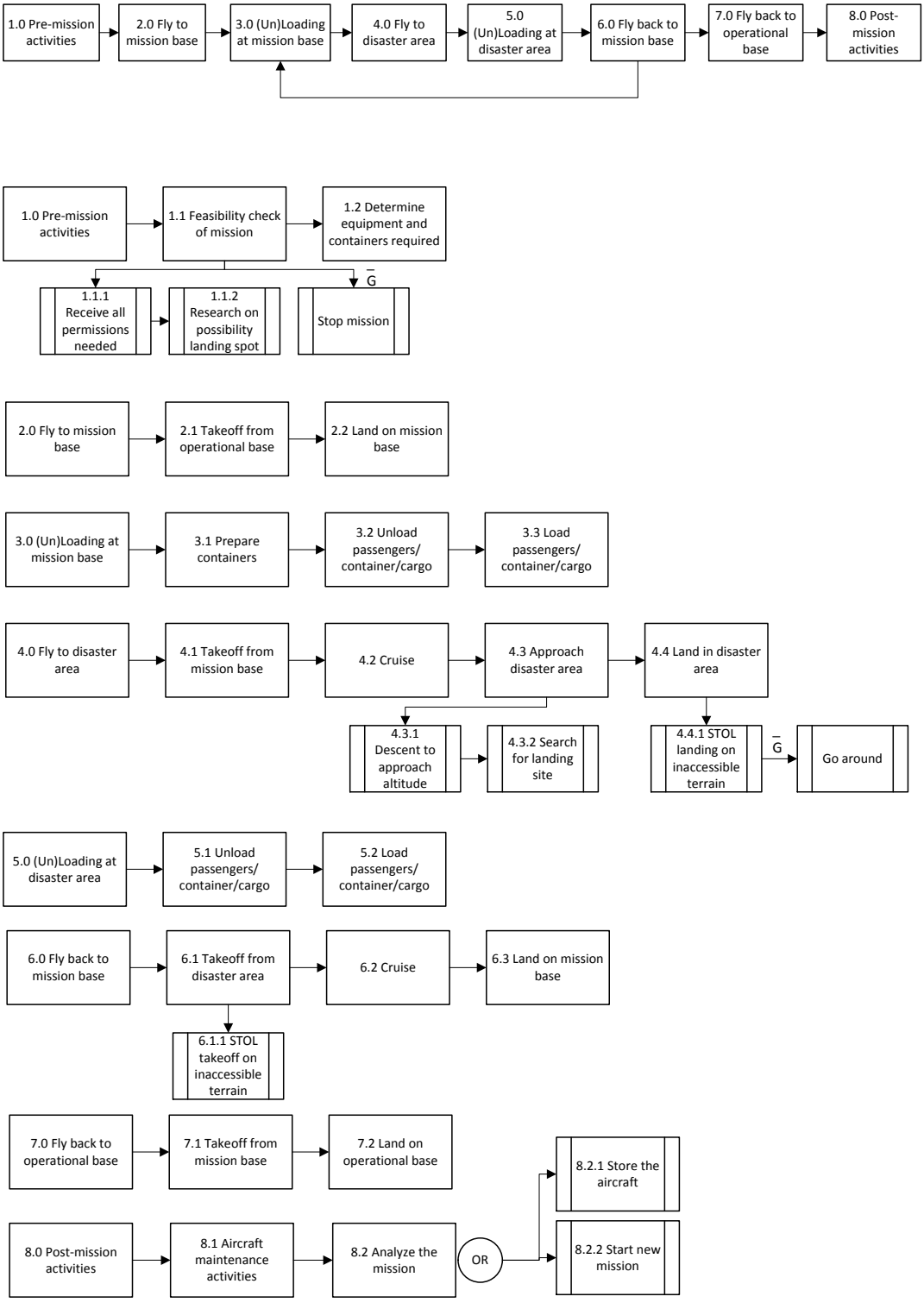

Figure 1.3: Functional Flow Diagram

1.3 Selection of Technical Modifications

In the mid-term report [2], the Antonov An-74 has been selected as the aircraft to be developed further. Several possibilities to improve the performance had been proposed. Furthermore, after the mid-term review, the main stakeholders requested to improve its takeoff and landing performance by reducing the runway length required. This would increase the number of missions in which the aircraft can be used to provide help; the shorter it can land and takeoff, the more often the aircraft is a useful tool to help during missions.

The design team has decided to focus on improving the STOL performance and worked out several means for doing this. These will be proposed in this section. A schematic is shown in Figure 1.4. It should be mentioned that, after a preliminary investigation, some options will not contribute significantly to the STOL performance, and will therefore not be further examined. However, as they may improve the general performance, the team advices to further investigate these in a later design phase.

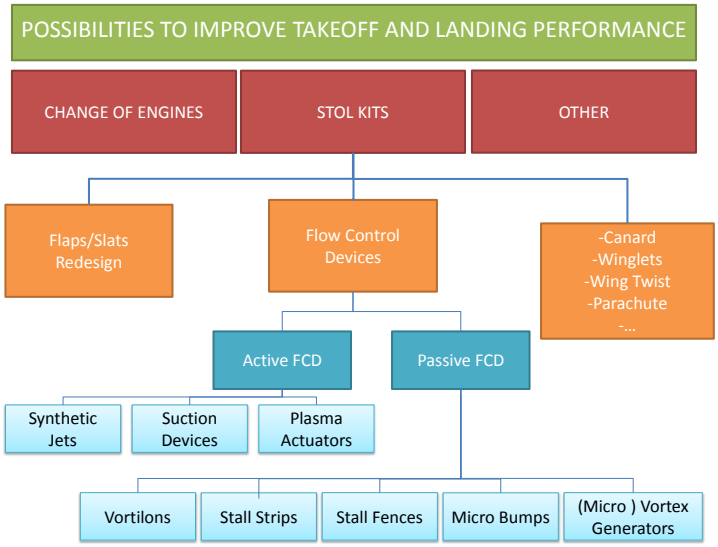

Figure 1.4: Diagram of possible technical modifications

1.3.1 Change of Engines

One of the most common upgrades to aircraft is the replacement of the engines. By changing the existing engines to alternative powerplants, an operator can directly improve the performance of the aircraft and tune operational characteristics such as emissions, fuel consumption and maintenance to those most suitable to the operator's policies. The Antonov An-74 is unique in terms of being a STOL aircraft powered by turbofans, enabling higher cruise speeds when compared to propeller configurations. In order to preserve this advantage and ensure design cruise conditions, only turbofan engines were considered.

Flight, takeoff and landing performance can be directly augmented by the additional thrust or lighter masses offered by alternative powerplants. Both increased thrust and lighter engine mass bolster aircraft performance by the same principle: increasing the net attainable acceleration. Acceleration is important for STOL takeoffs as the distance required is proportional to the thrust to weight ratio of the aircraft. Similarly the climb rate can also be improved. Landing, however, only benefits from lighter engines as stall speeds decrease with lower vehicle weight. Technically, higher thrust engines can provide greater thrust reversal to shorten landings but such mechanisms are not permitted during certification. Furthermore, in light of rough terrain landings, thrust reversal can generate considerable debris in front of the aircraft, increasing the risk of ingestion and foreign object damage. Specific to the Antonov An-74 is the engine relation to wing lift: the turbofans are placed above the wings thus their exhaust generates additional lift (upper surface blowing). Newer engines could exploit this effect even more and further improve takeoff and landing [7].

Operational characteristics of alternative powerplants are most prominent during the prolonged flight stages of the aircraft's operation. For a given weight, additional thrust is of little application for an aircraft during cruise, but reduced fuel consumption and emissions translate to lower operational costs and fainter environmental footprints with a greater flight range. Additionally, modernized engines tend to progressively emphasize lower maintenance requirements; translating to lower maintenance costs and higher operational readiness. Hence newer engines, even of the same power rating as those replaced, may still be an attractive option for an operator in the long run.

While engine upgrades are relatively common retrofits, such modifications are not without drawbacks. The acquisition costs of a new or even used engine are considerable. In addition to the acquisition costs are the integration costs; varying dimensions, thrusts and weights potentially mean structural considerations such as pylon redesign while system integration means ensuring compatibility with fuel, control and avionic subsystems. Flight performance considerations must also be taken into account; varying engine masses and locations can affect flight stability and must be accounted for. Extensive integrations, beyond increased development costs, mean longer development and certification times [8]. The scale of such considerations is highly dependent on the chosen engine, and ultimately the desirability of an engine upgrade is a trade-off between the performance improvement and the integration/cost constraints. Higher thrust engines can substantially improve takeoff performance and lift from upper surface blowing, but will incur more integration difficulties. Meanwhile lighter, modernized engines equivalent in power rating to the existing engines will decrease operational costs, improve STOL by decreasing weight and be easier to integrate albeit at the forfeit of upper surface blowing improvements.

Since the engine can have such a significant impact on the aircraft's performance, this retrofit possibility will be investigated further in Chapter 2.

1.3.2 Flaps/Slats Redesign

One of the most effective options to increase landing and takeoff performance is by using leading edge and trailing edge (respectively, LE and TE) high lift devices. They are standard devices on almost any aircraft.

The main principle behind flaps is to temporarily increase the camber of the airfoil in order to increase lift for a certain angle of attack α; this also causes a drag increase. Since the flaps can be retracted, the drag increase is only when flaps are extracted. Basic flap configurations (plain flap, split flap, single-slotted flap) only increase the camber of the airfoil. More advanced and complex flap systems (Fowler type: double-slotted flaps, triple-slotted flaps) are more efficient, since they both increase wing surface and camber. [9]

In case of simple flap systems where the wing surface is not increased, the slope of the lift curve for the flaps is equal to the slope of the lift curve for the clean wing; $C_{L_{\alpha,flapped}} = C_{L_{\alpha,clean}}$. When wing surface is increased, $C_{L_{\alpha,flapped}} > C_{L_{\alpha,clean}}$. The effect of both types can be seen in Figure 1.5 (a). It is clear that the $C_L - \alpha$ curve shifts to the left for the flapped situation. For takeoff and landing, this is particularly useful since a higher lift coefficient is obtained for smaller α. [9]

The effect of LE devices can be observed from Figure 1.5 (b). In case only LE devices would be added (and thus no flaps), they are of little use. High lift coefficients can only be obtained at large values for α. However, in combination with TE devices, they have proven to be useful. As seen in Figure 1.5 (a), the flapped curve shifts to the left, thereby decreasing α at which $C_{L_{max}}$ is achieved. By adding LE devices, the flapped curve gets an extension, thereby again increasing α corresponding to $C_{L_{max}}$. TE devices increase the risk of separation already at the LE by lowering the stagnation point and creating strong adverse pressure fields on the wing section. By adding LE devices, the boundary layer is fixed to the wing from the LE onwards. [9].

The original aircraft (Antonov An-74) itself is already equipped with large, multi-slotted flaps. Inboard and outboard, there are double-slotted and triple-slotted flaps respectively [10]. Furthermore, slats cover almost the entire LE. In order to improve takeoff and landing performance, one could best replace the 'old' flaps by modern and more efficient triple-slotted flaps all-over the TE, and replace the 'old' slats by modern versions .

Replacing the flaps and slats may thus be a very efficient solution. However, there are several disadvantages related to this option.
Firstly, information concerning the original aircraft is scarce. The airfoil, as well as the exact type of flaps and slats, is unknown. One could argue that modern flaps and slats are more efficient than the original devices. However, the

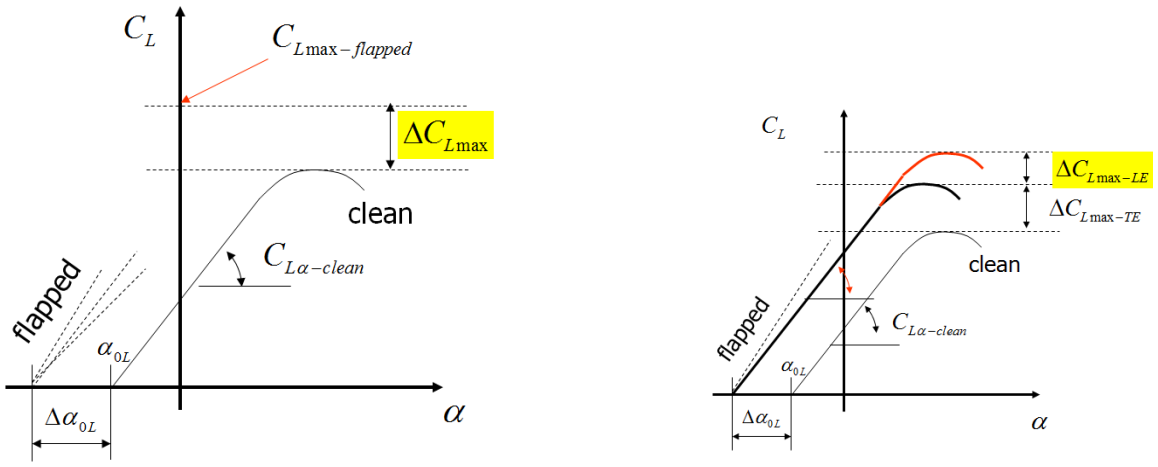

(a) Flaps addition (b) Slat addition

Figure 1.5: Effect of flaps and slats on performance

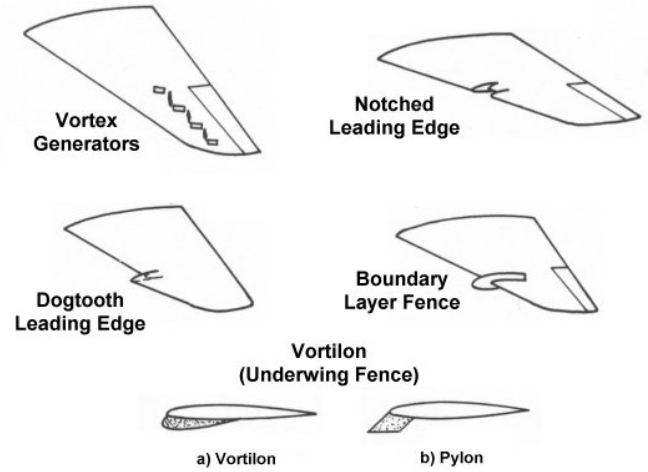

Figure 1.6: Passive Flow Control Devices

extent to which the new devices would increase performance is thus hard to determine. Furthermore,the Antonov An-74 was first build early 1980's. The extent to which new flaps and slats increase performance is thought to be rather limited.
Secondly, redesign of flaps and slats is costly. In case of triple-slotted flaps, the complete wing will need to be redesigned in order to ensure the flaps can be retracted properly. Furthermore, flaps and slats are expensive devices. Development costs are high as well since triple-slotted flaps are complex systems.
Using both arguments, the redesign of flaps and slats is not considered as a feasible option. Possibly, redesign of the complete wing is necessary, leading to high costs. Furthermore, due to limited availability of information, it is unclear as to what extent the performance will increase.

1.3.3 Passive Flow Control Devices

Airflow management devices are common on aircraft. Next to the active flow control category, the passive wing vortex devices are commonly applied. These can be subdivided in several sub-categories (Figure 1.6), of which the most important will be considered. [11]

The purpose of wing vortex devices is to create vortices in a predictable and controlled manner. The airflow experiences an increase in its forward momentum. Often, vortices are unwanted because they generate drag. However, they can be important in order to delay flow separation and thus wing stall. [11]

Stall Strips

A stall strip is a triangular strip mounted to the leading edge of the wing near the root. The purpose of the strip is to actually cause stall. This sounds counter-intuitive but there's a logical explanation. When occurring on the outboard part of the wing, stall can cause a sudden lift drop which is very undesirable. By using stall strips stall is induced gradually, starting at the root and therefore the stall situation is more controllable. The stall strips function as a subtle warning before stall occurs. [12] This could be useful for some aircraft, also for the Flying Hospital in order to increase safety. However, it does not increase the STOL performance, and will not be considered further throughout the rest of the report.

Stall Fences

Stall fences are vertical thin plates mounted on the wing parallel to the fuselage, as can be seen in Figure 1.6. There are different views as to how a stall fence works and what they do. The inventor of the stall fence, Wolfgang Liebe [13], claimed that the cross flow caused stall and that by blocking this flow the wing tip would be prevented from stall.

According to Kate Bernard [14] the fences increase controllability during low speeds by preventing the boundary layer from drifting towards the wing tips. Especially on swept wings, this boundary layer thickens towards the wing tip causing separation at the ailerons and decreasing controllability. Due to the fences the spanwise extension of the boundary layer is blocked.
Another possibility is given by Karl Nickels [15]. He explains that at the inboard of the fence the $C_{L_{max}}$ is increased while on the outboard the $C_{L_{max}}$ is decreased. This is favourable for the stall characteristics of the wing tip. It means that the aircraft can fly under a higher α without stall occurring.
The final function of the stall fence is to create a vortex to delay flow separation. The vortex is formed on the inboard side of the fence and transfers energy from the free stream to the boundary layer so that it sticks to the airfoil longer.

The real effect of the stall fence is probably a combination of all the above. It will definitely have some effect on the stall characteristics of the wing and therefore reduce the stall speed. This allows for a lower approach speed. The only disadvantage of the stall fence is that it creates a significant amount of drag because it is relatively large. Stall fences on modern aircraft are replaced by smaller vortex generators to decrease drag. Mainly due to this reason, this option will not be further considered throughout the report.

Vortilons

Vortilons are a specific type of vortex generators. It serves the same purpose as stall fences, but vortilons are located below the wing and thus make vortices on the underside of the wing. Depending on the design of the vortilon, there may also be a second vortex that can travel around the leading edge and over the wing upper surface. [11]

Vortilons are aerodynamic devices, fixed to the wing leading edge, generating vortices. Their purpose is to generate a high-energy vortex, thereby energizing the airflow over the wing. In regular operations, the airflow flows streamwise over the wing. During stall, the airflow will quickly transit to a spanwise flow, causing a rapid decrease in wing lift. By adding vortilons and inducing a vortex wake, this transition phase from chordwise to spanwise flow can be delayed; furthermore, the vortex energy can keep the airflow attached to the surface of the wing, even at high angles of attack. This also helps retaining aileron effectiveness, even if the wing root area is stalling. [16]

It is true that vortilons generate strong vortices, which would imply a drag increase. This drag increase is limited, and the increased manoeuvrability at low speeds will provide a safer aircraft. Furthermore, the drag at high speeds is lower than that for the stall fences. [11, 16]

Since these devices generate relatively large drag when compared with other devices that will be considered, it will not be considered further in this report.

Micro Bumps

Using micro bumps is an option for passive flow control devices. Micro bumps can be used as vortex generators by implementing small bumps in the surface of the wing. This option for passive flow control was not chosen because it generates extra drag over the wing. This would reduce the effect of the thrust so that improvement in takeoff

distance is not possible. Additionally the bumps did not show significant improvement in flow control experimentally because it does not produce enough vortex strength [17]. This eliminates micro bumps as a modification possibility for the vortex generator selection.

(Micro) Vortex Generators on Wing/Flaps

(Micro) Vortex Generators are devices placed on the wing/flaps. They are placed a certain distance ahead of the separation point, in order to re-energize the boundary layer. The separation point will then be delayed, or even removed. The aircraft can fly slower, at high α, without separation occurring. The stall speed will thus be decreased, hence the touch-down speed as well; the aircraft will need less runway distance.

Conventional vortex generators generate a relatively large amount of drag. When placed on the wing, they are exposed to the flow permanently. Micro vortex generators are smaller, hence generating less drag. They can be as effective as the conventional devices.

(Micro) Vortex Generators can be an efficient way in order to reduce the runway length required. Therefore, they will be considered further in Chapter 2.

1.3.4 Active Flow Control Devices

Active flow control devices are devices that need energy to generate vortices. These delay the detachment of the flow in order to avoid separation. It can be classified in three different categories, namely synthetic jets, suction devices and plasma actuators.

All these different active flow-control devices require extra energy for their use. Synthetic jets are produced by 'movement of a diaphragm inside a cavity' [18], whereas suction devices need a pump to be able to suck the flow. Plasma actuators need a high voltage device to produce the plasma needed for flow control. Because of this reason, active flow-control devices were eliminated from the modification choices. Installing a device that produces the required energy would make the system more complex and more maintenance intensive.

Synthetic Jets

Synthetic jets act as vortex generators; small holes in the wing exhaust jets of air, thereby re-energizing the boundary layer. The flow is first ejected through the hole and then sucked back in so that the net mass flux equals zero [19].

Suction Devices

Suction devices used for active flow-control suck the air locally from the specific hole on the wing. This way, part of the flow is removed but it creates a downward force so that the detachment of the flow is delayed [20].

Plasma Actuators

A plasma actuator is a device that uses high voltages to produce low-temperature plasma. The plasma ionizes the surrounding air molecules, which in turn accelerates them through the electric field. Collisions between the accelerated ions and neutral particles cause a shift in momentum of the flow creating an overall body force. At high angles of attack this body force ensures that the flow stays attached longer [21].

1.3.5 Canard

A canard is a small lifting surface located near the nose of the aircraft. The function of a canard is to provide extra lift and overall stability while causing less induced drag. There is some doubt on the effectiveness of the canard in order to improve the STOL performance. Pro's of the canard compared to conventional configuration are [22–24]:

- Carry 20 to 25% of the total aircraft weight, thus wings can be smaller
- Preventing stall of the wing

- In case of unstable aircraft, the canard has a high $C_{L_{max}}$ and drag advantage
- The canard shifts the center of gravity forward, and thereby increases the stability margin

There are also some drawbacks:

- The 3rd lift surface causes extra drag
- $C_{L_{max}}$ of the main wing must be limited to prevent main wing stall
- The nose down pitching moment created by the flaps cause the canard to stall at high speed
- Reduction of the overall lift due to inboard downwash caused by the canard
- The distance between the aircraft's c.g. and the vertical tailplane is small when using a canard. The aircraft thus requires a large tailplane

Nevertheless, the canard could be useful to prevent stall. The canard stalls first and loses lift, thereby creating a nose down moment and resultantly a lower angle of attack.
A concept that mitigates some of the disadvantages is the stall recovery shield [25]. It is a retractable device that is located at the nose, where it acts as a retractable canard, and at the tail end of the fuselage. The fact that the device is retractable brings advantages to stability and drag because the surfaces are not fixed. The shields will be deployed using computer software.
The canard will not be used for the Flying Hospital in this design phase, because of its many disadvantages. The contribution of the canard will not be significant to the STOL capabilities. For the design modification, focus is to increase the STOL performance; since there are more efficient options than the canard to improve STOL performance, it will not be further investigated in this report. However, the addition of a canard or recovery shield can provide a significant increase in safety; it is advised to further investigate this option in a subsequent design phase of the Flying Hospital.

1.3.6 Winglets

Winglets are small lifting surfaces mounted to the wing tips. The main purpose of winglets is to reduce the induced drag. The definition of induced drag has been explained in Anderson [26]. As can be seen in Figure 1.7, the resultant of the lift force is not in the vertical direction. The vortices at the tip create a velocity component downwards. Due to this downwash the resultant of the lift force is tilted backwards. The horizontal component that has been created due to the α_i is called "induced drag". According to Boeing [27] their blended winglet spreads the tip vortices along the trailing edge of the wing and thereby creates a sidewash velocity which leads to a resultant thrust force that reduces the induced drag.

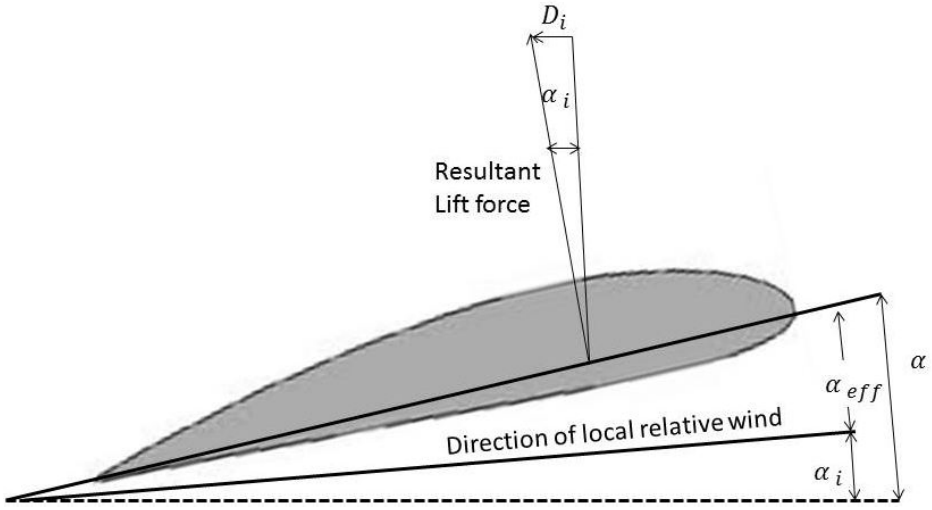

Figure 1.7: Induced Drag

The downwash effect of vortices on the whole wing is also reduced when the span of the wings is expanded, but this requires a stronger and heavier wing structure. Winglets are a good alternative to spanwise extension of the wing. According to Withcomb [28] the winglets decrease drag by 20% and double the lift over drag ratio compared to simple wing extension. A disadvantage of wing tips is that they tend to flutter. The winglets are not a useful concept to consider further in this design stage; this stage focuses on increasing the STOL performance. As can be seen in Figure 1.8, winglets do not have a significant effect on takeoff and landing for the weight range of the Flying Hospital. For this reason, they will not be considered further in this report. However, as winglets provide certain advantages, it is advised to further investigate this option in a later design stage.

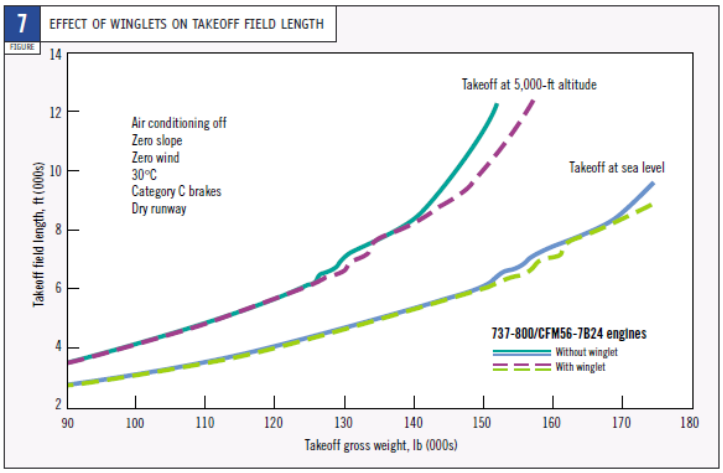

Figure 1.8: Effect of winglets on takeoff and landing [27]

1.3.7 Wing Twist

During aircraft design stages, the choice can be made whether to apply twist or not. It improves the stall characteristics of a certain configuration. By applying twist, one can assure that the inboard section of the wing stalls first. This is due to the fact that the tip is twisted down (Figure 1.9), and the angle of attack at the tip will thus be lower near the tip. If α of the wing increases and approaches stall conditions, the outer board section will experience a relatively low α, hence it will stall later. Stall at the outer part of the wing should be avoided in any case because the ailerons are located here. They are necessary to provide roll control in the event of a stall.

Adding twist to the original aircraft (Antonov An-74) is only possible in case the complete wing will be redesigned. As this is a costly operation, this option will not be considered here. There are more effective and cheaper solutions available for the design problem. Furthermore, due to the limited availability of the Antonov An-74 data, it is unknown whether the wings already have twist or not.

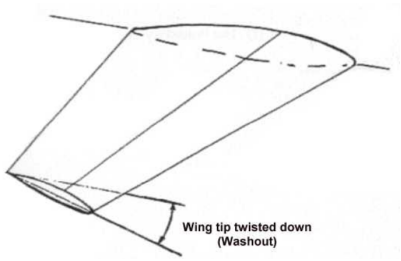

Figure 1.9: Wing twist [29]

1.3.8 Parachute

In 1911 the Italian Giovanni Agusta invented the first drogue parachute [30]. The drogue parachute can be attached at the back of the aircraft to create extra drag during landing. At touchdown the parachute will be shot out of

the chute installation that is usually at the point where the tail is attached to the fuselage. The drogue parachute is developed for rapid deployment at high speed. At relatively high speeds, like the landing speed, a conventional parachute will be torn apart. When rapidly deployed, the parachute will create a significant amount of drag that gives the aircraft an abrupt pull while landing. This way the landing distance can be decreased. Usually drogue parachutes are used for fighter aircraft or on icy landing strips.

Due to this modification, the landing distance of the aircraft can be decreased significantly. However it also comes with disadvantages. Firstly, a parachute is hard to be repacked so that the parachute can be reused. It takes a significant amount of man-hours and a highly developed folding technique to pack the parachute back to its initial size. Some parachutes even need a press to put the chute in the desired shape. If the parachute is not repacked properly then it might have problems with deployment the next time it has a high deployment risk. Secondly, the forces the parachute exerts on the aircraft are very high. It will be hard for an untrained pilot or passengers to withstand. Additionally, the sensitive medical equipment the aircraft needs to carry will most likely be damaged. However this equipment is needed to perform the mission successfully. Thirdly, a common problem with parachutes is that they pick up moisture when being on the ground. When the aircraft is then at high altitude this moisture will freeze which leads to significant problems during deployment. Also, parachutes are prone to maintenance problems.

Due to the large amount of work involved in order to use the parachute, it is not advised to use such a labour-intensive tool in disaster areas. Therefore, this option is not seen as a good solution in disaster areas.

1.3.9 Conclusion on Selection of Technical Modifications

To summarize this section on the selection of modifications it is concluded that:

- Change of engines and the addition of (micro) vortex generators will be further examined in Chapter 2.
- The addition of winglets and a canard can provide a significant improvement to the aircraft's performance, but not the STOL capabilities. Since the team focuses on increasing the STOL performance, these options will not be worked out further in this report. However, the team advises to investigate these options in a later design stage, because they can improve the performance significantly.

1.4 Budget Breakdown

An estimated budget breakdown of the technical budgets is made in this section. These technical budgets have the tendency to grow during the process of development. To account for this tendency a contingency value showing sufficient margin for the remaining development is assessed. Since an already existing Antonov An-74 is chosen, it is important to not cross certain limits. Here the MTOW is the most crucial in maintaining a safe design. Other technical budgets for the Flying Hospital are empty, payload, fuel and maximum takeoff weight, cost and some important performance parameters such as takeoff and landing distance, cruise velocity and range. These values will be derived from the standard Antonov An-74 with additions due to the retrofitting that will be carried out.

1.4.1 Weights

The weight budget breakdown consists of the major components contributing to the maximum takeoff weight. These components are the structural weight, propellant weight and payload weight. Payload weight can be subdivided into the weight of medical equipment, container weight, passengers and supplies like water and food, as can be seen in Table 1.2. Maximum weights are determined by the mission goal. When the aircraft is flying to pick up the hospital containers, range is the dominant factor and it should be covering the maximum range with maximum fuel capacity and no payload. When the hospital containers are loaded, the goal is to fly to the disaster, drop containers and fly back to the mission base. Therefore, only that amount of fuel will be loaded. Furthermore, the driving requirement then becomes speed and STOL performance. Therefore, sufficient fuel for engine high speed configuration needs to be carried without compromising the STOL capabilities. These figures can be found in Table 1.2.

1.4.2 Costs

The budget allocation for different scenarios discussed in the market analysis, Section 3.5, is of utmost importance for a non-profit organization such as the Red Cross. Purchase price or development price is a key factor since the

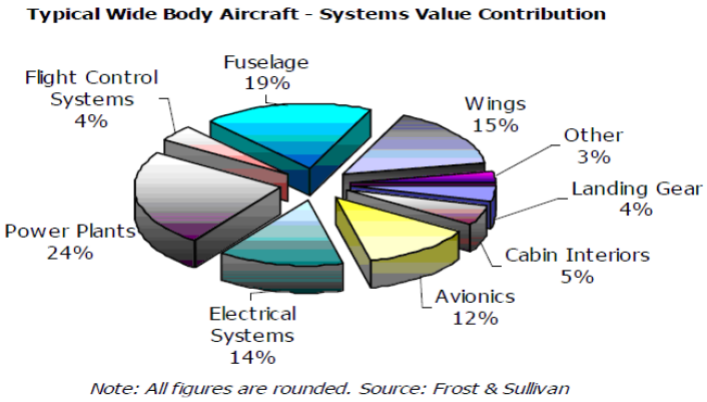

Figure 1.10: Power not used for propulsion distributed over different components [31]

budget of the Red Cross is restricted by donations. Production costs in terms of retrofitting or reconfiguring depend greatly on the design chosen. The amount of missions, depending on disasters, is of impact on the ground time and therefore on the service, fees and maintenance costs. After a financial budget by the Red Cross is defined, further budget allocation can be worked out. For now the advice is to keep costs to a minimum. Looking at the three different possible design scenarios for the budget allocation, the costs can vary from small to very large depending on the size and VTOL/STOL capabilities of the aircraft. The costs in Table 1.2 are calculated using the Aircraft Operating Cost Calculator [32].

1.4.3 Performance

Performance is largely depending on the mission requirements. Range, maximum speed, cruise speed, stall speed and takeoff/landing area are to be given estimated values in the budget allocation, since they are critical factors regarding the aircraft objective. In lesser degree of direct mission importance are aircraft ceiling and fuel consumption. Range is important in terms of minimum range since the aircraft has to reach remote parts of the world from a major airport in the vicinity. As can be seen from Table 1.2, range depends on the flight mission objective. Flights from the base to hospital destination and back require large range and almost no payload, therefore maximum range is the main goal. Flights from the disaster zone to the mission base is dependent on the availability of landing strip possibilities and aircraft speed. During emergency, getting to the disaster zone and back as quick as possible prevails. However, if there is very limited landing strip available, then the STOL capabilities become dominant and the aircraft performance should be optimized around that point. In general, a larger range, smaller takeoff- and landing distance will imply less total weight. The ratio of the fuel to cargo weight depends strongly on the mission objective and the surrounding environment.

For completeness, also the properties of the modified aircraft are provided in Table 1.2. These values were derived in Section 2.7.

1.4.4 Contingency Management

For the contingency management the Technical Performance Measurement procedure is used. The TPM method is an useful tool to account for contingencies. Since this project involves an already existing off-the-shelf product, contingencies can be limited to the retrofitted parts. The most important aspect, regarding the mission, are the STOL and payload capabilities. These are changed by retrofitting the aircraft. For the contingencies this means that the landing distance, takeoff distance, range and maximum payload are important. Since the landing and takeoff performance are to be optimized as much as possible, the weight is left the most applicable for contingency management. The minimum requirement for the mission was set to be 800 km [6]. This requirement is definitely reached, making contingency management unnecessary. In order to maintain structural functionality and survive certification procedure, the MTOW should not exceed the MTOW of the existing aircraft. The contingency percentage for the weight will therefore be extremely small. The weight is increased by approximately 472 kg when two other engines are used. Also the vortex generators contribute to the weight with 470 g. In order to compensate

Table 1.2: Weight, cost and performance budget allocation

Property/Aircraft	Antonov An-74-200	Antonov An-74 Flying Hospital
Max Payload [kg]	10,000	10,000
Staff [kg]	150	150
Crew [kg]	225	225
Containers [kg]	0	4370
Medical equipment [kg]	0	600
Max Fuel [kg]	13,200	13,200
Empty Weight [kg]	19,050	19,522
MTOW [kg]	36,500	36,500
Purchase price [€]	4,000,000	4,000,000
Retrofitting costs [€]	0	25,000,000
Range (Max. Fuel, 1.5 ton payload) [km]	3265	2908
Max speed [km·h^{-1}]	700	700
Approach speed [km·h^{-1}]	180	167
Cruise speed [km·h^{-1}]	600	600
Ceiling [m]	11,800	11,000
Takeoff distance (TOW = 28 ton) [m]	515	278
Landing distance (LW = 28 ton) with no reverse thrust [m]	514	456
Fuel consumption TO [g·(kN·s)$^{-1}$]	10.20	11.22

for the aforementioned changes, the maximum fuel weight, or the payload has to be reduced by 473 kg in order to maintain the MTOW.

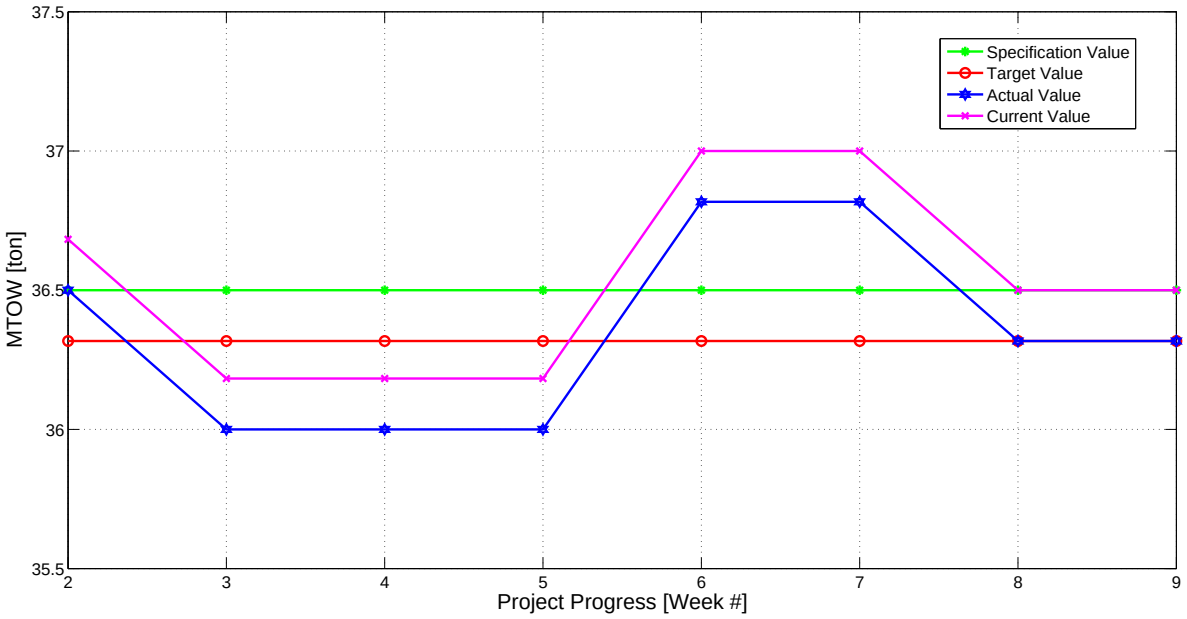

Figure 1.11: TPM method for the MTOW

Translated to the TPM procedure four values are needed: Specification, target, actual and current value. The values can be found in Figure 1.11. Here the MTOW is displayed next to the weeks of the project duration. The contingency value is very small, as discussed, and will have a value of 0.5%. The specification value will be the original Antonov MTOW plus the contingency value. The target value will be the original MTOW. The actual value specifies the actual MTOW at any moment in the design phase and is without contingency. The current value equals the actual value plus the contingency. From Figure 1.11, it can be seen that there is a slight increase in weight in week 6. This is due to the increase in weight of the new engines and vortex generators. In the final phase, the weight is reduced by a compensation in fuel. Finally, it is shown that the current value is exactly the same as for the original Antonov, proving the structural abilities are not compromised.

1.5 Risk Analysis

Risk is an uncertain event or condition which is inherent to every project. Risks can have a significant impact on the objectives of the project or mission, both negative and positive. This section describes different potential risks that can occur during the development and operational phase of the mission and Antonov An-74. The probability and impact of the risks on the project is desribed in a so-called risk assessment. From the risks found in the risk assessment a risk map was made. This tool maps all the risks based on the probability of occurrence and the consequence on the performance. Finally a risk mitigation strategy will be explained. Three potential risks are selected that present the most-likely threat to the project and a risk mitigation strategy is developed to reduce the probability of failure and includes actions to be taken in the event of failure. First the risks related to the mission are described and thereafter the risk related to the aircraft.

1.5.1 Mission Risk Assessment

This risk assessment describes the potential risk that can occur during the mission. The potential risks are grouped in technical/performance risk, schedule risk, cost risk and environmental risk.

Technical/Performance Risks

1. Technical malfunction or failure of the aircraft (unlikely - critical)
Any technical malfunction of the aircraft is considered to be critical for the mission. The impact on the mission however depends on the malfunction itself. For example, in case of a malfunction of an engine or one of the control surfaces, it does not necessarily lead to the end of the mission. An aircraft with a malfunctioning control surface is still able to reach a landing site. The probability of a malfunction or failure is unlikely to occur, because the Antonov An-74 aircraft is a robust, existing aircraft with a proven track record.

2. Pilot failure (unlikely - catastrophic)
The aircraft is controlled by the pilots and the ability to reach the disaster area depends on the pilots. A mistake or failure of the pilots will have a catastrophic impact on the mission, because the pilots have a vital role on the mission. However a pilot failure leading to catastrophic consequences is unlikely to occur. The probability can be reduced by selecting pilots based on training and experience.

3. Hazardous landing zone (likely - critical)
After a disaster, national resources are out of order, destroyed or too limited to cope with the size of the event. The aircraft must be able to penetrate into inaccessible terrain without the presence of a paved landing zone. The risks in landing in such hazardous area may result in damage of the landing gear which can have critical impact on the mission completion. Failure of finding a suitable landing zone also compromises the progress of the mission. Since the design is ought to operate in such rough terrain on most of its missions, the risks regarding the landing zone are critical and are most likely to occur.

4. Dimensional Risk (moderate - marginal)
Prior to the mission, it is estimated how many people need to be helped by the Flying Hospital. If this number is underestimated, there will be insufficient supplies to help all the patients requiring medical support. On the other side, an overestimation of the victims would result in additional costs and too much medical personnel and supplies transported to the disaster area. This event may occur as the situation in a disaster area is very hectic, but it has marginal impact on the mission, because medical help can still be provided although not in the most ideal way.

5. Safety of staff and supplies during the mission (unlikely - critical)
Safety has to be guaranteed for the crew, doctors and supplies during the whole mission. Since this safety involves protection from hazardous environment, from human factors such as rebellion or looting and contamination. This provides for uncontrollable risk in some amount. Therefore safety is a very important aspect and may have a critical influence on the condition of the staff and supplies. However, the Red Cross states in advance to all parties involved that they are neutral in the conflict and will only help all people in need. This way everyone benefits from the presence of the Red Cross and will cause the safety risk due to human factors to decrease. Furthermore, precautions are taken and special equipment is used in the aircraft and field hospital to protect staff and supplies from the hazardous environment or contamination.

Schedule Risk

6. Operational delays (moderate - critical)
Since the aircraft acts in response to a disaster or devastating impact, one of its key factors is to assist in the disaster area as soon as possible. Providing medical support rapidly is a main concern of the mission. Since time is important, delay has to be minimized. Examples of operational delays could be; if separate external parties that are needed to develop the medical relief mission are late and supplies or staff can not get access to the disaster area on time. Other operational delays could occur if the field hospital has problems while setting-up, if equipment does not work correctly or weather conditions prohibit the aircraft to fly. Operational delays may have a critical impact on the performed mission, since rapid departure is important in order to provide rapid medical support. The probability of an operational delay occurrence is moderate, since the operation depends on different external parties.

7. Preparation delays (unlikely - critical)
The aircraft should be able to accommodate all functional equipment necessary for specific categories of disasters. The medical equipment required for the operation depends on the disaster. Preparation delays have to be minimized since time is an important factor. Preparation delays could occur if the medical equipment is hard or time-consuming to get ready on the operation base for a relief mission. Or if resources needed for medical support such as medication, food and drinking water are not available or need to be transported from an external source. A preparation delay will have a critical impact on the mission. However, the probability of a preparation delay is unlikely for the mission because special containers are used that already include the necessary equipment and medical supplies. Extra supplies, food and water are managed on the operation base, which implies that these are easy to assess in case a disaster occurs. Preparation delays can even be reduced by providing training to staff in order to reduce the time needed to install the equipment and manage or distribute supplies.

8. Production errors (moderate - marginal)
Production errors can occur if unforeseen problems arise during the production phase. Production errors will result in a schedule delay during the fabrication process. If unforeseen errors arise during the operating phase this may result in technical or performance errors. Since production errors are likely to arise from the medical equipment, the operation will be able to continue and will only have a marginal impact on the mission. The medical equipment is designed specifically for the mission purpose and will therefore have a moderate likelihood of failure.

Cost Risk

9. Budget related risks (moderate - catastrophic)
Since the Red Cross is a non-profit organization funds are not unlimited. The project depends on funds provided by external parties such a governments and private donations. Sufficient funds are necessary to keep the aircraft operational and to provide medical support. Lack of funds will have a catastrophic impact on the operation to be performed and could even lead to abolition of the project.

Environmental Risk

10. Cultural and political barriers (rare - catastrophic)
The operation will be performed in different areas with different cultural and political situations which can influence the operation. The aircraft needs permission to land from local authorities. If the aircraft does not get permission to land, the aircraft will not be able to operate. Cultural and religious factors can play an important role in the operation in case local community does not want support. In more strict religious countries local communities could only want support from male doctors. These barriers can have significant impact on the operation. However, this is unlikely to occur because the operation is probably the only way to get support for the local people and the only way to get access to food and drinking water.

11. Hazardous disaster area or weather conditions (moderate - critical)
When providing medical relief in a disaster area, the conditions will not be optimal to perform surgery or other medical activities. However, in certain situations the environment limits the amount of activities of the Flying Hospital or even prohibits the mission to be performed. Examples could be an aftershock in case of an earthquake, flooded terrain or just harsh weather conditions in the area between the mission base and the disaster area or at the disaster site itself while the field hospital is in use. These conditions can have significant impact on the mission. The probability of occurrence is moderate as the disaster area in itself already implies that harsh conditions are present.

1.5.2 Mission Risk Map

The risk map is a matrix which is used to rank potential risks. The risks are ranked based on the probability of occurring and the consequence of occurring. The risk map is used to define a risk mitigation strategy to the three risks which present the greatest threat to the mission and where the largest reduction in risk is likely to be obtained. Figure 1.12 shows the risk map for the medical relief mission; the numbers in the risk map contribute to the numbering used for the risk assessment mentioned above.

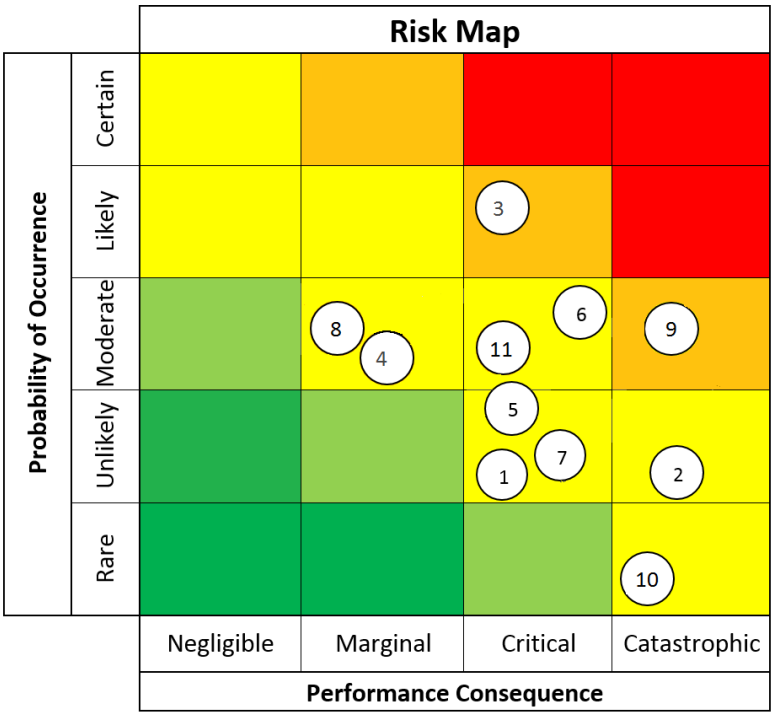

Figure 1.12: Mission risk map with numbers corresponding to the risks identified in Section 1.5.1.

1.5.3 Mission Risk Mitigation

The risk map in Figure 1.12 is used to identify the risks which are important to take into account while setting up a risk mitigation plan. Risks 3, 6 and 9, respectively a hazardous landing zone, operational delays and budget related restrictions, are most prominent on the risk map and will therefore be discussed below in the risk mitigation plan. In order to account for these risks, two options are available: minimize the impact and reduce the likelihood.

3. Hazardous landing risks

The risks regarding a hazardous landing zone can be minimized by the following points. A preventive measure can be manifested by using good area intelligence before beginning the mission. A primary risk is in the landing procedure which is highly dependent on the quality of the landing zone. By knowing on beforehand where to land the risk can be greatly minimized.

In case of failure in finding a suitable landing zone, a contingency plan can be drawn by using a landing gear or landing procedure which is able to land in such hazardous area.

6. Operational delays

Operational delays, actually any type of delays, brings a large risk to the feasibility of the entire mission since it prohibits the Flying Hospital to provide all the medical relief. Operational delays may have a critical impact on the performed mission.

A measure to prevent the risk problems in terms of operational delays can be in the form of safe-life or fail-safe design of the equipment used for the medical relief and one or multiple manuals describing how a mission in case of a specific disaster needs to be performed, how supplies are brought to the disaster site and managed at the field

hospital and how certain equipment needs to be deployed and used. In case of failure of a part of the equipment, back-up systems need to be available right away.

10. Budget related risks
The main stakeholder, the Red Cross, is a non-profit organization so its financial strength is greatly based on funds and (governmental) charity donations. Given this fact the aircraft design has restricted funds. By preventing exorbitantly high costs, contracts can be made with the Antonov An-74 design and production companies.
Contingency plans in this case are very hard and also result in the critical performance consequence. Residual value has to be accounted for so if funds are depleted possibilities in reselling the project are possible.

1.5.4 Aircraft Risk Assessment

This risk assessment describes the potential risks for designing and operating the Antonov An-74 as a Flying Hospital. The potential risks are grouped in technical/performance risk, schedule risk and cost risk.

Technical/Performance Risks

1. Takeoff and landing performance (likely - critical)
The runway and takeoff distance of the Antonov An-74 is dependent on the weight of the aircraft and therefore also on the payload. It can be dangerous to load too much into the aircraft when the area of the landing zone is uncertain. Not being able to land in the designated landing zone increases risk in mission failure and therefore has critical impact. This risk is greatly depending on the technical design in terms of STOL capabilities like robust landing gear and stall speed. Since every mission consist of multiple takeoff and landing maneuvers the probability of occurrence is likely.

2. Technical malfunction or failure of the aircraft (moderate - critical)
Any technical malfunction of the aircraft is considered to be critical. The impact and consequences for the aircraft however depends on the malfunction itself. An aircraft may still complete its flight profile or perform a safe landing if an engine or one of the control surfaces has a failure. The probability of a malfunction or a failure is moderate to occur because the aircraft to be used to perform the mission is an existing retrofitted aircraft and does not have a proven track record and there are uncertainties involved in the retrofitted parts of the aircraft.

3. Retrofitting (unlikely - critical)
Retrofitting the aircraft with for example new engines, slats or other devices will be accompanied by technical risks. Since for the combination of the aircraft with these new devices no track record exists, the risk factor for an aircraft failure when retrofitting is enlarged. Before the retrofitted aircraft is used in operation, it has to go through an extensive testing phase. Failure after the testing phase and certification is unlikely but still can be critical for mission completion.

4. Safety (moderate - critical)
Safety has to be guaranteed for the staff and equipment when flying to the disaster zone. Since this safety involves protection from hazardous environment like weather but also from human factors such as pilot or loading errors, the aircraft has to be fail-safe. Therefore safety is a very important aspect and may have critical influence on the staff's safety risk.

5. Maintenance (unlikely - critical)
Maintenance is an important part to stay airworthy and has a large impact on the safety of the airplane, the crew and the equipment. Insufficient maintenance could result in any technical malfunction or even failure of the aircraft. Furthermore the aircraft could be in maintenance at the moment a disaster strikes and not being able to perform the mission. However this is unlikely the occur, since well-trained and well-experienced maintenance workers are available, also extensive planning can reduce the risk of an airplane in maintenance at the moment a disaster strikes. Risks involved with maintenance will affect the mission and can therefore be considered as critical.

6. Foreign Object Damage (FOD) (unlikely - critical)
Foreign object damage is airplane damage caused by foreign objects such as birds, debris and stones. Foreign objects can seriously damage the aircraft, especially when objects hit critical parts of the airplane. Objects hitting the cockpit or the engines could result in malfunction or even failure of the aircraft. When a disaster strikes it

could be possible that the landing zone is covered with debris and the debris could fly into the engines. Since the Antonov An-74 has engines mounted on top of the aircraft, ground objects are unlikely to hit the engines.

7. Loading of the airplane (unlikely - critical)
The main purpose of the mission is to transport medical equipment and supplies to the disaster area. The aircraft will be loaded with a container fitted with medical equipment. When loading the aircraft one should keep in mind that the center of gravity of the airplane always needs to stay between the nose and main landing gear, otherwise the aircraft will tilt and could get seriously damaged. Furthermore the payload should be strapped in the airplane so that the payload cannot move during flight. Moving payload could result in a crash. Both situations will have a critical impact on the mission. One of the retrofit options applied on the airplane is a loading monitor, which could assist the loading of the airplane and could give information about the position of the center of gravity. The loading monitor reduces the risk of misplaced payload.

8. Weather related risks (moderate - marginal)
Basically there are two risks related to the weather for the airplane. First of all, hot environmental conditions in the disaster area increase the takeoff and landing distance of the airplane. Secondly hot and tropical environmental conditions increase the maintenance required for the aircraft. These risk are considered moderate to occur because these conditions can be taken into account before the mission actually starts and one can anticipate on that by reducing the payload to be carried and therefore the takeoff and landing distance. The impact on the mission is marginal since these risks do not conflict the completion of the mission, as the weather conditions are carefully taken into account beforehand.

Schedule Risks

9. Production/Development time (likely - marginal)
The discussed aircraft is available at the time being. Depending on the amount, type of retrofitting and specialized design, the development- and production time is subject to risk. Since the aircraft has to be redesigned for the Red Cross, this schedule risk is depending on several factors. This is not directly critical for the mission. The retrofitted aircraft requires additional testing to become airworthy. This is likely to result in a longer production and development time depending on the type of retrofitting.

Cost Risks

10. Retrofitting costs (unlikely - critical)
Retrofitting the aircraft can be a large cost risk involving calculations, tests, certification and more retrofitting expenses. The aim of retrofitting an aircraft is to be less cost expensive than designing an aircraft from scratch.

1.5.5 Aircraft Risk Map

Also for the aircraft risk assessment, the risk map will be used to rank potential risks. Thereafter the three most critical risks for the Antonov An-74, which can be reduced with the best results, are identified. Figure 1.13 shows the risk map; the numbers correspond to the numbering used for the risk assessment mentioned above.

1.5.6 Aircraft Risk Mitigation

The risk map diagram in Figure 1.13 is used to identify the risks which are important to take into account while setting up a risk mitigation plan. Risks 1, 2 and 9, respectively the takeoff and landing performance, technical malfunction or failure of the aircraft and production/development time, are most prominent on the risk map and will therefore be discussed below in the risk mitigation plan.

1. Takeoff and landing performance
This aircraft is designed to be used on unprepared surfaces: its robust undercarriage and high-flotation tires allow operations on sand, grass or other unpaved surfaces. More powerful engines are mounted to the airplane, this will reduce the takeoff and landing distance due to the more powerful thrust. Furthermore the airplane can be equipped with a loading monitor, which assists the loading of the airplane and can provide information about the

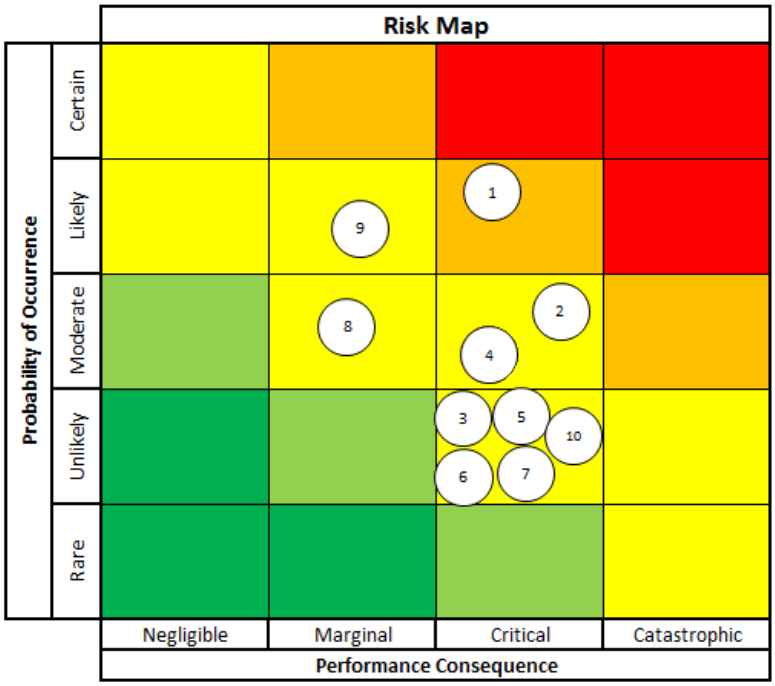

Figure 1.13: Aircraft risk map with numbers corresponding to the risks identified in Section 1.5.4.

position of the center of gravity and the amount of payload on the airplane. Intelligence of the disaster area can provide information about factors which will influence the takeoff and landing performance of the airplane. Hot environments increase the takeoff and landing distance of the airplane; to lower the distance the amount of payload should be reduced. Mitigating this risk will increase safety.

2. Technical malfunction or failure of the aircraft
Any technical malfunction or failure of the aircraft will influence the progress of the mission. To reduce the risk of a malfunction or failure, the aircraft with the retrofitted part should be tested and certified. Testing the aircraft can reveal critical parts and problems in the design arising in this phase of the development and additional improvements can be made before the aircraft starts its life-cycle. Furthermore maintenance needs to be performed to keep the aircraft airworthy and to identify defects on a short note so the defects can be repaired to reduce the risk of a malfunction. Maintenance procedures could assist the maintenance and provide information about the frequency of inspection intervals.

9. Production/Development time
The production and development time is already reduced by redesigning an existing aircraft. The production program has to be scheduled tight so the risks of delays are reduced and uncertainties can be detected and solved in an early stage. Clear production manuals can assist the production of the airplane. Employees with sufficient technical knowledge should be appointed. Furthermore production processes could be performed in parallel to reduce the production time.

1.6 Operational Record of Antonov An-74

The Antonov An-74 is a development of the Antonov An-72 and was designed to be used as polar transport aircraft. The series production of the Antonov An-74 started in 1985 but the first flight of the Antonov took place in 1983 [33]. Ever since there were only 7 accidents of an Antonov An-74 recorded. The first accident happened on September 16^{th} 1991 near Lensk Airport in Russia. The aircraft was overloaded so lost height and crashed just after takeoff. On November 27^{th} 2006 the most tragic occurrence happened. An Antonov 74T-200 crashed during takeoff from Tehran-Mehrabad Airport while performing a military mission. All occupants but one were fatalities of that accident. The last accident occurred on March 30^{th} 2010 in Ivanovo-Severny AB in Russia because of an

engine failure [34].

From the 7 accidents that happened up until now, 5 are hull-loss accidents. So, one can conclude that the aircraft does not crash very often. However, if it crashes chances are that the accident is a hull-loss occurrence. Moreover, from the 7 accidents only 3 of those were fatal. Therefore one can conclude that the aircraft is built reliant and robust. This is needed because the aircraft is built for arctic missions so not everywhere maintenance is possible. The Antonov An-74 has a proven operational record and is a safe as well as reliant aircraft choice.

2 | Detailed Design

In the detailed design chapter, certain technical modifications as proposed in Chapter 1 will be examined. In Section 2.1, engine modifications are described. This leads to changes in the upper surface blowing, which is analyzed further in detail in Section 2.2. Additionally, the effect of adding vortex generators is analysed; for a design overview, see Section 2.3. A deeper investigation and feasibility evaluation of the structural characteristics of the aircraft are carried out in Section 2.4, in order to determine the loads on the structure and to help determined structural implications of the retrofitting options. In Section 2.5, the stability and control aspect is discussed. It considers the appropriate c.g. locations, lay-outs of the different loading possibilities and corresponding mitigation actions to avoid instability as well as its subsequent disastrous consequences. The material characteristics part (Section 2.6) discusses the material aspect of the aircraft and the different design options therein. Finally, the technical performance results of the proposed modifications are summarized in Section 2.7.

2.1 Engine Modifications

In the following section, the engine modification is described. First, the best suitable engine for the mission was chosen. The engine performance is evaluated and the engine improvement is shown followed by a sensitivity study, verification and validation. Finallly, recommendations are given.

2.1.1 Engine Selection

To improve the performance of the Antonov An-74 the existing engine, namely the Ivchenko Progress D-36, will be replaced. To choose an appropriate engine, a literature study was necessary. It was found that Antonov has experience with replacing the engines with newer engines [35]. The Rolls-Royce BR710 and the General Electric CF-34-8 were named as possibilities. Therefore, these engines were chosen as modification possibilities as well as developments of the D-36 and the CF-34-8. These developments are the D-436 series out of which the D-436-T1 and the D-436-T3 were chosen. Additionally, the GE CF-34-10 was compared as well. The cost of installation would be cheaper if the manufacturer already has an experience with the type of engine. Furthermore, less testing will be required since some relevant data may be available already. During the engine selection process, much attention was paid to the thrust to weight ratio as this is an important parameter for decreasing the takeoff distance. An overview of the engine parameters of the different engine possibilities can be found in Table 2.1.

Table 2.1: Overview engine possibilities [36–40]

	Ivchenko Progress D-36 2A	Ivchenko Progress D-436-T1	**Ivchenko Progress D-436-T3**	GE CF-34-8E	GE CF-34-10	BR710-C4-48
Thrust [kN]	63.7	75.02	92.2	64.52	83.68	68.42
Bypass ratio TO	5.6	4.95	5	5	5	4.2
Pressure ratio	20	23.2	26	28.3	29	24
Fan diameter [m]	1.33	1.39	1.373	1.33	1.4	1.219
Length [m]	3.192	3.03	4.17	3.15	2.5	4.66
Weight [kg]	1124	1250	1360	1150	1700	1850
Thrust-to-weight ratio	56.67	60.02	67.79	56.10	49.22	36.98
SFC TO [g·(kN·s)$^{-1}$]	10.20	10.48	11.22	11.04	10.75	17.81
TET [K]	1450	1520	1580	1498	1510	1470

One requirement for the design choice is the size. The existing engine should be replaced, so the dimensions of the new engine should not differ too much from the previous one. Antonov has experience with the BR710-C4-48 engine that has a length of 4.66 m. Therefore, the engine should not exceed the length of this engine. Furthermore, to achieve a shorter takeoff distance the engine should have a high thrust to weight ratio. If this ratio is too low then the additional weight will counteract the additional thrust gained through the new engine so that no improvement

in takeoff distance will be achieved.

The chosen new engine for the Antonov An-74 will be the Ivchenko Progress D-436-T3 engine. It has a significantly higher thrust to weight ratio than the Ivchenko Progress D-36 2A which is needed to improve the takeoff distance. The engine has reverse thrusters which will be needed to reduce the landing distance. Its size is in the allowable range since the fan diameter only slightly differs from the D-36 2A and the length of the chosen engine does not exceed the length of the BR710-C4-48 engine. The weight of the D-436-T3 differs by 236kg from the D-36 2A. Thrust can be increased to 92.2 kN which represents a significant increase of 45%. With an increase in weight of 21% the thrust to weight ratio increased by 20%.

2.1.2 Engine Performance

Engine Layout

The D-436-T3 is an unmixed 3 spool turbofan engine with one fan stage. The number of stages for the LPC, HPC, HPT, IPT and LPT are 6, 7, 1, 1 and 3, respectively. An overview of the D-436-T3 engine including its stages and the numbering of the engine positions can be found in Figure 2.1.

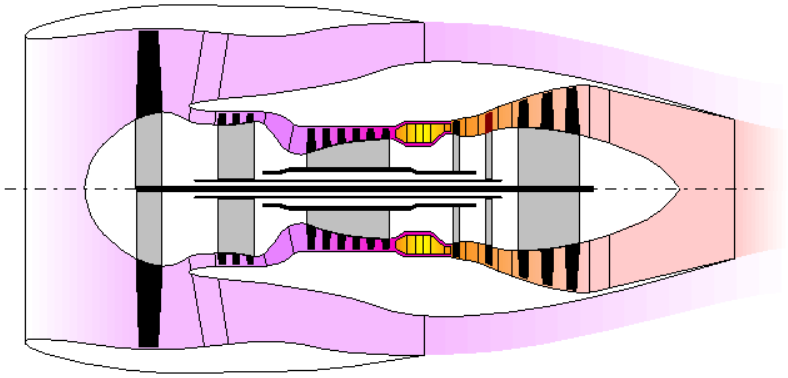

Figure 2.1: Layout of D-436-T3

Simulation Model

With the help of the GasTurb©software several internal parameters can be calculated, such as pressure, temperature and speed. However, different parameters are needed as input such as pressure ratios for compressors, inlet mass flow rate, burner exit temperature, bypass ratio and isentropic efficiencies at various stations [36]. The component pressure ratios are needed for each stage of the engine. Exact values are hard to find so engineering experience and experimental data is used to predict the behavior of the engine. With all these parameters set, the model was run to calculate the thrust and SFC of the engine. Additionally, the mass flow, temperature and pressure were calculated at each thermodynamic station. The input parameters for different models can be calculated from that. Furthermore, one can find all pressure ratios as well as core and propulsive efficiency of the system. An overview of all the parameters and their values can be found in Appendix A.

To estimate the flow behavior over the wing behind the engine, a simulation is performed as is explained in Section 2.2. This simulation needs several input values derived from the D-436-T3 engine. To calculate the dynamic viscosity over the wing, the exit temperature is needed. Because the engine is a high bypass engine, the temperature needs to be calculated with respect to the mass flow of the bypass and the core of the engine. This gives a value of 417 K. Using the same method velocity and density can be calculated resulting in a velocity of 306.9 $\mathrm{m{\cdot}s^{-1}}$ and a density of 1.12 $\mathrm{kg{\cdot}m^{-3}}$ over the wing. Furthermore the overall mass flow of the engine can be calculated by adding the mass flow of the core, the mass flow of the bypass and the fuel mass flow so that the final exit mass flow of 307.9 $\mathrm{kg{\cdot}s^{-1}}$ is achieved. Moreover, the exit area of the engine is 0.8 m^2. With the help of these inputs, the lift on the wing due to the modification of the engine can be calculated. The results of this calculation can be found in

Subsection 2.2.7.

To calculate the performance difference between the D-36 engine and the D-436 engine, the D-36 has to be modeled with the GasTurb©software as well. The outputs of the GasTurb©modeling will be the input for the MATLAB modeling predicting the Coanda performance behind the engine. Similar to the method used for the D-436-T3 engine the characteristics for the D-36-2A were calculated. An exit velocity of 253.73 $m \cdot s^{-1}$ and an exit temperature of 392.94 K are obtained. The mass flow of the existing engine equals to 253.1 $kg \cdot s^{-1}$ and the D-36 exit area is equal to the exit area of the D-436-T3 engine whereas the exit density equals 1.13 $kg \cdot m^{-3}$.

Acceleration

Due to the change in engine the the exit velocity increases. Moreover, the acceleration of the aircraft increases as well. The acceleration of the Antonov An-74 can be calculated. The results can be found in Table 2.2. The acceleration was calculated for MTOW and for OEW. Additionally, the two different engines, the D-36 2A and the D-436-T3, were taken into account. The change in acceleration of the aircraft when loaded at MTOW equals 44.7%. Because of these changes the aircraft can reach its takeoff speed more quickly so that the takeoff distance can be reduced.

Table 2.2: Acceleration of empty and fully loaded AN-74 with existing and new engine

	D-36 2A MTOW	D-36 2A OEW	D-436-T3 MTOW	D-436-T4 OEW
Thrust [kN]	63.7	63.7	92.2	92.2
Weight [kN]	358.065	186.8805	358.065	186.8805
Acceleration [$m \cdot s^{-2}$]	0.177901	0.34086	0.257495	0.493363

Emission Index

Another important value to be considered is the emission index of NO_x. Major airports have emission regulations and it is a part of sustainable development to keep this value as low as possible. A general formula to calculate the EI_{NO_x} value can be found in Equation 2.1 [41]. However it is stressed that this formula is a general formula. The emission index is dependent on the combustion chamber design which is not taken into account in this equation. The calculated EI_{NO_x} for the D-36-2A engine equals 0.568, whereas the EI_{NO_x} for the D-436-T3 engine is 0.809. This is mainly due to higher fuel flow rate and turbine entry temperature.

$$EI_{NO_x} = 0.004194 \cdot T_4 \cdot (\frac{P_3}{439})^{0.37} \cdot e^{\frac{T_3 - 1471}{345}} \tag{2.1}$$

Noise

After evaluating the emission index, the noise level was determined. Since more and more airports introduce noise limits the change in noise of the engine modification has impact on the system. However the Flying Hospital is going to fly a humanitarian mission so the noise level is not of primary importance. It would be possible to get exceptions for takeoff or landing on an airport that is strict with the noise level.

In the ICAO Noise Data Base [42] one can find data about the noise tests with an Antonov An-72 that had the D-36 2A engines mounted on it. These results of the tests can be found in Table 2.3. One can see that the Noise Level at approach is equivalent to 98.3 EPNdB. The engine noise occurs mainly due to the noise of the fan blade. This is dependent on the tip speed of the fan blades. Using the GasTurb©software, one can determine the value for the tip speed of the fan. It equals to 350 $m \cdot s^{-1}$ for both the existing and the new engine, D-36 2A and D-436-T3 respectively. Therefore, one can assume that the noise level of the D-436-T3 engine does not increase with respect to the D-36 2A engine.

Table 2.3: Noise data of D-36 2A [42]

	Lateral / Full-Power	**Approach**	**Flyover**
Noise Level [EPNdB]	90.5	98.3	89.3
Noise Limit [EPNdB]	94	98	89
Margin [EPNdB]	3.5	-0.3	-0.3

2.1.3 Engine Improvement

From the EI_{NO_x} value calculated above one can conclude that there is room for improvement for the D-436-T3 engine in terms of specific fuel consumption. To optimize the SFC the GasTurb©software is used. Since the aircraft is mainly flying in cruise condition, the optimization was performed for cruise at 11,000m altitude and at a Mach number of 0.75. The thrust the engine produces under this conditions equals 17.54 kN whereas the SFC is 17.86 g·(kN·s)$^{-1}$ [36]. Additionally, the overall pressure ratio is increased to 28.

For the optimization procedure the inlet corrected mass flow and the burner exit temperature were chosen as variables. The net thrust and the overall pressure ratio (OPR) were set to be constrains for the optimization procedure. The figure of merit was the specific fuel consumption that should be minimized in this optimization process. During the optimization process the software continuously changed the variables and constrains within the desired range until the minimal value for SFC is reached. This process is an endless loop so at a certain moment, when the SFC is only changing within a negligible range, the process needs to be stopped manually. The optimization procedure gives the characteristics for the engine to reach a minimum SFC that was determined to be 17.33 g·(kN·s)$^{-1}$. The associated inlet corrected mass flow decreased significantly to 108.5 kg·s^{-1} and the burner exit temperature was decreased to 1400 K. Additionally the thrust during cruise was increased to 17.7 kN during the optimization process.

From the optimization, a summary of key characteristics can be given to show the improvement between conventional and improved cruise condition of the D-436-T3 engine. The overview can be found in Table 2.4. While the thrust is increased by 1% the SFC is decreased by 3%. During cruise this adds up to a significant reduction of fuel consumption per flight. This means that the engine produces more thrust while burning less fuel because its propulsive efficiencies increase by 4%. Additionally, the emission index EI_{NO_x} was decreased by 7%. The engine emits less emissions using less fuel, while producing more power. In terms of sustainable development, this is a substantial improvement.

Table 2.4: Parameters of engine in conventional and improved cruise condition

Ivchenko Progress D-436-T3	**Cruise**	**Cruise improved**	**Difference**
Thrust [kN]	17.5	17.7	1%
SFC [g·(kN·s)$^{-1}$]	17.9	17.3	-3%
Prop. Eff. [%]	70.5	73.2	4%
EI_{No_x} [-]	0.37	0.34	-7%

The software is also able to do parametric studies to show the influence of parameters towards each other. In Figure 2.2, one can see the influence of the burner exit temperature of the specific fuel consumption and net thrust in yellow squares and magenta triangles respectively. One can see that if the burner exit temperature increases the net thrust and the SFC increases as well but to different extend.

2.1.4 Sensitivity Analysis

To analyze how sensitive the engine is to surrounding changes the engine was modeled under tropical conditions using GasTurb©. In these conditions the temperature equals 31°C and humidity equals 80%. From these new inputs, the maximum thrust was calculated to be 84.26 kN whereas the SFC was increased to 11.1 g·(kN·s)$^{-1}$ so the performance of the engine decreased. This means that the takeoff distance will be longer than at ISA conditions, or that the aircraft is not allowed to carry as much payload as before. There are very sophisticated calculations and predictions for different environments. So the effect on the change of the system is predictable and limited. The crew has to take that into account during the planning phase of the mission. Therefore it may be necessary to search for a longer landing strip or the payload of the aircraft needs to be reduced to still takeoff within the same

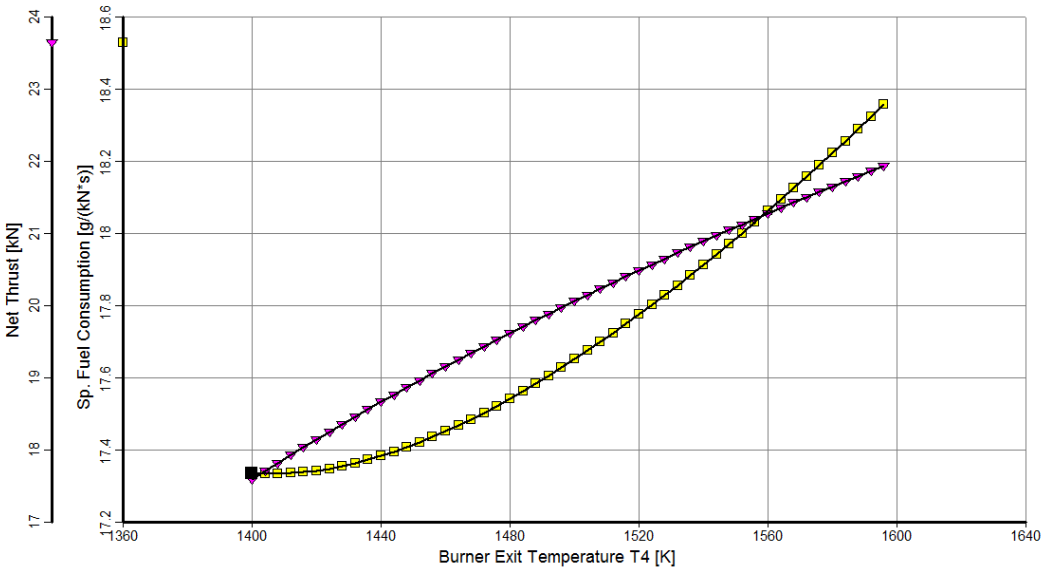

Figure 2.2: Burner exit temperature dependence

takeoff distance. Furthermore there could not be found anything about D-436-T3 engines having an engine loss or being involved in an accident. But to be more certain about the engine's performance under different circumstances, tests need to be run. The engine then can show its performance under real conditions.

2.1.5 Verification and Validation

The results can be verified, such that through the extensive use of the GasTurb©software by engine engineers one can emanate the result it produces are correct. Input parameters were taken from Janes [36] or the engine manufacturer Ivchenko Progress itself [40]. These parameters were taken from a direct source so they are assumed to be correct. The engine manufacturer needs to run tests in order to verify the parameters they want to sell the aircraft with. Every engine needs to be certified. During this phase also a significant amount of tests are performed. Verification is performed by comparing the parameters found in the reliable sources to the parameters calculated by the GasTurb©software. The results can be found in Table 2.5. One can assume that results that differ within a 10% range are verified. It can be seen in Table 2.5 that the biggest difference equals 9.75%. Therefore, the results are verified.

Table 2.5: Verification data

	Ivchenko Progress D-36 2A	Verification Data GasTurb©	Difference [%]	Ivchenko Progress D-436-T3	Verification Data GasTurb©	Difference [%]
Thrust [kN]	63.7	63.51	-0.3	92.2	92.25	0.05
Pressure ratio	20	21.95	9.75	26	26.03	0.115
SFC TO [g·(kN·s)$^{-1}$]	10.20	10.02	-1.76	11.22	10.68	-4.81

The system cannot fully be validated since no validation data was provided. One needs to run tests in order to validate the performance of the engine and also to show how the engine is performing when mounted on the aircraft. The engine has a significant effect on the structure and on several modifications made to the An-74. Not every effect can be predicted by calculation, so real life tests are required.

2.1.6 Recommendation

Detailed investigation will be required to evaluate engine performance. Both engines, the D-36 2A and the D-436-T3 engine, are produced by Ivchenko-Progress which is a Ukrainian company. Little can be found about those

engines especially when searching in English. Therefore only the key parameter of each engine could be found. The component pressure ratios were chosen using expert experience. The pressure ratios of the engine are precisely selected with respect to the aircraft and the environment it will be working in so with more precise data the engine can be modeled more exact as well. Similarly there was little to be found about the price of the engine. The price of the D-436-148 engine was found to be around €3M for two engines [43] so one can assume the D-436-T3 engines are priced similarly however further investigations and negotiation need to made in order to determine the exact price of the modification.
Additionally, further investigations could be made in terms of improvement of the engine. The engine improvement process was modeled using the GasTurb©software but there could be more investigations of how to change the engine so that it achieves the improvements and what kind of influences are linked to that changes. This can also be done by further testing of the engine which is also needed for validation process of this engine modeling as described in Subsection 2.1.5
To decrease maintenance costs, sensor monitoring and health monitoring systems for the engine can be installed. These systems can monitor the behavior of the engine so that problems with the engine can be detected earlier on. They can be fixed before bigger problems are caused. This would decrease maintenance cost significantly and safety can be improved. If these improvements will be installed further research is needed about the specific interaction of the system and the engine.
The final recommendation of improvement would be the securing of the engine to the wing. Since the engine was modeled as mass point further investigation will be needed if a 45% increase of thrust would be withstood by the structure. Also the center of gravity of the engine changes since the new engine is about 1m longer than the existing one. This moves the center of gravity of the aircraft to the front which is beneficial for the aircraft stability. Resulting from this the influence of the center of gravity change to the structure of the wing needs to be looked into detail. Higher moments and forces will be acting at the structure so this is crucial for safety. However the exact structure needs to be known for that which is not the case for the current model as described in Section 2.4. A fail-safe attachment of the engine to the wing will be inevitable for the security of the aircraft.
With further investigations the replacement of the D-36 2A engine with the D-436-T3 engine could be a successful modification of the An-74 for the use of the Flying Hospital.

2.1.7 Conclusion

The change in engine from the D-36 2A to the D-436-T3 results in performance changes. The thrust increases by 45% while the weight increases by 236kg. This results in an thrust to weight ratio increase of 20%. Therefore, the takeoff distance can be decreased since the acceleration increases by 44.7%. The exit velocity is increase to that the takeoff speed can be reached more quickly. Additionally, the EI_{NO_x} and the SFC increases slightly. The engine change is also beneficial for the upper surface blowing effect elaborated in the following Section 2.2.

2.2 Upper Surface Blowing Effects

The retrofitting of new engines on the An-74 will have considerable implications for its lift generation due to the unique configuration of the aircraft's engines. The An-74 is the sole aircraft in production that uses upper surface blowing (USB): exhaust air from the engine flows over the upper wing surface, generating additional lift. By placing larger engines on the aircraft, the USB operation, and resultantly the takeoff and landing capabilities of the Flying Hospital, will be improved.

2.2.1 Upper Surface Blowing Principles and Operation

As previously mentioned, USB configurations consist of generated jets of air being blown along a wing surface. For the An-74, USB is accomplished by the engine exhaust adhering to the upper wing due to the Coanda effect: the tendency of a jet to adhere to a nearby curved surface. This USB configuration is illustrated in Figure 2.3. The purpose of applying USB is to obtain additional lift resultant of two mechanisms:

- Momentum of the (exhaust) jet being vectored downwards by the wing trailing edge.
- Changes in the local pressures of the airfoil surface immersed in the jet.

Concept USB aircraft have demonstrated the massive lift gains of the configuration with C_L values approaching 10 [44]. Such high lift is excessive for cruise conditions and, as such, USB is mainly exploited during takeoff and

landing phases where flaps can be deployed to present appreciable curvature for the jet stream. Hence most of the analysis in this section will pertain to landing and takeoff conditions with only stability considerations explored during cruise conditions. Large lift is not the only advantage of such a setup; blown wing segments are more resilient to flow separation, so outer, non-blown segments stall first characterized by loss of control surface effectiveness and a more gradual loss of lift when compared to conventional aircraft. Unfortunately, USB configurations are not without their downsides as they do entail considerable drag and moment penalties to be taken into consideration.

There are several methodologies developed for calculating the lift generated by a USB configuration. The most advanced is the combination of Navier-Stokes equations with panel methods; however, this method requires high fidelity and is generally complex with a considerable emphasis on detailed geometry. Due to An-74 data being scarce and the limited timespan of the given project, such a thorough analysis was unfeasible. Panel methods served as a potential alternative but again succumbed to a considerable reliance on detailed geometry. This led to the selection of a method by Keen, which combines Spence Jet Flap theory and Circular Stream Line theory (CST) and is both relatively quick and applicable in light of little geometrical data [45]. The Jet Flap theory accounts for the momentum vectoring aspect of the lift while the CST accounts for the pressure distribution upon the blown surface including viscous interaction between jet stream and free stream air.

2.2.2 Geometrical Modeling and Configuration

Detailed engineering drawings for the An-74 USB system were, unfortunately, unobtainable and instead a simplified model was constructed on the limited data available. This model was constructed under considerable assumptions and simplifications in terms of the geometry, but it is believed that the relative percent changes measured from this system would apply to the actual Antonov when retrofitted. A more accurate analysis could only be executed with the actual An-74 geometries. Figure 2.3 shows the model used for the USB analysis. The following assumptions were made in terms of the geometry and parameters:

- The span of the USB blown sections is equivalent to the engine exhaust diameter. Thus nozzle spread angle is 0. This assumption is made as the nacelle configuration of the engine is completely unknown and will resultantly increase the jet coefficient, C_j, introduced later.
- The engine nozzles are rectangular in shape. This assumption is made by the CST and simplifies the jet thickness distribution over the wing making C_j uniform along the blown span.
- The ratio of the jet thickness to flap curvature is below 0.3. This is fundamental to the CST theory. Without knowing the specific jet and flap properties of the An-74, it is impossible to gauge the validity of this assumption but for other USB aircraft it is generally the case.
- The nozzle kick-down angle (downward deflection of the exhaust jet directly by the engine) is zero.
- After leaving the trailing edge, the exhaust jet becomes parallel to the free stream velocity after a finite distance. This means no thrust is lost (full thrust recovery) and is valid for flap deflections approximately near and below 40° [45].
- Since the original airfoil of the Anonov An-74 is unknown, the assumption is made to use the airfoil TSAGI12-IL as the base airfoil. This Russian airfoil is used in most Antonov airplanes of the same class. Flap chord ratio is 0.2 and the average chord in the blown section is 4.3 m. The engine nozzle is placed at 20% of the local chord with no lift generated up to that point. These numbers were derived from available data and planform figures [46].
- The flap mechanism is of a simple configuration shown in Figure 2.3. In reality the An-74 flaps are more complex being multi-slotted and with gaps. A detailed analysis of such a system is beyond the scope of this project.
- The exhaust nozzle/nacelle (assumed optimized for the aircraft) between existing and retrofit engines remains identical, including area and height. This assumption is unavoidable due to the lack of data available for the engines and nacelles.

Further, engine parameters are taken as those calculated in Section 2.1. Three flight conditions were evaluated for changes in USB with the retrofitted engines: takeoff configuration at V_2 speed with 17° flap deflection, cruise conditions as defined in Section 2.5 for stability analysis and lastly landing conditions with 30° flap deflection and

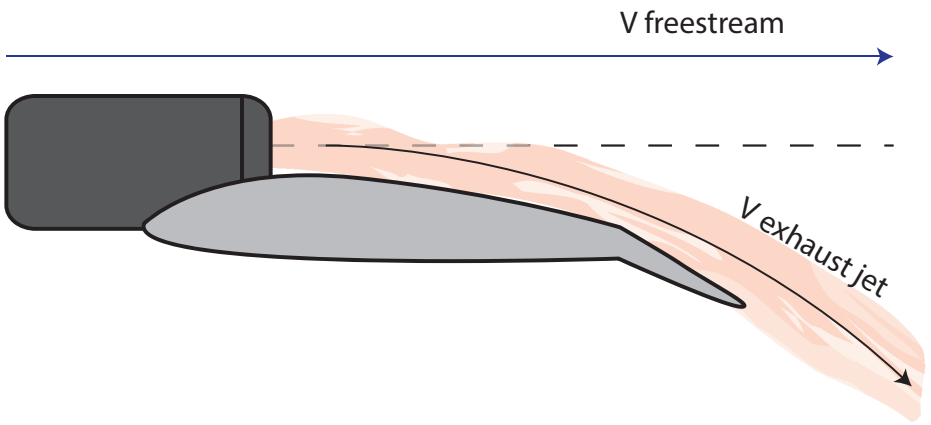

Figure 2.3: Simplified USB configuration used for analysis

V_A. These speeds and flap settings were obtained from the An-74 flight manual [46]. It was found that for flapped conditions, the percentage changes in lift, drag and pitching moment were the same when comparing the existing and the proposed retrofit engines.

2.2.3 Spence Jet Flap Theory

In the mid 1950's, Spence published his work on inviscid incompressible flows past a thin 2-D airfoil. Later, his theories where extended to cases were the jet enters the flow tangentially along a deflected flap. This section gives a simple overview of his theories and how this can be used in the specific case of the Flying Hospital. These theories are used because of their success in analyzing jet-flap wings and they are relatively simple.
Spence assumed that the jet flow returns to the undisturbed free-stream direction. This assumption led to a differential equation for the problem using a Fourier series, together with a function that describes the singular behavior of the flow at the trailing edge. The momentum flux coefficient, C_j, was then used in a 9-term interpolation.

Lift Coefficient

In the Fourier series method, mentioned before, the lift coefficient is given by Eq. 2.2.

$$C_l = 2\pi\alpha + 2\pi B_o + 4\pi A_o \tau \tag{2.2}$$

where α stands for the angle of attack and τ is the jet deflection angle relative to the chord line. A_o and B_o are the Fourier coefficients and are given by Eq. 2.3 and Eq. 2.4.

$$A_o = 0.2817 C_j^{1/2} + 0.0259 C_j + 0.0124 C_j^{3/2} \tag{2.3}$$

$$B_o = 0.0917 C_j^{1/2} + 0.0880 C_j + 0.0041 C_j^{3/2} \tag{2.4}$$

If the flow over any control surface, e.g. a deflected flap, has to be investigated, the equation for lift coefficient has to be adjusted to deal with the extra lift that this control surface creates. The sectional lift coefficient of this control surface is given by Eq. 2.5.

$$C_l = 2\pi\alpha + 4\pi B_o \alpha + 2(\chi + sin\chi + 2\pi D_o)\delta_f \tag{2.5}$$

In which B_o stays the same. The flap deflection, δ_f, is assumed to be equal to the jet angle. And χ is given by Eq. 2.6.

$$\chi = 2sin^{-1}\sqrt{E} \tag{2.6}$$

where E is the ratio of flap chord to airfoil chord. D_o is given by Eq. 2.7.

$$D_o = A_o - \frac{1.931 E^{1/4}}{4\pi}(C_j^{-0.9621E^2+0.5785E+0.1639}) \tag{2.7}$$

Pitching Moment Coefficient

The general form of the pitching moment around the leading edge in case of a pure jet flap is given by Eq. 2.8.

$$C_{m,le} = (-\frac{1}{2}\pi + E_o)\alpha + F_o\tau \tag{2.8}$$

with,

$$E_o = -0.3057C_j^{1/2} - 0.2466C_j + 0.0406C_j^{3/2} \tag{2.9}$$

$$F_o = -1.5868C_j^{1/2} - 0.6945C_j - 0.0437C_j^{3/2} \tag{2.10}$$

As can be seen in the functions for E_o and F_o, these coefficients are functions of the blowing coefficient C_j. In the case of a flap at the trailing edge, the change due to the aft flap must be accounted for in the angle of attack. A superposition of the original flap contribution and the jet effects on the deflection lead to Eq. 2.11.

$$C_{m,le} = (-\frac{1}{2}\pi + E_o)\alpha - (\frac{1}{2}\chi + sin(\chi) + \frac{1}{4}sin(2\chi))\delta_f + G_o\delta_f \tag{2.11}$$

With a functional relation for G_o that is given by Eq. 2.12.

$$G_o = -0.3318C_j^{1/2} - 1.0332C_j + 0.0842C_j^{3/2} \tag{2.12}$$

Which is valid for a flap chord ratio of 0.30. The quarter chord moment coefficient as a result is then given by Eq. 2.13,

$$C_{m,0.25c} = \frac{1}{4}C_l + C_(m, le) \tag{2.13}$$

which is valid for 2D thin airfoil theory.

2.2.4 Circular Streamline Theory

Goal of this section is to introduce the circular streamline theory and how it is used to approximate the surface pressures induced on the curved surface wetted by the jet exhaust flow of the engines. An approximation is used since an analytical solution is not possible. Therefore the nearly circular attached flow streamlines (Coanda effect) can be represented by a potential flow. A typical wall-jet velocity profile is shown in Figure 2.4.

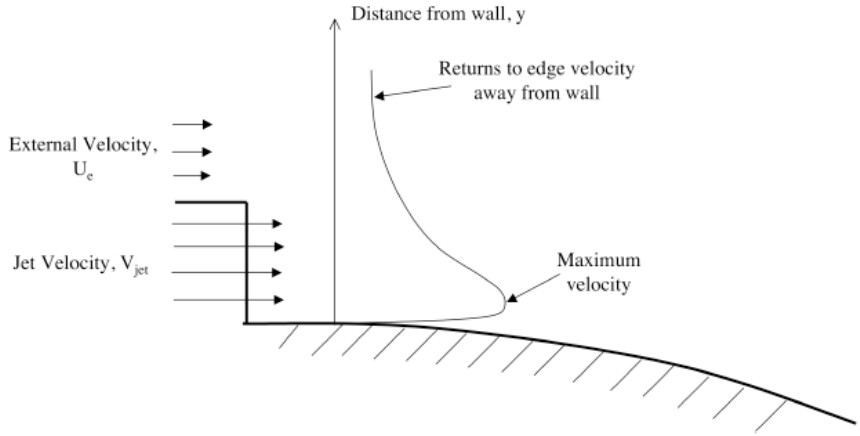

Figure 2.4: Typical wall-jet velocity profile over the airfoil [45]

From Figure 2.4 it can be seen that the farther away from the airfoil, the lower the velocity of the flow and it can be modeled with a potential flow vortex. Such a vortex is given in Figure 2.5 which displays a concentric circular vortex field.

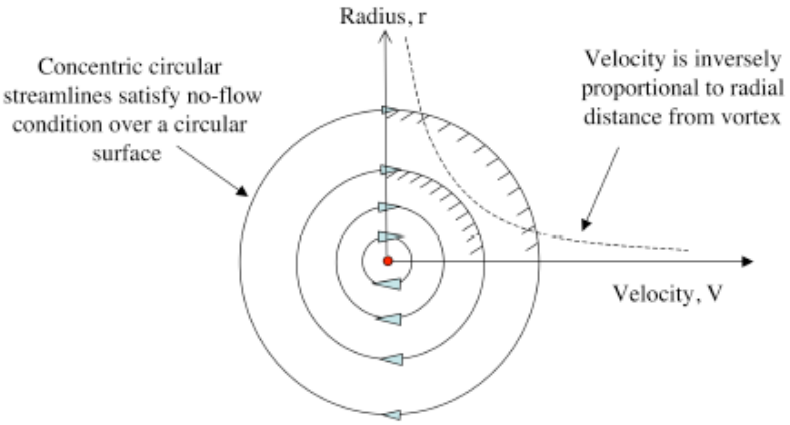

Figure 2.5: Streamlines and velocity profile produced by a point vortex [45]

2.2.5 Pressure Difference Calculation

Using Bernouilli's equation for incompressible flow, with the velocity in terms of the vortex strength Γ_{PV}, this results in an equation for the pressure difference Δp that is a relation between jet and freestream velocity. The thickness of the jet is given by the difference in radius R and $R+t$.

$$\Delta p = (p_{localstatic} - p_\infty) + \frac{\rho_{jet}}{2} R_{ref}^2 (U_e - nV_{exit})^2 (\frac{1}{(R+t)^2} - \frac{1}{R^2}) - \rho_{jet} R_{ref} U_e (U_e - nV_{exit}) (\frac{1}{R+t} - \frac{1}{R}) \quad (2.14)$$

Lift, Drag and Pitching moment

To calculate the lift and drag forces and the resultant pitching moment, the airfoil is split into n small segments of equal length. This is found useful since the surface geometry can change and the number of calculations is high. Figure 2.6 displays this plan of splitting up the airfoil in tiny sections.

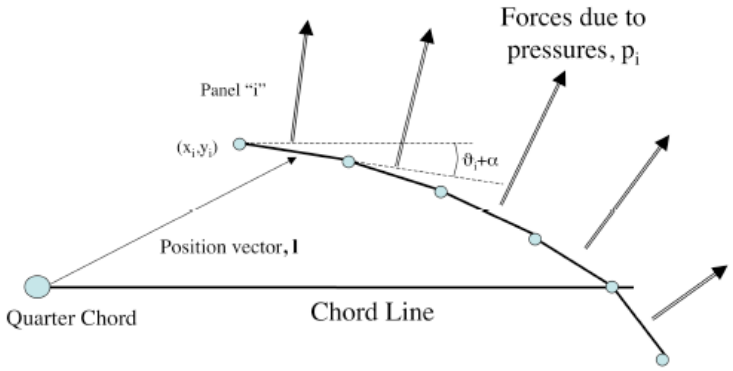

Figure 2.6: Drawing of a USB surface discretized into small segments [45]

Normal vector of one piece is then given by Eq. 2.15.

$$\mathbf{N}_i = cos\theta_i \mathbf{i} + sin\theta_i \mathbf{j} \quad (2.15)$$

From this, the induced pressure in both x and y directions for any panel is given by Eq. 2.16.

$$f_{x,i} = p_i s_i cos\theta_i \quad (2.16)$$

$$f_{y,i} = p_i s_i sin\theta_i \quad (2.17)$$

Total force in either x or y direction is then the sum of the forces on each panel. The 2D lift and drag increments due to induced surface pressure are then given by Eq. 2.18 and Eq. 2.19.

$$\Delta C_l = \frac{1}{q_\infty c} \sum_{i=1}^{N} p_i s_i cos\theta_i \tag{2.18}$$

$$\Delta C_d = \frac{1}{q_\infty c} \sum_{i=1}^{N} p_i s_i sin\theta_i \tag{2.19}$$

The moment about the aerodynamic center, created by the pressure distribution, is the product of the determined force vector and the position of the individual panel, given by l.

$$\Delta C_{m,ac} = \frac{1}{q_\infty c^2} (\mathbf{F} \times \mathbf{l}) \tag{2.20}$$

This results in the following equation for quarter chord moment coefficient, Eq 2.21.

$$\Delta C_{m,0.25c} = \frac{1}{q_\infty c^2} \sum_{i=1}^{N} p_i s_i (y_{m,i} sin\theta_i - (x_{m,i} - 0.25c) cos\theta_i) \tag{2.21}$$

Hence, given the surface geometry and the flow conditions, the lift, drag and pitching moment increments can be approximated due to induced surface pressures.

Drag Estimation

The total drag of the subsonic airfoil consists of two parts; skin friction drag and pressure drag. The pressure force comes from the jet flow that acts as drag. Skin friction is the other factor, this can be estimated in the standard manner using a form factors approach [45, 47]. The friction drag coefficient is given by Eq. 2.22.

$$C_d = (C_{F,fs}(\frac{S_{fs}}{S_{ref}}) + C_{F,jet}(\frac{S_{jet}}{S_{ref}})) \tag{2.22}$$

In which fs stands for normal flow and 'jet' stands for the area exposed to the exhaust. FF is the form factor of the airfoil, as given in Eq. 2.23.

$$FF = 1 + 1.8(\frac{t}{c}) + 50(\frac{t}{c})^4 \tag{2.23}$$

The skin friction coefficients are determined by Eq. 2.24.

$$C_F = \frac{0.455}{(log_{10}(Re_c))^{2.58}} \tag{2.24}$$

2.2.6 Modelling Program

The calculations described in Section 2.2.2 were implemented into a MATLAB code in order to facilitate rapid and modifiable execution. Supplementing the MATLAB was input data generated by XFoil for the initial pressure distributions and surface coordinates of the TSAGI airfoil [48]. The overall code can be seen to consist of several modules as follows:

1. **Generation of base airfoil data.** Coordinates for the TSAGI12-IL airfoil were input into XFoil. Geometric modifications (flap deflections and scaling) were then applied (hinge point $\frac{x}{C} = 0.8$, chord scale = 4.3). For each flap deflection case the XFoil algorithm was then run to generate C_p plots over the airfoil surface using relevant speeds from the flight manual and correlating Reynolds numbers at mean blown chord. Note: XFoil did struggle with the used TSAGI coordinates. For certain test conditions large iterations were required and occasionally (ex. flaps at 40°) no convergence could be found. Output from this module consisted of airfoil coordinates and C_p over the airfoil.

2. **Import and geometrical analysis of airfoil.** The outputs of the previous module were imported into MATLAB. Coordinates were used to plot the airfoil and calculate the local radius of curvature for each surface panel exposed to jet flow. Local radius of curvature was calculated by polynomial approximation: a fifth degree polynomial was fit to the top airfoil coordinate data. This polynomial was then differentiated twice in order to evaluate the local radius of curvature at each segment via Eq. 2.25. The accuracy of this method is shown in Figure 2.7. The fit is generally very close except at the beginning of the flap where polynomial curvature is less. Lastly the angle/slope of each airfoil surface panel relative to free stream horizontal velocity was calculated.

$$R = \frac{[1 + (\frac{dy}{dx})^2]^{3/2}}{|\frac{d^2y}{dx^2}|} \tag{2.25}$$

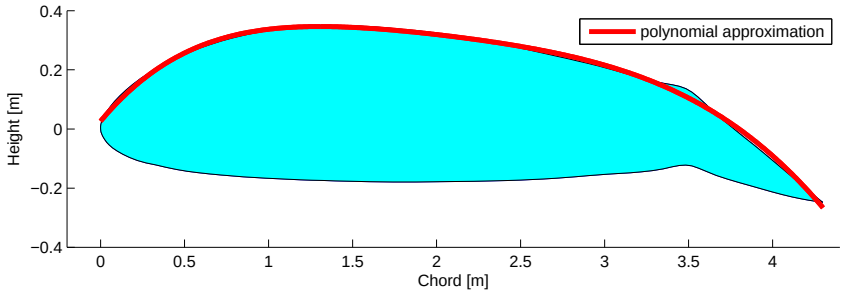

Figure 2.7: Polynomial approximation of surface for local radius of curvature

3. **Input of engine and free stream parameters.** Basic geometrical data and free stream properties as discussed in Section 2.2.2 were input. From this data C_j could be calculated as well as empirical correctional factors required by the CST method.

4. **Perform CST analysis.** Using the base C_p values from Xfoil, calculated radii of curvature and jet properties, the δP along the airfoil top (blown surface) was calculated via Eq. 2.14.

5. **Perform Spence Jet Flap analysis.** Executed Spence calculations as documented in Section 2.2.3.

6. **Superimpose CST, Jet Flap and XFoil data.** First CST and XFoil pressures were converted to lift forces, drag forces and moments via the panel process documented in Section 2.2.4. Resultant force vectors were plotted along the airfoil surface as in Figure 2.8. Finally, the calculated coefficients of all methods were summed and correctional factors (from the third module) applied.

2.2.7 Summary of Effects of Retrofitted Engines on USB

Table 2.6 documents the changes in parameters between the existing and retrofitted engines according to the UBS model. Note, the total coefficients include empirical correction factors as documented in CST theory. The other configurations exhibited the same exact percentage changes in lift, moment and drag when compared between the two engines. This is expected as the governing equations, Eqs. 2.14 and 2.5, are constant for the same flight conditions except for the engine exhaust velocity and C_j. The larger, retrofit engine has a higher exhaust velocity that results in lower pressures on the airfoil surface and thus additional lift. Similarly a larger mass flow increases the C_j resulting in a larger contribution from the Jet Flap theory. Samples of the pressure/force distribution data generated by the MATLAB code are presented in Figures 2.8 to 2.11. These figures clearly illustrate the pressure change being a function of the airfoil local radius of curvature, with larger pressure forces occurring at regions of higher curvature.

A number of observations can immediately be drawn regarding the obtained results. The calculated C_l, C_d, and C_m values were large compared to similar configurations in Keen's work [45]. Verification and validation of the USB analysis can be found in Section 2.2.8 and shows that larger drag and moment values are expected. Higher lift on the other hand is most likely due to a large C_j, resultant of a lack of data on the engine nacelles and nozzles. While the coefficient magnitudes themselves were very high, their relative change between engines seemed reasonable.

Table 2.6: Calculated 2D values for USB system at takeoff conditions

Coefficient	existing Engine	Retrofit Engine	Difference
C_l Jet Flap	9.53	11.93	25%
C_l CST	3.62	4.78	32%
C_l total	12.74	15.70	23%
C_m Jet Flap	-1.97	-2.52	28%
C_m CST	-0.33	-0.48	44%
C_m total	-2.30	-2.99	30%

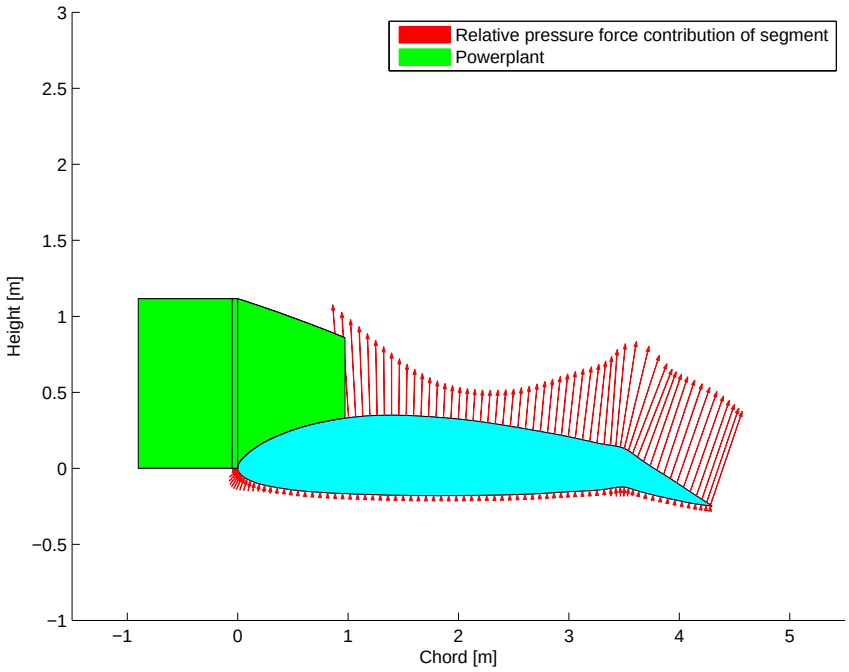

Figure 2.8: Model CST contribution of USB under $\alpha = 2°$ and flap deflection 17° with existing engine

The net effects on the aircraft by the retrofitted engine in terms of the USB system were established by evaluating the ratios between the USB blown and non-blown segments of the wing. The wing planform area was divided into two segments corresponding to the blown and non-blown areas as seen in Figure 2.12 for the non blown sections, the C_l, C_d and pitching C_m of the mean chord were generated via XFoil for the TSAGI airfoil. The relative contribution of the blown segments was then calculated by Eq. 2.26 for all three coefficients C_l, C_d and C_m.

$$relative\ contribution\ blown\ wing\ segment = \frac{C_{blown}S_{blown}}{C_{blown}S_{blown} + C_{nonblown}S_{nonblown}} \tag{2.26}$$

Based on the available geometry the USB area was estimated to be approximately 4.9 m^2 and the remaining non-blown wing area as 94 m^2. The results of Eq. 2.26 are summarized in Table 2.7 showing the contributions of the blown USB sections to the overall wing in takeoff configuration. Despite a small surface area the USB sections accounted for a large percentage of the drag and pitching moment of the entire wing when flaps are deployed. Such performance was understandable considering the magnitude of the calculated coefficients and USB configurations are known for incurring large moments and drags [49]. In cruise conditions, where the exhaust jet deflection is less, the USB contributions to the wing performance were considerably less.
Table 2.8 contains the end effects of the new engines on the overall aircraft performance. It can be seen that, according to the MATLAB results, during takeoff and landing configurations, the relative changes in lift, drag and moment due to the new engine are the same. This is expected: the only parameter changed between the cases is the jet velocity. In cruise the coefficients changes differ from those when flaps are deployed. This is expected as no flap deflection means less curvature so lift, drag and moment contributions from CST greatly decrease and the Jet

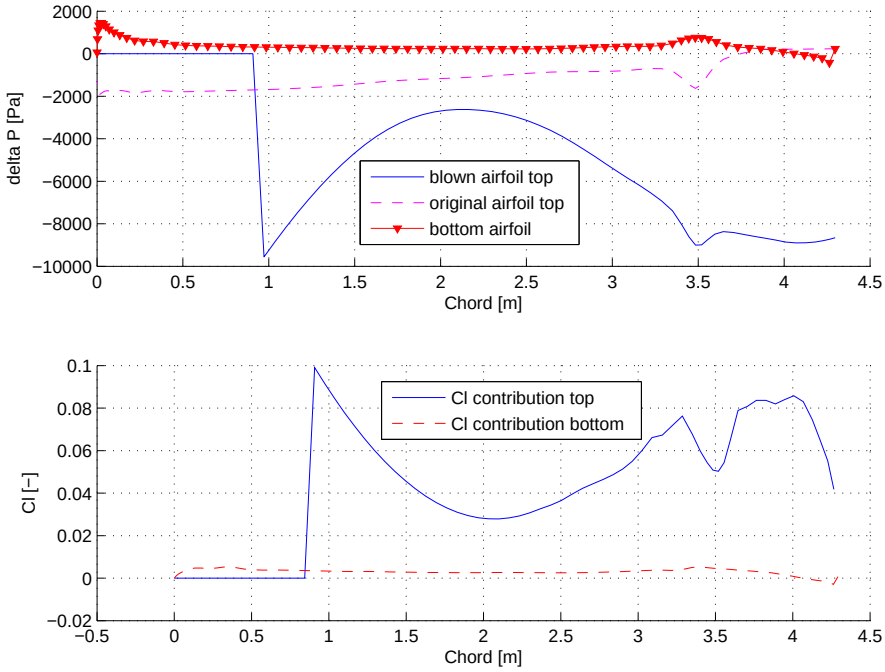

Figure 2.9: C_p and C_l distributions of USB under $\alpha = 2°$ and flap deflection 17° with existing engine

Table 2.7: Contribution of blown segment to the wing with 17° flap deflection (existing engine)

	Contribution to wing by USB segment
Lift	34%
Drag	42%
Pitching Moment	39%

Flap contribution becomes dominant. Furthermore, at cruise, the aerodynamic conditions are different: the ratio between jet velocity and free stream decreases. The change in wing induced moment at cruise is investigated further in Section 2.5 for the implications on stability. For landing ground run ,engines are assumed to be idle or in reverse thrust (with clamshell preventing airflow over the wing) thus no USB is present. Overall it appears the retrofit of the more powerful engines will lead to increased STOL performance. The additional lift in these conditions is about 8% and outweighs the increment in drag incurred.

Table 2.8: Net effect of retrofitted engines and USB on aircraft

	α	**Lift**	**Drag**	**Wing Moment**
TO Ground Run	2°	+7.7%	+2.0%	+15.6% pitch down
Cruise	0°	+3.6%	+5.3%	+18.5% pitch down
Landing Approach	8°	+7.7%	+2.0%	+15.6% pitch down
Landing Ground Run	0°	0%	0%	0%

2.2.8 Verification and Validation of USB Analysis

The verification of the USB analysis consisted of independently confirming the inputs, intermediate calculations and outputs of each code module. In doing so, syntax errors, inconsistencies or any other complications could be identified and addressed. No analytical method was available for comparison to the numerical solution: solving an analytical solution to the model was unfeasible given project time constraints. The major difficulty encountered during verification was the implementation of the TSAGI airfoil into XFoil: the original coordinate file was incom-

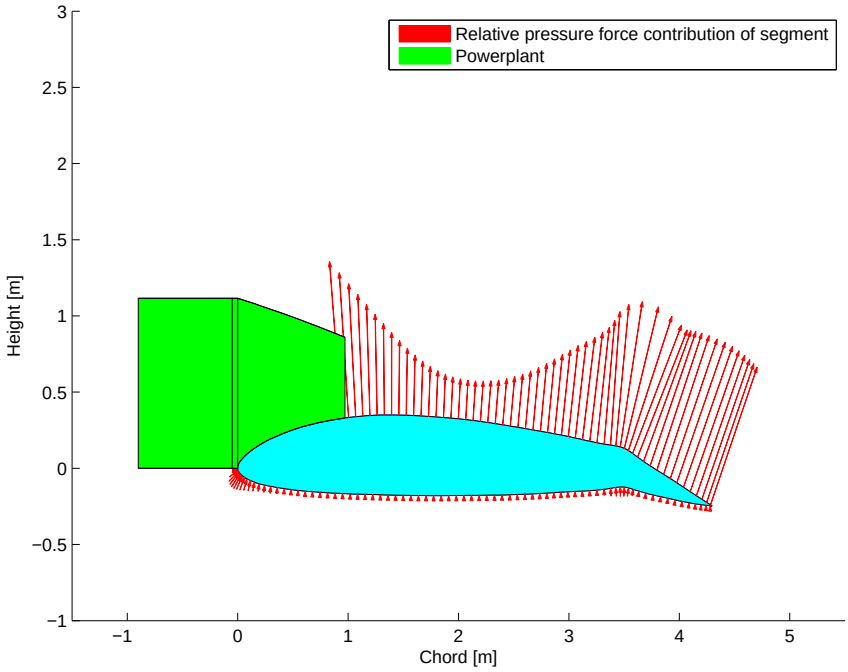

Figure 2.10: Model CST contribution of USB under $\alpha = 2°$ and flap deflection 17° with retrofitted engine

patible and even after modifications Xfoil struggled to converge onto solutions for given configurations that were resultantly omitted.

The validation of the USB model was done by comparison to Keen's work. Keen provided sample input and output data for the YC-14 aircraft that he applied to CST and Spence theory [45]. For validation of the created USB model, input data identical to Keen's was used and the resultant output compared to that of Keen. Results of this comparison can be seen in Table 2.9. It is important to note that variation in results was expected: the created code had differences from the simplifications used by Keen. Most notable of these differences were: Keen's flap was more intricate as opposed to the simple flap modeled, his model included lift forward of the engine nozzle, he did not take the bottom surface of the USB airfoil into account and Keen assumed constant curvature where the used model calculated local curvature around the TSAGI airfoil. The flap and curvature differences are suspected of accounting for the large deviations between the created model and Keen's data for C_d and C_m. In terms of the pitching moment Keen's method may over-predict the coefficient, so a smaller C_m from the created model is not necessarily a concern. Otherwise, Keen's methods tend to correlate very well with experimental data (the reader is referred to his work for more details) so correlating to his values is assumed to be sufficient for the An-74 analysis at the given level of design. It was found that the C_l of the two data's had negligible deviation while the C_d and C_m had considerable deviations due to the aforementioned model differences. Lastly, it is interesting to note the limitation of using a polynomial to approximate the airfoil surface: the rapid bend at the flap joint is poorly accounted for. In practice this segment has a very large radius of curvature and thus lift and pitch moment which is not modeled by the created code. A proposed remedy for this is to use multiple polynomials at different segments of the airfoil.

2.2.9 Sensitivity Analysis

C_l, C_d, and C_m were analyzed for their sensitivities to changes in engine parameters. Figure 2.13 illustrates the values of these coefficients for a given mass flow and varying exhaust density/velocity as well as increasing mass flow and density with constant velocity. In the case of constant mass flow it can be seen the USB system is relatively robust and follows linear trends. In the case of constant mass flow and varying exhaust density/velocity the trends follow exponential curves (less robust). It was noted that for certain input combinations negative drags could be obtained. These were resultant of very low exhaust velocities produced by high density jets (for a constant mass

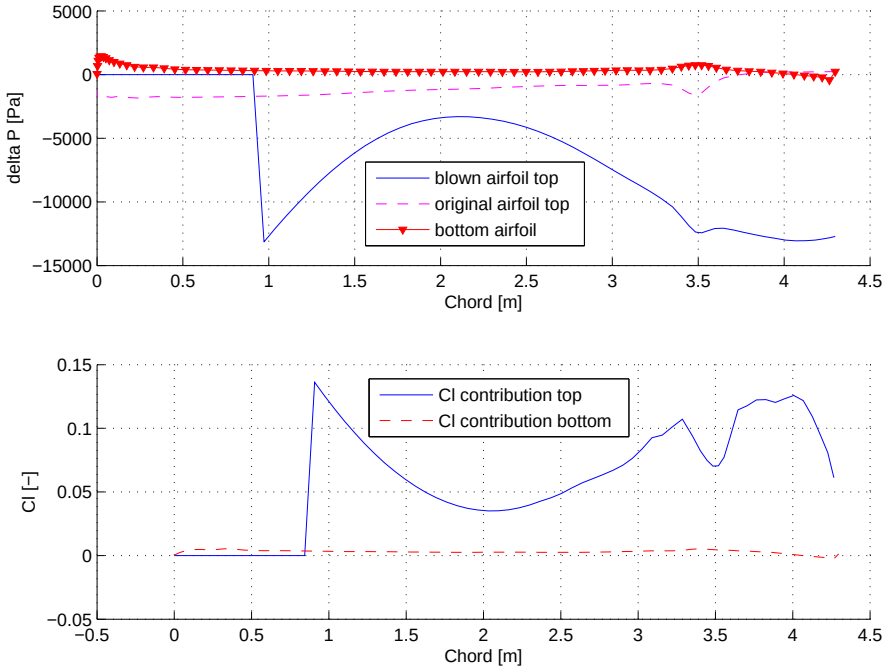

Figure 2.11: C_p and C_l distributions of USB under $\alpha = 2°$ and flap deflection 17° with retrofitted engine

h

Table 2.9: Model results compared to those of Keen for the YC-14 ($\alpha = 2°$, flap def. $= 30°$)

	Keen's result	**Model result**	**Difference**
ΔP radius of curvature: 1.71 m	-3.88 [kPa]	-4.58 [kPa]	+18%
ΔP radius of curvature: 10.06 m	-19.06 [kPa]	-19.84 [kPa]	+4%
C_l	9.39	9.36	$<$ -1%
C_d	0.20	0.26	+30%
C_m	-2.27	-1.16	+49%

flow). The low velocities meant the upper surface had very small pressure drops and even pressures above free static. These higher pressure regions would push the airfoil forward hence negative drag. In practice such engine conditions are impossible, at takeoff and landing the jet velocity will never be below free stream and exhaust densities are generally low.

2.2.10 Recommendations

USB analysis is very complex and presents many opportunities for further analysis. The USB model documented was simple, and a more intricate model with less assumptions may certainly present possibilities for possible future work. Most crucially, a refined model with actual An-74 geometries will be essential for a complete understanding of new engine effects on the Coanda effect and subsequent STOL performance. For really thorough analysis, the complete flap system may be modeled including multiple flaps and resultant gaps. In terms of model accuracy, other methods such as Navier-Stokes equations with panel methods can be used, provided sufficient time and resources. The interaction of bolstered USB system with the rest of the aircraft was disregarded in this analysis due to time constraints. For a final design of the Flying Hospital it would be important to examine the interaction of a stronger Coanda effect with other aspects of the aircraft. A prime example is the tail, USB aircraft tend to complicate empennage design due to large pitching moments and large downwash on the horizontal stabilizer. Thus if changing the USB the empennage must also be evaluate along with flight dynamics of the modified aircraft as a whole (another example consideration is roll moment in case of a single USB failure: high asymmetric lifts could quickly compromise the aircraft's stability). It is possible for large changes in the USB system to require redesigns of stabilizing and control surfaces elsewhere on the aircraft thus adding development time and risks. For further

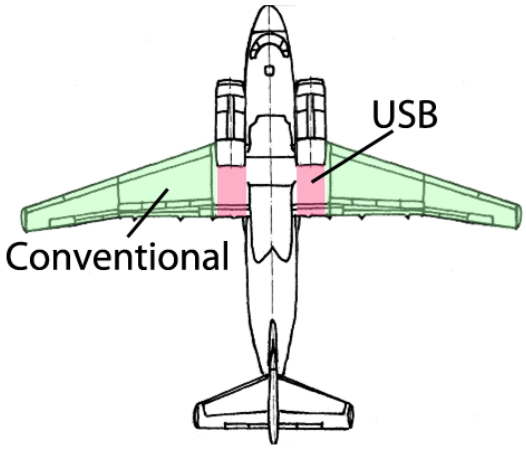

Figure 2.12: Assumed USB and non-blown areas of the An-74 wing [46]

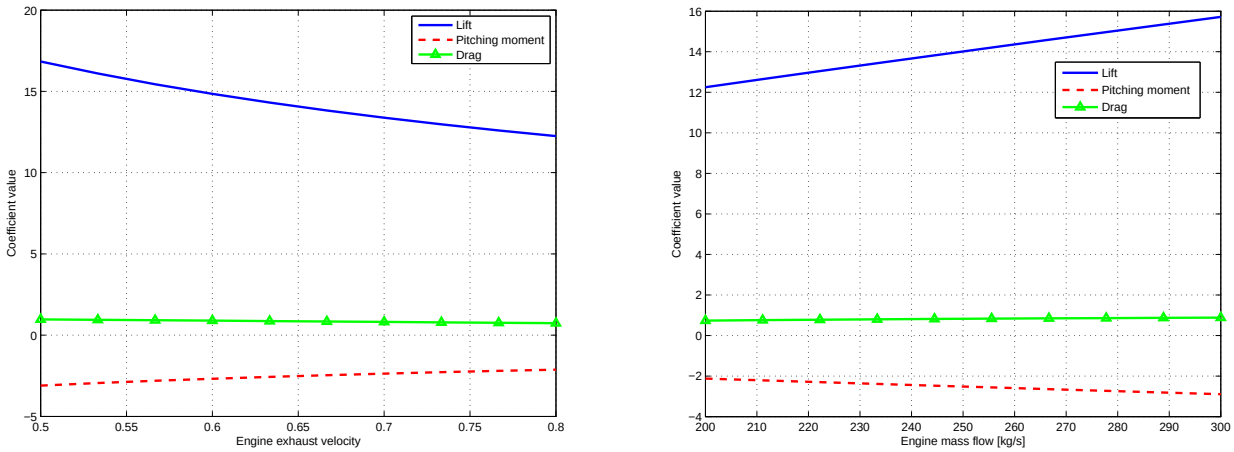

(a) Sensitivity of coefficients to varying engine exhaust density and(b) Sensitivity of coefficients to varying engine mass flow and density velocity

Figure 2.13: USB sensitivities

development of the Flying Hospital these risks would have to be taken into account.

2.3 Vortex Generators

As an improvement to the Antonov An-74 in terms of aerodynamics, the (micro) vortex genrators (Figure 1.6) were chosen as the most efficient solution in Section 1.3.9. To select the most effective configuration, the VGs have to be analyzed first on which a design can be based.
Three methods were considered for the analysis of VGs. The first method is to create a CFD model. This is a computer program in which a 2D or 3D geometry can be loaded. The program then simulates a flow over the geometry and analyzes the properties of the model. Creating such a model would take a considerable amount of time and experience in making CFD's. Besides that, being able to work with the program within a few days would de difficult due to time constraints.
Another possibility would be to make an analytical model. Unfortunately this would require a basic knowledge of advanced fluid mechanics so this method is also not recommended.
A literature study is the most feasible solution when considering current time limitations. It would consist of reading papers to look for relevant examples, correlations and experimental results.

At first, the design conditions and strategy are explained. The sizing of the VGs is shown thereafter, followed by the properties of the vortices. Then, there is elaborated on the drag produced by the devices. The treatment of performance of the VGs and the overall performance of the VGs is provided thereafter. Manufacturing considerations and a sensitivity analysis are then outlined. Verification and Validation is provided thereafter. Finally, recommendations are given.

2.3.1 Design Conditions

During the calculations and reasoning processes in this section on vortex generators, several assumptions will be made regarding the design conditions. Since the primary objective is to improve the aircraft's STOL capabilities, the focus lies on these conditions.

At first V_s, the stall speed, can be derived from the approach speed. The relation between stall speed and approach speed is given in Eq. 2.27 [9]; since the approach speed of An-74 is 180 km·h^{-1} (Table 1.1), the stall speed is 38 m·s^{-1}. The stall speed is taken as the reference speed during the analysis. In principle, the speeds considered during landing and takeoff are in the range $V_{approach} - 0$ and $0 - V_{LOF}$ respectively. However, as a reference value, the stall speed is used.

$$V_s = \frac{V_{approach}}{1.3} \tag{2.27}$$

According to aerodynamics theory, generally α increases when the flying velocity decreases; this way, a higher C_L causes more lift to be generated for a lower speed. Since both $V_{approach}$ and V_{LOF} are higher than V_s, α related to V_s will be higher than the α at $V_{approach}$ and V_{LOF}. This discussion has the purpose to prove that the α at which approach descend and takeoff climb are performed correspond to lower values for α than the α at which separation occurs.

Secondly, an appropriate range considered for angle of attack during climb and landing is in the range $4° - 8°$ [50]. Therefore, in the design process, the following is set: $\alpha = 8°$. During ground run, $\alpha = 0°$; the aircraft is in horizontal condition, and since data regarding twist, dihedral, etc are unavailable, these values have been set to 0 degrees.

In theory, a certain speed corresponds to a certain α. This would mean that $V_{approach}$ and V_{LOF} also correspond to a certain α. However, due to limited availability of information on the An-74 (airfoil, flaps, ...), it was not possible to find a correlation between speed and α. Due to this reason, α was set to a reasonable value of $\alpha = 8°$.

Thirdly, it should be noted that the aircraft will need to be operational in a wide variety of operating conditions. Furthermore it is important to keep this in mind during the design process. However, in order to simplify the process standard sea level conditions will be considered. Thereafter, a sensitivity analysis will be made in order to examine how the different conditions affect the design. Since standard sea level conditions are considered, the following parameters are used: $\rho = 1.225$ kg·m^{-3}, $T = 288.15$ K, $p = 101325$ Pa, $\mu = 1.79 \cdot 10^{-5}$ Pa·s.

Fourthly, since both V_s and environment conditions are defined, it can be determined that M = 0.14.

Fifthly, the Reynolds number was calculated using Eq. 2.28. Since this is also a function of chord length, a range for Re was defined: $4.93 \cdot 10^6 < \text{Re} < 14.55 \cdot 10^6$. For simplifications, one value has been specified as a reference: $Re = 10 \cdot 10^6$.

$$Re_c = \frac{\rho V_s c}{\mu} \tag{2.28}$$

Finally, due to limited availability of data regarding An-74, the airfoil assumed is TSAGI12-IL (12% thickness). It is a typical airfoil used on Antonov aircraft.

2.3.2 Preliminary Design Strategy

During the design process, several design choices were made. These concern such things as the type (conventional VG, LPVG, ...) of VG placed on the wing, the location, ... This section concerns the main strategy involved in order to improve the STOL (Short Takeoff and Landing) performance. In following sections, the sizing and performance changes due to the addition of VGs, etc will be added.

At first, it is necessary to define what exactly is meant with improving STOL performance, and how this should be done. In order to minimize the ground run for both takeoff and landing, V_r (i.e. the speed at which the aircraft rotates and loses contact with ground) and V_s (i.e. theoretically the speed at which the aircraft is able to land) should be minimized respectively. Being able to operate at high values for C_L is advantageous in terms of reducing these speeds and thus requiring less runway length, both during landing and takeoff. During takeoff, drag should be minimized in order to reach V_r over a shorter distance. For landing, drag is actually beneficial in order to decelerate the aircraft quicker.

Configuration of VGs

Vortex generators are particularly useful for separation alleviation. There are two configurations where they are particularly useful:

1. The separation of the flow over a clean wing is located very close to TE (99% of the chord length), even at relatively high values for α. However, if the flaps are extracted, the separation point moves considerably forward to ∼50% of the flap chord length. Langley Center carried out an investigation placing VGs at 25% of the flap chord length, thereby re-energizing the boundary layer and delaying the separation point. By delaying the separation point, the lift generated increases whereas the drag decreases. Furthermore, separation alleviation due to VGs placed on the flaps causes a global effect on the flow over the entire wing due to the enhanced circulation effect: VGs increase the suction pressure on the upper surface of the complete wing (slat, wing and flaps). Due to the narrowing of the downstram wake, the generator-induced attached flow increases performance significantly, certainly for $\alpha = 8°$: C_L is increased by ∼10%; C_D is reduced by ∼50%; L/D is increased by ∼100%. Furthermore, it should be noted that VGs do not affect $C_{L_{max}}$. [50]

2. VGs are placed at 20%-30% of the local chord length. It is shown [51] that, for low Re applications ($500 \cdot 10^3 < \text{Re} < 2.0 \cdot 10^7$), the transition point on the upper surface of the wing could be moved from 75% to 85% of the local chord length. Extending the transition point is useful in order to increase the extent of the laminar boundary layer, which causes lower drag than the turbulent boundary layer. By using analogies, one can assume similar effects for higher Reynolds numbers, in the order of $Re = 10 \cdot 10^6$.

For passive flow control devices, e.g. conventional VGs and LPVGs, this comes at the disadvantage of having additional drag due to the devices themselves. However, this drag increase is compensated for by the large performance increase caused by the VGs. Furthermore, if the VGs are fixed on the flaps, they can be stored when not in use.

This section is concluded by the design choice that will be further worked out to check the feasibility in the rest of the VG discussion. In Section 2.3.8, conclusions will be drawn based on the worked out design and a final design is proposed. The design that will be examined is the following: on the two inboard wing sections (Figure 2.17), VGs are placed at 25% of the flap chord length. This ensures that during landing, when the Fowler flaps are almost completely extracted, VGs are exposed to the airflow. During the takeoff roll, drag is the most important factor to

consider. It is common practice to have the flaps extracted less than during landing, hence not exposing the VGs and not having the VGs' device drag.
Furthermore, during the ground roll $\alpha = 0°$; in this condition, separation alleviation is not important to consider, since it only occurs at higher values for C_L. In case high climb rates and steep paths are required after takeoff, higher values for α and C_L are needed. In this case, the flaps can be extracted to the landing configuration after takeoff, so the VGs are exposed to the airflow. By using this principle of changing the flaps from takeoff configuration (during takeoff roll; low drag) to landing configuration (after takeoff; higher C_L, higher drag), one can combine STOL capabilities with high climb rates and steep paths.
Over the two inboard wing sections, VGs will be placed at 20% of the local chord length. These will be exposed to the airflow continuously, thereby extending the transition point and reducing drag. These are particularly useful during the takeoff run.
On the outboard wing section, no flaps are placed. Using a Javafoil analysis of the clean wing, it is found that the separation point is already close near the TE. Furthermore, it is unknown whether the aircraft has negative twist; however, if negative twist is applied on the original aircraft, the inboard sections will stall first. It is also true that VGs close to the tip will either:

- be very small (order of $1/10^{th}$ of a mm), which will cause high production costs; or
- if VGs are set to a minimum value for h, they will cause relatively large drag

It is thus not a good idea in terms of performance and cost, to place VGs at the outboard wing section.
To summarize: over the two inboard wing sections, there are 2 rows of VGs; at 20% of the wing chord and at 25% of the flap chord. On the outboard section, there are no VGs.

Type of VGs

In Section 1.3.9, the choice was made to use passive flow control devices. At this point of the design, two additional choices concerning the type of VG need to be made: at first, it will be explained whether conventional or micro vortex generators will be used. Secondly, the particular type will be selected. For this section, research and experimental data from the Langley Center [50] has been used.

Conventional VGs (CVGs) have a height (h) which is approximately equal to the height of the boundary layer (δ): $h/\delta \sim 1$. The other type considered is Micro VGs (MVGs), also referred to as Low-Profile VGs (LPVGs), which have a device height in the range $h/\delta \sim 0.2$ to $h/\delta \sim 0.5$. The main purpose of VGs is to reduce the separation distance as much as possible. This can be done by two means:

- delay the separation point
- reduce the reattachment distance

The total effect on the separated region is shown in Figure 2.14 (a) for the various types of VGs. From this figure, it is clear that both the CVGs and MVGs vane-types affect the separation similarly. MVGs are as effective in delaying the separation distance as CVGs. This does not mean that both are as efficient. Experiments carried out show that the highly 3D nature of the flows, as well as pockets of recirculating flow, indicate that vortices produced by CVGs are stronger than necessary. MVGs generate vortices, small enough to avoid separation; no excessivly strong vortices are generated, and there are hardly any packets of recirculating flow as a result.
Possible disadvantages of MVGs include the cost of manufacturing. In case a MVG is used with $h/\delta = 0.2$, VGs will need to be manufactured with dimensions in the order of $1/10^{th}$ of a mm; it is possible to make these, however the manufacturing cost will be high.
To summarize, it is examined that MVGs with $h/\delta = 0.2$ are as effective, but produce less drag when compared with CVGs. However, they are more difficult and expensive to manufacture. As a result, it has been chosen to set $h/\delta = 0.5$; this is also the suggestion of [51]. It combines reasonable values for drag, good performance and relatively easy manufacturing.

The two main types of vane-type VGs are shown in Figure 2.14 (b). As co-rotating and counter-rotating vanes are both valid options, there is opted for the counter-rotating vanes. This is due to the fact that these are most commonly applied in real aviation and thus will lead to lower manufacturing costs.

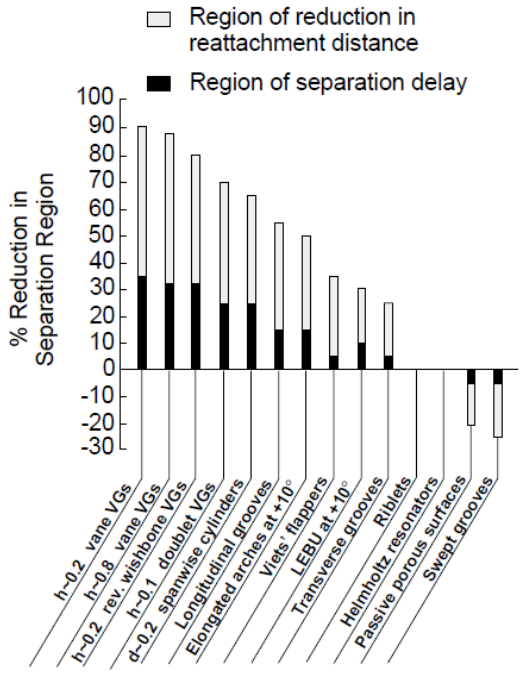

(a) Types of vortex generators and effect on separation region [50]

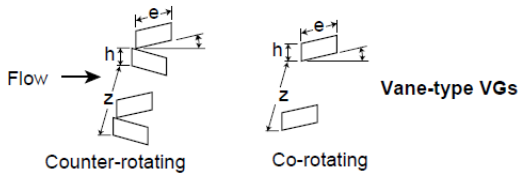

(b) Types of vane-type vortex generators [50]

Figure 2.14: Types of vortex generators

2.3.3 Detailed Sizing

Boundary Layer Thickness

Based on a Javafoil analysis, the boundary layer thickness of the flapped airfoil was determined. It is shown in Figure 2.15. At 20% chord the boundary layer thickness is 0.8 mm per m chord length and on the flap at 85% chord the thickness is 5.1 mm per m chord length.

Device Height

In principle all devices (except those on the inboard section) will be unique. However, for the ease of manufacturing, the choice has been made to round the device height h to the nearest mm; e.g. if calculations show that $h = 1.3$ mm, it is rounded to $h = 1.0$ mm. One can argue that this will have an effect on performance (effectivity, drag, ...). However, as shown in Figure 2.14 (a), VGs with h in the range $h/\delta = 0.2$ to $h/\delta = 0.8$ are approximately as effective. When $h/\delta = 0.5$, there is thus some margin for rounding. The effective height of the devices is shown in Figure 2.16 (a).

Device Dimensions

As explained above, the device height h is known; it is possible to design the counter-rotating vanes. Every pair of vanes has the configuration as shown in Figure 2.16 (b). Device height h is defined per pair of devices. Based on these, the other dimensions are known.

Device Locations

In 1995, a VG study was carried out by ESDU [52] in order to find the optimal VGs. As these provide an efficient design, these parameters will be used in our design. For the values, see Table 2.10.
The exact locations on the wing for the VGs can be seen in Figure 2.17. Each cross or circle represents a pair of VGs, one toed-in vane and one toed-out. Furthermore, based on the aspect ratio of the vane vortex generator (A_v), it is possible to determine the planform area of the vane vortex generator, together with its reflection (S_v) by using Eq. 2.29.

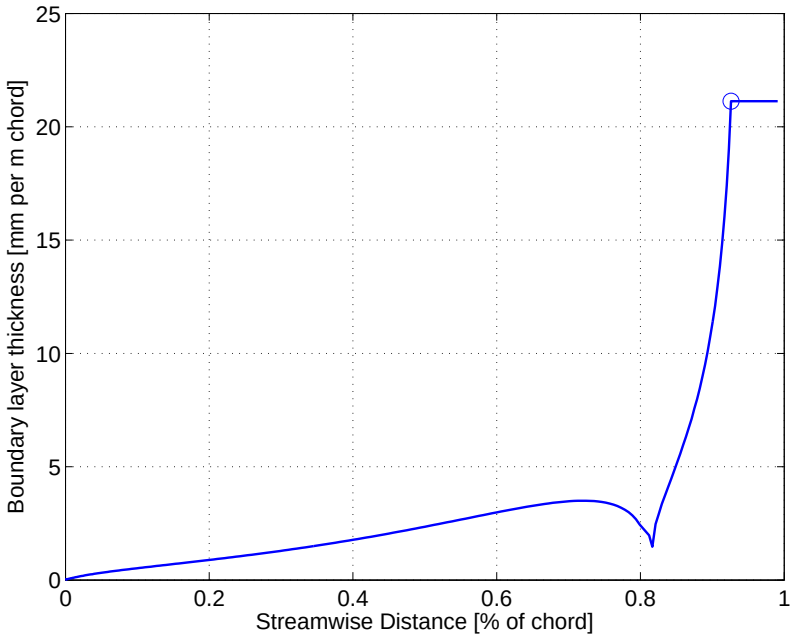

Figure 2.15: Thickness of boundary layer (flapped configuration)

Table 2.10: ESDU optimal vortex generator design parameters [52]

Property	**Value**
D/h	10
d/h	2.5
A_v	0.8

$$S_v = \frac{4h^2}{A_v} \tag{2.29}$$

In order to determine the angle of incidence of the VG relative to the stream direction (α_v), Figure 2.18 has been used. As defined in Table 2.10, $A_v = 0.8$. Due to the shape of the VGs used (Figure 2.16), the taper ratio $\lambda_v = 0°$. Furthermore, as determined for the VGs, $k_v = K/(hU_e)$ is close to 1. Based on these parameters, it can be determined that $\alpha_v = 30°$.

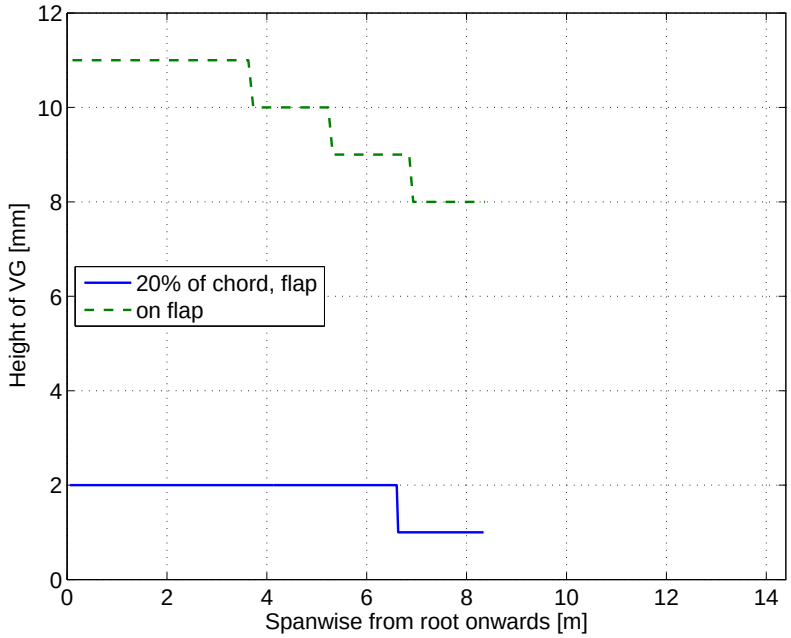

(a) Device height (flapped configuration)

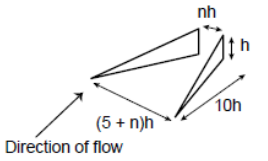

(b) Device dimensions [50]

Figure 2.16: Device height and dimensions

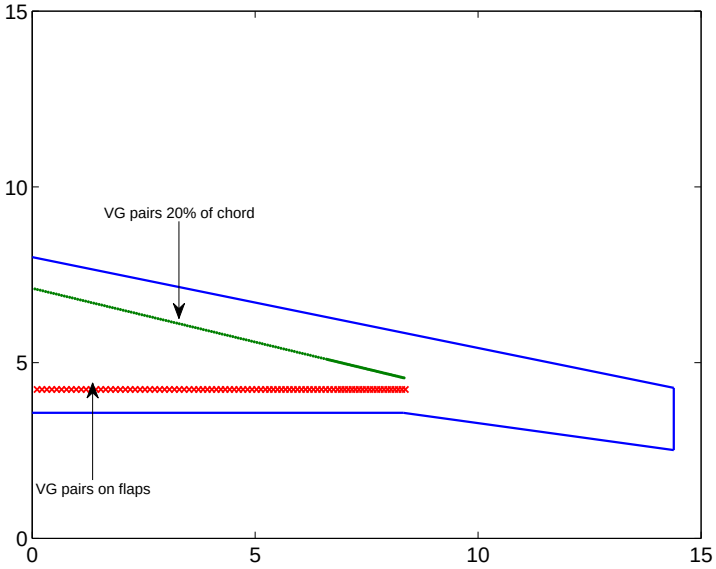

Figure 2.17: Location of vortex generators

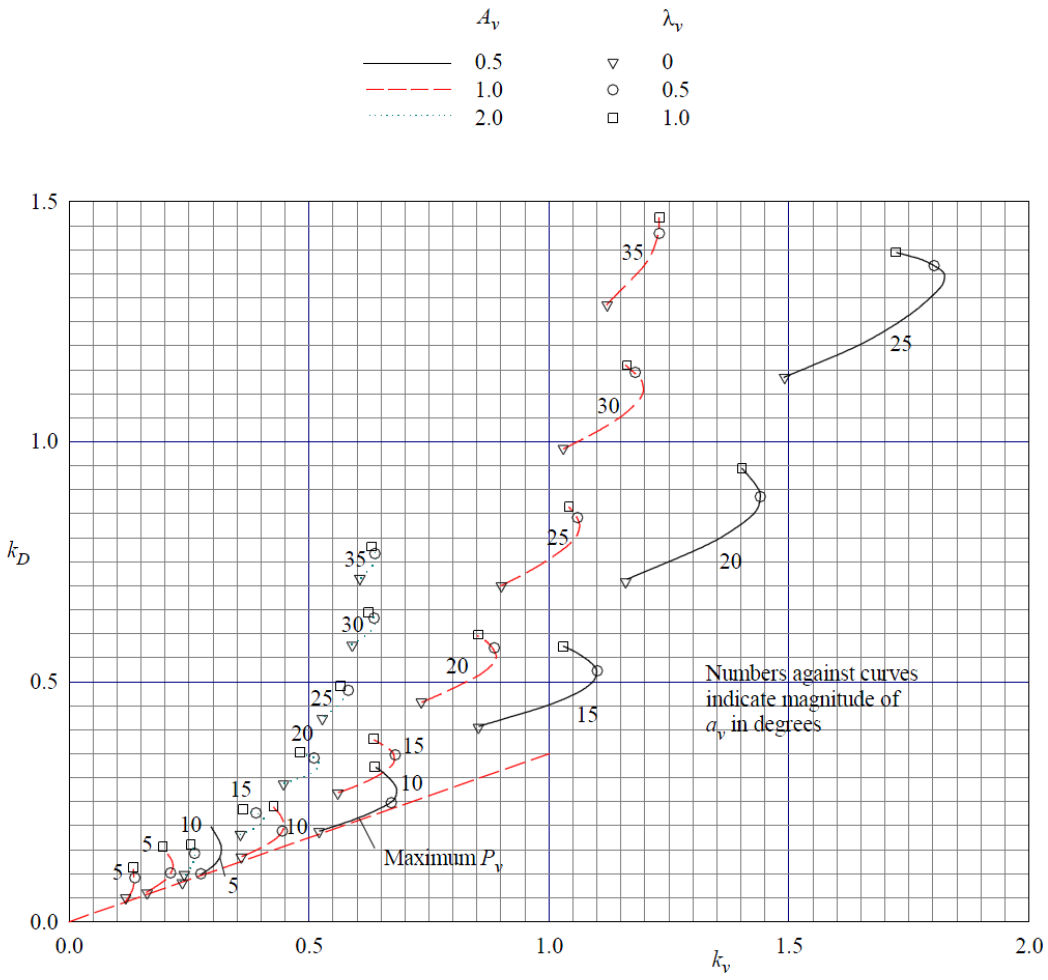

Figure 2.18: Correlation used to determine α_v [53]

2.3.4 Vortex Strength and Decay

In this section, vortex strength and decay will be determined. The latter part also includes the magnitude of the core radius as a function of the streamwise distance.

Vortex Strength

In order to determine the vortex strength, it is necessary to calculate the wall friction velocity, and the skin friction coefficient re-written in terms of velocity units. This is done by using Eq. 2.30, as mentioned in [54].

$$u_\tau = U_e \cdot \sqrt{c_f/2} \tag{2.30}$$

The boundary layer edge velocity (U_e) and skin friction coefficient (c_f) are derived using Javafoil data by plotting V/V_∞ and c_f for the flapped wing configuration in Figure 2.19. Considering that $V_\infty = V_s = 38$ m·s^{-1}, the results are summarized in Table 2.11.

Table 2.11: Input and output data concerning friction velocity calculations

VG Location/Property	V/V_∞ [-]	U_e [m·s^{-1}]	c_f [-]	u_τ [m·s^{-1}]
Flapped; $0.2 \cdot c$	1.80	68.4	0.0025	2.4183
Flapped; on flap	1.25	47.5	0.0014	1.2567

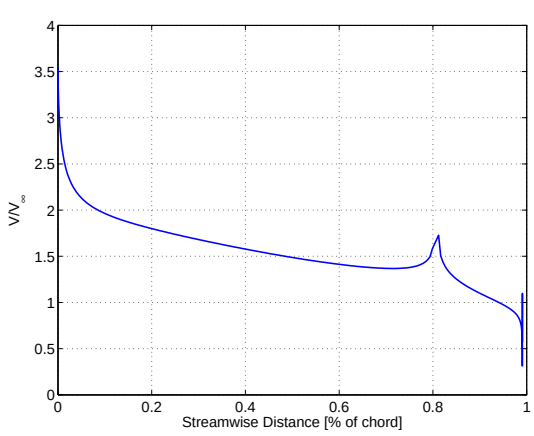

(a) Velocity ratios

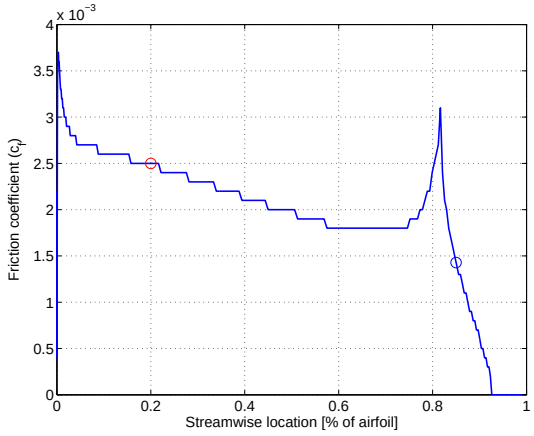

(b) Friction coefficient

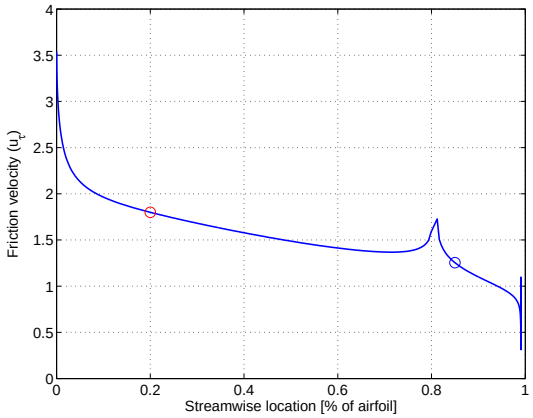

(c) Friction velocity

Figure 2.19: Airfoil properties (U_e and c_f) used to determine u_τ

Based on the two values of u_τ determined before, one can calculated the non-dimensional effective VG height (h^+) by using Eq. 2.31.

$$h^+ = \frac{u_\tau \cdot h}{\mu} \tag{2.31}$$

By combining the values for h with the appropriate values for u_τ, one can determine h^+ for each device. Langley Center [50] performed experiments and was able to find a good correlation between non-dimensional circulation and non-dimensional effective height (Figure 2.20 (a)). Air Force Research Laboratory [54] further elaborated on [50]; it was derived that, for counter-rotating vanes with $d = 2h$, $h/h_e = 1.55$. Even though $d = 2.5h$ in our design, the value for h/h_e for $d = 2h$ is thought to be a good approximation. It is the data with the black circle in Figure 2.20 (a). Based on this data, it is possible to plot non-dimensional height versus non-dimensional circulation (based on h instead of h_e), as in Figure 2.20 (b).

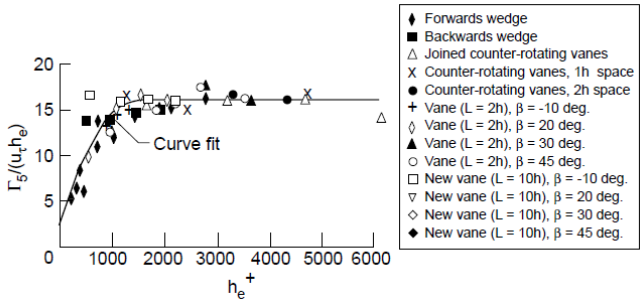

(a) Non-Dimensional circulation based on effective height versus non-dimensional effective height [50]

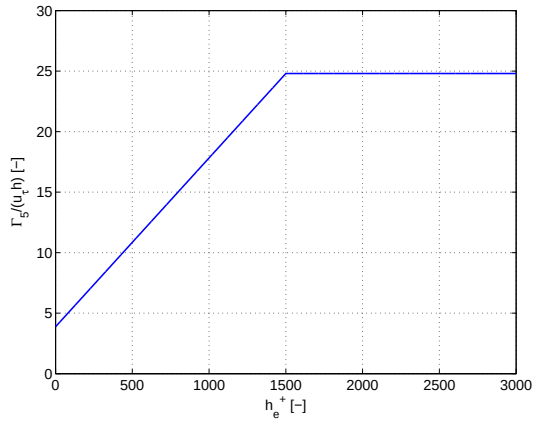

(b) Non-Dimensional circulation based on device height versus non-dimensional effective height

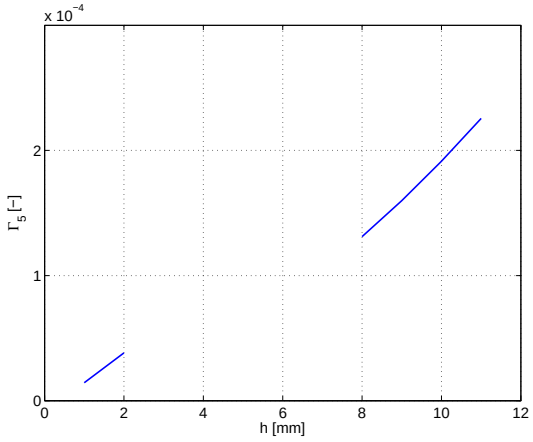

(c) Actual vortex strength

Figure 2.20: Determination of vortex strength at 5h downstream (Γ_5)

For every device, u_τ and h are defined. Using the correlation derived in Figure 2.20 (b), the vortex strength at 5h downstream the VG, shown as Γ_5 can be determined. As can be seen in Figure 2.21 (a), the decay during the first 5h can be neglected. Therefore, it can be assumed that the initial vortex strength is equal to Γ_5 as shown in Figure 2.20 (c).

Vortex Decay

The vortex created by a VG is very small directly behind the device. Further downstream, the vortices grow larger and larger and start to interact with neighbouring vortices. When the vortices of two neighbouring VGs overlap friction occurs and the initial strength of each vortex is reduced rapidly. The smaller the distance between the VGs, the more interaction between vortices. Besides the other vortices also the interaction with the main surface boundary layer, turbulence and pressure gradients cause dissipation. Variations in the stream velocity cause

disturbances in the vortices which leads to decay.
The dissipation of the vortex strength is given by Eq. 2.32

$$\frac{dK}{dx} = -\frac{kc_f K}{h} \tag{2.32}$$

Provided that the edge of the vortex does not touch the surface $k \sim 1.0$. Rewriting this equation and assuming that c_f and h vary only slowly with x gives a differential equation. Solving this equation results in Eq. 2.33.

$$\frac{K(x)}{K_i} = e^{\frac{-c_f(x-x_i)}{h}} \tag{2.33}$$

Using $K_i = 1$ the decay of the vortex strength can be assessed as a percentage of K_i. As can be seen in Figure 2.21 (b) the vortex decay is minimal for the first 11h. This had been validated with results from [50]. As can be seen in Figure 2.21 (a) the vortex decay of counter-rotating low-profile VGs is almost horizontal for the first 11h in streamwise direction for a spacing of 2h. The spacing of the VGs used for the Flying Hospitals is 2.5h. This means that there is a relatively large space for each vortex to extend before interacting with other vortices or the main surface boundary layer. That is why the vortices maintain most of their initial strength.

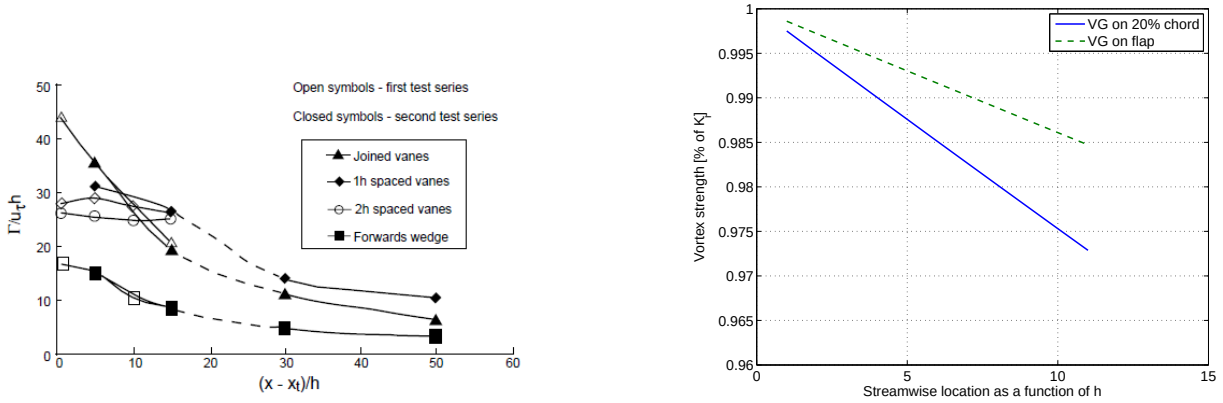

(a) Vortex strength up to 50 h downstream [50]

(b) Vortex decay as % of original vortex strength (K_i)

Figure 2.21: Vortex decay in streamwise direction

Core Radius

The radius of the core becomes larger as the vortices extend in streamwise direction. The radius of the core increases with x, the streamwise location on the wing. Eq. 2.34 gives the core radius for a vortex behind a MVG of height h. This equation can only be used prior to interaction with neighbouring cores.

$${r_c}^2 = 0.15h^2 + 4\left(\frac{\nu_E(x - x_i)}{U_e}\right) \tag{2.34}$$

In Eq. 2.34, ν_E is the effective kinematic viscosity which is related to the kinematic velocity. An appropriate value is $\nu_E = 35\nu$. There are more than 500 VGs on the wing thus calculating the increase of core radius for each VG would result in more than 500 plots. Therefore only the core radius of 4 VGs located at the root and towards the tip will be analyzed. Figure 2.22 shows the core radius at several locations of 4 VGs at the ends of the VG strips. It follows from Figure 2.22 that the radii of the VGs at the ends of the strip on the flap are the same. The radii VGs at the ends of the strip at 20% chord are also the same. This is probably because the heights of the two VGs on one strip are almost the same while the heights of the VGs on the 20% chord and those on the flap are different.

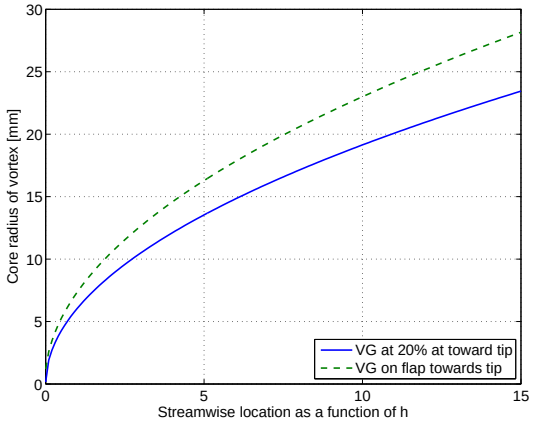

Figure 2.22: Core radius

2.3.5 Direct Drag Contribution of Vortex Generator Array

Since the VGs are fixed surfaces they will produce drag forces that contribute to the overall drag of the aircraft. C_D of each VG can be calculated and summarizing all these drag coefficients gives the total drag coefficient. The drag of an individual vane is given in Eq. 2.35. Whether the sign of the equation is positive or negative depends on the configuration of the vane. Toed-out requires the plus and Toed-in the minus.

$$\Delta D = D_v cos\sigma \pm L_v sin\sigma \tag{2.35}$$

Rewriting Eq. 2.35 using Eq. 2.38 gives Eq. 2.39 for each individual vane.

$$\Delta D = \frac{1}{2}\rho_\infty {U_\infty}^2 \delta C_D S \tag{2.36}$$

$$D_v = \frac{1}{2}\rho_e {U_e}^2 C_{D_v} \frac{S_v}{2} \tag{2.37}$$

$$L_v = \frac{1}{2}\rho_e {U_e}^2 C_{L_v} \frac{S_v}{2} \tag{2.38}$$

$$\Delta C_D = \frac{\frac{1}{2}\rho_e {U_e}^2 \frac{S_v}{2}}{\frac{1}{2}\rho_\infty {U_\infty}^2 S}(C_{D_v} cos\sigma \pm C_{L_v} sin\sigma) \tag{2.39}$$

The freestream density (ρ_∞) and the local density at the edge of the boundary layer (ρ_e) are assumed to be the same. Furthermore $C_{D_v} = A_v k_v/2$ and $C_{L_v} = \pi A_v k_v/4$ where $A_v = 0.8$ and $k_v = K/hU_v$. There are in total 172 vanes on a wing of which 86 are toed-in and 86 toed-out. The results are shown in Table 2.12. During landing both VGs on the flaps and VGs on 20% chord will be used. The flaps will only be extracted half during takeoff, such that the VGs are still inside the airfoil. In this configuration only the VGs on 20% chord will contribute to drag.

Table 2.12: Drag contribution

	ΔC_D one wing	ΔC_D total
VGs at 20% chord	0.0002	0.0004
VGs on flap	0.0012	0.0024
T.O. Configuration	0.0002	0.0004
Landing Configuration	0.0014	0.0028

The drag increase during landing caused by the VGs on the flaps is significant but it will not have a negative influence on the landing performance of the aircraft. Instead it slows down the aircraft. The drag increase during takeoff however is more important. The drag caused by the fixed VGs will act not only during takeoff and landing but also during cruise speed where it will not improve the performance of the aircraft.

2.3.6 Performance Effects due to Vortex Generators on Flap

During the descend and climb phase of landing and takeoff respectively, $\alpha = 8°$. During takeoff climb, high C_L is necessary to get high climb rates; during landing, high lift coefficients are used to reduce V_s; if C_L is increased in Eq. 2.40, V_s decreases. During the takeoff ground run, drag should be minimized and device drag is disadvantageous; during the landing ground run, drag is not an issue and helps slowing down the aircraft. Furthermore, separation occurs at the flap. The reasons mentioned above are all reasons that justify the placement of vortex generators on the flaps: they are relatively close to baseline separation, and can be stored in the wing in case they are not required and will not induce negative impact.

In this section, first the input and output of Langley Center [50] will be provided. Thereafter, the concept is applied on the aircraft and the effects will be discussed.

$$V_s = \sqrt{\frac{L}{\frac{1}{2}\rho C_L S}} = \sqrt{\frac{W}{\frac{1}{2}\rho C_L S}} \tag{2.40}$$

Literature Study on Vortex Generators on Flaps

As discussed in Section 2.3.2, Langley Center carried out a study concerning VGs where the devices were placed at 25% of the flap chord. Baseline separation occurred at 45% of the flap chord. For $\alpha = 8°$ it was found that lift is increased by $\sim 10\%$, drag is decreased by 50% and L/D is increased by $\sim 100\%$. [50]

In Section 2.3.2, it was decided to place VGs at 25% of the flap chord. This was due to the fact that the Langley Center study offered promising results, for a configuration that is highly similar to our situation. For the similarities, see Table 2.13.

Table 2.13: Similarities between experimental study [50] and design conditions concerning vortex generators placed on flaps

	Experimental Study	**Design Conditions**
α [°]	8	8
Re [-]	$9 \cdot 10^6$	$10 \cdot 10^6$
M_∞ [-]	0.2	0.15
VG Location [$\% \cdot c_{flap}$]	25	25
Baseline Separation [$\% \cdot c_{flap}$]	~ 45	~ 50

As explained before, the performance effect of the VGs will be based on literature data. Except for the actual airfoil being used (which is unknown for An-74), the study has several similarities. This makes it possible to use the outcome of the study in our design. Below, the results of this study are discussed.

The pressure distribution of both the baseline case (VG off) and the VG on case is shown in Figure 2.23 (a). It is clear that VGs on the flap cause an enhanced circulation effect, and by means of this they have a global effect on the flow over the complete wing. The generators increase the suction pressure over the complete configuration (slat + wing + flap), which causes a significant increase in lift. It is found that the wing, flap and slat contribute to $\sim 60\%$, $\sim 25\%$ and $\sim 15\%$ of the lift increase respectively. For $\alpha = 8°$, the total lift increase is $\sim 10\%$; during a ground run ($\alpha = 0°$), the lift increase is 5%. See Figure 2.23 (b).

When placing VGs on the wing (flaps), the devices cause a drag increase. However, they ensure separation is alleviated at moderate to high values for α. This may lead to the fact that there is a drag reduction for that range of α. This can be seen in Figure 2.23 (c); for moderate to large values of α, C_D is lower for the VG on case. However, the tendency of the curves shows that for $\alpha = 0°$ $(C_D)_{VG-on} > (C_D)_{VG-off}$. This is logical, since there is no separation (and thus not performance increase by placing VGs); however, there is the device drag. Since $\alpha = 0°$ during the takeoff ground run, it is common practice to not expose the VGs on the flaps during takeoff. This can be done by retracting the Fowler flaps such that the VGs are not exposed. In order to slow down the aircraft during the landing ground run, it is advised to expose the VGs to the airflow, hence generating additional drag.

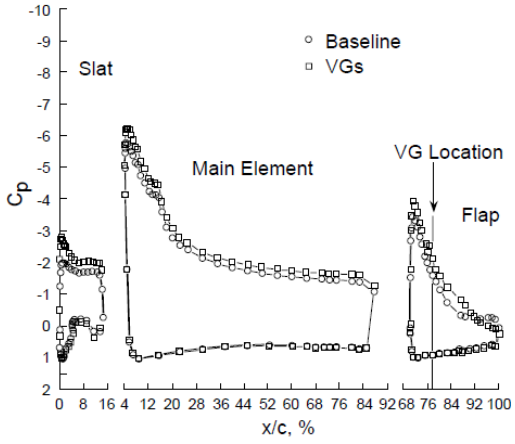

(a) Pressure distribution

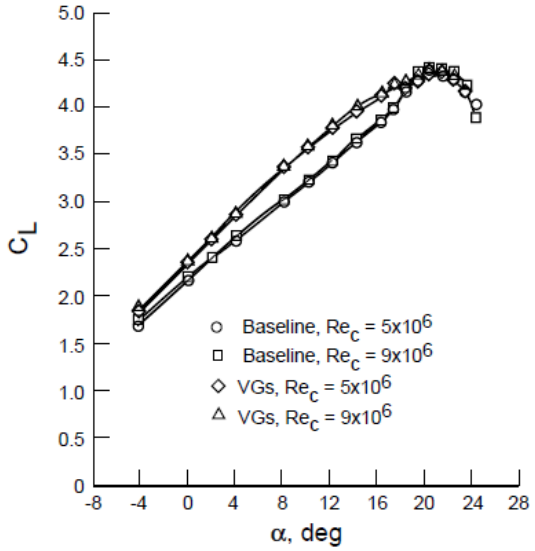

(b) $C_L - \alpha$ curve

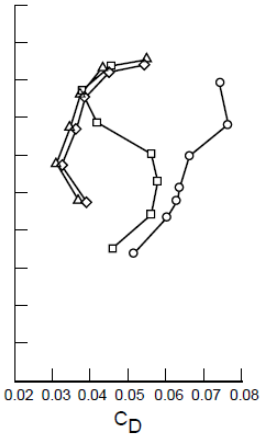

(c) $C_D - \alpha$ curve

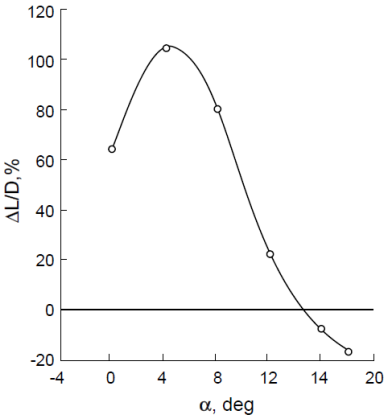

(d) L/D curve

Figure 2.23: Output of literature study on vortex generators on flaps [50]

Finally, the L/D ratio is increased by $\sim 100\%$, as can be seen in Figure 2.23 (d).

In case VGs are designed such that vortices produced are just strong enough to overcome baseline separation, full flow control is possible without generating too large vortices that cause drag. [50]

Concept Application on Aircraft

Due to the fact that the VGs are placed on Fowler type flaps at 0.2·c, it is possible to expose and store them when needed such that the ground run can be minimzed. During the takeoff ground run ($\alpha = 0°$), drag should be minimized; during landing ground run ($\alpha = 0°$), drag should be maximized. During both the climb phase of takeoff and descend phase of landing, $\alpha \sim 8°$.

It is thus common practice to ensure that the VGs are exposed during the complete landing phase to alleviate separation during the descend phase, and to maximize drag during the ground run. During takeoff climb, they can be exposed to increase climb rates.

The effect of the devices on the complete aircraft will be discussed in Section 2.3.8. At first, it is necessary to determine the effect of the VGs on the part they influence, i.e. the two inboard wing sections. The results are

summarized in Table 2.14. Note that device drag (for the VG devices on the flaps only) was determined in Section 2.3.5.

Table 2.14: Effect of vortex generators on flaps during takeoff and landing

	α	VG Position	Alleviation Alleviation	Drag	Lift
TO Ground Run	0°	Not exposed	No	Base Ground Run	Base Ground Run
TO Climb	8°	Exposed	Yes	Base $\alpha = 8°$ - 50%	Base $\alpha = 8°$ + 10%
Landing Descend	8°	Exposed	Yes	Base $\alpha = 8°$ - 50%	Base $\alpha = 8°$ + 10%
Landing Ground Run	0°	Exposed	No	Base Ground Run + Device Drag (Δ_{C_D}=0.0028)	NA

2.3.7 Performance Effects due to Vortex Generators on Wing

In Section 2.3.2, it was stated that VGs were placed at 0.2·c on the two inboard sections. A study carried out by [51] showed that the upper surface laminar flow can be extended by 10% for $500 \cdot 10^3 < \text{Re} < 2.0 \cdot 10^6$ in case VGs are placed in the between 0.2·c and 0.3·c. In case the laminar flow is extended, drag is reduced since a laminar boundary layer causes less drag than a turbulent boundary layer. This would be very useful during takeoff, where drag minimization is important in order to minimize the ground roll.

The VGs will be placed on the upper surface of the wing, and will be there continuously generating drag. It should thus be ensured that the drag decrease due to the enlarged laminar flow region is larger, in absolute magnitude, than the drag induced by the devices themselves. An iteration was performed that determined both the direct device drag of the fixed devices (Section 2.3.5), as well as the drag reduction due to extent of laminar boundary layer (see calculation below). After the iteration, it was found that the spacing of the VG pairs (D) needs to be increased from $D = 10h$, which was assumed in Table 2.10, to $D = 30h$.

When an analysis is performed in Javafoil, it is found that the transition point is at 0.01·c for the conditions described in Section 2.3.1. One might argue that VGs placed at 0.2·c will not have an effect in order to move the transition point to 0.04·c. However, using the analogy of the VGs placed on the flap, it is assumed to be achievable. In case the VGs were placed on the flaps, there was a global effect over the entire wing due to the enhanced circulation effect. [50] The same effect is assumed to cause the transition point to move by 3% (0.01·c to 0.04·c), hence reducing the drag.

Since the spacing D increased by a factor 3, it is assumed that the laminar flow extent will not be 10% as shown in [51]. Therefore, it is assumed that the transition point is delayed by 3% of the chord length.

To summarize: due to the vortex generators located at 0.2·c on the two inboard sections, it is thought that the transition point moves from 1% to 4%. This would include a drag reduction, since a laminar boundary layer causes less drag than a turbulent boundary layer. D has increased from $D = 10h$ to $D = 30h$, such that the drag reduction due to the laminar flow extent would exceed device drag. In this section, a first approximation is made by doing a 2D friction drag estimate. The airfoil is idealized as a flat plate at $\alpha = 0°$. The zero angle of attack approximation is realistic for takeoff conditions. Pressure drag and induced drag should be added as well in order to come up with the exact value; however, since the analysis concerns the effect of the boundary layer, skin friction drag is calculated.

Methodology

The principle is the following: until the transition point x_{tr} (Figure 2.24), the flow is laminar (region A). From that point onwards, the boundary layer becomes turbulent (region B). However, region C is now counted for double. The total friction drag is the following:

$$D_{f,total} = D_{f,A} + D_{f,B} - D_{f,C} \tag{2.41}$$

For the calculations, the wing is split up in several sections. Every section has a reference chord length (c) and a width (w). Based on these values, various calculations were performed. The more sections, the more the solution

will converge to the actual solution.

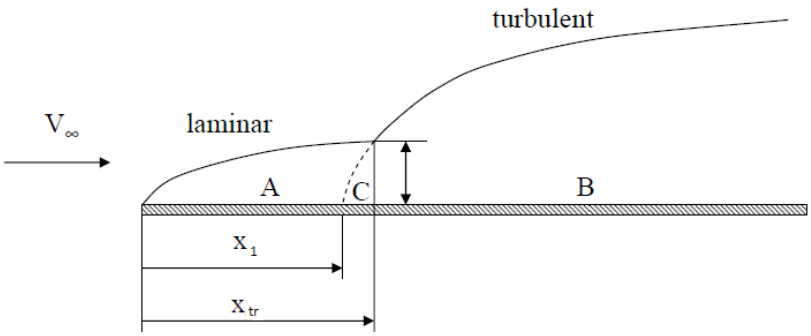

Figure 2.24: Flat plate under $\alpha = 0°$ for drag reduction calculations [55]

The formulas needed for this approach were found in Anderson [26]. For Laminar Boundary Layers, the boundary layer thickness and friction coefficient can be determined by using Eq. 2.42 and Eq. 2.43 respectively.

$$\delta = \frac{5x}{\sqrt{Re_x}} \tag{2.42}$$

$$c_f = \frac{1.328}{\sqrt{Re_c}} \tag{2.43}$$

Turbulent Boundary Layer thickness and friction coefficient can be calculated using Eq. 2.44 and Eq. 2.45 respectively.

$$\delta = \frac{0.37x}{(Re_x)^{0.2}} \tag{2.44}$$

$$c_f = \frac{0.074}{(Re_c)^{0.2}} \tag{2.45}$$

Case 1: 1% Laminar Flow

At first, the baseline case is considered where transition occurs at 1% of the local chord length; this thus means that $x_{tr} = 0.01 \cdot c$. The parameter x_1 is determined based on the property that at this point the laminar and turbulent boundary layer have the same thickness:

$$\begin{aligned} \delta_{lam} &= \delta_{turb} \\ \frac{5 \cdot 0.01c}{\sqrt{Re_c}} &= \frac{0.37 \cdot (x_{tr} - x_1)}{(Re_c)^{0.2}} \\ x_1 &= x_{tr} - \frac{5 \cdot 0.01c}{\sqrt{Re_c}} \frac{(Re_c)^{0.2}}{0.37} \end{aligned} \tag{2.46}$$

For region A, the friction coefficient is calculated using Eq. 2.43 where Re_c:

$$Re_c = \frac{\rho V_s 0.01c}{\mu} \tag{2.47}$$

The dynamic viscosity μ and density ρ are set to the sea-level standard values $\mu = 1.79 \cdot 10^{-5}$ Pa·s and $\rho = 1.225$ kg·m^{-3}. The velocity used in the calculations is the stall speed $V_s = 38$ m·s^{-1}.

One $c_{f,A}$ is determined, it is possible to determine $D_{f,A}$ by using Eq. 2.48:

$$D_{f,A} = c_{f,A}\frac{1}{2}\rho {V_s}^2 0.01cw \tag{2.48}$$

Since the wing is split up in multiple section, c and w are the sectional chord length and width respectively.

For region B, the same principle is used as for region A. The main difference is the fact that c_f for the turbulent boundary layer is used (Eq. 2.45); moreover, Re_c is now defined as in Eq. 2.49:

$$Re_c = \frac{\rho V(c - x_1)}{\mu} \tag{2.49}$$

Based on $c_{f,B}$, one can determine $D_{f,B}$ using Eq. 2.50.

$$D_{f,B} = c_{f,B}\frac{1}{2}\rho {V_s}^2 (c - x_1)w \tag{2.50}$$

For region C, the friction coefficient is calculated using Eq. 2.45, where Reynolds number is determined using Eq. 2.51. The friction drag coefficient for region C is then obtained by using Eq. 2.52

$$Re_c = \frac{\rho V(0.01c - x_1)}{\mu} \tag{2.51}$$

$$D_{f,C} = c_{f,C}\frac{1}{2}\rho {V_s}^2 (c - x_1)w \tag{2.52}$$

Total friction drag can now be determined using Eq. 2.41. Furthermore, since there are two wings, the result should be doubled.

If the wing (2 inboard sections) is subdivided into 100,000 sections, $D_{f,total} = 176$ N.

Case 2: 4% Laminar Flow

The same reasoning can be followed for the 4% laminar flow; for the calculations, $x_{tr} = 0.04 \cdot c$. The laminar flow region is extended due to the vortex generators placed at $0.2 \cdot c$.

If this particular case is worked out, it is found that $D_{f,total} = 174$ N.

Comparison and Discussion Results

Based on the results as described above, it is clear that there is a reduction in skin friction drag from 176 N to 174 N. It is equivalent to 1.47% decrease in skin friction drag for the two inboard wing sections.

In order to check whether this is a reasonable value, Eq. 2.53 is used. C_d is set to 0.01; according to Javafoil, this is a reasonable value for the TSAGI airfoil used.

$$\begin{aligned} D &= c_d\frac{1}{2}\rho {V_s}^2 S \\ D &= 0.01 \cdot \frac{1}{2} \cdot 1.225 \cdot 38^2 \cdot 98.53 \\ D &= 1508\, N \end{aligned} \tag{2.53}$$

It is found that the calculated skin fraction drag is approximately one eighth of the 2D drag calculated using c_d. This can be explained by the fact that skin fraction drag is not the only contributing factor to the calculation.

The authors also had contact with experts within Delft's Faculty of Aerospace Engineering concerning the critical assumption that, at high Reynolds numbers, the transition point is moved by 3%. It is true that a laminar flow is more difficult to maintain in case of high Reynolds numbers, like the Reynolds numbers experienced at speeds around V_s. The boundary layer is more susceptible to transition due to contamination, dirt, precipitation, etc.

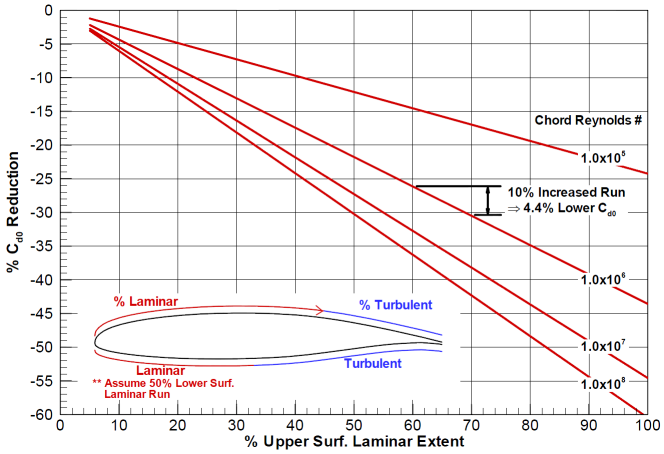

Figure 2.25: Correlation reduction in c_{d0} with increasing laminar flow extents [51]

However, the effect is not completely quantified. During takeoff, the Reynolds number will vary from $Re = 0$ (start of takeoff; $V = 0$ m·s^{-1}) to $Re = 14.55 \cdot 10^6$ ($V_s = 38$ m·s^{-1}; Re at root). The analysis is performed for $Re = 10 \cdot 10^6$, as stated in the design conditions in Section 2.3.1.

There were some doubts whether it is really feasible to move the transition point at high Reynolds number. In those cases, the transition point is very close to LE, as confirmed by Javafoil. Other sources, like [51] published a correlation between the laminar extent of the upper surface and the corresponding reduction in c_{d0}. This relation is shown in Figure 2.25. The Reynolds number for the case examined is set to $Re = 10 \cdot 10^6$, as derived in Section 2.3.1. For this linear relation and for that specific Reynolds number, it can be derived that a 10% increased run covers a $\sim$ 5% reduction in c_{d0}, which is $\sim$0.5% drag decrease per 1% extent of laminar flow. This result is similar to the result of the friction drag calculations before. There, a 3% laminar flow extent caused a 1.5% reduction in friction drag. Some sources claim it is feasible to delay the transition point. For further analysis, it is assumed to be possible. However, the authors advise further investigation concerning this subject in order to determine whether it is actually feasible to delay the transition point at high Reynolds number.

Concept Application on Aircraft

The VGs placed at 0.2·c are exposed continuously to the air. This has the disadvantage that device drag is always present. In Section 2.3.5, it is found that the device drag for the devices at 0.2·c is $\Delta_{C_D} = 0.0004$, in case these are spaced $D = 30h$. When comparing this value of Δ_{C_D} with an average C_D value of an aircraft ($C_{D_{average}} \sim 0.030$), there is an increase of 1.35% in drag coefficient.

Due to the delay of the transition point from 0.01·c to 0.04·c, the drag reduction is 1.47%. This reduction is only achieved where the VGs are located, i.e. only the two inboard sections. Based on these calculations, the net effect would thus be a drag increase, which is unwanted and thus leads to the conclusion that this option should not be considered further in this report. The authors of this report however believe in the concept; according to [51], it is possible and offers promising possibilities. Probably, the analysis using correlations and experimental testing data is not accurate enough to determine the relatively small positive/negative performance changes. Since it was not possible to determine the actual effect of the VGs at 0.2·c, it will not be further considered in the remainder of the report as a modification of the original aircraft. However, it must be emphasized that it is a feasible option, which will need to be analyzed further.

As a final note, it should be noted that only friction drag (c_{d0}) has been considered in this analysis. According to Eq. 2.54, induced drag should be considered as well. By extending the transition point, friction drag reduces; induced drag remains similar. As shown before, the friction drag reduction is already smaller than the increase due to device drag, making the application inefficient according to the calculations. Since induced drag is not affected by the devices, the efficiency does not change either.

$$c_d = c_{d0} + \frac{{c_l}^2}{\pi A e} \tag{2.54}$$

2.3.8 Overall Performance Changes due to Vortex Generators

The configuration that will be used for the remainder chapter of the report:

- vortex generators are placed at $0.25 \cdot c_{flap}$ on the two inboard wing sections (Section 2.3.6)
- vortex generators at 0.2·c on the two inboard wing sections are not applied on the aircraft (Section 2.3.7)
- a total of 344 micro vortex generators divided over two wings

Based on the performance calculations performed in Section 2.3.6 and Section 2.3.7, the overall performance on the aircraft due to the vortex generators will be summarized.

In order to improve the STOL performance, V_s, V_r and the takeoff and landing ground run should be minimized. The performance improvements for the wing are summarized in Table 2.15. For further analysis, it is required to determine the actual improvement on the complete aircraft. As the wing is only part of the aircraft, the lift increase and drag reduction will thus be smaller, in absolute value, than the improvements for the wing only. In order to come up with results for the complete aircraft, it is assumed that the wing lift contributes 90% to the total lift. Furthermore, it is assumed that wing drag contributes 75% of the total aircraft drag.

Table 2.15: Aircraft performance changes due to vortex generators

	α	VG Position $0.25 \cdot c_{flap}$	Lift increase Wing	Drag Reduction Wing	Lift Increase Aircraft	Drag Reduction Aircraft
TO Ground Run	0°	Not exposed	0%	0%	0%	0%
TO Climb	8°	Exposed	10%	50%	9%	37.5%
Landing Descend	8°	Exposed	10%	50%	9%	37.5%
Landing Ground Run	0°	Exposed	NA	NA	NA	NA

2.3.9 Manufacturing and Materials

The manufacturing and material cost for VGs is relatively low. VG install kits for small, homebuilt aircraft are easily available. They can be made from aluminium [17] or polycarbonate [56] and can be manufactured seperately in pairs or on long strips. Figure 2.26 shows an example where the VGs are mounted to the wing in pairs.
One way to fit the wing with VGs would be to use polycarbonate as material. The advantage of polycarbonate is that it is light and flexible while aluminium is heavier and sharp. Since the height of the VGs is in the order of a few millimeters the manufacturing process should be very precise. Polycarbonate is a suitable material for 3d printing but it can also be manufactured using a mold. The main drawback of using polycarbonate is that it is expensive; making a mold and operating the printer is also very expensive. The alternative, aluminium, is more attractive since it is still reasonably light and cheaper than polycarbonate.
From the choice of material follows the weight of the VGs. Aluminium has a density of 2700 $kg \cdot m^{-3}$. The volume of the VGs can be calculated using the surface area of the VGs and taking the thickness as being 1 mm. The resulting weight is 446.4 g for two wings.
The cost of an aluminium sheet is approximately €20 [57]. Thus material costs are relatively low. The total costs of the MVGs however are very high. Besides the manufacturing costs there are also the certification costs. Even for small aircraft getting the VGs certified by the FAA will cost between €180,000 and €375,000 [58]. This is partly due to requirement of the FAA that the flight tests have to be repeated after installation of VGs. For the large Antonov, a preliminary cost estimation would be €400,000.

2.3.10 Sensitivity Analysis

The vortex generators were designed using real-life correlations; based on those, it is possible to perform a sensitivity analysis. Several parameters that have an influence on the performance will be investigated: VG dimensions, VG type, VG spacing and VG location. In Table 2.16, the sensitivity analysis is summarized.

Figure 2.26: Example of vortex generators in pairs on wing [59]

Table 2.16: Vortex generator sensitivity analysis - 5: very high sensitivity; 1: very low sensitivity

Parameter	**Sensitivity**
VG Dimensions	4
VG Type	4
VG Spacing D	3
VG Spacing d	5
VG Location	4

VG Dimensions

As you may have noticed, the VG sizing was based mainly on the height h, defined as a function of the local boundary layer thickness: h/δ. If this parameter changes, the dimensions of the complete VGs change.

The general rule for VG height is as following: the larger the device, the higher the vortex strength. This is however associated with a drag increase. Smaller devices are more difficult to manufacture, but the direct device drag is smaller. However, they must be located more accurately on the wing, since the vortex strength is smaller and the effectiveness region is also smaller.

It is clear that the dimensions do affect the performance. In the original design, it is chosen that $h/\delta = 0.5$. There is however a range in dimensions for which device drag and effectiveness are similar, i.e. from $h/\delta \sim 0.35$ to $h/\delta \sim 0.75$. If the devices are larger, device drag becomes an issue. For smaller devices, the location must be determined exactly in order to ensure effectiveness. Furthermore, dimensions will be in the order of 0.1 mm, making production expensive.

Based on the discussion above, it is thought that performance of VGs is very sensitive to its dimensions. However, since there is a range in which the performance is relatively similar, it does not receive the highest grade in terms of sensitivity.

VG Type

As became clear from Figure 2.14 (a), there are various types of vortex generators. It is clear that devices generating transverse vortices, e.g. spanwise cylinders, LEBU and elongated arches at $+10°$, are less effective than the CVGs and LPVGs. [50]
VG type thus plays an important role when considering the performance of VGs. There is however a range of VGs (CVGs and LPVGs) that have similar performance.
Performance is thus highly sensitive to the type of VG used. Since there is a range of VGs available that score similar, it does not receive the highest grade.

VG Spacing

Spacing, and thus the amount of VGs placed on the wing, influences the total performance change due to the VGs. The less VGs, the lower the direct device drag. However, the effectiveness of the system goes down.

In Section 2.3.3 (Table 2.10), the spacing D was determined based on literature data. It is thought that increasing or decreasing this value indeed affects the performance of the system. However, it is thought that a small change in D will not largely affect the performance and vice versa. For this reason, performance is thought to be reasonable sensitive to D.

Note that, since there is opted for the counter-rotating vanes, there is a pair of VGs. The spacing between the two elements of each pair (d) is crucial; if chosen too low or too large, the effectiveness decreases due to vortices cancelling each other out, too high or low vortex strengths, etc.

VG Location

LPVGs need to be placed accurately in terms of streamwise location on airfoil, in order to ensure that they maintain their effectiveness. CVGs are less sensitive to the exact location, since they generally generate too large vortices and their effectiveness further downstream is larger. The smaller the VGs chosen, the more sensitive the location becomes.

Since there is chosen for LPVGs with $h/\delta = 0.5$, the streamwise location on the wing is not crucial but needs to be chosen appropriately in order to maintain effectiveness.

2.3.11 Verification and Validation

The verification and validation of the VGs has to be done according to the definitions given by AE3205-11. For the verification of the MATLAB model an analytical analysis can be carried out. By calculating the parameters, dimensions and location of one device by hand and comparing them to the outcome of the program the MATLAB model can be verified.

A convenient device would be the one at the root at 20% chord. Table 2.17 shows the input at this point.

Table 2.17: Input for device at root, 20% chord

Property	**Value**
Boundary layer thickness [m]	$8.8705 \cdot 10^{-4}$
Chord length [m]	4.430
Ratio h/δ [-]	0.5
u_τ [m·s^{-1}]	2.4183
μ [kg·(s·m)$^{-1}$]	$1.79 \cdot 10^{-5}$
Non-dimensional Γ^* [-]	7.6443
c_f [-]	0.0025
ρ [kg·m^{-3}]	1.225
U_e [m·s^{-1}]	68.4
A_v [-]	0.8
U_∞ [m·s^{-1}]	38
S [m^2]	20.1
k_v ($\frac{\Gamma \cdot U_e}{h}$) [-]	1.3072

The first thing to calculate is the heigh of the vane with Equation 2.55.

$$\begin{aligned} h &= \delta \cdot ratio \cdot chordlength \\ &= 8.8705 \cdot 10^{-4} \cdot 0.5 \cdot 4.43 \\ &= 1.96 \cdot 10^{-3}\, m \end{aligned} \tag{2.55}$$

$$\tag{2.56}$$

For simplicity during manufacturing the value of 1.96 mm has been rounded to 2.00 mm. With the device height h^+ and the vortex strength Γ can be calculated using Eq. 2.31 and Eq. 2.58.

$$h^+ = \frac{2.4183 \cdot 0.0020}{1.79 \cdot 10^{-5}} = 268.15 \tag{2.57}$$

$$\begin{aligned} \Gamma &= \Gamma^* \cdot c_f \cdot h \\ &= 7.6443 \cdot 0.0025 \cdot 0.002 = 3.822 \cdot 10^{-5}\, m^2 \cdot s^{-1} \end{aligned} \tag{2.58}$$

The value for Γ is the same as the output of the program but the value for h^+ is 270.20.

The last property that will be verified is the drag coefficient. It will be calculated using Equation 2.39.

$$\Delta C_D = \frac{\frac{1}{2}1.22568.4^2 \frac{0.0020^2 \cdot 2}{0.8}}{\frac{1}{2}1.22538^2 20.1}(0.8 \cdot 1.307 cos(asin(\frac{1.307}{4\pi})) + \frac{\pi 0.8 \cdot 1.307}{4} \cdot \frac{1.307}{4\pi}) = 9.7581 \cdot 10^{-7} \tag{2.59}$$

The programs gives an output of $9.7598 \cdot 10^{-7}$.

To validate the VGs the chosen concepts can be compared to data from manufacturers that make VGs. A company called Micro Aerodynamics Inc [17] sells MVG-kits for small aircraft. On the website information can be found about the number of VGs on the wings and the performance improvements. The Antonov is larger than the aircraft for which the kits are provided. Nevertheless the site gives certain guidelines considering the performance improvement. For many aircraft V_s and V_r are reduced by 8% to 13%. For the Flying Hospital, the speeds are reduced by 5%-10%, which is within a similar range of the manufacturer's data.
The number of VGs installed on wings is approximately between 60 and 140 divided over 2 wings. Comparing this to the 344 VGs that will be installed on the Flying Hospital aircraft, these seem to be almost similar. Looking at the scale of wings, for the Lake LA-4-200 there's a kit with 138 MVGs divided over a wingspan of 11 meters. The Antonov has a wingspan of 31.89 m which is three times larger than the Lake. Considering that, the number of VGs on the Flying Hospital should be 414 which is relatively close to 344.

2.3.12 Recommendations

The study on VGs is concluded by giving some recommendations.

1. In general, it is advised to perform a CFD or analytical analysis in order to examine the effect of VGs in this specific case. In our study, literature data was used in order to size and determine the effect of VGs. Although this provides a very efficient way for performing a first study on this subject, it is advised to perform a CFD analysis in order to assess the performance more accurately. Also experimental wind tunnel tests would improve the understanding and would help determining the effectiveness of the VGs applied to this specific situation.

2. In Section 2.3.7, the reduction in drag of placing VGs at 0.2·c was determined based on the reduction in skin friction drag due to an extension of laminar flow. In order to get a more accurate result for drag reduction, it is advised to also take into account pressure drag and induced drag.

3. As studies at low Reynolds numbers have proven, the transition point can be delayed by placing VGs. The extent to which this can be done at higher Reynolds numbers was estimated in Section 2.3.7. However, the authors advise an extensive study in order to determine quantitatively the delay in transition point at high Reynolds numbers.

2.4 Structural Characteristics

A new type of engine will be used to improve the performance of the Antonov An-74. This engine can generate more thrust than the engine which is used in general, however will also increase weight. This section will analyze how the loads and stresses change due to the new engine and give a recommendation whether the structure needs modifications or reinforcements. The analysis in this section is divided in two parts. These parts cover the investigation of the loads and stresses on the wing and fuselage separately. Prior to the calculation of the loads and stresses, the assumptions used to simulate the structural behavior are stated. The wing and fuselage analysis is followed by the sensitivity analysis, the verification and validation of the methods used and recommendations for further detailed analysis.

2.4.1 Assumptions

In order to get a suitable simulation, which obtains appropriate results, a number of assumptions should be made in this stage of the design phase. Using these assumptions a general, simplified model of the real situation can be made, while the results can still be used to form a valid first conclusion with respect to the structure of the wingbox and fuselage. The assumptions are stated below and have been divided in primary assumptions (assumptions which have a direct and large impact on the solution) and secondary assumptions (assumptions which have an impact, but smaller than that of the primary assumptions).

Primary Assumptions Wingbox Model

- **The wingbox is thin-walled.** This is an important assumption, because it has multiple effects. The use of this assumption is justified, as the thickness of the spars is much smaller than the outer dimensions (height, width) of the wingbox. The first effect of this assumption is that higher order terms in the moment of inertia calculation can be neglected. However, it should be noted that deviations in the moment of inertia will have their effect on the normal and shear stress. Also, the thin-walled assumption ensures that the concept of shear flow can be used, which simplifies the calculations.
- **The engine is regarded as a point mass.** Due to the fact that the exact connection between the engine and the wing is unknown, transferring the weight of the engine to the wingbox structure is done as a localized point force. This implies that the weight of the engine appears as a dip in the shear force diagram and a kink in the bending moment diagram.
- **Drag forces on the wing structure are neglected.** Due to the fact that the airfoil is unknown and drag is dependent on the airfoil shape, determining the drag is not really possible this way. Thus, the shear force due to the drag is zero and no bending moment in chordwise direction is present, which implies that lower forces and stresses may be found. This is an important assumption, as every body moving through a medium creates drag.
- **Fuselage and wing tip effects on lift are neglected.** The fuselage and wing tips cause disturbances in the lift distribution, such as vortices, which complicate the analysis. While testing or flying the aircraft, the effects can not be neglected and may have a noticeable effect on the lift (and drag), so the assumption will give results that deviate from real life.
- **The lift force is assumed to act on the quarter chord line.** This ensures that the location of the lift is fixed on the wingbox geometry, which simplifies the equation for torsion. In real life, the lift results from the integral of the pressure difference over the airfoil, and therefore acts as a distributed load over the entire wing. So, a deviation in the torque with respect to real life can be seen due to this assumption.
- **The shear load due to lift can be decomposed into a torsion and shear component.** This assumption implies that the lift force can be decomposed into a shear force acting through the centroid of the cross-section and a torsion component due to the lift acting on the quarter chord line. The shear center of the wingbox lies very close to the centroid, which allows this approach. However, in real life, due to a asymmetrical wingbox or material imperfections which causes the wingbox to be more asymmetrical, there could be an error or the error could be larger than anticipated by analyzing the problem with this approach.
- **The overlap between two parts due to a sweep is neglected.** To simplify calculations, it is assumed that the wingbox in the swept parts continues until the half chord line reaches the connection of two parts at

the sweep. Therefore, a triangle-shaped segment of the wingbox is not analyzed. This part is illustrated in Figure 2.27. This approach is used for both sweep angles in the wingbox.

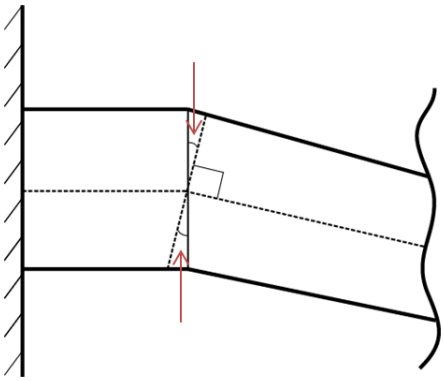

Figure 2.27: Parts at the sweep connection neglected by the simulation model, top-view

Secondary Assumptions Wingbox Model

- **When numerically calculating the loads on the wingbox, the wingbox is treated as a beam located at half chord.** This implies that the loads acting on the wingbox will be evaluated at half chord, which is of particular interest when considering torsion.
- **The wingbox is assumed to be symmetrical.** As the geometry of the wing and the cross-section of the wingbox is unknown, it is assumed that the wingbox has a symmetrical cross-section. The local curvature of the airfoil is neglected. This will simplify the calculations, but the model can still be used to give a percentage difference when different scenarios are analyzed. However, detailed real life results can not be obtained this way.
- **The taper angles are assumed to be small.** The governing equations include more errors when taper angles increase to large angles. For small taper angles a taper correction is enough to keep the error minimal. As the thickness of the wingbox varies with chord length, a taper is induced. However this will involve small angles, such that the equations are still valid. Since the actual geometry of the wingbox is unknown, and thus the taper angles due to the thickness can not be determined, it is hard to validate this assumption.
- **The material is isotropic.** The materials used in the wing are aluminum or titanium, which are both quasi-isotropic materials. In this case the effect of the assumption that the materials are isotropic is minimal.

Primary Assumptions Fuselage Model

- **The stringers can be replaced by booms.** The cross-section of the stringer has small cross-sectional dimensions compared to the dimensions of the complete cross-section and the distance of the centroid of stringer and the fuselage skin is small compared to the centroid of the complete cross-section. Therefore the stringers can be replaced by so-called booms. Booms are concentrated areas, located at the mid-line of the skin.
- **The normal stress is constant over the boom area.** Since the cross-sectional area of the stringers is small and the distance between the centroid of the stringer and the skin is small compared to the fuselage cross-section, it can be assumed that the normal stress of the cross-section of the stringer is constant. Therefore, also the normal stress over the booms can be assumed constant.
- **The fuselage skin carries only shear stresses and the booms carry only normal stresses.** The stringers of the fuselage carry mainly all the normal stresses in the cross-section and the skin is more effective in carrying shear stresses, it can be assumed that the booms carry all the normal stresses and that the skin carries all the shear stresses.

- **The forces and moments apply at the top of the fuselage.** The structure of fuselage is mainly subjected to the forces working on the wing-fuselage intersection and due to pressurization of the fuselage. To simplify the calculations, it is assumed that the forces and moments working on the root of the wing are transmitted to the fuselage and applied at the top of the fuselage.
- **The forces and moments, other than due to the wing and pressurization of the fuselage, are disregarded.** Other forces and moments than the aforementioned forces and moments are disregarded. Forces such as lift on fuselage are disregarded since these forces are much smaller than the forces applied on the wing-fuselage intersection. Secondly, to take these forces and moments into account a complete analysis of the aircraft is required. Due to the limited time-schedule this is not possible.

Secondary Assumptions Fuselage Model

- **The fuselage cross-section is circular.** Since technical drawings of the structure are limited, the cross-section of the fuselage is assumed to be circular with a radius of 1550 mm [60].
- **The skin thickness is assumed to be 1.5 mm.** The skin thickness of the fuselage of the Antonov An-74 is unknown. Therefore, it is assumed to be 1.5 mm. The thickness is based on the comparison of the thickness of other comparable aircraft with a pressurized cabin [60].
- **The stringer area is 70 mm^2.** As mentioned before, no reliable data of the structure is available. Therefore the cross-sectional area of the stringer is assumed to be 70 mm^2. The cross-sectional area is based on the stringers used in other comparable aircraft [60].
- **The material is isotropic.** The materials used in the wing are aluminum or titanium, which are both quasi-isotropic materials. In this case the effect of this assumption is minimal.

2.4.2 Wing and Fuselage Analysis

This section will describe the simulation method used to calculate and show the results of the forces and stresses in the wingbox and fuselage of the Antonov An-74. Two situations were investigated, when the normal, existing engine and if a new, stronger engine will be used. As the geometry of the entire wing and fuselage of the Antonov An-74 are difficult to obtain or determine, these dimensions can be determined from the technical sketches in the official Antonov An-74 aircraft manual [46]. Only the wingbox is used during the calculations. This can be justified, because all the forces and moments on a wing will be carried and transferred by the wingbox. First, the method of the wingbox MATLAB model is described, followed by the fuselage simulation. Finally, the results and conclusions are stated.

2.4.3 Wingbox Model Applied Theory

The theory required and the implementation of this theory in the MATLAB model to evaluate the normal and shear stress distribution throughout the wingbox of the Antonov An-74 is presented here. The relations used are derived from structural analysis theory [61]. Only one wing is considered in this model, as the other wing is assumed to have identical loads and thus the results can be mirrored.

Geometry and Reference Frame

The wingbox carries the loads acting on the entire wing. Due to this, the wingbox itself is used for the simulation model. The overall geometry of the wingbox is derived from technical drawings in the official Antonov aircraft manual [46] and is shown in Figure 2.28. As can be seen, the geometry of the wingbox consists of three parts. An unswept part (3.8 m) and two swept parts (both 6.1 m) with 12.2 and 13.8 degrees half chord sweep respectively for the mid section and outer section of the wingbox. The engine is positioned at 2.6 m from the root chord, still at the unswept section.

Three separate reference frames are used in the simulation model, due to the three different sections of the wingbox. The first reference frame is attached to the root of the wingbox, the unswept part, at the centroid of the cross-section. The positive z-axis points outwards along the length of the beam. The y-axis is positive in the upward direction, while the positive x-axis runs parallel to the root of the wingbox in the direction of the leading edge. The second and third reference frame are positioned at the middle and outward swept parts of the wingbox. The newly

defined reference frames have the same positive orientation as the first one, however are rotated by the half chord sweep angle. Figure 2.28 shows the reference frames, including the wingbox geometry.

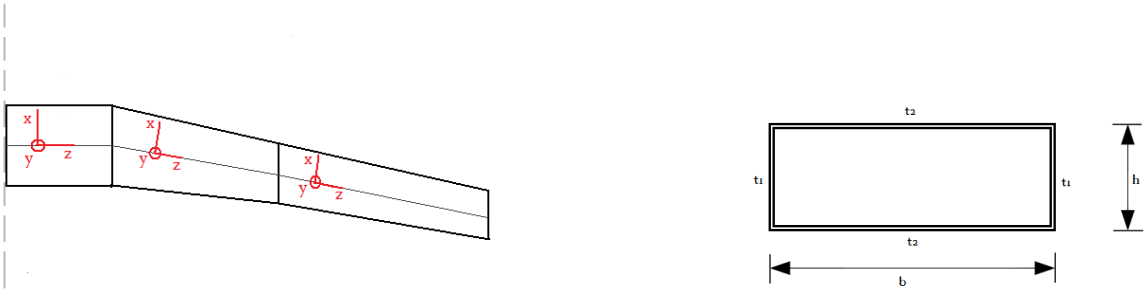

(a) Wingbox overall geometry, including reference frames, top-view

(b) Wingbox cross-section geometry

Figure 2.28: Layout of the wingbox

Wingbox Cross-Section

After the reference frames have been defined, the wingbox geometry and cross-section itself can be modeled in MATLAB. The simulation is performed numerically, which means that the model is discrete instead of continuous. Firstly, the wingbox structure is segmented with the use of a mesh, relative to the reference frame. The mesh is defined for each of the three wingbox sections. On the basis of these meshes, the chord length on the segments within a section can be determined, which is assumed to increase linearly from tip to the start of the unswept part. The bigger the amount of points in the mesh, the smaller a segment of a section and more accurate the results are in the end. Secondly, the number of elements per cross-section is defined. The cross-section consists of a front and back spar and a top and bottom skin, all with a thickness, height and length varying with respect to the chord length. As mentioned before, the geometry of the actual wingbox cross-section is unknown, thus the wingbox is assumed to have a rectangular box shape with equal thicknesses for the two spars and the two skins. The cross-section can be seen in Figure 2.28. The assumption of the rectangular shaped box induces that, from symmetry, the centroid of the cross-section is positioned in the middle of the wingbox. Also due to symmetry, the second moment of inertia I_{xy} is equal to zero. For the bending moment, only the moment of inertia around the x-axis is required. The generic equation and the equation when substituting the dimensions (widths, heights and thicknesses) of the wingbox, including the assumption that the wingbox is thin-walled and simplified, for the moment of inertia can be seen in Eq. 2.60 and 2.61. Note that the latter equation is used three times as the dimensions of the wingbox change according to the different swept and unswept parts and chord length.

$$I_{xx} = \int_A y^2 \, dA \tag{2.60}$$

$$I_{xx} = \frac{(t_1 + t_2) \cdot h^3}{12} + 0.5 \cdot b \cdot t_3 \cdot h^2 \tag{2.61}$$

Another property of the cross-section which will be of great importance in the calculations is the shear center of the wingbox. The shear center is evaluated by use of the shear flows, which will be calculated later in more detail. Due to symmetry all horizontal shear flows are equal and all vertical shear flows are equal. Therefore, the shear center will lie on the symmetry lines of the cross-section, which will be the same position as the centroid. This will give no problems in the unswept part, however in the swept parts the shear center may be positioned differently. Evaluating this possibility, the shear center in the swept sections for the assumed wingbox dimensions lies at most $1.5 \cdot 10^{-3}$ times the chord length away from the middle. This is less than 1 percent of the total width of the wingbox cross-section. Therefore it can be concluded that the shear center can be assumed to be located in the middle of the wingbox, at the same position of the centroid, without introducing any significant errors.

Wingbox Loading and Stresses

With the geometrical properties of the wingbox known, the loads to which the wingbox is exposed can be determined. Also in the determination of the loads and stresses, the wingbox unswept and swept sections will be treated

as three different parts with their own reference frame. These loads will consist of three modes, being a shear force, a bending moment and a torsion moment. This loading will result in a normal and shear stress distribution over the entire wingbox. Firstly, all calculations by the simulation model to obtain the shear stress distribution will be explained and secondly, the same is done for the calculation of the normal stress distribution.

Shear stress calculation approach

As the entire wing has a weight that needs to be carried by the wingbox, the weight of each segment is calculated. This is done by dividing the weight of the entire wing over the surface of the mesh segment in a section relative to the surface of the entire wingbox. The shear force due to the weight of the wing in a segment is obtained and will be used as a part of the total shear force calculation. In the unswept section of the wingbox, the engine is positioned. The engine is considered as a point mass and thus its weight will have a contribution to the shear force. This will induce a strong dip in the shear force diagram. Another part of the of the shear force is the lift. The lift force is orientated upwards and therefore of course in opposite direction to the weight. As the shape of the airfoil is unknown, the real lift distribution over the wing or wingbox can not be predicted. So, for this analysis a general lift distribution is assumed, which is linear of the spanwise length of the wingbox. To reflect the reality as best as possible, the Coanda effect is incorporated at the section where the engine is located. This is done by using a factor increase of the lift distribution. For the normal, existing engine this factor is 3, while for the new engine this factor increases with 23%. The calculation of the shear force starts at the tip of the wingbox and will run along the defined mesh segments along the span towards the root. As the three sections are treated within their own reference frame, the final value of the first section will be used as starting value for the second section and the final value at the second section will be used as starting value for the third, unswept section. The same approach is used at each mesh segment. The lift force and wing weight are added to the previous shear force. At a certain segment, in the unswept part, the engine weight is subtracted as well. The numerical formula used to determine the shear force along the span of the wingbox can be seen in Eq. 2.62, the forces which may contribute can be seen in Figure 2.29.

$$S_i = S_{i-1} + L_i \Delta z - W_{engine} \tag{2.62}$$

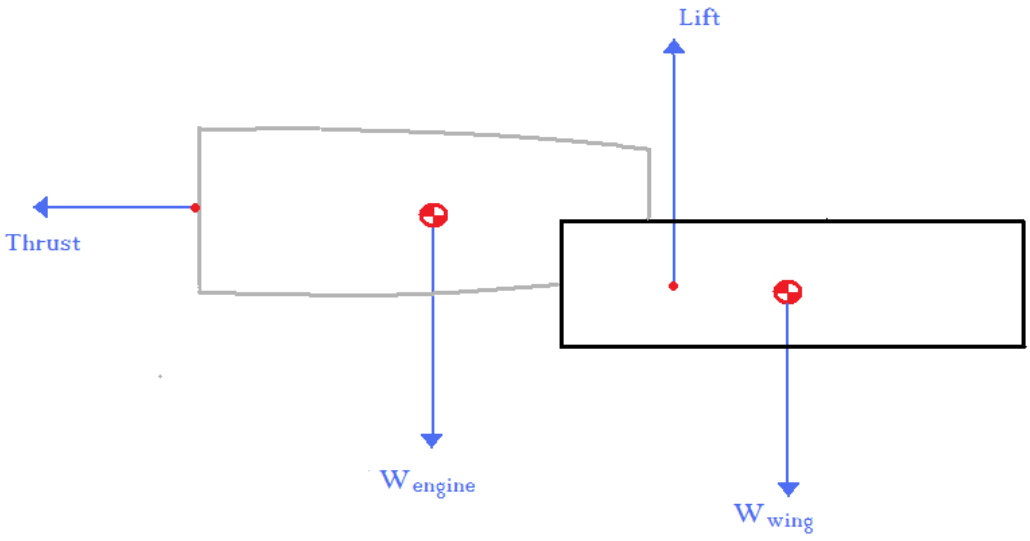

Figure 2.29: Cross-section of the wingbox including all forces

For the case of the wingbox, not only the shear force has a contribution to the shear stress. The torsion induced partly by the lift force and partly by the engine weight and thrust, also has an impact on the shear distribution. The model starts at the tip of the wingbox, taking into account all the segments on the outer swept section. In this section only the lift force has a contribution to the torsion, as the lift force acts on the quarter chord line and not in the centroid. The simulation model will run until the half chord line reaches the sweep connection. Here, one of the assumptions comes into play. As the connection of two parts is reached, the sweep will be incorporated in

the model. Therefore, a triangle-shaped segment of the wingbox is not analyzed. This part is illustrated in Figure 2.27. After the sweep is incorporated, the model will continue with the middle swept part with the same procedure. Again, the model will run until the half chord line reaches the connection with the unswept section and the sweep is taken into account in the same manner as before. Finally, the model will continue with the unswept section. In this section the engine is located. When the model reaches the location of the engine relative to the span of the wingbox, additional torsion contributions are included. These torsion contributions are induced by the thrust of the engine, which works at the top of the wingbox skin and by the engine weight, which is positioned 3.1 m before the centroid of the wingbox as derived from technical drawings from the official Antonov aircraft manual [46]. From Figure 2.29 the forces which induce a torsion can be derived. Eq. 2.63 and 2.64 show the formulas used to calculate the torsion in the sections and the rotation at the sweep connections.

$$T_i = T_{i-1} + L_i \Delta z \left(\frac{b}{2}\right) \tag{2.63}$$

$$T_0 = \sum L_i \Delta z \left(\frac{c_r}{4} - z_i \sin\left(\Lambda_{LE}\right)\right) \tag{2.64}$$

Now that the shear force distribution and the torsion distribution over the wingbox are determined, the defined cross-section of the wingbox is needed. The cross-section is used to calculate the shear flows. The cross-section in each mesh segment is divided in a number of elements, this is done over the entire span of the wingbox. The elements are specified for the bottom skin, rear spar, top skin and front spar separately. Not only the mesh elements per cross-section are defined, but also the x, y and z-coordinates are determined of the mesh, starting halfway at the bottom skin of the wingbox. These mesh elements in each cross-section will be used to evaluate the shear flow over the cross-section in each mesh segment, following from the thin-walled assumption. Also for the shear flows, the starting point of the calculation is halfway at the bottom skin and will continue via the rear spar to the top skin and front spar, back to halfway at the bottom skin again. The shear flow is split up into two parts, an open shear flow part and a closed shear flow part. Eq. 2.65 shows the numerical formula used for the shear flow calculation, where i counts along the mesh segments and j along the mesh points on the cross-section and is calculated using Riemann summation.

$$q_{i,j} = q_{i,j-1} - \frac{S_i}{I_{xx_i}} y_{i,j} t_{i,j} \Delta s \tag{2.65}$$

The torsion contribution due to the lift, engine thrust and engine weight can also be converted as a shear flow. This shear flow is calculated using Eq. 2.66, where A is the area of the cross-section and T, torque at the location to be evaluated. This shear flow is added to the already obtained shear flows. The shear flow caused by the torque acts in the same direction as the shear flow due to the shear force in the front part of the cross-section.

$$q = q_s + \frac{T}{2A} \tag{2.66}$$

As final computation, the shear stress distribution can be calculated with the obtained shear flow and the thickness at the specific point in the cross-section. The numerical formula used can be seen in Eq. 2.67, where again i counts the mesh segments and j the mesh elements within one cross-section segment.

$$\tau_{i,j} = \frac{q_{i,j}}{t_{i,j}} \tag{2.67}$$

Normal stress calculation approach

The determined shear force, per mesh segment, is now used to calculate the bending moment. However this is only one part of the bending moments present in the wingbox. The same approach is used as with the torsion. The calculation of the model will start at the tip and continues until it reaches the connection with the following wingbox section at half chord length. Then the bending moment is rotated and used as start for the following section, etc. The total bending moment of the previous segment is added to the bending moment at the evaluated segment. The second contribution is due to the Torsion, which generates a bending moment around the y-axis (instead of the x-axis like the shear force). This contribution only works on the unswept section starting at the location of the engine and runs towards the root of the wingbox. The numerical formulas used for each section and to take the sweep angle into account can be seen in respectively Eq. 2.68 and 2.69.

$$M_i = M_{i-1} + S_i \Delta z \tag{2.68}$$

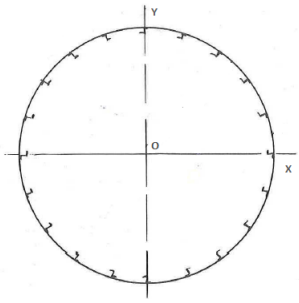

Figure 2.30: Cross-section of the fuselage structure with stringer and the skin

$$M_0 = \sum L_i \Delta z \left(z_i \cos \left(\Lambda_{LE} \right) \right) \tag{2.69}$$

The bending moment is used to obtain the normal stress distribution on the wingbox. Starting from the general equation for normal stress, but using the assumption that the wingbox has an axis of symmetry, the general equation can be simplified to Eq. 2.70. Where y and x are the dimensions from the point of the force to the centroid, which will increase from tip to root throughout the span of the wingbox as the y and x dimensions are dependent on chord length.

$$\sigma_z = \frac{M_x}{I_{xx}} y + \frac{M_y}{I_{yy}} x \tag{2.70}$$

2.4.4 Fuselage Model Applied Theory

The applied theory to calculate the stresses in the fuselage cross-section is explained here. First the geometry and the reference frame of the fuselage cross-section are described and thereafter the theory is explained. The applied theory to calculated the stresses in the fuselage is done by the method of idealization and will be explained in more detail in the next section [61].

Geometry and Reference Frame

Figure 2.30 shows the cross-section of the fuselage structure. The structure consists mainly of the skin and the stringers or stiffeners. It is the most critical structure since it carries all of the primary loads due to fuselage bending, shear, torsion and cabin pressure. The primary loads are carried by the fuselage skin and stiffeners to prevent buckling and to maintain the cross-section. Also can be seen in the figure that the stringers are spaced at regular intervals and are connected to the skin of the fuselage. As mentioned above the cross-section of the fuselage is assumed to be circular, therefore the x-axis and the y-axis are both axes of symmetry with the origin in the middle of the cross-section. Therefore the neutral axis of the cross-section passes through the origin of the fuselage.

Method of Idealization

The method of idealization is used to idealize complex structural sections into simpler 'mechanical model' forms which behave the same or nearly the same as the actual structure under given loading conditions. Furthermore the distance of the skin and the centroid of the stiffener is small compared to the distance of the centroid of the stiffener and the centroid of the complete section. Therefore, the normal stress over the stringers can be considered constant and the stringers can be replaced by concentrated areas, so-called booms, located at the mid-line of the skin. The stringers carry most of the normal stresses and the skin of the fuselage is more effective in resisting shear stresses. Therefore it can be assumed that the booms carry all the normal stresses and that the skin carries all the shear stresses.
Before the stresses in the fuselage can be calculated the structure needs to be idealized. Figure 2.31 shows the idealized cross-section of the fuselage in which the stiffeners are replaced by booms. The numbering in the figure corresponds to the numbering of the booms. The shear force and the bending moment on the fuselage are applied in the vertical plane on top of the cross-section.

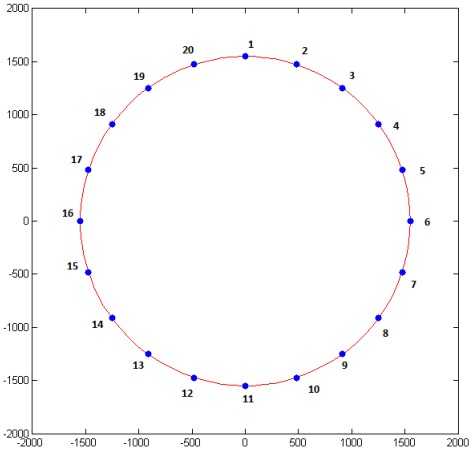

Figure 2.31: The idealized cross-section of fuselage with booms

Calculation of Boom Area and Moment of Inertia of the Cross-Section

The location of the booms is determined, so the next step is to determine the area of the booms. The area of the booms can be calculated by using Eq. 2.71, where n corresponds to the numbering of the boom in Figure 2.31. A_S is the cross-sectional area of the stiffeners, t is the skin thickness and s is the distance between the booms. y_n and y_{n+1} are respectively the distance between the boom and the neutral axis where n corresponds to the boom under consideration. The cross-section is symmetric and therefore the area of the booms is equal on both sides of the vertical axis, i.e B_2=B_{20}, B_3=B_{19}, B_4=B_{18} etc.... and B_1=B_{11}.

$$B_n = A_S + \frac{t \cdot s}{6}\left(2 + \frac{y_{n+1}}{y_n}\right) + \frac{t \cdot s}{6}\left(2 + \frac{y_{n-1}}{y_n}\right) \tag{2.71}$$

The areas of the booms are calculated as mentioned before and are used to calculate the moment of inertia of the fuselage cross-section. The moment of inertia about the x-axis is given by Eq. 2.72. The forces and moments on the fuselage are applied only in the y-direction and the moment of inertia around the y-axis is disregarded. B_n and y_n are respectively the area of the boom and the distance between the boom and the neutral axis in y-direction. r is the total number of booms used to idealized the structure.

$$I_{xx} = \sum_{n=1}^{r} B_n \cdot y_n^2 \tag{2.72}$$

Fuselage Loading and Stresses

Shear stress

The fuselage is subjected to a vertical shear force applied at the top of the fuselage at the vertical axis of symmetry. The shear force causes shear stresses in the structure of the fuselage. It is more convenient to work in terms of shear flow, i.e. shear force per unit length, rather than in terms of shear stress. The only force applied to the fuselage is a shear force in vertical direction S_y. There is no shear forces in x-direction $S_x = 0$, since the fuselage is symmetric the product second moment of area $I_{xy} = 0$. The torsion subjected to the fuselage is zero, since the torsion due to the right wing cancels out the torsion due to the left wing and only the primary loads on the fuselage are taken into account. The shear flow q_S in the cross-section can be calculated by using Eq. 2.73. The shear flow in a skin panel between two booms is calculated.

$$q_S = -\frac{S_y}{I_{xx}} \sum_{r=1}^{n} B_r \cdot y_r \tag{2.73}$$

Where S_y is the shear force in y-direction, I_{xx} is the moment of inertia of the cross-section. The shear flow skin panel 1,2 is zero, this is the section where the calculation of the shear flow starts. Furthermore, the cross-section is

symmetric, which implies that the shear flow in skin panel 10,11 is zero. Every time another skin panel is considered in the calculation, the boom at the beginning of the skin panel that is crosses in analyzed. For example in skin panel 2,3, only the first boom, boom 2 is taken into account. When the analysis moves to panel 3,4, boom 3 is analyzed.

Normal stress

The normal stresses in the fuselage are carried only by the booms. The fuselage is subjected to a bending moment which produces normal stresses in the cross-section. The normal stresses in the boom can be calculated with Eq. 2.74. M_x is the bending moment about the x-axis.

$$\sigma_n = \frac{M_x \cdot y_n}{I_{xx}} \tag{2.74}$$

Stresses due to pressurization of the cabin

The Antonov An-74 has a pressurized cabin with a maximum pressure differential of 0.49 bars [33]. Pressurization of the cabin results in two additional stresses in the structure of the fuselage; an axial stress and a circumferential stress. The axial stress in the fuselage due to pressurization is carried by the booms and the circumferential stress is carried by the skin perpendicular to the cross-sectional area of the skin.
The axial and circumferential stress are given by respectively Eq. 2.75 and Eq. 2.76.

$$\sigma = \frac{P \cdot r}{t} \tag{2.75}$$

$$\sigma_1 = \frac{P \cdot r}{t} \tag{2.76}$$

Where P is the pressure differential between the outside and the inside of the cabin, r is the radius of the fuselage and t is the skin thickness of the fuselage.

Von Mises yield criterion

The Von Mises yield criterion suggests that the material starts yielding if a certain yield strength is reached. The Von Mises yield stress can be calculated by Eq. 2.77 and takes into account all the stresses, both normal and shear, on the fuselage. σ_1 is the normal stress in the fuselage in longitudinal direction and σ_2 is the circumferential stress perpendicular to the cross-sectional area of the skin.

$$\sigma_v = \sqrt{\sigma_1^2 - \sigma_1\sigma_2 + \sigma_2^2 + 3 \cdot \tau^2} \tag{2.77}$$

2.4.5 Wingbox Model Results

This section presents the results for the numerical simulation model of the wing structure. The final results of this model give the normal and shear stress throughout the spanwise direction of the wingbox. The stresses are analyzed for two cases. When the existing engine and when a new, optimized engine is mounted on the wing. The new engine will be heavier and can generate more thrust, respectively 1124 kg & 63,700 N and 1360 kg & 92,200 N.

The numerical simulation gives the loads and stresses at every point in the mesh along the span of the wingbox. The loads, and thus also the stresses, increase closer to the root. An exception is found at the location of the engine. Here, the engine weight causes a dip in the shear force. The torsion has a sudden increase in magnitude due to the engine weight and thrust. Figures 2.32 and 2.33 show all the load and stress distributions for the entire wingbox. From these figures, it can be seen that the maximum normal, shear and Von Mises stress can be found at the sweep between the unswept part and the middle swept part. This could be true, or could be an error due to the lack of detailed depth of the model as the model can not predict the behavior at the sweep accurately. However, this is not a problem for further analysis. The results from tip to just before the engine are the same for the normal and new engine, as inputs, such as geometry, lift and wing weight, do not change in these wingbox sections. Only the results of the unswept part, from the engine location up to the root of the wingbox, have been analyzed in more detail.

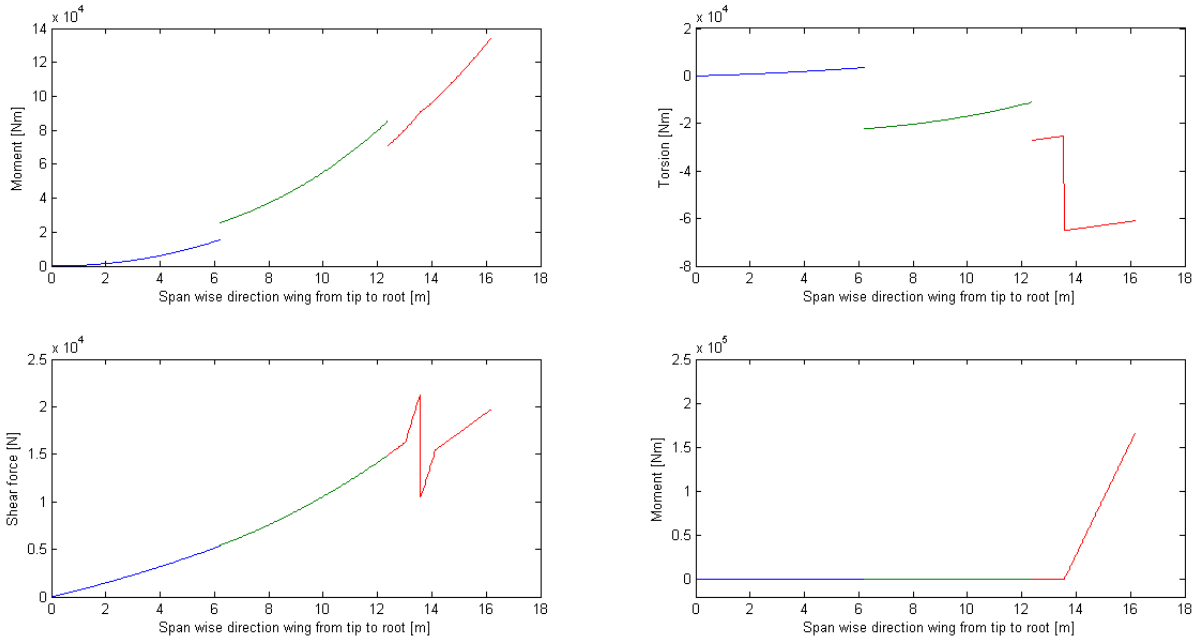

(a) Loads in case of the existing engine

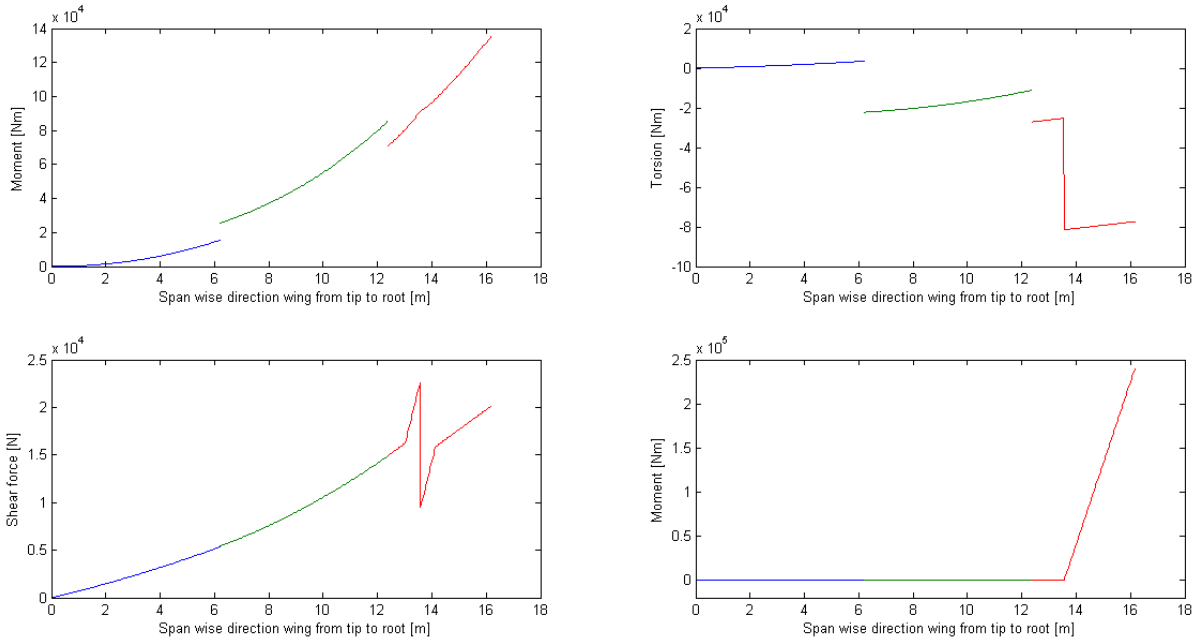

(b) Loads in case of the new engine

Figure 2.32: Loads on the wingbox in case the existing or new engine is used

Table 2.18 shows the results of the calculations. The table shows the maximum loads and stresses in the part where the engine can affect the results, as these are the most critical for the structure. Also, the percentage difference between the two cases is determined, because the actual cross-section of the wingbox is unknown but still usable results needed to be obtained. The maximum shear force can be found just before the engine position and thus its weight has an influence on this load. The Coanda effect has not only its contribution just behind the engine, but is more spread out over a part of the unswept wing section. As the Coanda effect of the new engine is higher,

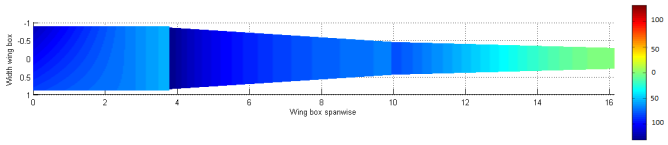

(a) Normal stress in case of the existing engine (MPa)

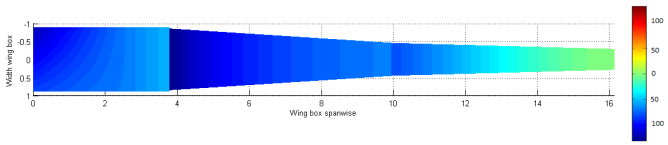

(b) Normal stress in case of the new engine (MPa)

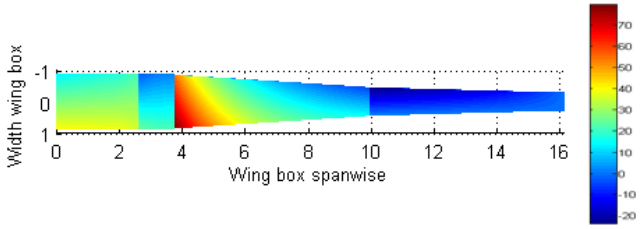

(c) Shear stress in case of the existing engine (MPa)

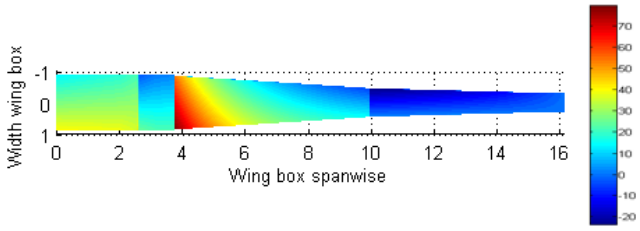

(d) Shear stress in case of the new engine (MPa)

Figure 2.33: Stresses on the wingbox in case the existing or new engine is used

due to the extra thrust it can generate, the maximum shear force is also higher. However, the engine is heavier, which influences the shear force distribution after the engine weight has taken into account. The lift force can not counteract the weight of the engine as much as in the situation with the normal engine, which result in a lower shear force at the root of the wingbox in case the new engine is mounted. Both moments, one due to the shear force and the other due to the thrust of the engine, are maximum at the root of the wingbox, as the arm of the moment increases throughout the span of the wingbox. Both moments are higher in case the new engine would be used. However, the moment due to the shear force (around the x-axis) differs not as much as the moment due to the torsion (around the y-axis) relative to the normal engine. This is due to the dip in shear force at the location of the engine and the fact that the lift force can not counteract this weight as much as for the normal engine. The maximum moment due to the thrust is much higher as the new engine generates almost 45% more thrust, the difference is 30.9%. The torsion has three contributions; the lift force, the engine weight and the engine thrust. The engine weight and thrust both increase for the new engine, while the lift increases due to the Coanda effect. However, this lift increase is not high enough to counteract the new increased torsion contributions. The torsion for the new engine is 13% increased relative to the normal engine. This maximum is experienced at the location where the engine is positioned. The torsion decreases a bit towards the root of the wingbox, but still is higher in case of the new engine.

The normal, shear and Von Mises stress all increase in case of the new engine, respectively 2.8%, 12.5% and 5.6%. The maximum results can all be found at the root of the wingbox. As the normal stress consists out of two components, the moment due to the shear force and the moment due to the thrust, the maximum normal stress is found to be located more towards the front spar instead of in the middle of the cross-section. This is due to the

high contribution of the thrust moment. The maximum shear force is located around the same location; in the top or bottom skin towards the front spar. The reason is because the torsion component of the shear stress has the same direction as the shear flow component on the front side, thus the contributions add up to the total the shear stress. Connection effects with the fuselage are not taken into account, so the stresses continue to the root without any strange effect. This means that also the Von Mises stress is most severe on the place where the normal and shear stress are most critical.

Table 2.18: Difference in maximum forces, moments and stresses between the existing and retrofitted engine

	Existing engine	**Retrofitted engine**	**Difference**
Shear force [N]	21,208	21,650	2.0%
Moment (x-axis) [Nm]	13,390	13,496	0.8%
Moment (y-axis) [Nm]	16,590	24,010	30.9%
Torsion [Nm]	-70,587	-81,458	13.3%
Normal stress [N·mm^{-2}]	119.38	122.85	2.8%
Shear stress [N·mm^{-2}]	40.24	45.99	12.5%
Von Mises Stress [N·mm^{-2}]	138.23	146.42	5.6%

2.4.6 Fuselage Model Results

This section shows the results of stress calculations in the fuselage. The main forces and moments applied on the fuselage due to the wing and the forces due to pressurization of the fuselage are taken into account. The stresses are calculated for two different situations. The first situation is the aircraft with the engines currently mounted on the Antonov An-74. These engines produce 63,700 N of thrust each and have a weight of 1124 kg. The second situations is the aircraft with new engines, these produce 92,200 N each and have a weight of 1360 kg. Since no reliable technical drawings of the aircraft are available, the real structural capabilities are hard to investigate. To determine the percentage difference in stresses between the two situations, the structure is as closely as possible processed into the model, based on the available data and technical drawings.

Table 2.19 gives the results of the calculations. The values of the shear force and moment are the forces applied on the wing root, which are transmitted to the fuselage. The stresses are the maximum stresses in the fuselage. The maximum stresses are the most critical since failure of the structure will start at the section with the highest stresses. The last column shows the percentage difference between the existing and new engine. The first difference that can be seen is the difference in shear force, the new, heavier engine increases the shear force at the root of the wing by just 2.05%. The additional lift produced due to the Coanda effect counteracts the additional increase in weight of the engine. The small difference in shear force is favorable since the shear force is transmitted to the fuselage and therefore the difference in loading on the fuselage is insignificant. Since no torsion is applied on the fuselage the same percentage increase in shear stress is achieved, as the only contribution to the shear stress is the shear force. The new engine produces around 45% more thrust, the increase in thrust contributes to an increase of 21.19% in moment applied on the fuselage. The increase in moment due to the additional thrust results in an increase of 7.5% in axial normal stress. The main contribution of the axial stress is due to pressurization of the cabin which does not change by changing the engines. The same holds for the circumferential normal stress, the only contribution to the stress is due pressurization.

Finally the Von Mises stress in the fuselage is increased by 1.45%. The shear stress is increased in the case of the retrofitted engine, the other stress in the fuselage differs marginal for both engines and the increase in Von Mises is mainly due to the increase in shear stress. The Von Mises yield criterion combines the different stress in the fuselage to a single value. The Von Mises stress may never exceed the yield strength of the material used for the fuselage structure, otherwise the structure will start yielding and this finally leads to failure of the structure and the aircraft.

Figure 2.34 show surface plots of the normal and shear stresses of the fuselage wing intersection for the retrofitted engine.

2.4.7 Wing and Fuselage Structure Conclusion

The normal, shear and Von Mises stress in both the wing and fuselage are increased if the new engine would be used. However, for the fuselage this difference is much smaller than for the wing structure, as can be seen in Tables 2.18 and 2.19. It is difficult to say whether reinforcements are necessary, due to the lack of information on the

Table 2.19: Difference in forces, moments and stresses between the existing and new engine

	Existing Engine	**New Engine**	**Difference**
Shear force [N]	19,677	20,089	2.05%
Moment [Nm]	60,952	77,336	21.19%
Normal stress (Axial) [N·mm^{-2}]	35.1	37.8	7.5%
Normal stress (Circumferential) [N·mm^{-2}]	50.6	50.6	0.0%
Shear stress [N·mm^{-2}]	5.4	5.5	1.9%
Von Mises Stress [N·mm^{-2}]	44.9	45.6	1.5%

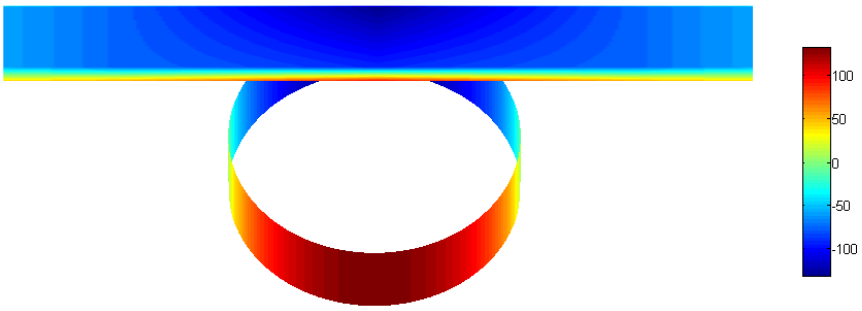

(a) Normal stress in the wing-fuselage section (MPa)

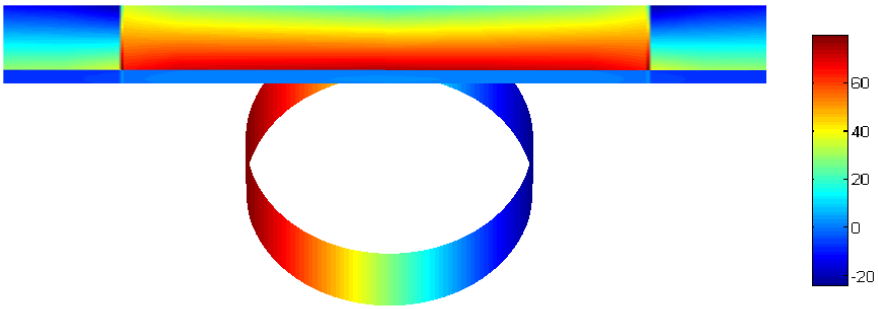

(b) Shear stress in the wing-fuselage section (MPa)

Figure 2.34: Surface plot of the normal and shear stress for retrofitted engine

structure and materials used in the structure and most importantly on the way the structure is already built. It is unknown if the wing and fuselage structure are already optimized and built to its limits. For the fuselage no modifications or reinforcements may be needed, as the percentage difference is quite low. For the wing structure it may be wise to reinforce or at least further investigate the need of reinforcements. Only the unswept wing structure from the engine location to the root and mostly the front part of the wingbox requires this approach, because only

in this area the stresses were increased relative to the situation where the existing engine is used. Possibilities for modifications or reinforcements for the structure where necessary are; increasing the thickness of the spars and skins, adding additional spars or stringers or using a different stiffer material. If the wing structure was built to its limits with the existing engines mounted, the thickness of the front spar, top skin and bottom skin needs to be increased by a factor of 1,15, including a safety margin. This needs to be done to make sure that the normal and shear stresses do not exceed the maximum stresses found in the wingbox if the existing engines were used.

2.4.8 Sensitivity Analysis

This sensitivity analysis is performed to investigate how the structural loads and stresses would change due to varying parameters. The situation where the normal or new engine is mounted to the wing is considered as the general case. Then, common parameters are changed in order to investigate their influence on the structure and also special or critical cases are covered. This is treated in theory and briefly, as the time schedule and unknown structural configuration do not allow a too detailed analysis. Further analysis should be done to investigate the actual structural changes in case of the special or critical situations.

Common parameters are the forces, such as wing weight, fuel weight and lift force. All cases are investigated in a manner such that the lift force counteracts the weight; a situation similar to cruise condition. An increase in wing weight will counteract the lift force distribution over the wing. This implies that the shear force will decrease in magnitude. The same reasoning can be given for the fuel weight, which will increase the entire structural weight. An increase in the lift distribution will have an opposite effect. High lift is advantageous for the flight performance of an aircraft, however the shear force acting on the wing will increase too. This also causes an increase in bending moment and thus in normal, shear and Von Mises stress. This increase may affect the structure of the wing, fuselage and the wing-fuselage intersection. In case a decrease in weight or lift force is established the situation is vice versa. A decrease in weight is preferable, however would imply a higher shear force and thus higher stresses in the structure.

One of the critical cases deals with the fuel weight, more precise the fuel consumption. When flying, the fuel stored in the fuel tanks positioned in the wing will be used. This implies that the weight will decrease and thus higher stresses will be present in the wingbox when flying with the same lift. Also, sudden releases of extra shear force can occur, as the fuel tanks are located on just a few places instead of being continuous throughout the span of the wingbox (for instance not behind the engine). Further analysis should reveal the hazards of fuel consumption while flying and what the most optimum way is to use fuel from the wings. The second case considers the center of gravity location in flight. As all the weight of the aircraft work in this point, a torsional moment occurs relative to the wing. When an aircraft needs to brake, the wing could break off the aircraft structure due to a critical backward center of gravity location, as happened before with other planes. A higher torsional moment occurs if the center of gravity moves backward relative to the wing weight. The final critical case considered is the deflection of the flaps while flying. Flaps extend the wing and thereby generate an extra lift force. This lift force acts on extended flap surface itself instead of at the position of the lift from the main wing. So, the lift due to the flap deflection causes an additional torsional moment opposite to that of the main wing. Due to the fact that the flap lift force acts behind the center of gravity of the wing and the main wing lift force acts in front of the center of gravity. In case of the Antonov An-74, the additional torsional moment adds up to the torsion from the engine weight and engine thrust. This causes the already existing torsion on the wingbox to increase in magnitude, which will lead to higher stresses. As said before, the time schedule does not allow for an analysis in such detail to calculate the consequences of flap deflections. However, if further analysis is performed this should be one of the issues to be investigated. Finally, dynamic loads could really be a limiting factor of the strength of the structure. Therefore, these loads should be considered. Dynamic loads could act on the structure in case the aircraft flies in windy conditions or if the pilot performs an extreme maneuver while flying. However, the MATLAB model used only simulates static loads on the wingbox and fuselage. It is recommended that in future analysis dynamic loads are taken into account.

2.4.9 Verification and Validation

This section describes how the verification of the wing and fuselage models is performed and gives a general approach for validation processes. Verification is performed by checking the simulation model with analytical calculations. This is done for the final results, but as well for the intermediate calculations. Validation of the simulation model is done by comparing the results with real life data. However, as no real life data could be obtained at this moment of the design phase, validation of the model is explained in theory.

Verification Wingbox Model

This section describes how the verification of the wing analysis is performed. The simulation model is divided into several unit codes in which each unit code performs a specific calculation, e.g. an unit to geometric properties of the wing, a unit to calculate normal stresses in the wing and so on. Verification have to be done to ensure the numerical codes performs well. To check if the simulation performs well, the numerical results are compared to analytical results. The verification of the wing consists of three parts. First the geometry of the wing is checked, thereafter the forces and moments on the wing and finally the calculation of the normal, shear and Von Mises stresses are verified.

Geometry of the wing

The first part of the numerical model defines the geometry of the wing. The verification starts with checking the calculation of the chord length. Secondly the cross-sectional geometry of the wingbox will be checked. The geometry of the wingbox is a function of the chord length, so if the chord length is within sufficient accuracy the geometry of the wingbox should be within the same accuracy. To be sure this is right, the geometry of the wingbox will be verified. Finally the moment of inertia will verified. Since the wing of the Antonov An-74 consist of three different parts, one unswept part and two swept part with different angles, the code will be verified on all the three parts to ensure the calculation are well performed on each part of the wing.

Table 2.20 shows the analytical and numerical results. As can be seen from the table, the deviation of the wingbox dimensions is negligible. The most important parameter to verify is the moment of inertia. The wingbox dimensions arise in the calculation of the moment of inertia, deviations in the wingbox dimensions will therefore also arise in the moment of inertia. The average deviation between the numerical and analytical results is 0.042% with a maximum deviation of 0.106%. It can be concluded that the wingbox properties are well calculated and that the numerical model performs well.

Table 2.20: Comparison of the analytical and numerical results of the geometric properties of the wingbox

	Analytical Results			**Numerical Results**		
	Unswept Part	**Swept Part 1**	**Swept Part 2**	**Unswept Part**	**Swept Part 1**	**swept Part 2**
Chord Length [mm]	1780	1361.54	773.54	1780	1361.50	773.50
Heigth Wingbox [mm]	178.0	136.15	77.35	178.0	136.15	77.35
Width Wingbox [mm]	1780	1306.63	740.85	1780	1306.60	740.90
Moment of Inertia [mm^4]	$1.17118 \cdot 10^8$	$3.8530 \cdot 10^7$	$4.0080 \cdot 10^6$	$1.1712 \cdot 10^8$	$3.8571 \cdot 10^7$	$4.0087 \cdot 10^6$

Shear force, bending moment and torsion calculation

The next step in the numerical model is the calculation of the forces and moments on the wing. The next verification step is therefore to check if the code is well programmed and calculates the forces and moments in the right way. The comparison of the analytical and numerical results is performed at the same location on the wing as for the comparison of the geometric properties. Table 2.21 gives the results of the numerical and analytical calculations. The average deviation of the shear force is 0.79% with a maximum deviation of 0.95%. The average and maximum error is below 1% and can be considered as negligible. The deviation is mainly due to rounding errors and the small deviation in the geometric properties which are used in the calculation of the forces and moments. The average deviation of the bending moment is 2.57% with a maximum deviation of 2.9%.

The deviations for the bending moment are significantly higher than the deviation for the shear force. This is mainly due to the fact that the errors in the calculation of the shear force and the geometric properties also arise in the calculation of the bending moment on the wing. This would also mean that it will have a greater impact on the deviations of subsequent calculations, such that this has to be taken into consideration further on in the report. However for this calculation, the deviation is acceptable. Finally the torsion has a maximum deviation of 2.4% with an average deviation of 1.6%. As already mentioned before, the deviation is acceptable. The error can be considered as insignificant, but will accumulate in further calculations. It is important to take this situation into consideration further on in the calculations of the shear stresses in the wing.

Normal stress and shear stress calculations.

The final step of the verification process is the verification of the normal and shear stress calculation. Table 2.22 gives the values of the analytical and numerical calculations of the stresses in the wing. The average deviation of the normal stress is 2.21% with a maximum deviation of 2.43%. The maximum deviation of the shear stress is 4.35%

Table 2.21: Comparison of the analytical and numerical results of the shear force, bending moment and torsion on the wing

	Analytical Results			Numerical Results		
	Unswept Part	**Swept Part 1**	**Swept Part 2**	**Unswept Part**	**Swept Part 1**	**swept Part 2**
Shear force [N]	15,965.9	9407.4	2370.5	16,118.0	9384.6	2379.7
Bending moment [Nm]	98,578.0	46,498.0	3517.5	100,430.0	47,842.0	3619.5
Torsion [Nm]	-78,457.9	-18,101.9	1365.4	-80,352.0	-18,321.0	1381.1

with an average deviation of 3.57%. The deviations of both stresses are below 5%. This means that the errors can be considered insignificant and that the program performs well. The deviations in the stresses are mainly due to the deviations in the bending moment and torsion calculations. The deviations of the geometric properties are very small and these will not affect the deviations in the stresses to a large extend. To reduce the errors in the stress calculations, the force and moment calculations should be improved in further research. Improved accuracy of the force and moment calculations will result in more accurate stress calculations.

Table 2.22: Comparison of the analytical and numerical results of the shear stress and normal stress in the wing

	Analytical Results			Numerical Results		
	Unswept Part	**Swept Part 1**	**Swept Part 2**	**Unswept Part**	**Swept Part 1**	**swept Part 2**
Shear stress [MPa]	34.46	18.15	7.54	35.65	18.94	7.76
Normal stress [MPa]	74.91	82.44	34.94	76.36	84.44	35.73

Verification Fuselage Model

This section describes how the verification of the fuselage analysis is performed. The simulation model is divided into several unit codes in which each unit code performs a specific calculation, e.g an unit to calculate the position and the area of the booms, a unit to calculate normal stresses in the fuselage and so on. Verification has to be done to ensure the numerical codes performs well. To check if the simulation performs well, the numerical results are compared to analytical results.

Geometry of the fuselage and the location of the booms

The first part of the numerical model defines the geometry of the fuselage and defines the location and area of the booms. The location of the booms and the calculation of the boom areas is compared to the analytical results and the percentage difference between the numerical and analytical calculation is determined. Table 2.23 gives the values of the numerical and analytical calculation. From the comparison of the results it has been found that the highest deviation is 0.0027%. For both the calculation of the location and the area, the maximum deviation is small enough to be neglected.

Table 2.23: Comparison of boom location and boom area

	Analytical Results			Numerical Results		
	Boom 2	**Boom 9**	**Boom 15**	**Boom 2**	**Boom 9**	**Boom 15**
X coordinate boom [mm]	478.97	911.07	-1474.14	478.98	911.06	-1474.10
Y coordinate boom [mm]	1474.14	-1253.97	-478.97	1474.10	-1254.00	-478.98
Area boom [mm^2]	788.51	788.51	788.51	788.50	788.50	788.50

Moment of inertia of the fuselage cross-section

Before the stresses on the fuselage can be determined, first the moment of inertia of the fuselage cross-section has to be calculated. It has been found that the difference between the numerical and analytical calculations of the moment of inertia is $1.4945 \cdot 10^5 \text{mm}^2$. The percentage deviation is 0.00079%, therefore the error in the calculation can be neglected.

Verification of the stresses in the fuselage

With the geometric properties of the fuselage the normal and shear stresses can be calculated. The deviation between the analytical and numerical calculations of the geometry of the fuselage can be neglected. These deviations will however arise in the calculation of the stresses. Since the errors are very small this will not have large effects on

the calculations. The results of the analytical and numerical calculations can be found in Table 2.24. The average deviation of the normal stress is 0.056% with a maximum deviation of 0.075%. The average deviation of the shear stress is 0.0069% and the highest deviation is 0.0082%. And finally the average deviation of the Von Mises stress is 0.00463% with a maximum deviation of 0.00684%. Since the deviation for the stresses is insignificant, the error can be neglected.

Table 2.24: Comparison of the normal, shear and Von Mises stress in the fuselage

	Analytical Results			**Numerical Results**		
	Boom 2	**Boom 9**	**Boom 15**	**Boom 2**	**Boom 9**	**Boom 15**
Normal stress [MPa]	13.30	35.54	29.21	13.28	35.55	29.22
Shear stress [MPa]	1.43	1.43	-3.99	1.43	1.43	-3.99
Von Mises stress [MPa]	45.54	45.09	44.56	45.64	45.09	44.56

Validation

Validation is performed by comparing the results of the model with reference data obtained from real life cases or testing. As at this moment testing is not possible and real life data could not be obtained, a general overview of possible validation processes is given.

The first possibility is to use flight data of the Antonov An-74, which is the most preferable option as this is the best data that can be used for validation. This could be difficult to obtain, as this data is confidential. Another possibility is to build a testing system in a flying Antonov An-74 to obtain the loads and stress during flight. The load distributions, such as lift and weight, and normal, shear and Von Mises stress can than be compared between the MATLAB simulation model and the obtained real life data. If real life data can not be obtained, there is another possibility to get validation data, by testing. Testing can be performed in wind tunnels and stress benches, such that all necessary inputs of the validation data can be determined. When using test results as validation data, it is relevant to consider the nature of the data in order to better explain the discrepancies when comparing that data and the data from the MATLAB simulation model. This means that it is important to realize that the validation test data obtained is meant to emulate the real life situation. However, the data is still a result of another numerical simulation procedure or makes use of assumptions to illustrate the real life situation as best as possible. Also in case a test is used to obtain validation data, the load distributions and stress are compared with the simulation model.

When validation of the simulation model was performed by comparing the results with reference data obtained from testing, discrepancies could be seen. This should be because in the simulation model no effects of wing-fuselage interactions are taken into account, which should be visible in the testing results. The clamping effects of the wing-fuselage structure impedes free deflection of the wing structure in that part, therefore adding to stress concentrations and facilitating buckling effects. Another discrepancy could be due to the fact that in the simulation model the engine is calculated as a point mass and that in real life or test models this is not the case. This implies that the stress values computed by the simulation model are less spread out than the validation data. Also, it could be that the simulation model overestimates the stresses relative to the test validation data, which can be due to the thin-walled assumption, which affects the calculation of the centroid and moment of inertia. Finally, local failure can not be seen in the simulation model, however could be present when testing the structure.

2.4.10 Recommendations

Although the numerical simulation model provides a first analysis of the wing and fuselage structure, in case of a new engine design there is still room for improvement. This simulation model only works as a first analysis for this problem, because of the lack of geometry and aerodynamic inputs of the Antonov An-74 aircraft and tight, relatively short time schedule in which this analysis needed to be performed. This improvement can be done in two ways, improving this first detailed analysis or building an entire new model with the use of a more detailed program and complete inputs. In this way, more accurate results can be obtained for the general model and more special cases can be analyzed.

Regarding changes in the simulation models for the wing and fuselage itself, the entire connection between the wing sections could be analyzed instead of neglecting a small part. Incorporating the exact connection could result in

the conclusion that a stronger structure is needed or not. Further optimization could incorporate taper corrections and the actual position of the shear center in the swept parts. If done accordingly, this would increase the accuracy of the output. Finally, it is recommended to use a more accurate mesh, such as a Gaussian grid. Compared to the grid used in this simulation model, a Gaussian grid may handle the numerical integration more accurately. However, instead of optimizing this model, it may be preferable to analyze this aspect of mounting new engines to the Antonov An-74 to a more detailed level. First of all, the entire structure is necessary to perform any more detailed analysis. This could be the entire structure of the aircraft or just the structure of the wing, wing-fuselage intersection fuselage near the wing. The best way to perform any further analysis is by implementing the structure in a program that makes use of the finite element method (FEM). The finite element method is a numerical technique which can determine outputs with more accuracy than the MATLAB program used. However, it requires a longer implementation time and more specific knowledge to analyze a certain structure. The extra time and knowledge is recommended when further detailed analysis is done, as the additional accuracy of the finite element method will generate results which are more accurate to real life than the MATLAB simulation results. This better accuracy in results is obtained by the use of a different grid. The new grid will define the mesh more precisely over the structure and will not only use rectangles, but also other shapes to include difficult geometries into the calculations. This implies that the total wing-fuselage structure can be analyzed in the same simulation model. The finite element method does also include bending and twisting at any point in the structure, instead of only analyzing stress distributions. Another advantage of a FEM is that the model is numerically stable. Numerically stable means that errors in inputs or intermediate calculations do not accumulate towards the end results.

When using a finite element method, it is recommended that all the general loads and stresses, all possible failure modes due to these loads and stresses and all critical situations are analyzed. Some of these are covered in Section 2.4.8, such as structural defensibility when fuel is consumed in flight or due to a change in c.g. and structural strength when an additional torsion is exerted due to flap deflections. However, these are covered in a more general way as the tight project schedule did not allow for a detailed analysis on these situations. This analysis may consist of a stiffness and strength visualization of the structural components of the wing, fuselage, wing-fuselage intersection and the section where the engine is mounted. This will give better insight in the critical design parameters. The strength visualization should be performed not only for normal and shear stress, but also for buckling, bending and twisting of the structure and possible structural failure due to vibrations induced by the engine. Also, foreign object damage or other risk investigation, such as in case of engine failure, can be analyzed. Finally, it is necessary to incorporate dynamic loads and stresses in the FEM program when performing further analysis. Dynamic loads occur when the aircraft is flying in windy conditions or if the pilot performs an extreme maneuver. In these cases, additional loads act on the wing. These dynamic loads are not simulated by the MATLAB model used as this model only considers static loads. However, dynamic loads could really be a limiting factor for the strength of the structure.

So, overall it is recommended that a more detailed analysis is performed on the structure of the wing, engine and fuselage. The use of the models presented here is not preferable, a finite element method should be used. When using a finite element method model for further analysis, the duration of the project must allow for such an analysis. This model can analyze the structure in more detail and generate results with a higher accuracy. Also, the model can perform analysis on more cases, such as different failure modes, special and critical situations, which is preferable in a more detailed design phase.

2.5 Aircraft Stability and Control

The aircraft stability and control section will focus on the changes made to the weight distribution of the airplane. The center of gravity is depended on the different aircraft components and the way the aircraft is loaded. In this section the methods used to calculate weight components, load factors, weight estimations and loading diagrams will be discussed. Subsequently, the stability and controllability of the airplane will be treated. The section is concluded with a sensitivity analysis, verification & validation of the numerical models used and recommendations for future project phases.

2.5.1 Component Weights

Methods

In order to make a good weight estimation which can be used to determine the stability and controllability of the aircraft, a few methods are possible to determine these matters. In the design process of aerospace systems in terms of weight estimation, several steps are determined. The steps consist of four classes. The first three classes regard the conceptual and preliminary design. Class I consists of early conceptual methods. Class II describes the conceptual stage methods. Class III contains the preliminary design methods. The final class, Class IV, involves the pre-production stage methods. This final stage method is used when the exact geometry of each component and the characteristics of the material are known. In order to achieve a good indication of the weight of the different components in the airplane, the Class II approach is the method most suitable at this point in the design process. It will provide a clear indication of the weights and will act as a good basis for further calculations on the balance of the aircraft in terms of center of gravity locations and resultantly in the stability and controllability of the aircraft.

Class II Method

To apply Class II methods it is required to have availability of geometric data of the aircraft. From the technical sketches of the Antonov An-74 in Figure 2.35, these dimensions are determined. The technical drawing originates from the official Antonov An-74 aircraft manual [46]. The data extracted from the technical drawings of the Antonov is collected in Table 2.25. This is done by careful measurements and adding a scale factor. This table is combined with additional data of the aircraft from Janes' All the World Aircraft [33]. This leaded to a very important list of parameters for the aircraft. By comparing handmade measurements with the official aircraft data the estimations were checked. In order to calculate the weight of the individual components, these parameters are of main importance.

Table 2.25: Aircraft parameters

Parameter	Description	Value	Units
t/c	Thickness to chord ratio	0.12	[-]
AR	Aspect ratio	10.30	[-]
b	Wing Span	31.89	[m]
S	Wing Area	98.53	[m^2]
$\Lambda_{0.5c}$	Semi chord sweep angle	16.00	[deg]
Λ_{LE}	Sweep angle Leading edge	17.00	[deg]
λ	Taper ratio	0.35	[-]
c_r	Root Chord	4.43	[m]
c_t	Tip Chord	1.54	[m]
MAC	Mean aerodynamic chord	3.55	[m]
S_h	Horizontal tail surface	24.64	[m^2]
S_v	Vertical tail surface	16.46	[m^2]
b_h	Horizontal tail span	10.27	[m]
b_v	Vertical tail span	3.81	[m]
c_h	Chord tail	2.84	[m]
l_h	1/4 wing to 1/4 h. tail	13.89	[m]
l_v	1/4 wing to 1/4 v. tail	12.29	[m]
z_h	V. root to h. tail	3.81	[m]
l_f	Fuselage length	25.20	[m]
h_f	Fuselage height	3.10	[m]
Ne	Number of Engines	2.00	[-]
N	Number of Tanks	7.00	[-]
t_{rh}	H. tail max root thickness	0.48	[mm]
S_r	Rudder area	3.07	[m^2]
t_{rv}	Max thickness	0.53	[m]

In order to give a first estimation of the weights, an overview of the different components is established. This overview consists of three sections; the operational empty weight, the payload and the fuel. These three sections can be split up into more detail.

Operational Empty Weight

The actual calculations of a Class II method to obtain a estimation of the structure weight are split up into categories for different types of aircraft. For every aircraft category a different set of equations is available. The categories are;

- General Aviations Airplanes
- Commercial Transport Airplanes
- Military patrol, Bomb and Transport Airplanes
- Fighter and Attack Airplanes

Since the Antonov An-74 design is treated as a transport aircraft and based upon a commercial model, the set of equations for the Commercial Transport Airplanes is used. Within this category several methods are available to calculate the component weights. Large errors may be observed when different methods are used within the same aircraft category. It is stressed to never combine component weight estimates from one method with those of another. The methods are listed below;

- Cessna Method
- USAF Method
- Torenbeek Method
- GD Method

The Cessna method should be applied only to low performance airplanes with maximum speeds below 200 kts. The USAF method is applied to light and utility type airplanes with maximum speeds up to 300 kts. The Torenbeek method for Commercial Transport Airplanes applies in most cases to light transport airplanes with takeoff weights above 12,500 lbs. For commercial transport airplanes also the GD method may be used. The most suitable method should be chosen, which is the Torenbeek method. For the most influential aircraft parts in terms of weight, the equations for the component weight calculations using the aforementioned method are given for the Antonov An-74. Apart from these large contributing parts, all other minor components are calculated. For these calculations reference is made to the work of J. Roskam [62] and especially the work of E. Torenbeek [47]. For the sake of brevity the entire calculations are not described in this report.

Structure Weight:

$$W_{struct} = W_w + W_{emp} + W_f + W_n + W_g \tag{2.78}$$

Wing Weight:

$$W_w = 0.0017 W_{MZF} \left(\frac{b}{cos(\Lambda_{1/2})}\right)^{0.75} \left\{1 + \left[\frac{6.3cos(\Lambda_{1/2})}{b}\right]^{0.5}\right\} (\eta_{ult}^{0.55}) \left(\frac{Sb}{t_r W_{MZF} \Lambda_{1/2}}\right)^{0.3} \tag{2.79}$$

Empennage Weight:

$$W_{emp} = W_h + W_v \tag{2.80}$$

Horizontal Tail Weight:

$$W_h = K_h S_h \left[3.81 \left(\frac{S_h^{0.2} V_D}{1000 cos(\Lambda_{1/2_h})^{1/2}}\right) - 0.287\right] \tag{2.81}$$

Vertical Tail Weight:

$$W_v = K_v S_v \left[3.81 \left(\frac{S_v^{0.2} V_D}{1000 cos(\Lambda_{1/2_v})^{1/2}}\right) - 0.287\right] \tag{2.82}$$

Fuselage weight:

$$W_f = 0.021 K_f \left[\frac{V_D l_h}{w_f + h_f}\right]^{0.5} (S_{fgs})^{1.2} \tag{2.83}$$

The value of K_f takes the following values in the above equation:
1.08 for a pressurized cabin, 1.07 for a main gear attached to the fuselage and 1.10 for a cargo airplane with cargo floor. These effects are multiplicative for airplanes equipped with all of the above.

Nacelle Weight:

$$W_n = 0.065 T_{TO} \tag{2.84}$$

Landing Gear Weight:

$$W_g = K_{g_r}[A_g + B_g(W_{TO})^{0.75} + C_g W_{TO} + D_g(W_{TO})^{1.5}] \tag{2.85}$$

The coefficients for the Landing Gear Weight calculation are given in Table 2.26.

Using the above mentioned Torenbeek method for the Class II calculations, the whole structure in terms of weight components is calculated. The load factor is of importance in some of the equations, this factor will be treated in Section 2.5.2. Finally the results of the calculations using the Torenbeek method are listed in Table 2.27.

Gear Component	A_g	B_g	C_g	D_g
Main	40.0	0.16	0.019	$1.5 \cdot 10^{-5}$
Nose	20.0	0.10	0.00	$2.0 \cdot 10^{-6}$

Table 2.26: Landing gear coefficients

Table 2.27: Antonov An-74 weight estimations

Component	Mass [kg]	[%]	C.G. from nose [m]	Moment [Nm]
Wing	3403	18	10.84	361704
Fuselage	3383	18	11.54	382,904
Landing gear Main	2641	14	7.01	181,593
Nacelle	2211	12	21.05	456,646
Landing gear nose	451	2	25.17	111,344
Horizontal tail	354	2	25.17	87,378
Vertical tail	347	2	23.62	80,344
Engines	1020	6	3.81	38,063
Engine starting	546	3	3.81	20,375
Fuel tanks wing	467	3	3.45	15,794
Fuel tanks center	159	1	10.94	17,118
Auxiliary power unit	1490	8	6.55	95,667
Instrumentation, avionics and electronics	671	4	7.14	47,000
Flight controls	541	3	12.06	64,010
Hydraulics	149	1	11.54	16,863
Auxiliary gear	86	0	3.81	3227
Electrical System	70	0	12.06	8289
Air conditioning, pressurization, de-icing system	62	0	12.06	7348
Baggage and cargo handling equipment	31	0	5.77	7348
Oxygen systems	24	0	12.06	2815
Oil systems	0	0	0	0
Armament	0	0	0	0
Guns, launchers and wpn provisions	0	0	0	0
Flight test instrumentation	0	0	0	0
Furnishings	52	0	3.81	1932
Operational items	45	0	11.36	5052
Paint	99	1	11.36	11,065
Ballast	91	0	0.00	0
Not accounted for	91	0	12.06	10,732
Total	18,484	100	11.27	2,029,031

Payload

Next to the structural components, the payload is a major contributor to the weight. Regarding this payload, a couple of items are taken into account. First the pilots and crew are incorporated. For the Antonov's mission the crew consists of two pilots, namely the captain and the first officer. For the crew, the navigator, flight engineer and loadmaster are counted. Apart from the pilots and crew, the cargo has the most influence to the payload weight. The cargo area of the Antonov has dimensions of 10.50 m (l) · 2.15 m (w) · 2.20 m (h). This cargo area provides enough room to store up to two medical containers. The combined weight of two containers is estimated based on existing containers. In the Flying Hospital case custom-made containers are to be designed, which may result in an increase or decrease of weight. This is dependent of the use of material and construction. The assumption now is that per container the empty (tare) weight is 2185 kg and 300 kg for interior and equipment. The total weight of two containers can therefore reach up to approximately 4970 kg. The equipment weight is based upon existing medical containers.

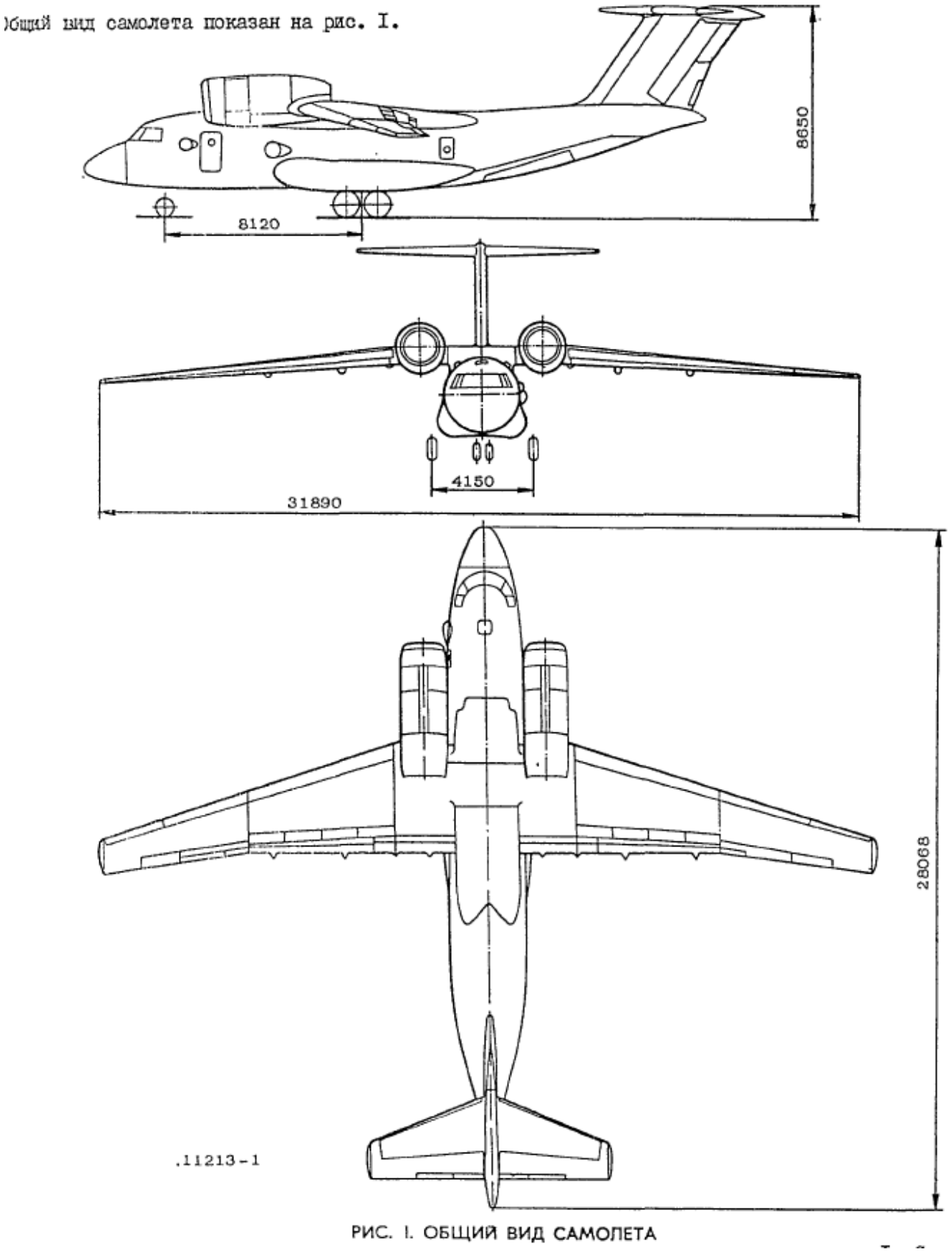

Figure 2.35: Technical drawing Antonov An-74 [46]

Fuel

The maximum fuel capacity for maximum range is 13,200 kg fuel as found in literature [33]. This maximum fuel load is taken into account in order to calculate the maximum loading abilities of the aircraft.

2.5.2 Load Factors

In order to make a good estimate of the loading diagram, the load factor has to be established. The load factor is used in methods for the weight calculations of several parts of the aircraft. A few examples of these are the wing and fuselage components. When setting up a load limit diagram, several steps are identified, these will be explained below.

Maneuver Loading

The maneuver load diagram, displaying the limit load factors during maneuvering, consists for the Antonov of 6 stages as seen in Figure 2.36. The first curve represents the maximum normal component load. This curve from 0-A is defined by Eq 2.86.

$$n = \frac{qC_{Lmax}}{(W/S)} \tag{2.86}$$

Where the line $n = 1$ crosses this curve, the stall speed is located. From the Airworthiness Certifications CS-23 [63] & CS-25 [64] the maximum positive and negative limit load factors for different aircraft are retrieved. Since the Antonov An-74 is a transport aircraft with a load larger than 50,000 lbs, a maximum load factor of 2.5 is found. The maximum negative limit load factor is -1. This is represented in Figure 2.36, respectively line A-D and line F-H. The speed at point D represents the dive speed V_D. This speed is based on the relation between the Mach number during cruise and during a dive. The next line, D-E, is a line from point D to the $n = 0$ axis at the same stall speed. The last curve H-O is given by the negative form of Eq. 2.86. The maximum load factor used in the calculations is therefore set to 2.5.

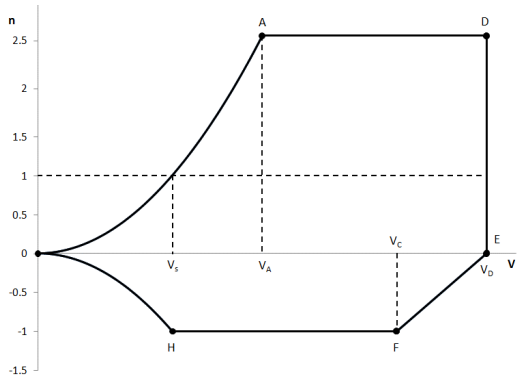

Figure 2.36: Manuever load diagram

2.5.3 Loading Diagram

Using the load factor from Section 2.5.2 and the aircraft parameters from Table 2.27 combined with the discussed method, a final loading diagram can be developed. This is done by creating a MATLAB program. The program calls all parameters and calculates based upon user inputs like number of crew and number of containers in cargo area what the final loading diagram will look like. This diagram is very important in order to stay within safety limits with respect to the center of gravity. The output is given in Figure 2.37. The extreme forward and aft c.g. position must be compatible with the limits dictated by the aircraft stability during loading. The safety margin is often 2% of these extremes in aviation. Since the redesigned Antonov An-74's primary function is to transport mission critical equipment, a safety factor of 5% is more suitable in this situation regarding mission safety while in hazardous environment. In the discussed figure, first the pilots and crew board the aircraft. Next the first and second container are loaded. Subsequently the fuel in the wing tanks is loaded and finally the center tank is filled. Using the MATLAB program, different scenarios can be plotted, each with different loading diagrams and therefore

different c.g. limits. For the sake of brevity only one, most common, example of a loading diagram is given, see Figure 2.37.

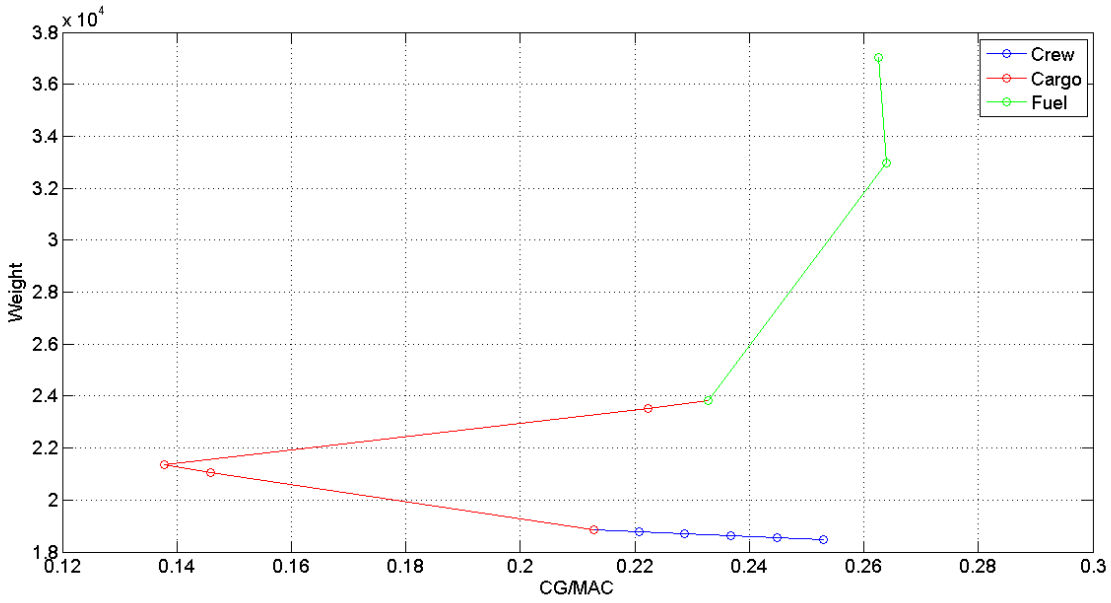

Figure 2.37: Loading diagram

2.5.4 Stability

Takeoff Center of Gravity

After having calculated the center of gravity of the empty aircraft, now fuel and cargo can be loaded and the new center of gravity could be calculated using Eq. 2.87.

$$x_{cg_{total}} = \frac{W_{ac}x_{cg_{ac}} + W_f x_{cg_f} + W_p x_{cg_p}}{W_{ac} + W_f W_p} \tag{2.87}$$

where: ac = aircraft, f = fuel and p = payload.

The values from the equation are computed using the MATLAB tool based upon the weight estimations developed in the previous sections.

Longitudinal Stability

The aircraft has to be stable throughout flight, most importantly during cruise. Therefore the relevant stability diagrams have to be drawn to demonstrate the allowable center of gravity range. A MATLAB code was developed to demonstrate the variations in center of gravity and stability margins corresponding to different flight times and different (potential) retrofitting options. The aircraft, throughout flight phases and with any retrofitting done, must be able to react to disturbances in angles of attack by generating an opposite pitching moment to restore the previous state of equilibrium. For this to occur the relative positions of components, being net center of gravity location and the neutral point, are very important to consider.

Neutral Point

The neutral point is a very important point in stability and control of a aircraft. It is defined as the point where the resultant of the lift force variations due to a perturbation is applied. The neutral point can be calculated by first determining the lift increments in the main wing and tail in terms of the angle of attack increment. The relations for the lift variations for the tailless aircraft and aircraft tail are shown in Eq. 2.88 and 2.89 [65].

$$\Delta L_{A-h} = C_{L\alpha_{A-h}} \Delta\alpha \frac{1}{2}\rho V^2 S \tag{2.88}$$

$$\Delta L_h = C_{L\alpha_h} (\Delta\alpha - \Delta\varepsilon) \frac{1}{2}\rho V_h^2 S_h \tag{2.89}$$

Lift Coefficient

To determine the neutral point location for the Antonov An-74, numerical values have to be used. To perform the calculations, a perturbation resulting in $\Delta\alpha$= 1° is assumed. Also using cruise altitude conditions and speed, the following values can be obtained for the lift change by using Eq. 2.88 and 2.89 mentioned in the previous section. Where $C_{L\alpha_{A-h}}$ and $C_{L\alpha_h}$ are the slopes of the $C_L - \alpha$ graphs. Their numerical values are calculated in the following sections using the DATCOM method. In order to determine the slope of the curve, the point about which to take the slope needs, i.e. the trim angle of attack needs to be determined. That can be done as follows;

$$C_L = C_{L_{A-h}} + C_{L_h} C_L = \frac{2W}{\rho V_c^2 S_T} = \frac{2 \cdot 36500}{0.412707 \cdot 166.66^2 \cdot (98.53 + 24.6426)} = 0.0517 \tag{2.90}$$

To obtain a total cruise lift coefficient of 0.0517, the aircraft has to be flying at 0°. At that angle, $C_{L\alpha_{A-h}} = 0.1292$ and $C_{L\alpha_h} = 0.095$. Therefore, the change in lift is obtained with Eq. 2.91 through 2.94:

$$\Delta L_{A-h} = C_{L\alpha_{A-h}} \Delta\alpha \frac{1}{2}\rho V^2 S \tag{2.91}$$

$$= 0.1292 \cdot 0.01745 \cdot 0.5 \cdot 0.412707 \cdot 166.66^2 \cdot 98.53 = 1273N \tag{2.92}$$

$$\Delta L_h = C_{L\alpha_h} (\Delta\alpha - \Delta\varepsilon) \frac{1}{2}\rho V_h^2 S_h \tag{2.93}$$

$$= 0.1292 \cdot (0.01745 - 0) \cdot 0.5 \cdot 0.412707 \cdot 166.66^2 \cdot 24.6426 = 234N \tag{2.94}$$

From Figure 2.38, and using the given airfoil data, the neutral point can be computed about the neutral point assuming that the forces of lift act at the quarter chord point, using the moment equilibrium formula, Eq. 2.95 [65].

$$\Delta M_{np} = \Delta M_{ac} + \Delta L_{A-h}(x_{np} - x_{0.25c_w}) - \Delta L_h (x_{0.25c_h} - x_{np}) = 0 \tag{2.95}$$

Therefore, for aircraft stability, the center of gravity must always be in front of the neutral point.

Stability Diagrams

Eq. 2.96 [65] describes the position of the stick-fixed neutral point as a percentage of mean aerodynamic chord in terms of the horizontal tail size.

$$\bar{x}_{np} = \bar{x}_{ac} + \frac{C_{L_{\alpha h}}}{C_{L_\alpha}} \left(1 - \frac{d\varepsilon}{d\alpha}\right) \frac{S_h l_h}{S\bar{c}} \left(\frac{V_h}{V}\right)^2 \tag{2.96}$$

Where:

$$C_{L\alpha} = C_{L\alpha_{A-h}} + C_{L\alpha_h} \left(1 - \frac{d\varepsilon}{d\alpha}\right) \frac{S_h}{S} \left(\frac{V_h}{V}\right)^2 \tag{2.97}$$

assuming a stability margin of 5%, Eq. 2.96 is then re-written to become Eq. 2.98.

$$\bar{x}_{cg} = \bar{x}_{ac} + \frac{C_{L_{\alpha h}}}{C_{L_\alpha}} \left(1 - \frac{d\varepsilon}{d\alpha}\right) \frac{S_h l_h}{S\bar{c}} \left(\frac{V_h}{V}\right)^2 - 0.05 \tag{2.98}$$

Eq. 2.96 and 2.98 are plotted in Figure 2.38 to illustrate the stability margins within which the aircraft's center of gravity can mobilize.

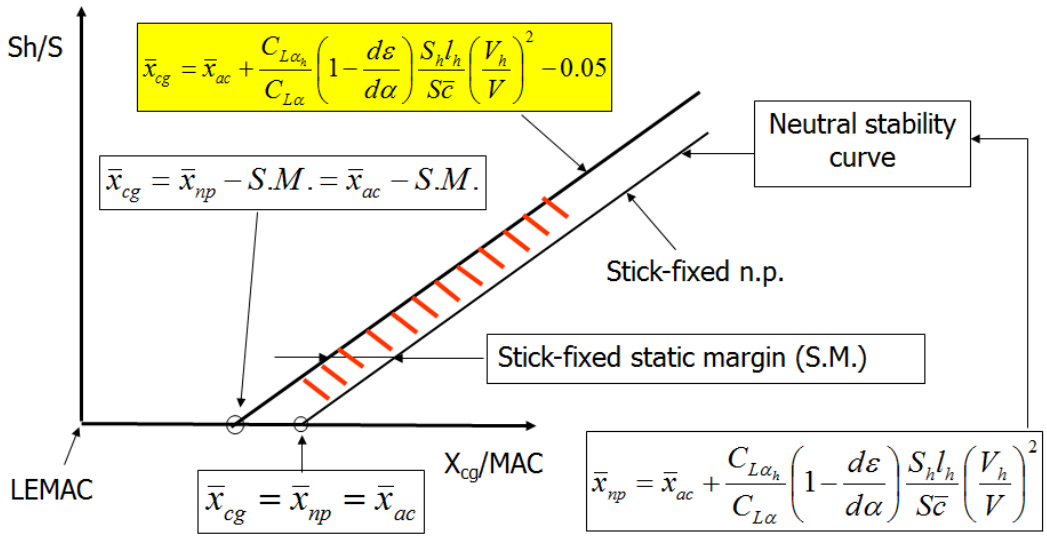

Figure 2.38: Stick-fixed static margin [65]

2.5.5 Equation Parameters

Tail-Wing speed ratio $C_{L\alpha_h}$

The air velocity that the tail experiences is usually different than the one that the wing experiences due to the presence of the fuselage. However, the tail/wing speed ratio $\frac{V_h}{V}$ is equal to 1 because of the T-tail configuration [65]. The tail is higher than the wing and fuselage. Therefore, these do not upset the airflow that the tail eventually experiences. That results in the tail experiencing the same flow velocity as the wing.

Tail Lift Rate Coefficient $C_{L\alpha_h}$

The horizontal tail lift rate coefficient, $C_{L\alpha_h}$, can be computed using the DATCOM method [65] expressed in Eq. 2.99.

$$C_{L\alpha_h} = \frac{2\pi A_h}{2 + \sqrt{4 + \left(\frac{A_h \beta}{\eta}\right)^2 \left(1 + \frac{tan^2(\Lambda_{0.5C_h})}{\beta^2}\right)}} \tag{2.99}$$

For the cruise mach number Eq. 2.100 can be used.

$$\beta = \sqrt{1 - M^2} \tag{2.100}$$

Aircraft Lift Rate Coefficient $C_{L\alpha}$

The aircraft lift rate coefficient, $C_{L\alpha}$, could be computed using equation 2.97. However, the component $C_{L\alpha_{A-h}}$ needs to be knows first. Eq. 2.101 [65] is used to determine this parameter value.

$$C_{L\alpha_{A-h}} = C_{L\alpha w}\left(1 + 2.15\frac{b_f}{b}\right)\frac{S_{net}}{S} + \frac{\pi b_f^2}{2S} \tag{2.101}$$

where, b_f is the span of the fuselage section shown in Figure 2.39 and S_{net} is the difference between the wing area and the projection of the central wing part inside the fuselage.

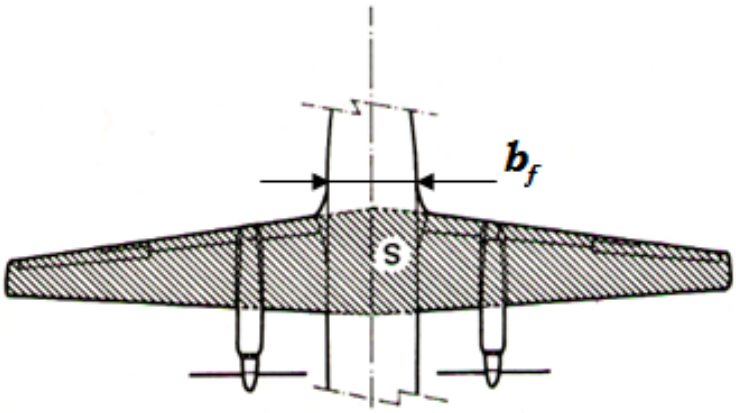

Figure 2.39: Aircraft wing area and fuselage span [65]

Aerodynamic Center

The aerodynamic center is influenced by the nacelles and jet steam vector. When taken into account, the resultant aerodynamic center is represented by Eq. 2.102 [65].

$$\bar{x}_{ac} = \bar{x}_{ac_{wf}} + \bar{x}_{ac_n} + \bar{x}_{ac_T} \tag{2.102}$$

Wing and Fuselage Aerodynamic Center

The wing and fuselage contribution to the aerodynamic center, ac_{wf}, can be calculated using equation 2.103 [65].

$$\left(\frac{x_{ac}}{\bar{c}}\right)_{wf} = \left(\frac{x_{ac}}{\bar{c}}\right)_{w} - \frac{1.8 b_f h_f l_f}{S\bar{c}C_{L_{\alpha_{wf}}}} + \frac{0.273}{1+\lambda}\frac{b_f c_g (b-b_f)}{\bar{c}^2(b+2.15b_f)} tan\Lambda_{1/4} \tag{2.103}$$

Where, C_g is the mean geometric chord S/b. The other geometric parameters can be found in Figure 2.40.

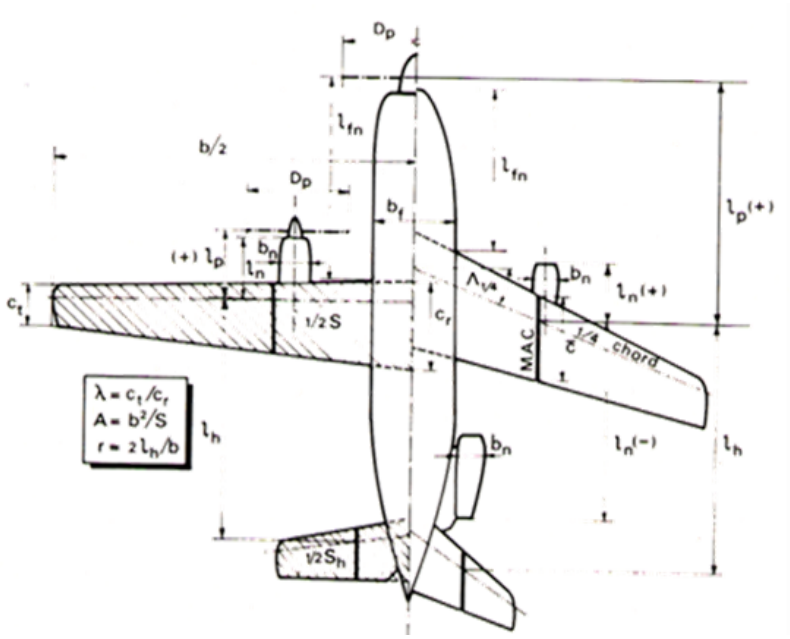

Figure 2.40: Aircraft geometric parameters [65]

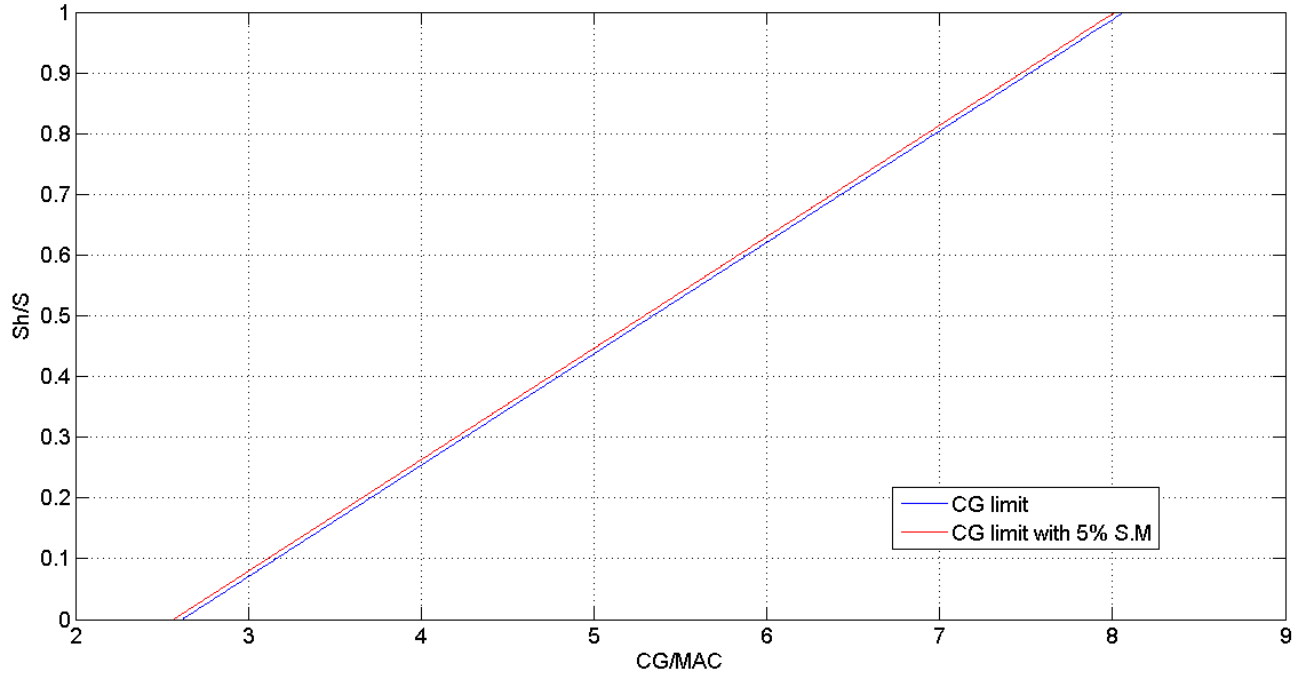

Figure 2.41: Maximum center of gravity location for stability

Nacelles's Aerodynamic Center Contribution

The nacelles also contribute to the aerodynamic center location on the aircraft. This contribution is quantified in Eq. 2.104 [47].

$$(\bar{x}_{ac})_n = \sum k_n \frac{b_n^2 l_n}{S\bar{c}(C_{L_\alpha})_{wf}} \tag{2.104}$$

Where, $k_n = -4.0$ for the Antonov An-74 [47].

Jet Thurst's Aerodynamic Center Contribution

The thrust vector has an effect on the aircraft's aerodynamic center. If the thrust line is above the center of gravity, the distance z_T is negative and so the a.c and n.p move aft, making the aircraft more stable and vice versa. If the thrust vector is aligned with the center of gravity, the thrust vector has no contribution to the aerodynamic center [65]. This relation can be illustrated using Eq. 2.105.

$$\left(\frac{x_{ac}}{\bar{c}}\right)_T = -\sum \frac{T z_T}{W\bar{c}} \tag{2.105}$$

2.5.6 Stability Results

When all the equations and assumptions above are taken into account, and the aircraft parameters of the Antonov An-74 are used as inputs, Eq. 2.98 is plotted in Figure 2.41.
Making use of a MATLAB program, the center of gravity of the aircraft is computed, given a certain fuel, cargo and crew loading or distribution. It then computes the allowable center of gravity locations. A statement whether the current aircraft is stable or if a tail re-design needs to be carried out is generated as output.

2.5.7 Aicraft Trimming

Aircraft trimming is very important during cruise for stability and control. To ensure a trimmed flight, the net moment of the aircraft should be equal to zero. This is best achieved via one of three methods:

- Alter the lift using wing or tail control surfaces.

- Move the c.g. of the aircraft to result in moment equilibrium.
- Redesign the tail or wing for the new aircraft moments.

The easiest and most efficient method is to use the control surfaces. If those are not enough to accommodate for the high moment of the aircraft, the location of the center of gravity can be adjusted. This is done either before flight by properly positioning the crew and cargo, or during flight by pumping fuel to appropriate locations. Since re-designing and rebuilding the tail and wing are the most time consuming, costly and demanding methods, these shall be avoided as much as possible for the Antonov An-74 in question. A MATLAB program calculates the center of gravity location necessary for aircraft trimming. As fuel is consumed during flight, the center of gravity relocates. This shifts the aircraft away from its trimmed position. There is no existing system on board of the Antonov An-74 to keep the center of gravity exactly on the trim point constantly during flight. However, the trim position can be regained manually using the moments of the forces generated by control surfaces of the wing and tail. For the Antonov An-74, Figure 2.42 shows the net forces and moments of the aircraft. The distance denoted as x is the design distance between the quarter chord point of the mean aerodynamic chord and the center of gravity for aircraft trim with the given wing, tail and flight configurations.

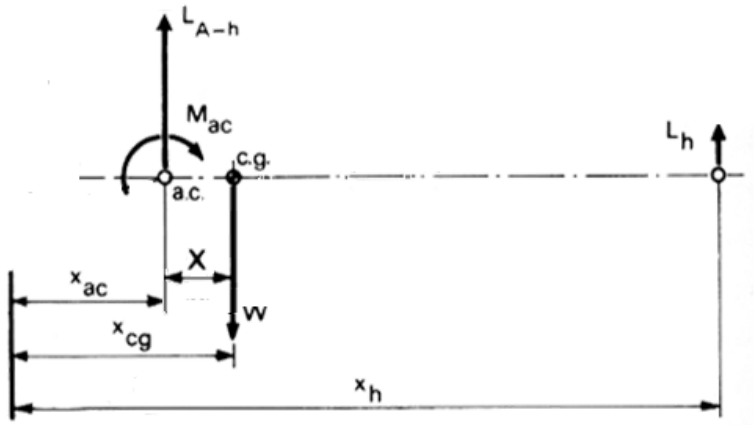

Figure 2.42: Trim equation parameters [65]

The equation for moment equilibrium is then equation 2.106.

$$M_{ac} + L_w(x_h - x_{ac}) = W(x_h - x_{cg}) \tag{2.106}$$

This equation is used in the MATLAB program to calculate the value of x. As long as the actual center of gravity location is not very far from this position, no major structural redesign is required.

2.5.8 Sensitivity Analysis

After all of the above calculations, three main results are obtained:

1. The most aft center of gravity location for stability
2. The ideal c.g. location for trim
3. The most possible forward and aft center of gravity location during loading and unloading

In case of loading and unloading, the sensitivity calculations of the design determines the actual center of gravity location with respect to the stability margin. These calculations should be done by a program within the aircraft itself and may be developed in a future design phase. If the distance is within reasonable limits, then minor reloading or redistribution of loads will rectify the problem. Furthermore, the loading diagram indicates the most possible aft location of the center of gravity in worst case (over)loading scenario. The sensitivity calculations determine how far away this extreme location is from the stability margin. In case the distance is large, the pilot can rest assured that whatever happens during disaster site evacuation, the aircraft is still stable and flyable. If the distance is small, care

should be taken during the evacuation or some redesign needs to be performed to re-enlarge that distance. If the center of gravity crosses the stability point, then further re-design must be considered. During flight, the sensitivity analysis also calculates how far the center of gravity is from the trim point, that distance also indicates the extent of the redesign needed to ensure trimmed flight throughout cruise. The sensitivity analysis measures these distances, however actual values of what is an acceptable risk are subject to the pilot's decision and preference.

2.5.9 Verification & Validation

The programs used to compute the values and limits for the stability and control of the Antonov An-74 need to be verified to ensure their viability and integrity. This can be done by means of double calculations. On one hand, the MATLAB code will be used to derive the results. On the other, calculations will be performed manually and results are obtained. The two results will then be compared and the difference measured. If there is a difference, then the code needs to be revised and corrected then re-run. This process will be iterated until the MATLAB program output is exactly corresponding to the manual calculation results. This ensures that the code is correct and if free from errors. Furthermore, for the stability code, extreme values will be input for loads and their locations, the output of the code must be that the aircraft is unstable for those values. If not, then the code needs to be rectified.

The Fokker-VFW F-28/600 is used for validation of data. This aircraft is chosen since the MTOW lies close to the Antonov's MTOW. In wing, tail and fuselage group the components are almost identical with some deviations possible. For the landing gear a large difference with respect to the Antonov is observed. When comparing the main landing gear of both aircraft it is seen that the Antonov has a much more robust and larger landing gear, therefore the deviance in weight is clarified. For the other weight components almost identical values are found when comparing and thus conclusion can be assessed that calculation methods are valid.

2.5.10 Recommendations

In this section some recommendations regarding the stability and control are given. First the monitoring options are discussed and finally the redesign options are listed.

Monitoring Options

The stability of the aircraft has to be monitored during loading, flight and unloading to avoid accidents or mishaps. Therefore, some monitoring mechanism have to be devised to ensure the aircraft stability at all times. The best system to perform such a function is the weighing of the aircraft. The conventional weighing scales are not a feasible option because of their size and weight and because of the nature of the mission. The aircraft will be used anywhere in the world where a disaster occurs, and there is a high probability that those scales will not be available. Therefore, a second option is the use of pressure sensors. Pressure sensors could be placed in the landing gears. Either inside the hydraulic system or inside the tires. The sensors can detect the pressure values of the air inside the tires or the fluid inside the hydraulic system. These pressures are strongly related to a fluctuation in weight of the aircraft and its distribution. Therefore, a relation can be devised between the pressure distribution over the different hydraulic systems or tires and the weight distribution. The sensors will send the measured values to a central processing unit. That unit will compute the c.g. location and loading of the aircraft. The output will be the location of the center of gravity, the remaining stability margin, indications of overload area and possible actions to be taken to regain stability. These will be displayed in real time to the pilot in the cockpit during loading, unloading, when fuel is consumed or when people or cargo move during flight. Development of such a system is dependent on the safety margin of the sensitivity analysis. It is beyond the scope of this report. However, it can be further investigated in subsequent phases of the project.

Redesign Options

For the current mission requirements and cargo loads, there is no need to redesign the aircraft for stability reasons. However, if the center of gravity falls outside the stability limit with future requirements or cargo loading, the following actions can be taken to rectify the situation and regain stability [65]. These further designs can be investigated by other Design Synthesis Exercise groups or by MSc. students for an in dept investigation of the possibilities in their Master Thesis.

- The design of the tail plane should be altered to change its area in order to improve stability.

- The tail plane position can be changed to increase the moment arm of the tail lift force. That can be achieved by lengthening the fuselage.
- Redesign of internal aircraft systems and re-positioning of components placing the heavier components more to the front.
- Design a fuel active control system using pumps and intermediate tanks to relocate fuel appropriately for stability
- Using a canard on the aircraft nose. This will enable the extension of the stability margin by moving the center of gravity forward. It could also provide a more efficient and faster recovery from stall due to the large moment arm of forces generated by that surface and therefore larger moments to regain stability and controllability.
- Using stall recovery kits [25]. These, also originally intended for stall recovery, could also be used with the primary objective of regaining stability. The same principle used in stall recovery kits could be applied to recovery from an instable position. The stall kit is placed at the very front of the aircraft, therefore due to the large moment arm, small forces from the stall kit surface result in a relatively large moment bringing the aircraft back to stability or trim position.

2.6 Material Characteristics

The previously described and applied modifications not only require structural adjustments, but also require an analysis on the material properties of the structural components. This is mainly because the modifications introduce new operating conditions for the material; these conditions include altered loads and temperatures. This section will elaborate on general material properties in order to get an insight on how the material will behave under new circumstances.

Figure 2.43 illustrates a stress strain curve, engineering strain is classified as the deformation of a solid material due to stress [66]. This curve indicates the altering stages that a material goes through during different loading conditions. The material behaves linearly w.r.t the applied stress during low stress levels. Increasing the applied stress results in yielding of the material. Yielding of material is defined as the phenomenon where the material deforms plastically; the material does not regain its original shape after it is relieved from the applied loading. Increasing the loading even further results in the failure of material, this happens at the materials' ultimate stress; The new loading conditions should not exceed the materials' yield stress, the material must remain in the linear region in order to comply with the airworthiness authorities. Another operating material should be selected if this requirement cannot be satisfied.

Several assumptions can be applied while analyzing materials, the main assumptions that are applied in this section are the linearity and the isotropic behavior of a material. The linearity assumption indicates that there is a linear relationship between the stress and strain in a structure. The isotropic behavior indicates that the material properties are independent of the loading directions. This is a reasonable assumption since most parts of the Antonov An-74 consist out of metals, which are isotropic.

2.6.1 Mechanical Strain

The previously mentioned assumptions can be used to establish a mathematical relationship between the stress and strain in a structure. Figure 2.44 illustrates the three dimensional application of normal stresses on a unit cube. The stresses in the x, y and z directions are related to the three dimensional normal strains which are given in Eq. 2.107, Eq. 2.108 and Eq. 2.109 [67] respectively. One can observe that the strain in a particular direction is a function of all the applied stresses on the material, this gives a reason to analyze the material more thoroughly for failure during the new loading.

Section 2.4 denoted that the normal stresses in the wing increased by 2.8%. The material strain decreases by a factor of 1.028 when one assumes a linear relationship between the normal stress and normal strain, and that the stress increase occurs in three dimensions. The material behavior should be observed due to this decrease in strain.

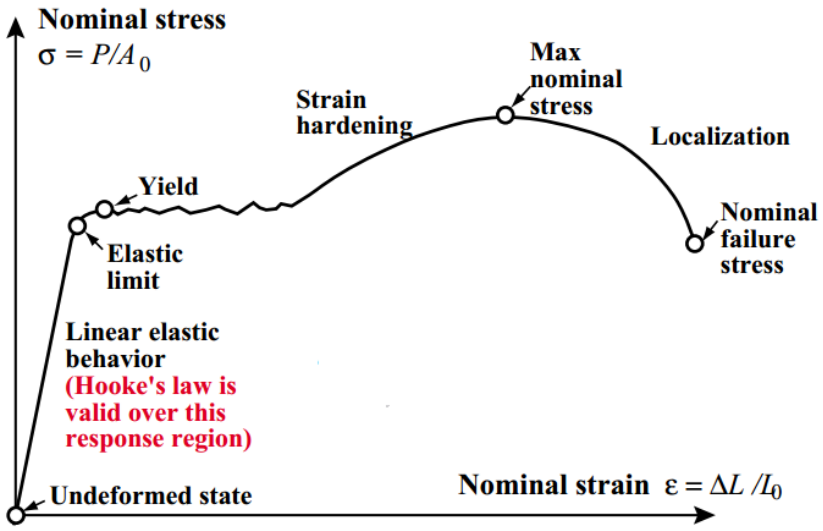

Figure 2.43: Stress strain relationship [67]

The same principle holds for the normal stresses in the fuselage of the aircraft, there is an increase of 7.5% in the normal stress in the fuselage. This implies that the material strain is reduces by a factor 1.075.

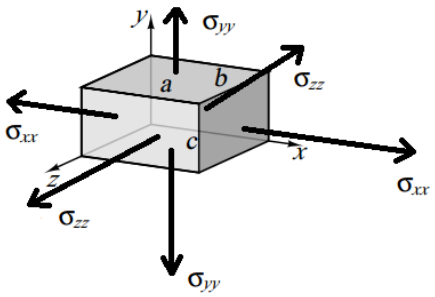

Figure 2.44: Three dimensional plane stress [67]

$$\epsilon_{xx} = \frac{1}{E}(\sigma_{xx} - \nu\sigma_{yy} - \nu\sigma_{zz}) \tag{2.107}$$

$$\epsilon_{yy} = \frac{1}{E}(\sigma_{yy} - \nu\sigma_{xx} - \nu\sigma_{zz}) \tag{2.108}$$

$$\epsilon_{zz} = \frac{1}{E}(\sigma_{zz} - \nu\sigma_{xx} - \nu\sigma_{zz}) \tag{2.109}$$

The material is also subjected to shear stresses, these stresses result in shear strains in the material. The shear strains and shear stresses are related to each other and are given in Eq. 2.110, Eq. 2.111 and Eq. 2.112 [67] respectively. Section 2.4 indicated that the shear stresses in the wing increased with 12.5%. The shear strain decreases by a factor of 1.125 when one assumes a linear relationship between the shear stress and shear strain, and that the stress increase occurs in three dimensions. The same principle holds for the shear stresses in the fuselage of the aircraft, there is an increase of 2.05% in the fuselage shear stress. This implies that the material strain is reduced by a factor 1.0205.

The normal strains and shear strains can collectively be expressed in matrix form in order to obtain a detailed overview on the applied stresses and resulting strains. Eq.2.113 [67] gives a matrix equation that includes the shear and normal stresses on the right hand side, and the strains on the left had side of the equations. This relation is of utter importance when the aircraft material is subjected to new circumstances and thus this relation can be used to verify the materials' capabilities to operate in new conditions.

$$\gamma_{xy} = \gamma_{yx} = \frac{\tau_{xy}}{G} = \frac{\tau_{yx}}{G} \tag{2.110}$$

$$\gamma_{yz} = \gamma_{zy} = \frac{\tau_{yz}}{G} = \frac{\tau_{zy}}{G} \tag{2.111}$$

$$\gamma_{zx} = \gamma_{xz} = \frac{\tau_{zx}}{G} = \frac{\tau_{xz}}{G} \tag{2.112}$$

$$\begin{bmatrix} \epsilon_{xx} \\ \epsilon_{yy} \\ \epsilon_{zz} \\ \gamma_{xy} \\ \gamma_{yz} \\ \gamma_{zx} \end{bmatrix} = \begin{bmatrix} \frac{1}{E} & -\frac{\nu}{E} & -\frac{\nu}{E} & 0 & 0 & 0 \\ -\frac{\nu}{E} & \frac{1}{E} & -\frac{\nu}{E} & 0 & 0 & 0 \\ -\frac{\nu}{E} & -\frac{\nu}{E} & \frac{1}{E} & 0 & 0 & 0 \\ 0 & 0 & 0 & \frac{1}{G} & 0 & 0 \\ 0 & 0 & 0 & 0 & \frac{1}{G} & 0 \\ 0 & 0 & 0 & 0 & 0 & \frac{1}{G} \end{bmatrix} \begin{bmatrix} \sigma_{xx} \\ \sigma_{yy} \\ \sigma_{zz} \\ \tau_{xy} \\ \tau_{yz} \\ \tau_{zx} \end{bmatrix} \tag{2.113}$$

2.6.2 Thermal Strain

Not only the external loads differ after retrofitting a new engine, but also new thermal conditions arise. The main temperature change is at the aft of the engine in proximity of the upper side of the wing. Al the components behind the engine are made out of titanium [36] to coop with high temperatures and thus high stresses. With the new engine, the temperature of the flow leaving the engine significantly increases. The existing Ivchenko Progress D-36 2A generates an exit temperature of 392.94 K, whereas the new Ivchenko Progress D-436-T3 produces an exit temperature of 417 K. This implies that one has to analyze the thermal behavior of titanium. The basic relation between material strain and temperature is given in Eq. 2.114 [67] where α is the coefficient of thermal dilation, a measure of the expansion rate of a material [67]. The thermal strain is mainly caused due to the fact that the material tries to expand because there is a temperature difference. However the material is constrained by fastening systems. This retards the expansion process and generate thermal stresses in the structure. The coefficient for thermal dilation of titanium is given in Eq. 2.115 [68], the additional thermal stress can be determined with the temperature difference and Eq. 2.116, where the Youngs' modulus of titanium is 110.3 GPa [68]. The calculated thermal stress is then 22.822 MPa which is a first order approximation in a one dimensional direction. This is a significant increase in normal stress, this implies that one needs to consider the additional strains that are produced due to the thermal stress and observe the stress strain curve to predict the yielding behavior of the material.

$$\epsilon_{thermal} = \alpha \triangle T \tag{2.114}$$

$$\alpha_{titanium} = 0.000086 K^{-1} \tag{2.115}$$

$$\sigma_{thermal} = E \epsilon_{thermal} \tag{2.116}$$

2.6.3 Recommendation

Both the thermal and mechanical strains produce stresses in the material. The material behavior can be investigated with the appropriate resources and time. This in order to conduct thorough research to prove the airworthiness of the material. However, this is not in the scope of this project and thus is recommended for future projects and thesis's .

2.7 Results of Technical Modifications

In previous sections, the change of engine and addition of VGs were discussed together with their effects on the STOL performance. In this section, the contributions were integrated in the original aircraft; it is examined to what extent the performance is improved. At first, the method used will be explained in Section 2.7.1. Secondly, the actual results are provided in Section 2.7.2.

2.7.1 Method

With the detailed analysis of the modifications completed, the net performance increase of the aircraft could now be evaluated. Emphasis was placed on the landing and takeoff performance of the aircraft as these phases are most critical for the innovation and operational aspects of the Flying Hospital. However, the modifications proposed in this chapter will affect cruise performance, therefore this phase was also investigated to a lesser extent.

Landing Performance

The landing performance of the aircraft was evaluated by conventional flight mechanics equations [69]. In order to complete these calculations, the basic landing characteristics of the aircraft, $C_{L\ landing}$, $C_{D\ landing}$ and V_s, had to be derived. Additional variables and constants, documented in Table 2.28 were either taken from standard atmospheric data or extrapolated from known An-74 data.

Table 2.28: Landing variables and constants

Variable or Constant	Value	Source/Derivation
$S_{landing}$	118.2 m^2	120% S (flap chord ratio 0.2)
ρ	1.225 $kg{\cdot}m^{-3}$	Sea level S.A.
μ	0.25	[70]
h_{screen}	35 ft	Obstacle height civil aircraft regulation
γ	3°	Typical descent angle
T	0	Assumed idle thrust, no reversing

The flight mechanics equations rely on characteristic V speeds of the aircraft from which the $C_{L\ landing}$ could further be derived. The approach velocities, $V_{approach}$, of the stock An-74 were known from the flight manual and are reproduced in Figure 2.45. From these velocities the remaining V speeds could be estimated and $C_{L\ landing}$ calculated by the relations shown in Table 2.29 and Eq. 2.117 assuming steady flight. It was found that the original $C_{L\ landing}$ without modifications had a value of 1.5 (a low value compared to conventional numbers, but such deviation is expected when reverse engineering such parameters from limited data with unavoidable assumptions).

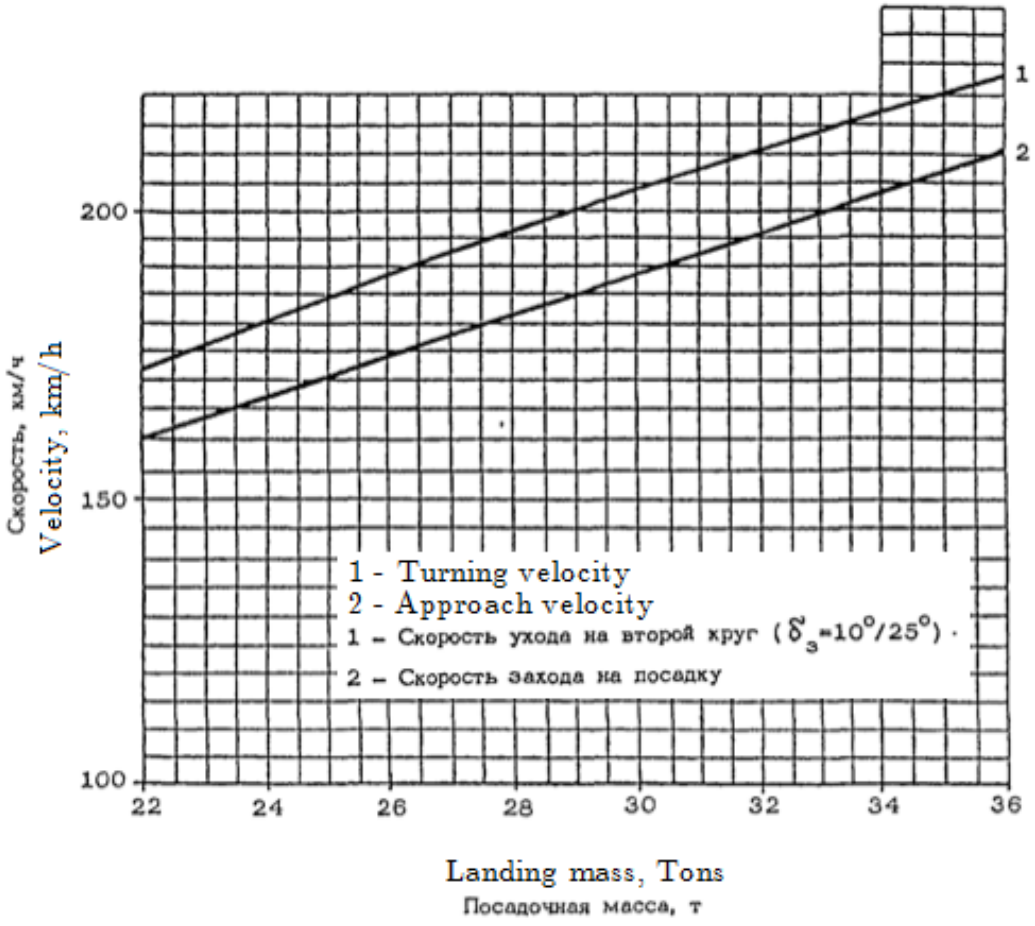

Figure 2.45: Approach velocities unmodified An-74 (line 2) [46]

Table 2.29: V speeds, relations as described in [69]

V **Speed**	**Relation**	**Value at unmodified vehicle weight 30 ton**
V_s	$V_{approach}/1.3$	40.2 m·s^{-1}
$V_{touch\ down}$	$1.15V_s$	46.2 m·s^{-1}
V_{screen}	$1.2V_s$	48.2 m·s^{-1}

$$C_{L\ landing} = \frac{2W}{\rho V_{approach}^2 S_{land}} \tag{2.117}$$

The value of $C_{D\ landing}$ was based on similar aircraft data available and set to 0.35 [71]. This estimate has considerable uncertainty that will permeate into further calculations; the An-74 configuration is relatively unique in shape and layout and thus likely deviates in drag coefficient from more conventional counterparts. With all variables and constants defined, Eqs. 2.118 to 2.120 were solved for multiple landing weights (and corresponding V speeds) to find the total landing distances. In order to evaluate the performance gains of the modified aircraft the same routine was used but with modified variables for the new parameters and coefficient changes (see Section 2.7.2).

$$a = \frac{g}{W}(T - \frac{1}{2}\rho V_{touch\ down}^2 S_{land} C_{D\ landing} - \mu(\frac{1}{2}\rho V_{touch\ down}^2 S_{land} C_{L\ landing} - W) \tag{2.118}$$

$$s_{ground\ run} = \frac{V_{touch\ down}^2}{2a} \tag{2.119}$$

$$s_{total} = \frac{\frac{V_{screen}^2 - V_{touch\ down}^2}{2g} + h_{screen}}{\sin\gamma} + s_{ground\ run} \tag{2.120}$$

Takeoff Performance

The takeoff performance was investigated in an identical manner as the landing performance. Variables and coefficients used are defined in Tables 2.30 and 2.31. Takeoff lift coefficient, $C_{L\ landing}$, was set as 60% of the landing coefficient based on statistics [72].The value of $C_{D\ takeoff}$ was based on similar aircraft data available and set at 0.31 [71]. Liftoff velocities, V_{LOF}, were obtained from Figure 2.46. After establishing all these inputs Eqs. 2.118 (replacing $V_{touch\ down}$ with V_{TO}) and 2.121 to 2.122 were solved for the total takeoff distance. As with the landing analysis, the process was repeated for the modified aircraft with updated variables (Section 2.7.2).

Table 2.30: Takeoff variables and constants

Variable or Constant	**Value**	**Source/Derivation**
$S_{Takeoff}$	103.5 m^2	105% S
ρ	1.225 kg·m^{-3}	sea level S.A.
μ	0.25	[70]
h_{screen}	35 ft	obstacle height civil aircraft regulation
γ	8°	typical takeoff angle
T	127.8 kN	full thrust existing engines

Table 2.31: V speeds, relations as described in [69]

V **Speed**	**Relation**	Value at unmodified vehicle weight 30 ton
V_{TO}	$\sqrt{2}V_{LOF}/2$	45.9 m·s^{-1}

$$s_{LOF} = \frac{V_{LOF}}{2a} \tag{2.121}$$

$$s_{total} = (\frac{{V_{screen}}^2}{2g} + h_{screen}) \cdot \frac{1}{sin(\gamma)} + s_{LOF} \tag{2.122}$$

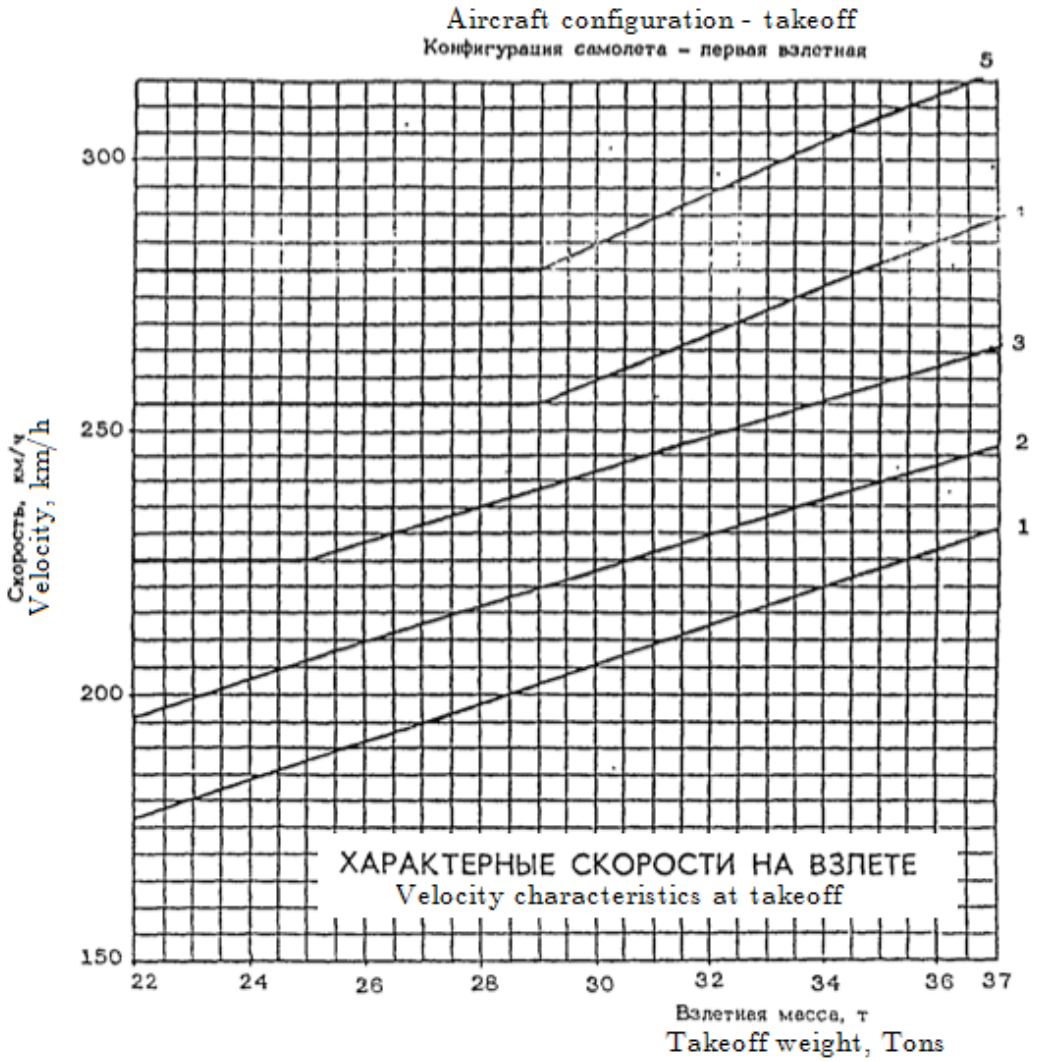

Figure 2.46: V_{LOF} unmodified An-74 (line 3) [46]

Cruise

The proposed modifications for the An-74 will result in different drag, lift and fuel consumption during cruise flight. These effects are brought about by the retrofitted D-436 engines (additional weight, higher SFC) and their effect on the upper surface blowing of the wing (lift and drag increase). The cruise of the stock and modified aircraft can be compared by Breguet range equation, Eq. 2.123.

$$Range = \frac{V}{g \cdot SFC}(\frac{L}{D})_{cruise} \ln(\frac{W_{start}}{W_{end}}) \tag{2.123}$$

2.7.2 Results

Effect on C_L, C_D and V_s

Based on the theory and method explained above, it is possible to determine the change in STOL performance due to the change in engines and the addition of the VGs.

As outlined before, the runway length required is determined by certain speeds (V_{LOF}, $V_{approach}$, $V_{touch-down}$), which are based on V_s. If it is possible to determine the change in V_s due to the modifications, and thus reduce V_{LOF}, $V_{approach}$ and $V_{touch-down}$, one can determine the change in runway distance required. For this, Eq. 2.124

is used:

$$V_s = \sqrt{\frac{2L}{C_L \rho S}} \tag{2.124}$$

In Table 2.32, the influence of the Coanda effect and the addition of VGs is summarized.

Table 2.32: Influence of Coanda effect and addition of vortex generators on takeoff performance

Takeoff	C_L	C_D	Thrust
Coanda	+7.7%	+1.9%	+45%
Vortex Generators	0%	0%	0%
Total	+7.7%	+1.9%	+45%

Since C_L is increased by 7.7%, V_s decreases by 3.4%. This means that V_{LOF}, given as a function of V_s, decreases by 3.4% as well. However, there is a small drag increase of 1.9%, which slightly increases the runway length required. The increased thrust during takeoff reduces the runway distance.

The effects during landing can be seen in Table 2.32. In the landing configuration, V_s is decreased by 7.2% due to a 16.7% increase in C_L. During the ground run, C_D change due to the Coanda effect is neglected since there is no forward thrust; possible reverse thrust will not have a Coanda effect. Also the C_D change of the VGs due to the direct device drag is neglected, since during the ground run spoilers are extracted; the VGs will be downstream of the spoilers and will thus marginally increase drag. To summarize: during landing, V_s reduces by 7.2% and thus $V_{approach}$ and $V_{touch-down}$ will decrease by 7.2% as well.

Table 2.33: Influence of Coanda effect and addition of vortex generators on landing performance

Landing	C_L
Coanda	+7.7%
Vortex Generators	+9.0%
Total	+16.7%

Interaction Between Modifications

In Chapter 2 the engine/USB modifications and vortex generators were designed with reference to the stock aircraft, independently of each other. Thus any interrelations and influences between these two were not considered. In practice these modifications will influence one another since vortex generators were placed in the exhaust path of the new engines. As a result, the vortex generators in this region would be exposed to a different airflow brought about by the Coanda effect of the USB. Operating in these conditions (higher air velocities) the vortex generators would produce higher boundary layer velocities and friction velocities (U_e and μ_τ) thus generating larger vorticity. This larger vorticity could be excessive and lead to additional drag. In practice this could be accounted for by reducing the size of vortex generators placed within the USB area. However, for the simplification of subsequent calculations the vortex generators and engine/USB interrelations were discarded; force contributions of each modification were assumed to be independent, enabling their direct summation when evaluating net modification influence on the aircraft.

Effect on Runway Distance Required

Based on the changes for C_L, C_D and V_s derived in previous section, it is possible to determine the new values for required runway using the method as outlined in Section 2.7.1. For the results, see Table 2.34 and Table 2.35. Results are also visualized in Figure 2.47. Available data on the An-74 confirmed the validity of the calculated takeoff distances for the unmodified aircraft at lower weights [35]. No data could be found from which to validate performance at higher weights.

It is clear that the new configuration, i.e. the original An-74 with modifications, has a greatly reduced takeoff distance. For a takeoff weight in the range 22-30 ton, the takeoff distance is reduced by 42%-55%. This is due

to the fact the new engine has an increased maximum power (+45%). For the MTOW of the modified aircraft the takeoff distance is 478 m; the aircraft is still STOL at this weight, which was not the case for the original aircraft.

The change in landing distance required is smaller, i.e. around 12%. For a maximum landing weight (36 tons) the total landing distance is 582 m. During landing, certification regulations state that no reverse thrusters can be used. Hence the increased power of the new engine has little effect. The Coanda effect causes an increase in C_L; furthermore, the VGs also cause an increase in C_L. Due to the increase in C_L, V_s decreases and the runway distance required will be smaller. The effect however is relatively small when compared to the takeoff situation.

On the other hand, if reverse thrust is applied, the effects are appreciable as seen in Table 2.36. This data was generated assuming a reverse thrust of 15% of the engine rated thrust, a low value compared to reference material [73]. Reverse thrust was assumed constant from touchdown to standstill, though in reality reverse thrust is decreased upon slowing down. The low reverse thrust value was intentional in order to compensate for this constant thrust assumption.

As expected, the reverse thrust made considerable reductions in the landing ground run. With the aforementioned reverse thrust settings the landing distance for the aircraft at maximum weight was reduced to 487 m. When compared to the landing distances of the modified aircraft without reverse thrust, total landing distances were reduced by ∼20%. When compared to the original aircraft without reverse thrust, total landing distances were reduced by ∼30%. While these improvements are significant and capitalize on the new engines' thrust, they are representative of optimal conditions. Realistically, STOL landings in rough terrain may inhibit, if not prohibit, the use of reverse thrust for risk of debris ingestion by the engines. As such the use and extent of reverse thrust is specific to individual landing conditions.

Table 2.34: Takeoff performance changes due to implementation of technical modifications (Sea-Level Conditions)

Takeoff Takeoff Weight	[ton]	22	24	26	28	30	32	34	36
Ground Run									
Before Modifications	[m]	293	326	376	456	552	668	809	982
After Modifications	[m]	151	165	194	223	261	305	355	411
Airborne Phase									
Before Modifications	[m]	55	55	56	59	62	65	68	71
After Modifications	[m]	52	53	53	55	59	61	63	67
Total Takeoff Distance									
Before Modifications	[m]	348	381	432	515	614	733	877	1053
After Modifications	[m]	203	219	247	278	320	366	418	478
Difference		-42%	-43%	-43%	-46%	-48%	-50%	-52%	-55%

Table 2.35: Landing performance changes due to implementation of technical modifications (Sea-Level Conditions)

Landing Landing Weight	[ton]	22	24	26	28	30	32	34	36
Airborne Phase									
Before Modifications	[m]	122	127	131	136	142	147	153	158
After Modifications	[m]	115	119	124	127	132	136	141	145
Ground Run									
Before Modifications	[m]	292	322	350	378	407	438	469	502
After Modifications	[m]	254	277	303	329	354	381	408	437
Total Landing Distance									
Before Modifications	[m]	414	449	481	514	549	585	622	660
After Modifications	[m]	369	396	427	456	486	517	549	582
Difference		-11%	-12%	-11%	-11%	-11%	-12%	-12%	-12%

Table 2.36: Landing performance changes due to implementation of technical modifications with reverse thrust as 15% rated thrust (Sea-Level Conditions)

Landing Landing Weight	[ton]	22	24	26	28	30	32	34	36
Airborne Phase									
After Modifications	[m]	115	119	124	128	132	137	141	146
After Modifications with Reverse Thrust	[m]	115	119	124	128	132	137	141	146
Ground Run									
After Modifications	[m]	254	277	303	329	354	381	408	437
After Modifications with Reverse Thrust	[m]	171	192	216	239	262	286	312	338
Total Landing Distance									
After Modifications	[m]	369	396	427	456	486	517	549	582
After Modifications with Reverse Thrust	[m]	287	311	340	366	394	423	453	484
Difference		-22%	-21%	-20%	-20%	-19%	- 18%	-17%	-17%

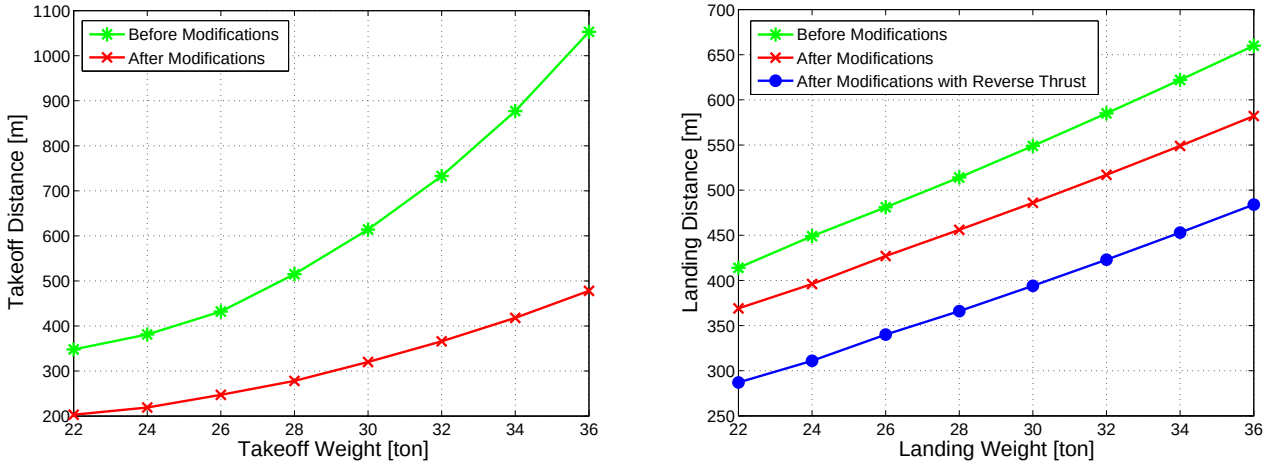

(a) Takeoff distance

(b) Landing distance

Figure 2.47: Performance change due to technical modifications (Sea-Level Conditions, reverse thrust = 15% of rated thrust)

Effect on Range

Due to the new engines, the range will be affected when compared to the initial values.
The initial aircraft with the existing engines has $SFC = 20.4$ g·(kN·s)$^{-1}$, i.e. twice SFC of a single engine. It is also mentioned by [4] that the range at a payload of 1500 kg equals 3200 km; furthermore, the maximum fuel weight equals 13,200 kg [33]. After rewriting the Breguet equation to Eq. 2.125, it is determined that $\frac{L}{D} = 8$. Cruise speed V is set to 167 m·s^{-1}.

$$\left(\frac{L}{D}\right)_{cruise} = Range \cdot \frac{\frac{g \cdot SFC}{V}}{\ln(\frac{W_{start}}{W_{end}})} \tag{2.125}$$

Due to the USB (Section 2.2.7), it was determined that L and D increased by 3.6% and 5.3% respectively when compared to the initial aircraft due to the Coanda effect of the new engines. These parameters are summarized in Table 2.37.
Using Breguet's equation, it is possible to set up a diagram relating payload weight to range. This is done by determining the range for various payload weights. Fuel is added until the tanks are full (13,200 kg of fuel) or MTOW (36,500 kg) is reached. The result is shown in Figure 2.48. It is determined that the range is reduced by ∼10-15%. Since the focus is to improve the STOL performance, the reduction in range is seen as a relatively small

Table 2.37: Results of Coanda effect on range due to new engines

	Unit	**Existing Engine Configuration Complete Aircraft**	**New Engine Configuration Complete Aircraft**
SFC	[g·(kN·s)$^{-1}$]	20.4	22.44
L	[-]	Base	Base + 3.6%
D	[-]	Base	Base + 5.3%
L/D	[-]	8/1	8.28/1.05 = 7.88/1
Range (Payload = 1500 kg)	[km]	3265	2908

disadvantage. This is mainly due to the fact that the initial aircraft already had a relatively large range. Therefore, the trade-off was made to improve the STOL capabilities and thereby limit the range.

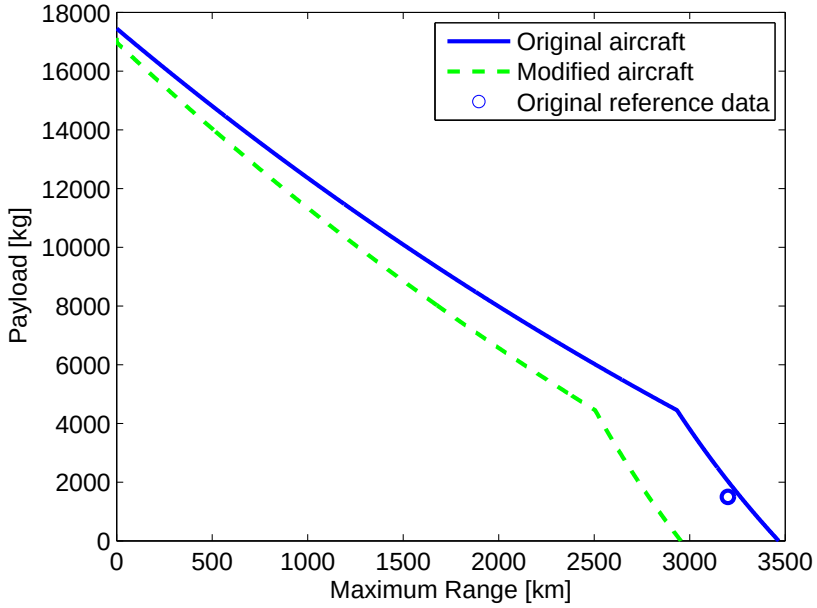

Figure 2.48: Maximum range for payload

3 | Implementation

In the implementation chapter, various global aspects of the system implementation will be discussed. In Section 3.1, the overall design and the logic used in the development of the Flying Hospital system is given. The corresponding Gantt chart is shown in Section 3.2 to illustrate the steps and planning of the different project phases, as well as the division of manpower and time resources. The cost breakdown structure then follows to illustrate the different project costs in Section 3.3; it is shown how the costs are distributed over the relevant parts and aspects of the project. In the manufacturing part (Section 3.4) the manufacturing aspect of the different retrofitting options, their feasibility, cost and other relevant manufacturing aspects are described. The market analysis and business model part (Section 3.5) discuss the different approaches that will be financially taken into account to realize the project as the most efficient costs and returns. Market prospects will be presented and opportunities of growth are illustrated. Due to the growing importance of the environmental aspect of projects, a sustainability strategy was developed to minimize the environmental footprint of the project and system as a whole. This will be carried out in the sustainable development strategy in Section 3.6.

3.1 Project Design and Development Logic

The future course of the project has to be planned. Therefore, Figure 3.1 illustrates the future activities of this project in a flow diagram. The concept, preliminary and detailed design have been done in the past ten weeks, during the Design Synthesis Exercise.
The next block is the supplier identification; this is where connections are made with the suppliers of required materials and companies willing to apply the retrofits to the aircraft. Also, an Antonov An-74 supplier is sought in this phase. The process is continued with the acquisition of the aircraft; this phase elaborates on obtaining the aircraft from the suppliers that have been identified in the previous phase.
After the aircraft has been bought, the aircraft is stripped of unnecessary equipment and parts. This is followed by retrofitting the aircraft by the companies that have been found and contacted in the supplier identification phase. The retrofitting leads to a first prototype of the system. This prototype is tested for any inconsistencies and other failures. The aircraft is certified after all the tests have been conducted.
An additional loop has been created that returns to the retrofitting of the aircraft when the aircraft failed to pass the certification procedure. The production of the aircraft is started after the system is certified in order to arrive at the final delivery phase, where the retrofitted aircraft is presented to all stakeholders and customers.

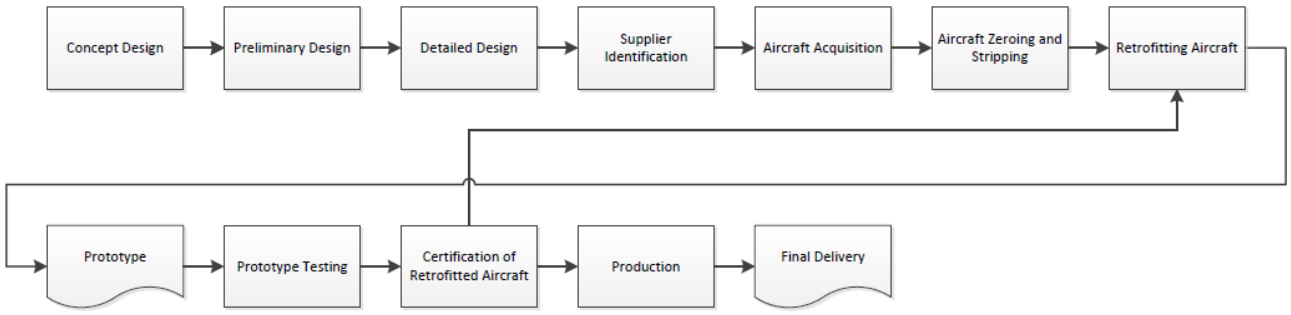

Figure 3.1: Future project development

3.2 Gantt Chart

Figure 3.2 provides the Gantt chart for the future project activities, the activities are planned for a lead time of three years. The first column indicates all the activities to be conducted, the second column denotes the starting date of the activity, the third column gives the end date of the activity. The fourth column indicates the total

days required for each phase of the project. The fifth and last column indicates the horizontal time bar for each project phase. Emphasis is laid upon the certification of the retrofitted aircraft since this is often time consuming and important for the future of the project.

ID	Task Name	Start	Finish	Duration
1	Concept Design	3-5-2013	8-5-2013	4d
2	Preliminary Design	8-5-2013	3-6-2013	19d
3	Detailed Design	3-6-2013	5-7-2013	25d
4	Supplier Identification	8-7-2013	25-10-2013	80d
5	Aircraft Acquisition	25-10-2013	2-1-2014	50d
6	Aircraft Zeroing and Stripping	2-1-2014	26-3-2014	60d
7	Retrofitting Aircraft	26-3-2014	21-10-2014	150d
8	Prototype testing	21-10-2014	18-5-2015	150d
9	Certification of Retrofitted Aircraft	18-5-2015	19-2-2016	200d
10	Production	19-2-2016	7-7-2016	100d
11	Final Delivery	7-7-2016	15-7-2016	7d

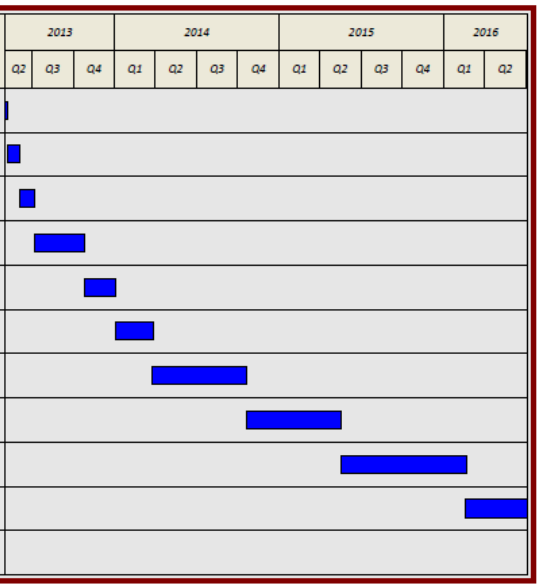

Figure 3.2: Gantt chart for future activities

3.3 Cost Breakdown Structure

In a previous section dealing with the project design development logic, the post-DSE activities of the Flying Hospitals project have been worked out and these are structured in the Gantt Chart. The Gantt Chart gives the post-DSE activities in chronological order and states how long they take per individual activity. In this section, the costs that are involved with these post-DSE activities are identified and explained.
As can be seen in Figure 3.3, the activities can be split into two phases. The first phase is from the end of the DSE up to the testing of the prototype. This phase includes aircraft acquisition, retrofitting of the aircraft, the zeroing and stripping of the aircraft as well as the prototype testing. Second phase deals with the certifications process, the production of the final design and the final tests.
It is clear from Figure 3.3 that the first phase (including acquisition and retrofitting) costs the most. These two activities, with €4M and €25M account for almost 90% of all post-DSE activity costs. This is due to the retrofitting being the most important part of the project assessment. Therefore this sole activity is the far most important post-DSE activity when it comes to expenses (€25M). The retrofitting of the aircraft is estimated to be almost 80% of the costs in the three years after the DSE project. All values for expenses are estimates collected from earlier studies in the mid-term report [2] and documents provided by the Global Peace Partners [74]. Total costs of the lead time are stated in Figure 3.3 being €32.5M. However, after the first production, some steps - and thus costs - will not be covered again when producing future aircraft. The steps that can be skipped are the prototype testing and certification of retrofits. This reduces overall costs by €750k.

3.4 Manufacturing Plan

During the determination of post-DSE activities, it was clear that the most important and costly activity is the retrofitting of the Antonov aircraft. This is the phase in which the technical changes to the aircraft are integrated and thus the manufacturing takes place. This section focuses on the manufacturing required to include the changes that have to be made to the structure and interior of the aircraft. All technical concepts are investigated on whether manufacturing is required and if it is required, then the specific adjustments that have to be manufactured are elaborated upon.

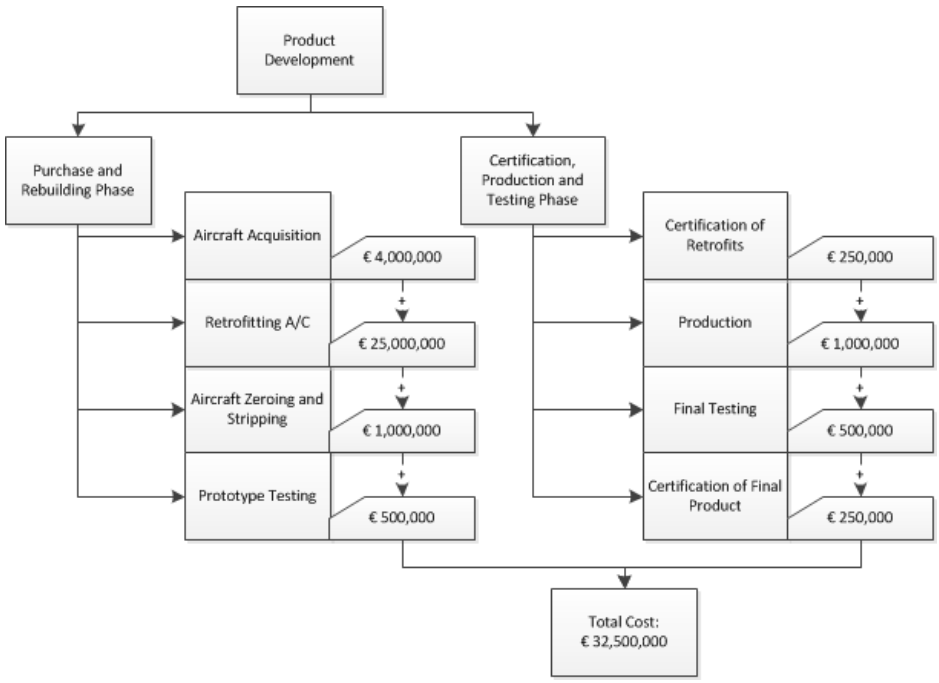

Figure 3.3: Cost break-down structure of the post-DSE activities

3.4.1 Retrofitting of the Wing

Most modifications will take place on the wing section of the aircraft. Besides the integration of a new type of engine, two technical changes require manufacturing after the DSE project. One of these changes involves the addition of vortex generators (VG) to the flaps of the main wing. In the VG technical section, the material chosen for this application was aluminum. Because of its reasonably low density and lower costs with respect to polycarbonate kits, the aluminum was chosen as the material for this purpose. Thickness of the VGs is chosen as one millimeter. Together with a density of 2700 $kg \cdot m^{-3}$, this results in a weight of 473.3 grams for the two wings.
The second change to the wing is the structural reinforcement that may be required at the engine's supporting structure. Since a new, heavier engine shall be put on the wing, the shear stresses and normal stresses increase. This may result in reinforcements, as was discussed in the technical detailed design section about the wing structure, Section 2.4. Local reinforcement, as well as the wing-fuselage integration need to be strengthened.

3.4.2 Retrofitting of the Fuselage Interior

Although the wing is the main part that may require changes in its structure and material used, the fuselage also requires changes. The interior of the aircraft has to be stripped to make sure that no superfluous weight is taken. This means that systems that are not required for the Flying Hospital mission and either contribute to weight or space in the fuselage, are removed. This clears space for the container based mission of the Flying Hospital as well as the loading system for the container. As mentioned in the operations and logistics Section 4.1, to be able to load the container on the aircraft, extra changes to the rear ramp and the loading system are required. As stated before, this implementation, as well as the changes to the wing structure and layout shall be manufactured in the retrofitting phase during the aftermath of the DSE.

3.4.3 Overview Manufacturing Plan

Figure 3.4 shows a brief overview of the steps within the manufacturing plan. As mentioned before in this section, three steps are taken to retrofit the Antonov An-74 into a Flying Hospital. These steps consist of the stripping the interior of the aircraft, the manufacturing of the possible needed structural reinforcements and the manufacturing of the vortex generators. All the activities are concurrent processes. To work as efficient as possible, the just-in-time (JIT) procedure is used. This procedure implies that all products needed for the assembly are delivered just before the time the product is needed. In this way, no storage costs are necessary for the products in the assembly phase. Also, the three activities can be performed at the same time to minimize the waiting time, as the Flying Hospital

will be used as quick as possible. If these activities are performed, the Flying Hospital can be assembled. The assembly and previous activities do not have to be performed by one specific company. Outsourcing may be a preferable solution, as companies with specific technical experience can manufacture parts for the Flying Hospital (i.e. the vortex generators) and this may decrease the production risks and costs. Once all activities are finished the aircraft is delivered to the customer.

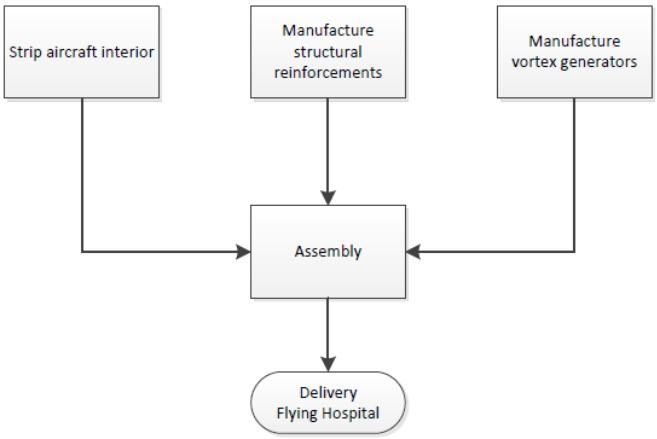

Figure 3.4: Overview manufacturing plan

3.5 Business Model and Market Analysis

The Flying Hospital must be economically sustainable in addition to its large social and health benefits during disasters. It must be operable in a cost efficient way that will allow the Red Cross and other operators to keep their costs down, or maybe even make profits.
This chapter will describe a business model that will result in the most efficient and perhaps profitable operation of the Flying Hospital. This will make it of interest to both non-profit organizations and private entrepreneurs. In both cases, disaster victims will always benefit from the Flying Hospital existence and operation along with investors, governments and relief organizations.
This section is broken down into four main sections; business model, costs, returns and market share

3.5.1 Business Model

The business model of the Flying Hospital is based primarily with the goal of sustainability. Possibilities for profitability will also be considered to cover organizations whose objectives do not allow profitability in their operating guides. The Flying Hospital system composes of multiple elements namely: aircraft, hospital, medical flight and technical crew, and medical service recipients.

Aircraft

The aircraft's main function is to transport the hospital equipment, tools, supplies and evacuees to and from the disaster site. The aircraft transport function can be acquired either via lease, a purchase, or a contract. The organization using the aircraft can lease the aircraft from its owner if the purchase capital is not available. This will allow the organization access to the aircraft at all times. The organization could also contract the transportation of tools, people and equipment to aircraft owners and operators. That way, only transport fees will be incurred, and if the organization is a disaster relief organization then there is a possibility to arrange those transport service at discounted rates or even receive them as a form of donation. Alternatively, if the organization of interest is commercial, or enough capital is available, the aircraft can be purchased outright. Tables 3.1, 3.2 and 3.3 describe the advantages and disadvantages of the three options:

Lease:

Table 3.1: Advantages and disadvantages of aircraft lease

Advantages	**Disadvantages**
Small investment capital	Expensive on the long term
Operation and maintenance included	Storage costs
Guaranteed Availability 24/7	Idle time costs
Wide scope of transport purposes	Cannot be used to external purposes
Flexibility within internal operations	Crew and control personnel costs
No vehicle cost fluctuations	Subject to operating cost fluctuations
No extra costs for normal wear and tear	Liability for operational mishaps
Leases are tax deductible	Limited usage [negotiable]
Gap insurance covers total loss damage	Excess wear and tear costs
Possibility of sub-lease	Customizing not allowed
No residual value risk	Risk of early termination penalty

Contract:

Table 3.2: Advantages and disadvantages of transport contract

Advantages	**Disadvantages**
Small investment capital	Expensive on the long term
Operation and maintenance could be included	Storage costs
Guaranteed Availability 24/7	Idle time cost
Wide scope of transport purposes	Cannot be used to external purposes
Flexibility within internal operations	Crew and control personnel costs
No vehicle cost fluctuations	Subject to operating cost fluctuations
No extra costs for normal wear and tear	Liability for operational mishaps
Leases are tax deductible	Limited usage [negotiable]
Gap insurance covers total loss damage	Excess wear and tear costs
Possibility of sub-lease	Customizing not allowed
No residual value risk	Risk of early termination penalty

Purchase:

Table 3.3: Advantages and disadvantages of aircraft purchase

Advantages	**Disadvantages**
Very flexible	Storage and maintenance costs
Internal transport usage	Residual value risk
Transport service can be contracted out	Idle time risk
Ownership can be shared	Shared ownership conflicts
24/7 availability	Cost creep risks
Cheaper on the long term	Crew costs
No risk of vehicle usage cost fluctuations	Insurance and liability costs
Minimum time waste to approve transport	

Hospital

The mountable hospital provided by Hospitainer, or other potential suppliers, can be used outside disaster times as either a hospital, a training center or a hybrid combination. This can be either done for profit or in areas of interest to provide free or low cost medical care. The location of the hospital has to be in a low risk area and within the aircraft's range from areas of high disaster risk. The hospital can be used as a private hospital to provide different variation of medical, surgical, eye or dental services. The revenue of the hospital can be used to absorb the Flying Hospital costs during its disaster relief mission. The hospital could also be used to provide free or low cost medical care in rural areas during disaster free times. Alternatively the hospital could be used as a mobile training center to train people basics of relief and first aid. That way, if a disaster strikes, a larger section of the population has already some first aid and disaster relief basic awareness and training. During a disaster, the hospital can be transported to the disaster area to provide medical relief for the patients, post-surgery and general medical care instructions to their relatives. That way, patients will be less dependent on the relief organization's personnel. That will reduce the average cost per patient. In case of a non-profit disaster relief organization, the organization can use the hospital through three ways. The first is to own or co-own and operate the hospital outside disaster times. The second is to own or co-own the hospital but lease it out outside disaster times. The third is to not own the hospital but rent it during disasters. These possibilities are shown in Figure 3.5.

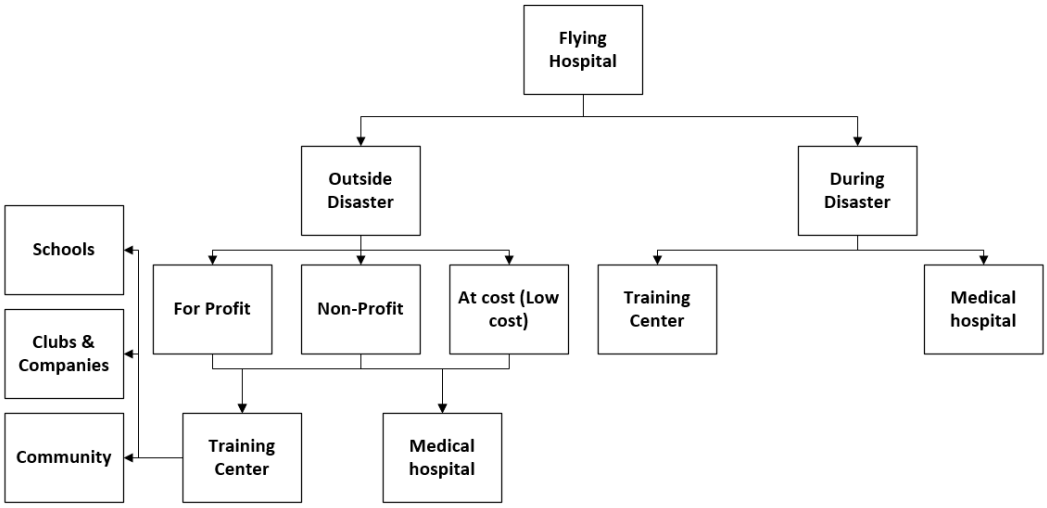

Figure 3.5: Hospital options

Medical, Flight and Technical Crew

The medical crew can either consist of employees of the operating organization or of contracted employees during the mission time. These employees carry out the medical care and instruction services. These also could be employees of the organization or private contractors. However, in case the transportation of the hospital is contracted out, the cost of these employees will be included in the transport cost service.

Medical Services Recipients

These are the main focus of the stakeholders of the Flying Hospital system both during and outside the disaster time. During the disaster time everyone and anyone in the vicinity of the Flying Hospital should be aided. Outside the disaster relief boundaries, these can either be recipients of charitable medical services or paying customers.

3.5.2 Costs

The cost of the Flying Hospital system is strongly dependent on the operating organizations objectives and method of investing. It also depends on the available investment capital and future cash flow forecasts. Therefore, a general overview will be given and an investment direction will be provided in the recommendations to suit the different objectives of different potential investors. The costs of the total system are broken down into five main categories: hospital costs, transport costs, administrative costs, relief operation costs, legal and compliance costs.

These categories are further broken down into subcategories as shown in Figure 3.6.
Some elements of the costs in Figure 3.6 can be estimated such as vehicle acquisition cost and taxes. However, the vast majority of costs are scalable and therefore strongly dependent on the operating party's objectives. An example of costs that can be pre-determined independently of the organization objectives and methodology are the total life cycle cost. These are typically; development, operations, maintenance, renewal and rehabilitation, depreciation and cost of finance and replacement or disposal. The development cost and operating cost are discussed below.

Development cost

The development costs for the Flying Hospital including acquisition of an existing aircraft [5] and retrofit possibilities are listed in Table 3.4. The Global Peace Partners hospital plane product has been used as reference to give an indication of the costs [74].

Operating costs

The operating cost of the airplane can be broken down into several smaller blocks, starting with direct and indirect costs. The direct cost consist of the cost directly related to the aircraft usage. The indirect cost also relate to the

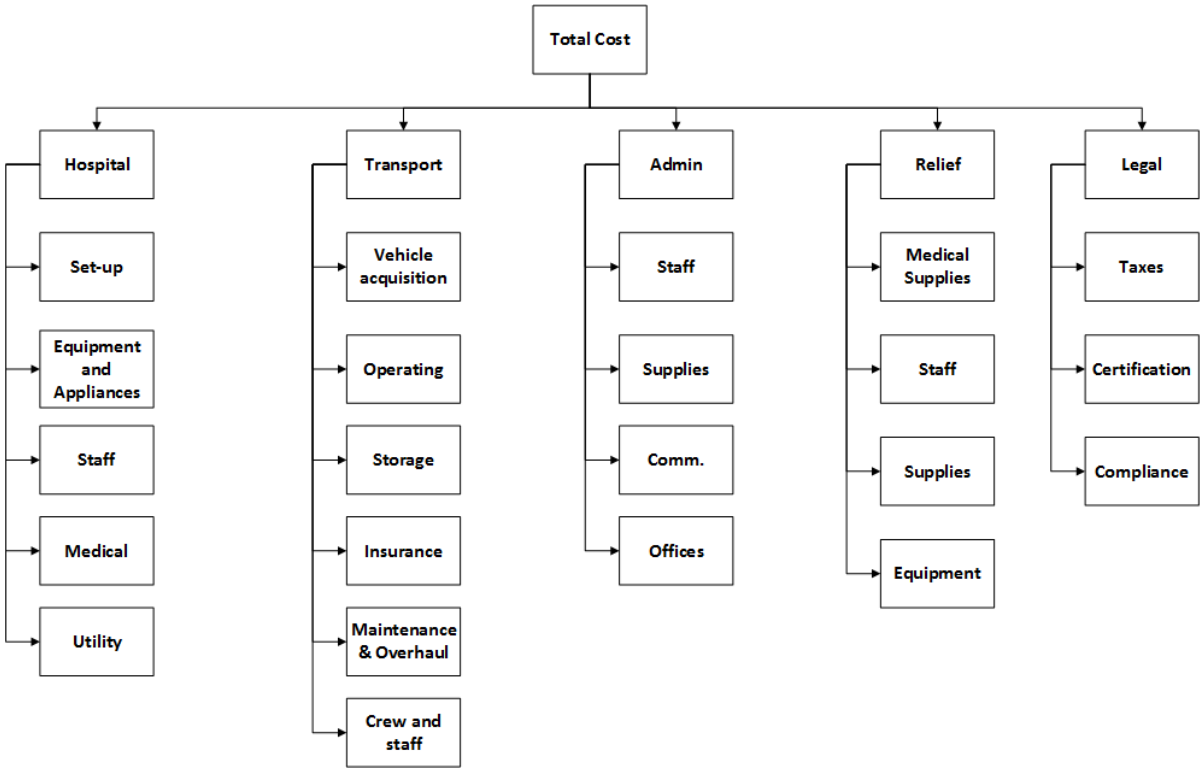

Figure 3.6: System cost breakdown

aircraft, but may consist, among others, of annual costs or marketing costs. The subdivision can be seen in Figure 3.7.

The aircraft costs also depend on whether the aircraft is fully owned, co-owned, rented, leased or having the transport service contracted out. Administrative costs also depend on whether a new administration will be set up to oversee the hospital operation or if it will be added to the responsibilities of already existing establishment and staff. Relief and operation costs also depend on the scale and location of the disaster, as well as the scope of the medical assistance provided, its duration and the funds available for that purpose. Finally, legal and compliance costs depend on the set-up form of the organization and its registration country regulations as well as staff location and aircraft storage location and operational scope. For all these reasons, it is impossible to pin point the costs of the system arbitrarily. This is very advantageous to the investing party. The Flying Hospital is very scalable and flexible. This allows it to be designed to fit a very large scope of investment potential, required performances and rates of return. Custom made system layout can be provided to suit the needs and investment requirement of different parties.

Table 3.4: Development cost

Development activity	**Estimated costs [€]**
Design phase	500,000
Project preparation	300,000
Supplier identification	200,000
Test phase	500,000
Legal/administrative	300,000
Book keeping/accounting	30,000
Promotional	25,000
Salaries/expenses/travel	300,000
Unforeseen/miscellaneous	30,000
Plane acquisition	4,000,000
Plane zeroing out and Stripping	1,000,000
Engine acquisition 2x	4,000,000
Retrofitting cargo airplane	15,000,000
Total estimated costs:	25,185,000

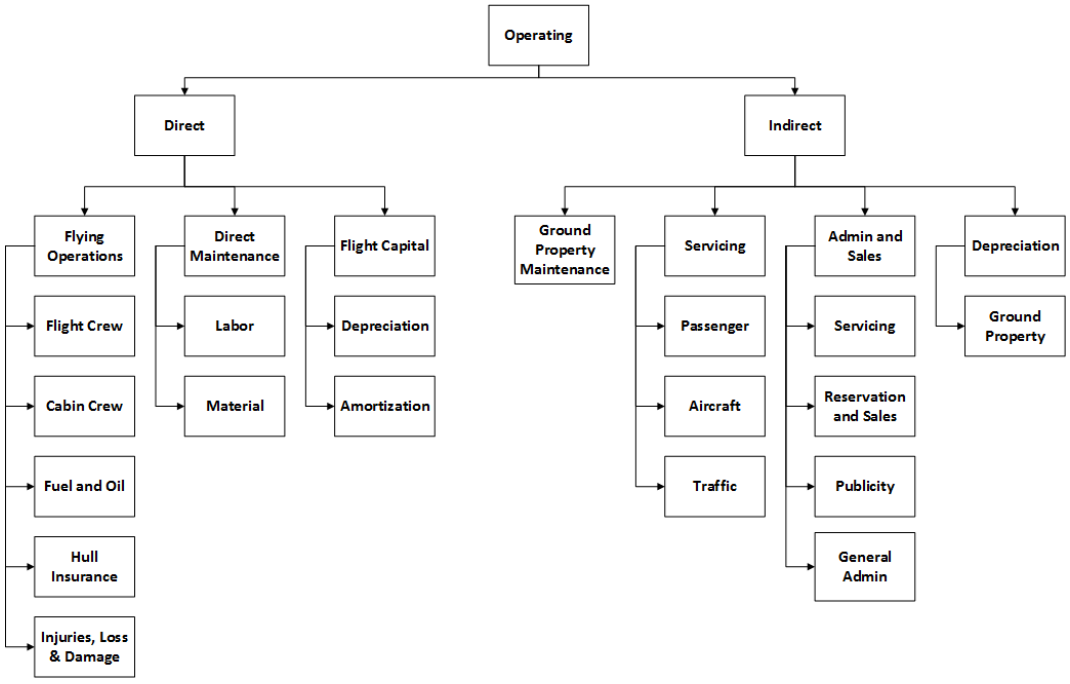

Figure 3.7: Operating cost breakdown

3.5.3 Returns

This section discusses the return opportunities on investment for the Flying Hospital, these are social and monetary returns. Both profit and non-profit organizations are concerned with both types of return with varying importance according to their objectives.

Social Returns

The more important type of returns for non-profit relief organizations are social returns. After a disaster, a lot of families lose their homes, their lifetime belongings, their memories. Some lose family members, parents and children, and many lose their health or even their lives. That can have a deep impact on the people struck by the disaster. This impact could be broken families, lifelong psychological damage and potentially a life of orphanage, homelessness or poverty. Disaster relief is not only about getting medical procedures done cheaply, it is mainly about re-establishing societies and improving lives. The Flying Hospital will be able to help thousands of people through what could be probably the most difficult times of their lives. The Flying Hospital will provide medical help in disaster zones. That help could save a child from being an orphan, families from getting broken, diseases from causing lifelong pain and suffering and prevent poverty from destroying lives and living standards that generations have worked hard for. These returns and advantages cannot be measured or quantified, however, they are the biggest returns of such programs as the Flying Hospital for non-profit organizations.

Economical Returns

A vital point for both profit and non-profit organization is financial feasibility and sustainability of the system. The Flying Hospital system is very strong in terms financial and sustainable aspects. There are potential returns in all elements of the system. These are explained below.

Income From Operating Hospital The hospital can operate outside disaster times as a private hospital, rescue or emergency center. This hospital can be set up in areas where it can provide needed medical help at a certain price. The hospital can be arranged to break even or make profits. This would help to cover disaster costs and be less dependent on donations and handouts. Moreover, the hospital can be either a standalone unit or an attachment that can be added and removed from already existing hospitals.

Income from Aircraft The aircraft can also be generating income for the owning party. It can be used during disaster relief to help victims. However, outside those times, it can be used as a normal cargo plane. It can be either used by the relief organization to lower its transport costs or it can be rented out to a cargo transport company and generate income.

Income from Donations and Contributions As more people are aided by the Flying Hospital, the social capital of the organization increases and its names strengthen and present in the disaster relief sector. This will grow the public support, awareness and trust in the organization's quick response, presence, and high efficiency. The implications of the better image having a direct impact on the contributions and donations from people, companies and governments.

Income from Disaster Insurance Certain local governments purchase disaster insurance for the local cities under their control. Using the Flying Hospital, due to its other income, the overall cost of disaster relief can be decreased significantly. This allows the owning organization to contract their disaster relief services with insurance companies. These contracts will ensure an income during disasters.

Income from Training Outside disaster times, the owning party can use the Flying Hospital as a training center. This center can provide training courses for school and university students, companies that want to teach their staff first aid skills such as lifeguard service providers or local hospitals. This training can be carried out at a cost that ensures some income to the owning company.

Savings due to Pre-Disaster Activities The disaster relief organization can also use the hospital in areas that are disaster prone before the disaster actually happens. The population can be provided with low cost or free courses on disaster relief and first aid. Although this does not have apparent direct returns, it could prove to be very cost effective during disaster time. That is because a larger portion of the population has some basic disaster relief skills. This means that more people could be saved when a larger portion of population is trained and actively

participating. Putting less demand and pressure on external staff and efforts. This could bring down the cost of disaster relief by needing to bring in less staff and lower the per capita cost of relief as often relief happens outside the Flying Hospital coverage area.

3.5.4 Market Share

Now that the business model and returns on investment of the product have been discussed, the market share of the Flying Hospital is introduced. The market volume and market potential are dealt with. At the end of this subsection, the achievable product market share is explained.

Market Volume for the Product

The market volume exhibits the totality of all realized sales volumes of a special market. The volume is therefore dependent on the quantity of consumers and their ordinary demand. Since sales have not yet been realized the market volume cannot be defined at this point.

Market Potential

The market potential defines the upper limit of the total demand and therefore takes all potential clients into consideration. These potential customers are defined as: Governments, Ministries of Defense, Ministries of Education, Universities (Medical Schools), Hospitals, Hospital training facilities, Private individuals/companies, non-governmental organizations like United Nations (UN) and finally relief organizations.

Achievable Product Market Share

Looking at the service the Flying Hospital offers, a special segment in the huge market of medical relief combined with aerospace vehicles is opened. The segment of providing medical help and assistance in remote areas during disasters is a new niche where the Flying Hospital is the leading design, and at this point the only product. In the early stage a market share of 100% is possible in this market segment. Looking at other relief-possibilities: army, other health organizations or governments, can become future competitors. At present ORBIS the flying eye hospital, Global Peace Partners and Air Hospital Canguro are similar designs, yet at this point not competing in the market the Flying Hospital is trying to reach.

3.6 Sustainable Development Strategy

The implementation of sustainability in the report has already been discussed in the baseline report [6] and mid-term report [2]. The strategy for sustainability is to design a sustainable life cycle for the aircraft where the definition of sustainability is given by [75]:
"Sustainable Development is a development that meets the needs of the present without compromising the ability of future generations to meet their own needs."

3.6.1 Material supply

The first stage of the life cycle of the Flying Hospital is also the final stage of the aircraft used for it. Reusing parts of older aircraft becomes more and more accessible. Although reusing old material has its limitations it is also a cheap and sustainable solution because in the process of recycling, scarce materials can be reused and preserved creating a closed loop.

Reusing Aircraft Parts

The Antonov An-74 is an already existing aircraft. Second hand vehicles can be bought for a minimum price of $4M from several suppliers [5]. The aircraft does not have to be built from scratch so costs can be saved in this stage.
Because of growing environmental issues concerning the disposal of retired aircraft, Airbus has started the PAMELA initiative [76]. PAMELA stands for Process for Advanced Management of End-of-Life of Aircraft. The main objective of this initiative is to recycle and reuse retired aircraft by decommissioning, disassembling and deconstruction.

During the disassembling phase resalable parts and equipment are removed from the aircraft, checked and certified. These parts can be used as upgrades to increase the performance of the Flying Hospital. Examples of upgrades are stronger engines, adding winglets, extra flaps, slats or a canard.

Limitations

Reusing old aircraft parts brings along some issues. First of all the construction phase still requires the use of raw materials. Secondly, and most important, recycling used parts is limited by safety regulations. Materials that have been in service for a long time have a reduced quality. The quality of parts and materials should be checked thoroughly to prevent fatigue, corrosion, structural failure and system failure.

Sustainable materials

Some of the required components may not be obtainable or have insufficient quality. These components should be manufactured from scratch using sustainable resources and methods. A possible solution would be to use composites in the design. This type of material has a high strength, low-weight, high fatigue resistance and offers many possibilities when it comes to manufacturing [77], which is beneficial if one seeks for a sustainable design. A composite that can possibly be used is GLARE which stands for Glass Laminate Aluminum Reinforces Epoxy. GLARE has significant better properties than regular metal alloys. GLARE has for example a lower specific weight compared to metals; this property alone already makes the use of GLARE more appealing than metal alloys.

Another green material that can be used in the future, is the natural cork composite called AEROCORK. This material is a candidate to replace PVC foam and petroleum based materials in the aircraft industry [78]. This material is able to replace parts of the fuselage,wing and flaps of light weight aircraft. The parts that are replaced with cork can be reinforced by a carbon fiber sheet coating; this also retains the light weight nature of the material and improves the thermal capability of cork [79].

Sustainable materials impose great benefits in the aerospace industry, however there is also a major problem concerning sustainable materials. The certification process that the new material has gone through is time consuming and complex. This implies that the Flying Hospital operation can be retarded. Also the selected materials should not impose hazardous conditions for the laborers.

3.6.2 Manufacturing

The manufacturing stage will be about modifying the aircraft and adding additional components. The usage of resources such as energy and water should be limited in order to realize sustainability during this stage. Also one should be careful when working with hazardous materials, the waste of such resources should be brought to a minimum, this also holds for the greenhouse gas emissions. Also the produced waste e.g. hazardous residue, should be disposed in a sustainable manner and should never end up in the environment. The main goal is to design in such a way that the final product is durable and can be recycled easily.

Processes that use thermal methods often do not produce structures and materials that are easy to reuse. This is mainly because the thermal energy alters the grain structure of the material permanently. This implies one should take care in reusing heat affected materials since not only the geometry is prone to change but also its grain structure.

An advantage of using composites is the way in which they are manufactured. Fabrication methods for making composites are molding or casting. The consequence of these methods is that the resulting product is almost exactly the required shape; there is no need for cutting or shaping. It produces very little scrap material. This also reduces the labor hours required for each product, hence it is economically beneficial. The advantage of using cork is that it is a relative soft material. This gives a possibility to use lighter machinery that requires less energy and personnel operating it. Companies can also communicate with each other more, for example an aluminum manufacturer can size its aluminum sheets that it provide to an aerospace company according to the needs of the aluminum user. This skips the additional manufacturing process where the aerospace company has to cut or disassemble large metal sheets with heavy equipment because this is already done by the supplier.

3.6.3 Operational use

The engine of the Flying Hospital provides some improvements with respect to the existing engine. As can be seen in Subsection 2.1.3 the new engine was even optimized further for cruise condition so that it is more sustainable. Resulting from this procedure the emission of NO_x was decreased by 7% compared to the usual performance of the D-436-T3. Besides that the thrust increased by 1% and the propulsion efficiency by 4% through the optimization process. Thus because the performance of the engine is improved, it emits less. The last property is the specific fuel consumption (SFC) which is reduced by 3%. Even though this did not seem to be a significant improvement, it could save tonnes of fuel during the life cycle of the engine.
Since the definition of sustainability states that the needs of the present have to be met without compromising the needs of future generations, it is necessary to look at sustainable energy sources. From a sustainable point of view the engines should run on biofuel. The sustainable aspect of biofuel is that it has a small carbon footprint. The CO_2 emitted by the engine will be absorbed by the plants that will be used for the biofuel production. Thereby a closed CO_2 cycle is created, reducing the netto CO_2 emission to a minimum [80]. The aircraft does not require any modifications and the biofuel can be blended with existing fuel [81]. Biofuel seems to be a very sustainable solution, biofuel blends are already certified for commercial flights and large companies and governments are setting up projects to develop the biofuels further. Biofuel seems promising but there are also some disadvantages according to [82], especially for biodiesel. For example, its performance decreases in cold weather. Besides that the oil required for the biofuels has to be extracted from crops. These crops could have fed hungry people but instead, the potential food is used to fly an aircraft. This trade-off between food and fuel causes some concern. Other disadvantages are the fact that biodiesel is prone to grow mold, contains water and decreases power. Nevertheless the emissions are appealing: 78% less carbon dioxide emissions, 67% less unburned hydrocarbons, 48% less carbon monoxide emissions, 47% less particulate matter.

Another possible fuel source could be algae. More and more companies, among EADS, are doing research in the area of algae-based aviation biofuel. The first flight of an aircraft with pure algae biofuel took place at the ILA 2010 in Berlin with the Diamond Aircraft DA42 New Generation [83]. It is proven that this method has potential to reduce carbon emissions by up to 84% over conventional jet fuels. By 2030 EADS aims 'to have 10 % of their fleet flying on pure or blended biofuels' [84]. Additionally, because the algae-based aviation biofuel is more fuel efficient in flight than petroleum-based fuels it would make the aircraft more sustainable [84].

3.6.4 End-of-life

After 20 to 30 year of service most aircraft reach the End-of-Life stage. They are not of any use for the flight sector anymore and have to be disposed in some way. The disposal of the Antonov An-74 and the Hospitainer container should be dealt with in a sustainable way. There are several options for the End-of-Life of the aircraft. The easiest and least desirable way of disposal is to leave the aircraft at a bone yard, but there are more sustainable options. Most of them are combined in the PAMELA concept of Airbus [76].

Keep Operational

Retired aircraft are unable to serve in civil transport but they can be converted for cargo use. In this way they can be kept operational. Since the Flying hospital already consists of reused parts this will be very unreliable. Keeping the Flying Hospital operational will be a very unsafe solution, even as a cargo aircraft. However, the aircraft is still very useful as a ground-based training facility for the Red Cross.

Disassemble and Reuse

Another solutions is to remove and sell reusable components such as engines, landing gear and avionics. These parts can be repaired and put back into service. This solution is doubtful because the Flying Hospital already uses old components. These components will then be reused for the second time. After two life cycles they will probably not meet the requirements to be operational once again.

Dismantle and Recycle

When there are not any usable components on a retired aircraft it can be stripped down completely. Every component will be shredded into small pieces and sorted by material. Examples of removed materials are aluminium stainless steel, titanium, copper, titanium tires and some plastics. The obtained elements should be sorted and sent

to appropriate channels. The material can be used in the aerospace industry, sold to other industries, burned or recycled in any other way.

Reuse Components for Non-Aircraft Related Purposes

There are many examples of innovative ways to reuse old aircraft components. They can be converted to buildings, boats [85] or furniture. To offer residual value for the local community the hospital could be dismantled and reused as a local medical facility. A local hospital is very valuable in areas that are being reconstructed after a disaster. The surgery room in the Hospitainer container has all the equipment to serve as a local, independent surgery so it will be a great opportunity to start a small medical enterprise. An impression of the recycled Flying Hospital is given in Figure 3.8. The container can also be used as a local school, community room or for any other kind of medical help. The container is built so that it can withstand the environment for several decades so the container can be an addition to the local communities on a long term.

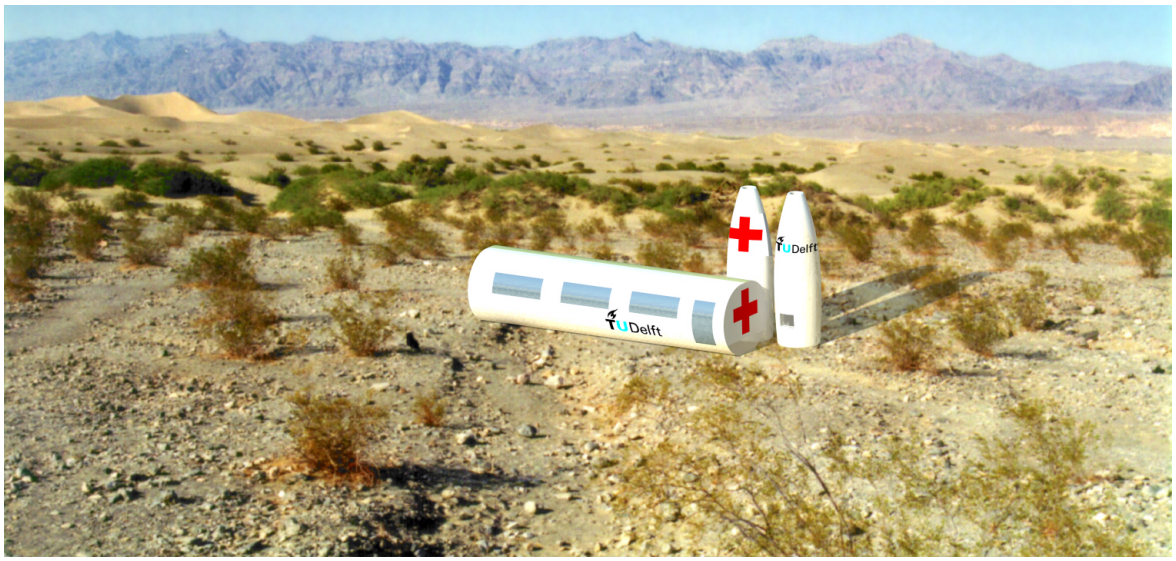

Figure 3.8: Recycled Flying Hospital

4 System Overview

As final chapter, system overview has the purpose to clarify the Flying Hospital system as a whole. In Section 4.1, the operations and logistics of the system is discussed . The communication flow is provided in Section 4.2. It describes the communication elements and their relevant order. Section 4.3 contains an analysis, which will determine the compliance with the different requirements of the system and the extent to which these requirements were met. Finally, a list of innovations is given in Section 4.4.

4.1 Operations and Logistics

For the operation of the system, it is of high importance to plan the mission correctly in advance. Once a disaster strikes, time is short to organize the aircraft and its necessities if immediate support is needed. Therefore the operations and logistics of the mission have to be well organized. This is done by the operational base. It is crucial to roll out the aircraft as fast as possible once it has become clear that it has to act in a disaster zone. This section will list the multiple places where the aircraft may be situated during its life cycle as well as what the equipment may consist of. Besides that, the layout of the aircraft and the logistical layout of the mission is written down.
The mission is split into three logical phases. Most important part is the operational phase. This is the time that the field hospital and the Hospitainer stands in the disaster zone and the Red Cross can provide medical care to the people in need. It may also be clear that this mission requires preparation and after-care. Therefore the pre-mission phase and the post-mission phase are there to make sure that at all times the mission can start by a well-prepared pre-mission phase and the cycle is completed with the post-mission phase.

4.1.1 Bases of the Mission

When operating the mission on behalf of the Red Cross, the Antonov will be positioned at various locations during the mission cycle. In case it is not operational, the An-74 is stalled at a position where storage is cheap and where it is close to potential disaster zones. However, it is not stored in a potential disaster zone because otherwise the risk of damaging the aircraft during a disaster increases. At that spot maintenance can be performed and trainings can be given. It is important that the aircraft can takeoff from that position immediately after the disaster strikes. When a disaster occurs, the An-74 flies from where it is stored to the position where is Hospitainer is located. The surgery in the container will be fully operational at a spot where no hospital is within reach. Therefore, a doctor can perform operations and other medical help where otherwise no help can be provided. When the Hospitainer is needed, it will be packed up and then picked up by the An-74. Since the aircraft is able to land on rough terrain it can pick up the Hospitainer even at a spot where no landing strip is located. After that, it will fly to the disaster area directly or it will stop at the mission base for organizational affairs.
The mission base is the location at the major airport closest to the disaster base. There the Global Peace Partners perform medical help on larger scale within a Boeing 747. From there supplies get transported towards the disaster area and patients or evacuees can be brought from the disaster area so that they can be helped by the Global Peace Partners. The transportation is done by the An-74 that shuttles between those two bases. The link between the mission base and the disaster area is of high importance. It may be clear that during a disaster, every injured human being should be helped as soon as possible. However, the An-74 should also have a high loading factor each flight. This is due to time and financial constraints.
At the mission base, the integration of the supplies also comes into place. These can be brought from the operational base to the mission base by normal cargo planes. The operational bases are the same as the logistic center of the Red Cross so that no new logistical network needs to be constructed. The mission and the success of it, basically revolves around getting the supplies at the disaster area on time. Therefore a brief introduction in the cargo system is given in the next subsection.
Once the aircraft reaches the disaster area, it can deploy the field hospital and the Hospitainer. Then it can provide help to the injured people in the main disaster zone. It can perform operations and it can provide shelter as well as other medical help. This is where the operational phase of the hospital starts. At this location there is the possibility of collaboration with the PAV EMS vehicle, a small gyrocopter which has an ambulance function. This smaller vehicle is be able to penetrate deeper into the disaster area because it can land vertically. Therefore it can bring patients to the hospital that cannot reach it themselves.

After the injured people in the disaster area are either evacuated or treated, the contribution of the Flying Hospital mission to that specific disaster is not necessary anymore. It will fly back to the place where it is stalled until its stocks and equipment are checked. From then on, the Flying Hospital is ready for action in a new mission to a disaster stricken area.

4.1.2 Cargo container integration

The entire mission and its success basically revolves around getting the right cargo to the right location on time. Therefore comes the necessity of looking into cargo with more detail, inspection and planning.
The Flying Hospital is made of and relies on different types of supplies. The supplies are those such as surgery rooms, equipment, perishables, food, water, etc. Hospitainer is a company of Dutch origin that provides containers which can be custom-made to a desired size. In this container a surgery room will be placed that will be ready to provide help on the spot. Loading of the Hospitainer can be done via loading trucks. An example of such a loading system is already incorporated in the original Antonov, as can be seen in Figure 4.1. To make the loading easier, the floor of the airplane will be stacked with smooth metal balls to reduce friction and allow the containers to slide easily into position. The most important design of the loading mechanism, is the hatch which can slide under the aircraft's belly as can be seen in the figure. By this configuration, a truck can drive up to the loading ramp. Unloading can be done in the same way using trucks on site. Another possibility is to manually load and unload the containers at location. This can be done by using Hospitainer's lifting device [86] as seen in Figure 4.2 in combination with a large jack which is able to lift the total weight of the container. In this manner, immediate on site manual loading and unloading can be done.

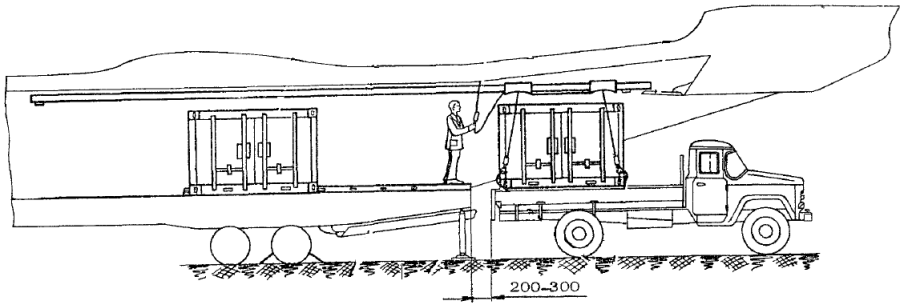

Figure 4.1: Truck, ramp and container integration system [46]

Figure 4.2: Manual container lifting device [86]

4.1.3 Pre-mission phase

Now that all locations (bases) during the mission are identified, the actions taken during the three different mission phases are pointed out, hence a time-wise overview instead of a location-wise overview is provided in this part. The first stage of the mission is the preparation of both the hospital itself as well as making sure the stocks are supplied. This is coordinated by the organizational base. The maximum amount of payload is set by the maximum payload that can be brought by the aircraft. The type of modular equipment and medicines is selected by the Red Cross, which has the best view on what type of disaster (earthquake, tsunami, famine) requires what kind of medical help. Once this is determined, the arrangement of the payload in the aircraft is defined. This is done to provide help as fast as possible, since a wrong configuration of the supplies can negatively influence the medical help procedure.
Once the mission is ready to fly, it flies to the mission base. At this moment, the disaster area has already been investigated and the landing spot of the aircraft is selected. This selection is based on finding a spot that can be used as runway and finding a possible operational location for deployment of the hospital. Also, before takeoff to the disaster area, it has to be sure that communication will be possible during the entire operational phase. Without communication the mission cannot be executed as desired. Therefore, the final check is that communication is possible during the entire execution of the operation.

4.1.4 Operational phase

In case the aircraft is ready for its flight towards the disaster area, the operational phase starts. Before flight from the mission base to the disaster area, the disaster area already has been investigated and possible landing spots are identified. When one of those landing spots is selected as the final mission operation base, the flight takes off and preparations have all been done to make sure that the mission can be fulfilled perfectly.
Once landed at the selected landing spot, the ground operation starts with unloading the containers and the deployment of the hospital. The storage and supplies as well as the crew will be unloaded from the aircraft. This is done to evacuate injured people from the disaster area or bring new supplies or containers from the mission base to the disaster area.
In the disaster area, the PAV EMS evacuation vehicle could come at help. This vehicle is capable of vertical takeoff and landing and thus can access even more destroyed places that might be unreachable by the Antonov aircraft. This enlarges the mission profile and the number of people that can be helped increases with it.
The continuous availability of the aircraft at the disaster side also asks for further check-up moments when it comes to possible technical or logistical malfunctions. At the site, the crew of the hospital should at all times be able to fix issues that could come across during the operation. The aircraft has to be operational, so it is checked by the personnel. Also, the medical equipment that is brought to the disaster area needs to be fail-safe for the mission life-time. Besides technical malfunctions, the logistics of the stocks are of high importance. This means that some of the crew is involved with the checks on the availability and the amount of medicines, water and food that was taken on board of the aircraft. The same crew shall investigate whether refilling of the stocks is required.

4.1.5 Post-mission phase

After the operational phase in the disaster area, the mission is assumed to end at some point. What happens then, is that the aircraft has to take off from the same spot as where it has landed and fly back to the mission base and then to the position where it is stored. Once back at this location the stocks are refilled for a possible new mission. Besides that, the technical malfunctions that may have come across, are checked and fixed. During the time that no takeoff is required to a new mission, the aircraft can be used to fulfill other needs such as the training of the Red Cross personnel to make sure that the new missions are executed as perfectly as possible. The entire logistics of the mission can be seen in Figure4.3.

4.2 Communication Flow Diagram

The communication flow diagram has the purpose to show how the information flows within the system as can be seen in Figure 4.4. The mission consists of four bases: the base of the Red Cross (organizational base), the logistic center of the Red Cross (operational base), the base of the Boeing 747 of the Global Peace Partners (mission base) and the base of the Flying Hospital (disaster area). These four bases require long distance communication between each other. Each communication string needs to go either way so to and from each communication block.

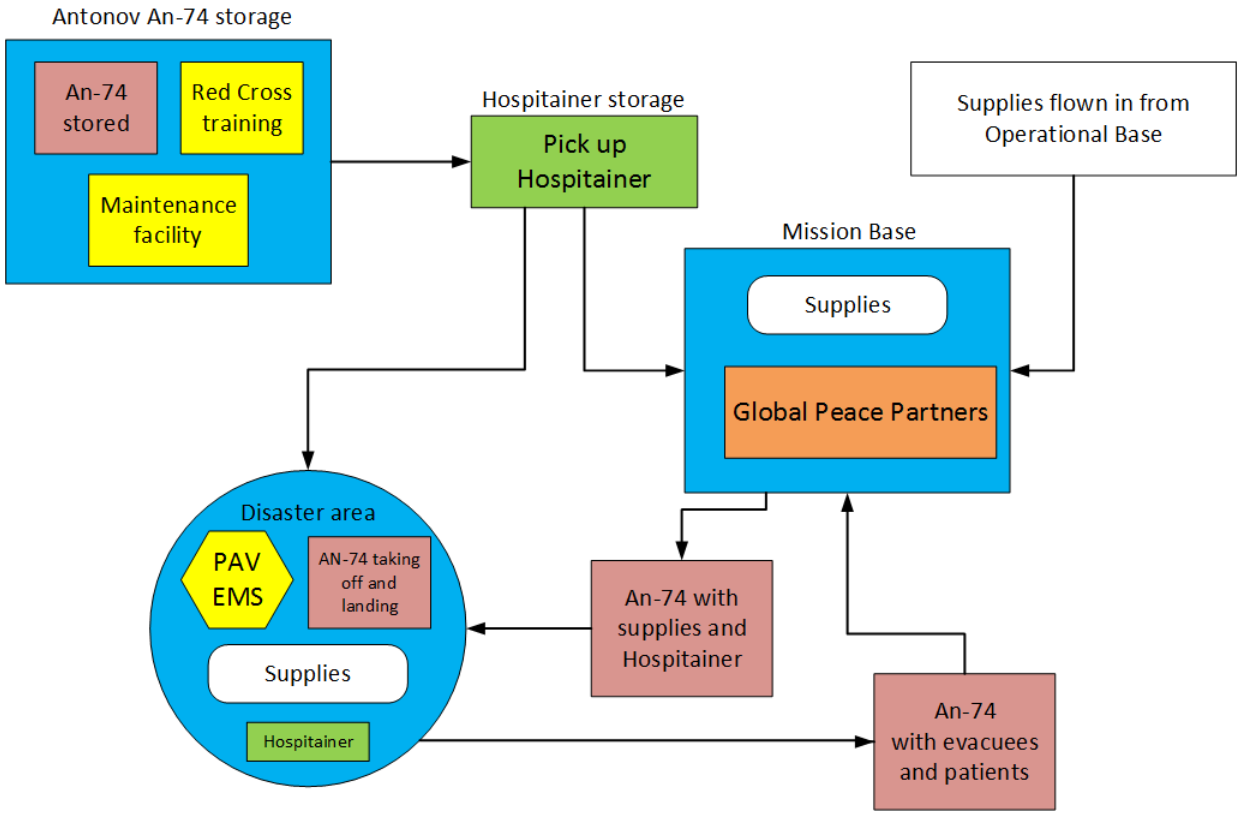

Figure 4.3: Overall layout of the logistics during the mission cycle

The organizational base needs to perform the post-mission activities as well as maintaining contact with other organizations that provide help in the disaster area. Furthermore it has contact to the main supplier to organize the allocation of the supplies. Also, the organizational base is in contact with the government of the country where the organizational base is placed and the government of the country of disaster. This is needed to get all the permissions needed for the mission and to stay up to date about the events happening around the disaster area. This information is also relevant for the field hospital in the disaster area so the organizational base has contact to the field hospital as well.

The four logistical centers of the Red Cross are the operational bases of this system as described in Section 1.1.1. During the mission the operational bases need to have contact to the main supplier, the organizational base and the mission base. The operational and organizational base together with the main supplier organize that the supplies arrive at the operational base and then get transported to the mission base. That is why there needs to be long distance communication to the mission base as well.

The mission base where the Global Peace Partners are providing medical help on a larger scale, has contact with the organizational base, the operational base and the communication person of the field hospital in the disaster area. This is needed to organize the supplies and to be updated about proceedings of other organizations and the government. Additionally there will be the Antonov An-74 aircraft shuttling between the mission base and the field hospital. This is needed to evacuate patients to the Global Peace Partners so they receive further treatment there. Both of these bases are in contact with the aircraft to give and receive information and instructions.

In the disaster area there will a field hospital of the Flying Hospital and the Surgery Hospitainer where surgery will be provided. Between these parts of the Flying Hospital there will be short distance communication possible. This way new medicine can be ordered when Hospitainer runs out of medicine. Furthermore, all staff in the field hospital will carry a short distance communication system with them. With the use of that system everyone can contact the medical aircraft, the communication manager and the rest of the staff. The communication equipment will be placed in a separate tent in the field hospital. That is where the communication manager will work from. He is

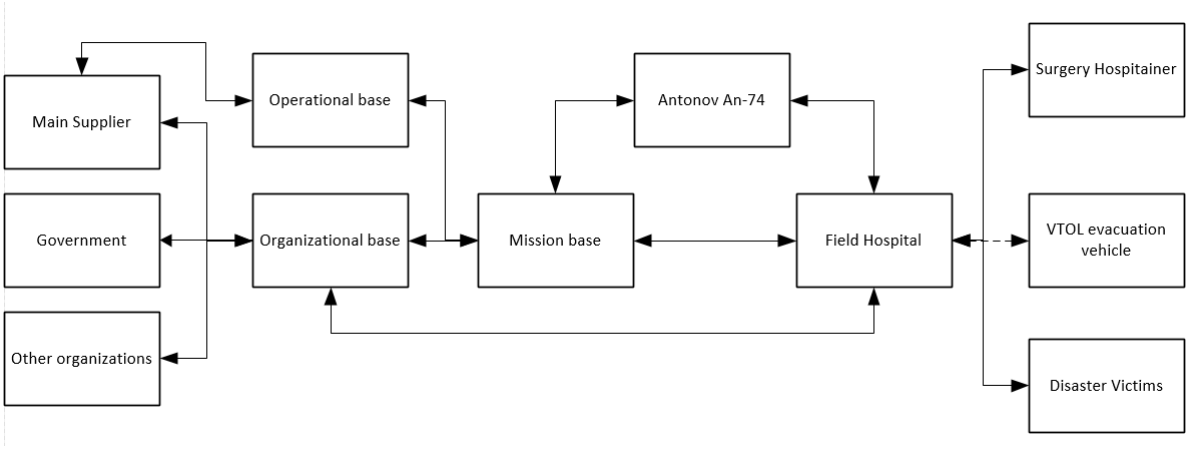

Figure 4.4: Communication flow diagram

responsible for the allocation of the supplies and keeps the crew up to date about proceedings. One staff member will be penetrating deeper in the disaster area so that it can be communicated to the local communities that there is a possibility of getting support. In case of cooperation with the personal air travel VTOL aircraft of DSE group 10, the communication manager will need to have contact to the personal aerial vehicle as well. This aircraft will be used to evacuate patients from inaccessible disaster area.

4.3 Compliance Matrix and Feasibility Analysis

This section describes whether the design requirements are met. The rationale why the design does not meet the requirements is explained in a so-called feasibility analysis. The Requirements Compliance Matrix presents the requirements of the design and indicates whether a requirement is met or not. The first column of the Compliance Matrix shows the section number referring to sections of this report where the requirement is explained in more detail. The compliance column gives the required value of a requirement, the actual value the design meets and the final column indicates whether a requirement is met or not. Values are only assigned to requirements where a specific value can be assigned. Table 4.1 shows the Compliance Matrix of the design. The requirements regarding the crew, patients, medical equipment and the hospital in collaboration with the Red Cross are disregarded in this technical report.

Feasibility Analysis
The feasibility analysis explains why the design does not meet the requirements or which modifications would be required to meet the requirement. As can be seen in the Compliance Matrix, two requirements do not meet the design or partially meet the design. The first requirement is; 'Ensure safety while airborne including system failure scenarios.' The chosen aircraft, the Antonov An-74, has a proven track record. However, further research is required to look into more detail to different system failure scenarios, since reliable data of the Antonov An-74 and the airplane's systems and subsystems is scarcely available. Especially for the retrofitted parts such as the engines, further investigation on the reliability and failure scenarios are necessary to guarantee the safety of airplane, crew and equipment.

The second requirement that is not met by the design yields; 'Provide back-up power in case of primary power source failure.' The airplane itself is equipped with a back-up power source in case the primary power source fails. The medical equipment inside the containers is powered by a generator or solar panels. There is no back-up power supply; the generator to provide power for the medical equipment can be repaired easily and a technician will be present at the disaster site in case of failure. A back-up generator can be transported to the disaster area in case the primary power source fails.

Table 4.1: Compliance Matrix

	Requirement Statement		**Compliance**	
Sec. No	**Requirement**	**Required Value**	**Achieved Value**	**Compliant**
1.1	Enabling penetration into disaster area from a major airport in the vicinity.			Yes
2.7	Enabling penetration into disaster area based on short-range operating envelope.	Range > 800 km	Range = 2908 km at max fuel and 1.5 ton payload	Yes
1.1	Enabling penetration into disaster area based on high-load capacity operating envelope	At least 2500 kg payload	Maximum Payload: 10,000kg	Yes
2.7	Enabling penetration into inaccessible terrain by STOL and VTOL capabilities.	Takeoff distance: 515 m Landing distance: 514 m	Takeoff distance: 278 m Landing distance: 366 m (with thrust reverser) TOW/LW: 28,000 kg	Yes
4.1	Seamless operational connectivity with large scale resources provided by the Boeing 747 and 757 medical support.			Yes
4.1	Availability to accomodate all functional medical equipment tailored to the specific need of the various categories of disasters.			Yes
4.1	Endurance: self-supportive and survivable for at least one week in hostile operating environment with climatically extreme conditions.	One week	With sufficient support, unlimited self-supportive and survivable	Yes
4.1	Easily replaceable by equivalent units on a demand controlled basis.			Yes
1.3	Modification and/or retrofitting of well-known aerial vehicles with a proven track record.			Yes
3.2	Lead time (from design to finalizing certification procedures) of 3 years.	3 years	Within 3 years	Yes
3.5	Low cost operations of the vehicle, minimal maintenance and docking costs.			Yes

	Requirement Statement		**Compliance**	
Sec No	**Requirement**	**Required Value**	**Achieved Value**	**Compliant**
1.1	Cheap, lean and potentially disposable vehicles with a residual value for the local community.	Cost as low as possible	€ 25.19 million	Yes
1.1	Reach a sufficient cruise speed.	> 500 km·h^{-1}	828 km·h^{-1}	Yes
1.1	Ensure safety while airborne including system failure scenarios.			Partial
1.1	Ensure crew and patient security.			Yes
1.1	Maintain storage conditions for supplies.			Yes
1.1	Maintain comfortable conditions for crew and patients.			Yes
1.1	Maintain operating conditions for medical equipment.			Yes
	Maintain sterilized environment when surgical units present.			Yes
1.1	Provide continuous power to subsystems.			Yes
1.1	Provide backup power in case of primary power source failure.			Partial
1.1	Accomodate long rang communication independent of local infrastructure.			Yes
1.1	Be able to navigate independently of local infrastructure.			Yes
1.1	As part of the self-reliance, operational consumables shall be carried in reserve in order to perform emergency maintenance.			Yes
1.1	Once the aerial vehicle reaches the disaster site, the hospital should be quickly deployable and operational.			Yes

4.4 List of Innovations

This list shows the innovations present in the rapport and lists the innovations which could possibly be used in future development of the Antonov An-74 Flying Hospital aircraft.

- **Retrofitted engine** A new type of engine will be used. This engine has never been used on an Antonov An-74 aircraft. However, it could be adapted to the needs of the Antonov An-74 Flying Hospital. The new optimized engine provides more thrust and has a higher thrust to weight ratio.
- **Increased exploitation of Coanda effect** At the moment the Antonov An-74 is the only production aircraft in use with the Coanda effect. As a new engine will be used, which has a higher maximum thrust, this phenomena will be more noticeable. This makes the aircraft really unique. The Coanda effect generates more lift on a certain part of the wing near the location of the engine.
- **Micro vortex generators** This aircraft will be one of few which uses micro vortex generators. The vortex generators are used to re-energize the boundary layer, which results in more lift and less drag. Since the vortex generators are placed on the flaps, takeoff and landing performance are increased while no additional device drag is generate during cruise.
- **Loading monitor** This device is used to help the loading of the aircraft while on a mission. Such a device yet to be developed to this extend, as the device can be used at any location in the world. It is an automated program, which can be controlled in the cockpit or outside the aircraft. The device consists of sensors in the wheels or landing gear. The sensors determine the weight of the aircraft on each landing gear, after which the center of gravity is determined. This center of gravity is checked with the limits of the aircraft. The output of the program is a statement indicating the stability of the aircraft and the need of reallocation of the loading is needed.
- **Stall recovery kits** These kits could be used to recover from a stall situation. However, these systems could also be used with the objective of regaining stability. The stall kit is placed at the very front of the aircraft. Therefore, due to the large moment arm, small forces result in a relatively large moment bringing the aircraft back to stability or trim position.
- **Canard on the aircraft** Using a canard on the aircraft nose enables the extension of the stability margin by moving the center of gravity forward. It could also provide a more efficient and faster recovery from stall due to the large moments, generated by small forces on the canard surface and the large moment arm. Furthermore, a more efficient controllability of the aircraft could be obtained. Also, the torsion of the lift force of the the canard will counteract the torsion of the lift force of the flaps and tail, which will result in a smaller torsion in the wingbox of the main wing. Of course, the lift force of the canard can be used to obtain an higher overall lift force.
- **Composite structures** As an existing aircraft is retrofitted to the needs of a Flying Hospital mission, some structural parts of the aircraft may be modified or reinforced. Modern technologies have made it possible to use other materials than metals. It could be preferable to use composite structures in certain parts of the aircraft if reinforcement are necessary.
- **Glass cockpit** A glass cockpit includes the latest instruments of piloting, navigation and communication. These systems help the pilot while performing the Flying Hospital mission, especially when the pilot needs to land in a hazardous environment.

Conclusion

Natural disasters and conflicts have struck various regions during the past decades, endangering populations and destroying local infrastructure. The loss of local infrastructure inhibits immediate relief and delays or prevents external aid by conventional means. The aim of the project is to create a preliminary design of a Flying Hospital system, incorporating medical equipment and facilities designed by the Hospitainer, to meet the needs of the Red Cross in extended penetration of disaster areas.

This report reflected on the detailed design phase of the project, including a brief overview of the design choices made in the conceptual design phase. In the detailed design phase, the modifications for the Antonov An-74, the chosen aircraft for the Flying Hospital mission, were investigated.

Mission Design
At first, a conceptual design of the mission and aircraft selection was made in the mid-term report. The Flying Hospital mission was determined by looking into different disaster types, rate of occurrence of disasters, typical injuries and past relief operations. Thereafter, potential aircraft types were analyzed and one aircraft type was chosen to be implemented in the Flying Hospital concept. Based on design criteria, the Antonov An-74 turned out to be the most suitable aircraft.

During the detailed design phase Red Cross, the main stakeholder, requested that the focus would shift towards low operational costs, minimal maintenance and docking costs. The developed mission needed to be adjusted. Additionally, the lead development time should not exceed 3 years, the retrofitted aircraft should perform STOL (Short Takeoff and Landing) maneuvers and should be able to reach any disaster area within 24 hours.
Therefore, the recommended system consists of multiple bases all over the world in areas close to disaster sensitive areas, such as Panama, Las Palmas, Dubai and Kuala Lumpur. These cities already have a Red Cross base (logistic center) and enable access to big parts of the world. The Antonov An-74 will be flying to an airport in the vicinity of the disaster area (the mission base) and into the disaster area itself. On the mission base, Global Peace Partners will help the Flying Hospital performing the medical relief mission. The Antonov was chosen for its good performance and robust design. This aircraft will transport supplies, a Hospitainer field hospital and medical staff. It may also evacuate people when necessary. The field hospital will be set-up entirely outside the aircraft, permitting the aircraft to shuttle back and forth from the disaster area to a base for additional supplies. Surgery will be performed in the specially designed Hospitainer, while other activities can be performed in the tents supplementing the field hospital. This system can be scaled larger and smaller in every aspect, in order to match best stakeholders' needs. When the Flying Hospital is not needed, the aircraft can be stored at a location where fees are low. The Hospitainer could be used in places where no regular hospital is available. Additionally, the PAV EMS Vehicle could be used as an additional vehicle within the disaster area, as this vehicle can penetrate even deeper into the disaster area to reach people that cannot be directly aided by the Flying Hospital.
The collaboration with the Global Peace Partners and PAV EMS Vehicle accomplishes a seamless connectivity between all parts the Flying Hospital system. This Flying Hospital system results in a resilient medical relief environment.

Risks can have a significant impact on the objectives of the Flying Hospital system. To prevent the occurrence of unexpected setbacks while developing the aircraft or performing its mission, a risk analysis was performed for both the mission and the Antonov An-74. The most critical risks for the mission are a hazardous landing zone, operational delays and budget related problems. These could be solved by using obtained detailed information about the disaster area, the use of standardized manuals and selling possibilities if funds are depleted respectively. However, in the latter situation it is difficult to mitigate the problem. For the aircraft the most critical risks are the takeoff and landing performance, malfunction or failure and the development time. Mitigation plans for these risks are respectively: using a specialized undercarriage or landing procedure, frequent intervals and predefined procedures for maintenance and an optimized technical production processes.

Detailed Design of the Modifications for the Antonov An-74
The Antonov An-74 had been selected as the aircraft for the Flying Hospital mission. Several possibilities to improve the performance, increasing the suitability for the mission and further development of the aircraft have been

proposed. For the stakeholders, the improvement of the takeoff and landing performance by reducing the runway length required was the main objective. This increases the number of missions in which the aircraft can be used. Technical aspects such as engines, the upper surface blowing, vortex generators, stability and control and structural strength have been investigated.

The first, most critical proposed modification to the Antonov An-74 was a change in engines. The stock D-36 2A engine could be changed to the Ivchenko Progress D-436-T3 during the modification process. This modern engine has an increased maximum thrust of 92.2 kN, while increasing the weight by just 236 kg compared to the D-36 2A. This leads to a significant thrust to weight ratio increase which is highly beneficial for a reduction in takeoff distance. Justifying the process, the D-36 2A engine as well as the D-436-T3 engine were modeled. The D-36 2A engine was modeled during takeoff, whereas the D-436-T3 engine was modeled during takeoff and cruise. Additionally, an optimization procedure for cruise condition was performed for the D-436-T3 engine.
The replacement of the D-36 2A engine by the D-436-T3 engine would result in a thrust increase of 45%. This is beneficial for the Coanda effect and upper surface blowing, so the aircraft will be able to takeoff within a shorter distance. The SFC and the emission index of NO_x slightly increased due to the increase in thrust. These parameters were decreased during the optimization procedure for cruise condition.

Once new engines were selected for retrofit, they were investigated in terms of USB (upper surface blowing) performance. USB is resultant of the unique configuration of the An-74 and consists of the engine exhaust being blown over the wing surface to generate large aerodynamic forces. The analysis of the USB system consisted of a model based on known An-74 geometries.

The model results indicated that the new D-436 engines, coupled with the existing USB configuration, would have an appreciable influence upon the STOL characteristics of the aircraft. The greater mass flow produced by the D-436 compared to the stock D-36 leads to increased momentum vectored downwards by the wing (resultant of the Coanda effect). Additionally, the higher exhaust velocity on the blown surface results in lower pressures and greater aerodynamic forces. Results indicated 8% and 2% increases in lift and drag respectively for the entire aircraft in flapped configuration, and 4% and 5% increases in lift and drag respectively for cruise configuration when compared to stock engines. New moments were found to be generated as well, necessitating future investigation in terms of flight stability. Increases in drag and pitching moment were inherited from the USB of the new engines but were deemed tolerable in light of the STOL benefits of the new lift. Ultimately, the D-436 engines were deemed to have a beneficial contribution to STOL at a minor expense of cruise efficiency, thereby adhering to the Flying Hospital mission requirements.

Retrofitting the aircraft with new engines required investigation of the structural capabilities of the airplane. The aim was to investigate the difference in normal and shear stress in the wing and fuselage due to the heavier and more powerful engine. The percentage increase in normal stress in the wing and fuselage is respectively, 2.8% and 7.5%. The increase in shear stress is 2.05% and 12.5% respectively for the fuselage and the wing. The impact on the structure due to the additional weight and thrust is small. The wing-fuselage intersection experiences the largest difference in stresses, consequently structural reinforcements may be necessary for this part of the structure. If the wing structure was built to its limits with the old engines mounted, the thickness of the front spar, top skin and bottom skin needs to be increased by a factor of 1.15, including a safety margin. This needs to be done to make sure that the normal and shear stresses do not exceed the maximum stresses found in the wingbox if the old engines were used.

To improve the stall characteristics of the aircraft, micro vortex generators were placed on the wings. In total, 344 micro vortex generators, divided over the two flap sections of the two wings, were placed at $0.25 * c_{flap}$ on the two inboard wing sections. The height h of the vortex generators is between 8 and 11 mm, defined as a function of the boundary layer thickness δ: $h/\delta = 0.5$. The aspect ratio is set to $A_v = 0.8$; the angle between the flow and vane is $\alpha_v = 30°$. The spacing between different pairs (D) and between elements of the same pair (d) are defined as: $D/h = 10$ and d/h=2.5. Total costs are approximately €400,000. The performance effects on the wing: for takeoff climb ($\alpha = 8°$) and landing descent ($\alpha = 8°$), drag is reduced by 50% and lift is increased by 10%. The improvements for the entire aircraft are 9% lift increase and 37.5% drag reduction during both takeoff climb and landing descent at $\alpha = 8°$. The sensitivity analysis showed that the spacing between devices of the same pair is crucial for the effectiveness of the vortex generators.

Due to all the proposed modifications to the Antonov An-74, stability and control of the aircraft could have changed.

The modifications were found to have a minor impact on the stability and control. Making use of the aircraft parameters and loading diagrams, scenarios were investigated in which cargo shifts the center of gravity over its limits. To prevent such situations in a medical relief mission, a program is fitted within the aircraft itself that uses the Antonov An-74 parameters to compute the center of gravity of the aircraft given a certain fuel, cargo and crew loading and distribution. It then computes the allowable center of gravity locations using stability calculations. Thereafter, it outputs a message stating whether the current aircraft is stable or if a loading redesign needs to be carried out. Implementation of such a system in the cockpit of the airplane would be of major relevance to the pilot or load master.

After determining the separate effect of the new engines, the upper surface blowing and the addition of vortex generators, it was investigated as to what extent their total effect influences the STOL performance. Due to the stronger Coanda effect and the addition of vortex generators, the total change in C_L during approach ($\alpha = 8°$) equals 16.7%. Stall speed, and thus also $V_{approach}$ and $V_{touch-down}$, are reduced by 7.2%. In case no reverse thrusters are used during the ground run, the runway length required reduces by 11%-12%. When reverse thrusters (15% rated thrust) were taken into account in the calculations, it was determined that landing distance is reduced from 17% to 22% (for a total takeoff weight of 36 tons and 22 tons respectively). During takeoff, the new engines with increased power (+45%) result in that the takeoff distance is reducing by 42% to 55% (for a total landing weight of 22 tons and 36 tons respectively). For a predicted typical operating weight of 28 tons, the takeoff and landing (with reverse thrust) distances of the aircraft were calculated to be approximately 280 m and 380 m respectively. Such short takeoff and landing performance enables the aircraft to perform its mission of accessing difficult areas, thus justifying the modification costs. The new engines have an increased specific fuel consumption of around 10%. Due to this, and the stronger USB, the range is reduced by 10%-15%. The vortex generators do not affect range, since they are hidden in the wing during cruise.

The retrofitting will enable the aircraft to be operated in all sorts of disaster where enough dry land for landing and takeoff is available. If case of floods, the hospital can be built on floating boats or platforms. In case of unavailability of dry landing strip, a further option is to use floating landing strips that need to be designed. The aircraft will however not be able to operate near volcanic eruptions due to the ash cloud presence. Further, nuclear disaster also cannot be covered due to the high radiation risk that the aircraft, equipment and crew are subjected to.

Mission Analysis and System Design
With the mission and aircraft having been further developed, aspects like mission risks, sustainability, compliance with stakeholders' requirements and the implementation of the design were investigated.

Having finished the conceptual and detailed design phases, the future implementation of the Flying Hospital was established. Investigated procedures included supplier identification and aircraft acquisition, stripping and retrofitting. Retrofitting will consist of mounting the new engines, with subsequent structural reinforcement, mounting of vortex generators and modifications to the rear ramp. These processes are envisioned to occur as a concurrent process, governed by just-in-time (JIT) principles.

Retrofitting leads to the initial prototype of the system. This prototype is to be tested and certified. After certification, the production of the aircraft is started and eventually leads to the final delivery phase. In this phase the retrofitted aircraft is presented to all stakeholders and customers. All these steps are projected to take approximately 800 days starting from the date of detailed design. Retrofitting, prototype testing and certification of the retrofits are scheduled to take 150, 150 and 200 days respectively. Aircraft acquisition, stripping and retrofitting along with prototype testing will account for 80% of costs with an estimated cost of €29 million. The certification process, final testing and production of the aircraft will cost €2 million. Adding other miscellaneous costs, the total cost of the lead time will be €32.5 M.

The business model for the Flying Hospital is mainly dependent on its potential buyers. The transport aircraft can be acquired by the customer either via lease, a purchase or a contract. The hospital units of the system, the medical containers, can operate in a manner which is most suitable for the need of the owner. During disasters the hospital can operate in its intended role as non-profit emergency relief. Outside disaster times it may be employed as a medical or training facility, either for profit or non-profit. Thus the aircraft and medical units can be used throughout the year, not only during disasters. All in all, the Flying Hospital concept proves to be very flexible due to its scalability and multiple roles it can fulfil for different buyers.

To implement sustainability in the design the life cycle has been adapted to fit the definition of sustainability. Besides reusing old components, new components will be created using sustainable materials such as AEROCORK and composites like GLARE. Furthermore the engine performance will be improved, this brings some benefits as for sustainability. The NOx emission can be reduced by 7% while the SFC is reduced by 3%. Another helpful option to reduce emissions and take into account sustainability, is the use of biofuels. When the aircraft reaches the end of its life it will be disassembled and sold in parts. Large components can be used for non-aerospace related purposes such as buildings.

The compliance matrix and feasibility analysis presented the requirements of the design and explained when the design did not meet a requirement. Most of the requirements were met. The requirements changed during the early detailed design phase due to stakeholders' needs. More focus was established on low operational and docking costs and minimal maintenance. Furthermore, the Red Cross had taken over all the medical organization, including the requirements for the crew, patients, supplies and medical equipment.

Overall, the Flying Hospital is a feasible candidate to fulfill the needs of a future humanitarian relief system. By applying selective modifications to the existing An-74 aircraft, a proven and quickly certifiable aircraft has been designed. The modifications, new engines and vortex generators, are expected to reduce takeoff and landing distances by approximately 50% and 12% respectively. Resultantly this will enable the Flying Hospital to access regions inaccessible to conventional means including larger aircraft. Upon accessing a disaster area, the Flying Hospital can then deploy modular medical containers which provide local aid and are sufficiently versatile to cover the majority of humanitarian needs. This system was determined to meet all stakeholder requirements in an economical yet environmentally sustainable manner. In doing so, the Flying Hospital may help define future humanitarian operations as rapidly responding, effective and versatile.

Recommendations

In this chapter, recommendations for further research, analysis, design and system additions related to the project are discussed. In the project the foundation was laid, but there still is a long road ahead to fully operate the Flying Hospital. By means of these recommendations, a view on future design is given. These recommendations primarily involve the technical design. As an overview, a list of innovations is given in Section 4.4. Possible future MSc theses or DSE projects can be found in the following section.

The first recommendation involves the engine. Further analysis can be done on the detailed design of the D-36 2A engine and D-436-T3 Ivchenko Progress engines. Detailed data needs to be obtained on the pressure ratios. At this moment these were carefully selected with respect to the aircraft and the environment it will be working in. Furthermore, a more specific analysis on the improvements of the new engine can be performed. This can be done in the form of testing. Finally, it can be investigated how to mount the engine to the wing in a suitable manner, as the dimensions with the existing engine differ, but no reliable data of the engine structure is available at this moment.

For the further elaboration of the Upper Surface Blowing (USB) of the wing, some recommendations can be given. The USB model was limited by the lack of data regarding the exact An-74 wing/USB geometries and D-36 engine characteristics. This was addressed with considerable assumptions in the generated model. Consequently, the accuracy of the model is not certain. While the precision of the calculations is likely sufficient, the low accuracy means that the calculated values deviate considerably from the true An-74 USB properties. In terms of the engine, nozzle geometry is highly determinant in USB performance, yet sufficient data could not be acquired. Creating an accurate model with actual data on the engine and wing is recommended to gauge the detailed effect of engine retrofitting on the An-74 in terms of STOL, stability and structural considerations.

For vortex generators (VGs) in general, it is advised to perform a CFD or analytical analysis to examine the effect of VGs in this specific case. In our study, literature data was used to size and determine the effect of VGs. Although this provides a very efficient way for performing a first study on this subject, it is advised to perform a CFD analysis to assess the performance more accurately. Also experimental wind tunnel tests would improve the understanding and would help determining the effectiveness of the VGs applied to this specific situation. The reduction in drag of placing VGs at $0.2 \cdot c$ was determined based on the reduction in skin friction drag due to the extension of laminar flow. To get a more accurate result, it is advised to also take into account pressure drag and induced drag. As studies at low Reynolds numbers have proven, the transition point can be delayed by placing VGs. The extent to which this can be done at higher Reynolds numbers was estimated. However it is advised to do an extensive study to determine quantitatively the delay in transition point at high Reynolds numbers.

With regard to the structure further research is necessary to investigate the current structural capabilities and to investigate whether reinforcements are needed. The wing-fuselage intersection has to be analyzed in more detail and the dynamic loads on the structure should be incorporated in further research on the structure. A proven method to investigate the structure is Finite Element Method. For any further analysis this method is recommended.

For stability and control with the medical container aspect in the existing Antonov design, it is essential that the loading and unloading of the aircraft is safe even in most hazardous situations. For this purpose, use can be made of monitoring sensors that display the stability of the aircraft by measuring the weight distribution. During loading, flying and unloading, it is very important that the c.g. stays within its limits. Further in depth, research on such a monitoring system is highly recommended. To increase c.g. performance during flight, research can be done on the tailplane, interior and fuel system alterations. Also adding canards and stall recovery kits can provide an increase in performance and are therefore subjects for further research.

There is enough room for improvements with regard to the sustainable aspect of this project. Further analysis can be done on the different types of materials that are possibly more sustainable than the currently used materials on the aircraft. One has to think in the sectors of composites, biomaterials and material that is still in development. It is also recommended to perform additional research on the methods to manufacture in a more sustainable manner, since this reduces a waste and undesired emissions. Also, one can elaborate further on the different kind of fuel used on the newly retrofitted aircraft. One can possibly find cleaner and cheaper fuels to operate the engine with. This

again makes room for further research on the emissions of the new engine and fuels. Also it is possible to perform an analysis on the material of the container. The container is made out of a metal alloy, this can be altered to a composite structure for certain benefits. Thus there are several sustainable topics that can be researched in the near future.

Other Recommendations

The aircraft can be fitted with additional features that increase the value of the aircraft. However, these were not feasible to investigate within the given time and resource constraints during the project. Therefore, they will be described in general terms in the following paragraphs. These need to be investigated further and designed to gain a technological advantage and add value.

Monitoring systems are a very good addition to the aircraft, especially in disaster missions. This is because there is not always enough time and resources to perform a full check of the aircraft during a disaster. The probability of having faults or breakdowns is higher than in normal operating conditions due to the hard landings on rough terrain, the nature of the mission and aircraft surroundings. For those reasons, a monitoring system can be designed to detect critical faults in those areas that are crucial for a successful flight. These have a general functionality as follows:

Hydraulics and tires Sensors can be placed inside the hydraulic systems and tires, any leaks of hydraulic fluid will result in variations in the measured pressure. Below critical levels, the system will alarm the pilot.

Structural integrity Every electrical conducting piece has a resistance that is corresponding to its geometry. A small electric current can be run through the different critical components. Any cracks, bends or changes in geometry will result in a change in resistance properties of the component. That resistance change can be detected by voltmeters and altimeters and reported by a processing unit to the pilot.

Glass Cockpit A glass cockpit uses digital instrument displays like LCD screens instead of the knobs and gauges. It can be adjusted to only display needed flight information. This makes it easier to operate the aircraft and enables the pilot to see certain warnings and blinking lights that he might overlook or miss during evacuation chaos in traditional cockpits.

Cameras Cameras can be fitted in different locations of the aircraft and feed directly into the cockpit. This will enable the pilot to have a ground level visual of aircraft surroundings. This can be very beneficial in crowded disaster sites where there is no ground support. It enables the pilot to see whether there are people or obstacles on the ground. In case of an engine fire, he can now sees this from the cockpit. In rough landing, the pilot can see whether there is structural damage to the aircraft.

Fire systems During rough landings, fuel leaks and engine fires are also likely due to structural or foreign object damage. Having fire sensors installed on wings and engines can also help detect a fire and take the appropriate measures since fuel tanks and engines are not visible for the pilot.

Amphibian system To provide the best and fastest medical help in case of a flooding, an amphibian system can be designed to fight down the water. This can be done in two ways. The first option is to cooperate with Damen Shipyards. This company can make a floating runway on which the Antonov An-74 can land. The other option is to make the Antonov An-74 amphibian by mounting pontoons to or under the fuselage. This way, the Antonov An-74 itself can land on water. In both options the medical relief mission can be performed on the water as the Hospitainer may float as well. However, another option is to only use the water to land and takeoff and to set-up the field hospital on a dry area close by. So, an amphibian system can have a big impact on how a medical relief mission is performed in case of a hydrometeorological disaster, such as a flooding.

Subsystem interaction the Antonov An-74 aircraft consists of multiple systems and subsystems, each performing a specific task. To understand the complexity, additional research has to be done on the mutual relations and interactions of the subsystems. It represents important relations between the electrical, hardware and software as well as data handling equipment of the system. Different subsystem failure scenarios have to be taken into account, since this influences the safety of system.

List of Future Research

This is a list of suggestions for future research projects like MSc theses or DSE projects. Since the retrofitting possibilities for the Antonov An-74 may need further research in the field of engines, vortex generators, Coanda effect improvement, stability and c.g. range improvements. These may be interesting activities in further studies.

- Design of a large VTOL cargo aircraft operable in 2050
- Medical supply by a UAV swarm in hazardous environment
- Coanda effect on new airplanes
- Redesign of tailplane to improve c.g. range
- Design an active fuel control system to improve stability
- Retrofit existing aircraft with canard
- Stall recovery kit on existing aircraft
- Calculation of dynamic loads on structure in hazardous environment using FEM
- Retrofit existing aircraft with bio-aviation fuel engines
- Retrofit existing aircraft with composite wings components
- Research into micro vortex generators
- Micro vortex generators analysis using CFD
- Research effect vortex generators on transition point at high Reynolds numbers
- Material selection for increase temperature at the aft of engine
- Upper Surface Blowing curvature optimization
- USB jet ratio optimization
- USB pitching moment reduction
- Propulsion behavior in hazardous environment
- Health and sensor monitoring systems for engines
- Improvement of engine mounting

Bibliography

[1] Andy Pasztor, Susan Carey, Gabriel Kahn, Joe Lauria, Charles Forelle, "Clogged Airport, Ruined Seaport Delay Aid," *Wall Street Journal*, January 2010 [visited on 02/05/2013].

[2] DSE - Group 15, "Flying Hospitals - Mid-Term Report," 30/05/2013.

[3] International Federation of Red Cross and Red Crescent Societies, "Humanitarian Logistics Centre." http://www.iweee.org/2013-las_palmas/presentations/humanitarian-logistics-centre-benjamine-budiman.pdf, 25.01.2013 [visited on 11/06/2013].

[4] Aviama, "An-72 Description." http://www.aviama.ru/content/72-voenno-transportnyi-samolet.html, 2013 [visited on 19/06/2013].

[5] Global Plane Search, "ANTONOV AN-74." http://www.globalplanesearch.com/search?gpsq=antonov+an-74, 2013.

[6] DSE - Group 15, "Flying Hospitals - Baseline Report," 03/05/2013.

[7] Terry Day, "The Coanda Effect and Lift." http://www.newfluidtechnology.com.au/THE_COANDA_EFFECT_AND_LIFT.pdf, 2008 [visited on 14/06/2013].

[8] EPI inc., "The Prime Directive - Powerplant Weight." http://www.epi-eng.com/aircraft_engine_conversions/prime_directive.htm, 06/19/2011 [visited on 14/06/2013].

[9] G. La Rocca, "Lecture Slides AE2101: Aerospace Design and Systems Engineering Elements II ," 2011-2012.

[10] AER, "Antonov An-74." http://www.aer.ita.br/~bmattos/mundo/airliner/an74_dir.htm, 2013 [visited on 14/06/2013].

[11] Jeff Scott, "Wing Vortex Devices." http://www.aerospaceweb.org/question/aerodynamics/q0228.shtml, 15/05/2005 [visited on 14/06/2013].

[12] Whitt, "Stall Origins and Performance." http://www.whittsflying.com/web/page3.265Stall_Origin_and_Performance.htmIsastallcoordinated?, [visited on 5/06/2013].

[13] D. A. Solfelt, "CFD Analysis of a T-38 Wing Fence," 2007.

[14] K. Bernard, "Improving Airplane Stall Characteristics with Fixed Devices." http://airspeedalive.com/writings/stallcharacteristics.html, April 2013 [visited on 05/06/2013].

[15] D. A. Solfelt, R. C. Maple, "CFD Analysis of a T-38 Wing Fence," 2008.

[16] Flying Magazine, "Hawker 800XP," vol. 129, 2004.

[17] Micro AeroDynamics Inc., "Micro Vortex Generators for Single and Twin Engine Aircraft." http://www.microaero.com/index.html, 2013 [visited on 14/06/2013].

[18] A. Agrawal, G. Verma, "Similarity analysis of planar and axisymmetric turbulent synthetic jets," *International Journal of Heat and Mass Transfer*, vol. 51, 2008.

[19] "Synthetic Jets." http://homepages.rpi.edu/~amitam/docs/Synthetic_jets.pdf, [visited on 11/06/2013].

[20] S. Budea, A. Ciocanea, "The influence of the suction vortex over NPSH available of centrifugal pumps," *U.P.B. Scientific Bulletin, Series D*, vol. 70, 2008.

[21] M. Kotsonis, L. Veldhuis, H. Bijl, "Plasma Assisted Aerodynamics for Transition Delay," *Springer Nederlands*, vol. 18, 2010.

[22] "Canard Efficiency Myths." http://www.apollocanard.com/4_canard%20myths.htm, 2012 [visited on 12/06/2013].

[23] Desktop Aerodynamics Inc., "Applied Aerodynamics: A Summary of Canard Advantages and Disadvantages." www.desktop.aero/appliedaero/configuration/canardprocon.html, January 2007 [visited on 13/06/2013].

[24] D. Stackhouse, "What are the advantages of a canard wing aircraft?." http://www.djaerotech.com/dj_askjd/dj_questions/canard.html, 14/02/2007 [visited on 13/06/2013].

[25] J.A. Stoop, "Towards a failsafe flight envelope protection: the recovery shield," 2012.

[26] J.D. Anderson, *Fundamentals of Aerodynamics*. McGraw-Hill, 2011.

[27] R. Faye, R. Laprete, M. Winter, "Blended winglets," [visited on 12/06/2013].

[28] G. Larson, "How Things Work: Winglets." http://www.airspacemag.com/flight-today/wing.html, Sept 2001 [visited on 5/06/2013].

[29] Doug Jackson, "Wing Twist and Dihedral." http://www.aerospaceweb.org/question/dynamics/q0055.shtml, 02/12/2001 [visited on 14/06/2013].

[30] "Drogue parachute." http://www.absoluteastronomy.com/topics/Drogue_parachute, [visited on 04/06/2013].

[31] A.Cervone, "Lecture Slides AE2203: Power and Propulsion," 2013.

[32] Freight Metrics, "Aircraft Operating Cost." http://www.freightmetrics.com.au/Air/AircraftOperatingCost/tabid/540/Default.aspx, 01/01/2013 [visited on 18/05/2013].

[33] J. Taylor, *Jane's All the World's Aircraft*. Jane's Information Group, 87th edition ed., 1996-1997.

[34] Aviation Safety Network, "Antonov 72 / 74." http://aviation-safety.net/database/type/type.php?type=04A, 05/05/2007 [visited on 20/06/2013].

[35] A. Gubler, "Replacing the Caribou: mission impossible?," *Defence TODAY magazine*.

[36] Janes, "Ivchenko-Progress D-436 ." https://janes.ihs.com/CustomPages/Janes/DisplayPage.aspx?ShowProductLink=true&DocType=Reference&ItemId=+++1306343&Pubabbrev=JAE_, 19/04/2013 [visited on 07/06/2013].

[37] N. Meier, "The CF34 engine family ." http://www.jet-engine.net/civtfspec.html, 03/04/2005 [visited on 07/06/2013].

[38] GE, "Civil Turbojet/Turbofan Specifications ." http://www.geaviation.com/bga/engines/cf34-family.html, [visited on 07/06/2013].

[39] Rolls-Royce, "BR710 ." http://www.rolls-royce.com/defence/products/tactical_aircraft/br_710.jsp, [visited on 07/06/2013].

[40] Ivchenko progress, "More detailed information about D-36 engine family." http://www.ivchenko-progress.com/welcome.do?id=165, 2004-2007 [visited on 14/03/2013].

[41] N. Antoine, I. Kroo, " Framework for Aircraft Conceptual Design and Environmental Performance Studies," *AIAA JOURNAL*, vol. 43, 2005.

[42] ICAO, "ICAO Noise Data Base." http://noisedb.stac.aviation-civile.gouv.fr/pdf.php?id=10181, 2002 [visited on 18/06/2013].

[43] "Price An-74." http://superjet.wikidot.com/wiki:d-436-cost, [visited on 14/05/2013].

[44] W.H. Mason, "High Lift Aerodynamics." http://www.dept.aoe.vt.edu/~mason/Mason_f/HiLiftPresPt2.pdf, [visited on 17/06/2013].

[45] W.H. Mason, "A Conceptual Design Methodology for Predicting the Aerodynamics of Upper Surface Blowing on Airfoils and Wings." http://scholar.lib.vt.edu/theses/available/etd-12072004-095231/unrestricted/EBKThesis_121004.pdf, 2004 [visited on 11/06/2013].

[46] ANTONOV Company, *Flight Manual Antonov An-74-200.* 2003.

[47] E. Torenbeek, *Synthesis of Subsonic Airplane Design.* 1982.

[48] UIUC Applied Aerodynamics Group, "UIUC Airfoil Coordinates Database." http://www.ae.illinois.edu/m-selig/ads/coord_database.html, [visited on 18/06/2013].

[49] J. Williams, S.F.J. Butler, "Aerodynamics of Jet Flaps." http://aerade.cranfield.ac.uk/ara/arc/rm/3304.pdf, 1963 [visited on 20/06/2013].

[50] John Lin (Langley Research Center), "Review of research on low-profile vortex generators to control boundary layer separation," *Progress in Aerospace Sciences*, vol. 38, 2002.

[51] M. Kerho & B. Kramer, "Enhanced Airfol Design Incorporating Boundary Layer Mixing Devices," *AIAA Aerospace Sciences*, vol. 41, 2003.

[52] I. Chisholm, K. Hackett et al., "Vortex Generators for Control of Shock-Induced Separation - Part I: Introduction and Aerodynamics," *ESDU*, 1993.

[53] I. Chisholm, K. Hackett et al., "Vortex Generators for Control of Shock-Induced Separation - Part II: Guide to use of Vortex Generators," *ESDU*, 1993.

[54] J. Betterton, K. Hackett et al., "Laser Doppler Anemotry Investigation on Sub Boundary Layer Vortex Generators for Flow Control," *ESDU*, 1993.

[55] H. Bijl, "Lecture Slides AE1101: Introduction to Aerospace Engineering," 2010-2011.

[56] Free Bird Innovations, Inc., "Freebird Aviation Australasia." http://www.freebirdaviation.com.au/vortex.html, 2010 [visited on 14/06/2013].

[57] Metal Supermarkets. https://www.metalsupermarkets.com/CART.ASPX, [visited on 17/06/2013].

[58] Mike Busch, "Vortex Generators: Band-Aids or Magic?." http://www.avweb.com/news/reviews/182564-1.html, 13/11/1997 [visited on 17/06/2013].

[59] Sebastien Heintz, "Installing Micro Vortex Generators (VG) on the STOL CH 701 Elevator." http://www.zenith.aero/profiles/blogs/installing-micro-vortex, 02/03/2009 [visited on 14/06/2013].

[60] Niu, C.Y. Michael, *Airframe Structural Design.* Hong Kong Conmilit Press LTD., 1st edition ed., 1998.

[61] Megson, T.H.G, *Aircraft Structures for Engineering Students.* Elsevier, 4th edition ed., 2007.

[62] J. Roskam, *Airplane Design, Part V: Component Weight Estimation.* 2003.

[63] European Aviation Safety Agency, "CS-23." http://www.easa.europa.eu/agency-measures/docs/certification-specifications/CS-23/CS-23%20Amendment%202%20(corrigendum).pdf, 08/09/2010 [visited on 13/06/2013].

[64] European Aviation Safety Agency, "CS-25." http://www.easa.europa.eu/agency-measures/docs/certification-specifications/CS-25/CS-25%20Amdt%2012.pdf, 12/08/2010 [visited on 13/06/2013].

[65] Gianfranco La Rocca , "Lecture Slides AE3201: Requirement Analysis and Design principles for A/C stability & control," 14/02/2013.

[66] "Stress strain and young's modulus." http://www.engineeringtoolbox.com/stress-strain-d_950.html, [visited on 14/06/2013].

[67] "Stress strain material laws." http://www.colorado.edu/engineering/CAS/courses.d/Structures.d/IAST.Lect05.d/IAST.Lect05.pdf, [visited on 14/06/2013].

[68] http://www.engineeringtoolbox.com, 2013 [visited on 19/06/2013].

[69] Mark Voskuijl, "Flight and Orbital Mechanics." Lecture Slides, 2011.

[70] Virginia Tech, "Takeoff and Landing Performance." http://www.dept.aoe.vt.edu/~lutze/AOE3104/takeoff&landing.pdf, [visited on 18/06/2013].

[71] Sadraey M., "Aircraft Performance Analysis." http://faculty.dwc.edu/sadraey/Chapter%203.%20Drag%20Force%20and%20its%20Coefficient.pdf, 2009 [visited on 18/06/2013].

[72] Denis Howe, *Aircraft Conceptual Design Synthesis*. 2000.

[73] George J. Noel, Eric Boeker, "Thrust Reverser Analysis for Implementation in the Aviation Environmental Design Tool." http://ntl.bts.gov/lib/35000/35600/35608/rtv-4f-fa4t-lr1.pdf, 06/2007 [visited on 20/06/2013].

[74] Dan Moody, "747 & 757 Hospital Planes." http://www.globalpeacepartners.org/files/Download/GPP_Technology_Planned.pdf, 21/10/2010 [visited on 21/05/2013].

[75] G. Brundtland, "Our Common Future," tech. rep., United Nations, March 1987.

[76] Acadamy, "Process for Advanced Management of End-of-Life of Aircraft," 2008.

[77] C. Lambert, "Advanced Aircraft Materials," tech. rep., SBAC.

[78] N.Santhanam, "Sustainable Aircraft Materials - AEROCORK." http://www.cleantick.com/users/narsi/pages/cleantech-in-aviation/updates/16087, 20/02/2012 [visited on 22/06/2013].

[79] A.Schwartz, "Airplanes made from cork may soon take to the skies." http://inhabitat.com/airplanes-made-from-cork-may-soon-take-to-the-skies/, 20/02/2012 [visited on 22/06/2013].

[80] S. Jaichandar1, K. Annamalai, "The Status of Biodiesel as an Alternative Fuel for Diesel Engine - An Overview ," *Journal of Sustainable Energy & Environment*, vol. 2, 2011.

[81] International Air Transport Association, "Fact Sheet: Alternative Fuels." http://www.iata.org/pressroom/facts_figures/fact_sheets/pages/alt-fuels.aspx, June 2013 [visited on 19/06/2013].

[82] Biodiesel-Energy-Revolution, "The Disadvantages of Biodiesel.." http://www.biodiesel-energy-revolution.com/disadvantages-of-biodiesel.html, 2010 [visited on 19/06/2013].

[83] EADS, "First flights worldwide with pure biofuel from algae." http://www.diamondaircraft.com/media/uploads/files/IW_ILA_Biofuel_eng.pdf, 2010 [visited on 19/06/2013].

[84] Mat McDermott, "World's First Flight Powered by 100% Algae Biofuels Completed." http://www.treehugger.com/aviation/worlds-first-flight-powered-by-100-algae-biofuels-completed.html, 22/07/2010 [visited on 19/06/2013].

[85] Simone Preuss, "Seven Amazing Airplane Buildings." http://1800recycling.com/2010/08/airplane-buildings/#.UZtLmrVkOso, 4/08/2013 [visited on 21/05/2013].

[86] Hospitainer, "Concept Description." http://hospitainer.com/39/mobility, 01/01/2013 [visited on 05/06/2013].

A | Appendix Engine

Station	W kg/s	T K	P kPa	WRstd kg/s
amb		288,15	101,325	
2	305,910	288,15	100,312	309,000
13	254,925	335,21	160,499	173,583
21	50,985	335,64	160,499	34,739
22	50,985	335,64	160,499	34,739
24	50,985	422,55	320,998	19,489
25	50,985	422,55	314,578	19,887
3	48,691	811,58	2610,995	3,171
31	43,082	811,58	2610,995	
4	44,067	1580,00	2480,445	4,215
41	46,616	1541,20	2480,445	4,404
42	46,616	1176,50	653,175	
43	49,676	1155,31	653,175	
44	49,676	1155,31	647,949	
45	50,695	1146,05	647,949	15,810
46	50,695	1072,26	477,405	
47	50,950	1070,33	477,405	
48	50,950	1070,33	477,405	20,841
49	50,950	825,54	145,509	
5	51,970	823,22	145,509	61,168
8	51,970	823,22	144,054	61,786
18	254,925	335,21	156,486	178,034
Bleed	0,000	811,58	2610,996	

Efficiencies:	isentr	polytr	RNI	P/P
Outer LPC	0,8780	0,8858	0,990	1,600
Inner LPC	0,8700	0,8783	0,990	1,600
IP Compressor	0,8400	0,8546	1,321	2,000
HP Compressor	0,8500	0,8853	1,967	8,300
Burner	0,9995			0,950
HP Turbine	0,8900	0,8734	3,453	3,798
IP Turbine	0,9126	0,9096	1,267	1,357
LP Turbine	0,9000	0,8856	1,009	3,281

FN	=	92,25 kN
TSFC	=	10,6765 g/(kN*s)
WF	=	0,98487 kg/s
s NOx	=	0,99194
BPR	=	5,0000
Core Eff	=	0,4129
Prop Eff	=	0,0000
P3/P2	=	26,0288
P2/P1	=	0,99000
P22/P21	=	1,00000
P25/P24	=	0,98000
P4/P3	=	0,95000
P44/P43	=	0,99200
P48/P47	=	1,00000
P6/P5	=	0,99000
P16/P13	=	0,97500
P16/P6	=	1,08631
P5/P2	=	1,45056
V18/V8,id	=	0,70333
A8	=	0,29055 m²
A18	=	0,79883 m²
XM8	=	0,73953
XM18	=	0,81318
WBld/W2	=	0,00000
CD8	=	0,95593
CD18	=	0,95443
PWX	=	50,00000 kW
WlkLP/W25	=	0,00000
WBld/W25	=	0,00000
Loading	=	100,00 %
e442 th	=	0,86084
WHcl/W25	=	0,06000
WIcl/W25	=	0,00500

Figure A.1: Overview of all calculated engine parameters